INVESTIGATION OF MICROBIOLOGICALLY INFLUENCED CORROSION (MIC) AND BIOCIDE TREATMENT IN ANAEROBIC SALT WATER AND DEVELOPMENT OF A MECHANISTIC MIC MODEL

A dissertation presented to

the faculty of

the Russ College of Engineering and Technology of Ohio University

In partial fulfillment

of the requirements for the degree

Doctor of Philosophy

Kaili Zhao

November 2008

This dissertation titled

INVESTIGATION OF MICROBIOLOGICALLY INFLUENCED CORROSION (MIC) AND BIOCIDE TREATMENT IN ANAEROBIC SALT WATER AND DEVELOPMENT OF A MECHANISTIC MIC MODEL

by

KAILI ZHAO

has been approved for

the Department of Chemical and Biomolecular Engineering

and the Russ College of Engineering and Technology by

_____

Tingyue Gu

Associate Professor of Chemical and Biomolecular Engineering

_____

Dennis Irwin

Dean, Russ College of Engineering and Technology

ABSTRACT

ZHAO, KAILI, Ph.D., November 2008, Chemical Engineering

INVESTIGATION OF MICROBIOLOGICALLY INFLUENCED CORROSION (MIC) AND BIOCIDE TREATMENT IN ANAEROBIC SALT WATER AND DEVELOPMENT OF A MECHANISTIC MIC MODEL (284 pp.)

Director of Dissertation: Tingyue Gu

Pipelines during and after hydrotesting are vulnerable to microbiologically influenced corrosion (MIC), which can result in severe pinhole leaks. Instead of the current MIC studies in the field practice, this study investigated the MIC phenomenon in hydrotesting under laboratory conditions, and a variety of issues that arose during this process are discussed.

The MIC process during hydrotesting was found to be dependent on water sources due to different concentrations of nutrients and native organisms. In order to accelerate the MIC process, a simulated worst-case scenario with a lab strain SRB (sulfate-reducing bacteria) and key nutrients added proved to be a useful approach. Furthermore, the technique of polymerase chain reaction (PCR) was adopted to MIC research for detecting very low concentrations of targeted planktonic microbes.

A novel MIC mitigation method, using biocides THPS (TetrakisHydroxymethyl-Phosphonium Sulfate) and glutaraldehyde, in combination with EDTA (Ethylene-DiamineTetraAcetic acid) was found to be more effective for controlling the growth of planktonic SRB. A mechanistic THPS degradation model, with great consistency to

experimental results, was developed to predict residual THPS concentration to assure that it does not fall below the desired minimum required for MIC control.

Based on the mechanism of biocatalytic cathodic sulfate reduction (BCSR), a first generation MIC mechanistic model was developed to predict the localized MIC pitting rate under certain conditions; thus providing a basis for a more comprehensive mechanistic MIC modeling. Futhermore, a new biomarker EPS (extracellular polymeric substances), a potential replacement of existing biofilm probes, was proposed to serve for locating biofilms.

Approved: _____

Tingyue Gu

Associate Professor of Chemical and Biomolecular Engineering

DEDICATION

To

Sheng Zhao and Yaqin Yang (my parents)

Aili Zhao and Yali Zhao (my sisters)

and

Na Li (my wife)

ACKNOWLEDGMENTS

I would like to express my sincere gratitude and appreciation to my academic advisor Dr. Tingyue Gu, not only for his insightful and continuous guidance during the course of my PhD study, but also for his invaluable suggestions and encouragement. Special thanks go to Dr. Srdjan Nesic, director of the Institute of Corrosion and Multiphase Technology (ICMT), for his support and professional training. I would like to acknowledge all my committee members for their full support in my PhD study.

I am indebted to Mr. Jie Wen, my co-worker through the entire PhD study, for his tremendous assistance and help both in my academic work and my daily life. I would like to extend my gratitude to the staff at the ICMT for always providing me support whenever I asked for help, and also to my fellow graduate students at ICMT who provided a friendly and relaxed environment to make my study and life in Athens colorful and unforgettable. I would like to acknowledge the project sponsors (U. of Texas M. D. Anderson Cancer Center, BP America, and Saudi Aramco) for their financial support and technical advice.

Finally, I am very grateful to my family members, my parents Sheng Zhao and Yaqin Yang and my two elder sisters Aili Zhao and Yali Zhao, who have given me such strong support no matter what, when and where. A special gratitude goes to my wife Na Li for her understanding and true love. Meeting and marrying her during my PhD study is my greatest achievement.

.

TABLE OF CONTENTS

Page

LIST OF TABLES

Page

LIST OF FIGURES

Page

CHAPTER 1: INTRODUCTION

Corrosion is a process of material deterioration reacting to its environment, and is a natural process of materials reverting towards the lowest energy states with the involvement of electrochemistry and thermo kinetics (Davis, 2000). There is a wide range of types of corrodible materials, such as metals and alloys, plastics, ceramics, wood and composites. The study of corrosion is a complex scientific field. The study of metal corrosion alone involves many aspects of pure or applied sciences including metal physics, chemistry, metallurgy and microbiology. Corrosion occurs in a variety of environments and, thus, can be classified as atmospheric corrosion, underground/soil corrosion, seawater corrosion and microbiologically influenced corrosion.

Microbiologically influenced (induced) corrosion (MIC), an important branch of corrosion studies, was documented as early as 1934 by von Volzogen Kuhr and van der Vlught as causing severe damages on metals (von Volzogen Kuhr and van der Vlught, 1934). Since then, MIC has increasingly becoming a concern in such industries as water treatment, chemical-processing, nuclear power generation, oil and gas industries. The consequences of MIC can be plugging of injection and disposal systems, corrosion of facilities, and souring of fluids and reservoirs, all of which present major safety and economic considerations in oil field operations (Bibb, 1986; Brennenstuhl et al., 1990; Flemming, 1996).

MIC in nature is an electrochemical process, in which “the presence of microorganisms is able to initiate, facilitate and accelerate the corrosion reactions” (Videla, 1996). Bacterial microbes associated with MIC are ubiquitous. In the

environment, they may be metal-reducing bacteria (MRB), metal-depositing bacteria (MDB), slime-producing bacteria, acid-producing bacteria (APB), and sulfate-reducing bacteria (SRB). SRB are most often cited as the major culprit in MIC. This is because they thrive easily, can live in an anaerobic and sulfate environment, and can produce hydrogen sulfide (H_2S) which can react with alloys (Li et al., 2005), stainless steel (Duan et al., 2006), and mild steel (Zhao et al., 2007). Corrosion with SRB presence frequently shows localized attacks beneath the SRB biofilm in the form of a thin and slimy film composed of sessile cells, extracellular polymeric substances (EPS) and water.

In industry, hydrotesting (hydrostatic testing) of pipe work is a routine practice for assessing system integrity before it is commissioned. A test system is usually pressurized to 10% greater than the anticipated future operating pressure, and treated water (seawater, produced water, and local river/well water) is typically employed as the flush fluid. According to Sanders (1998), the presence of biological organisms in these flush fluids can be a source of MIC, because in the oil and gas industry, it is common to leave the hydrotesting fluid in a pipeline system for many months. Incomplete and improperly conducted hydrotesting could also result in MIC. For example, if a system is not drained dry immediately or thoroughly after a test, microorganisms present in the residual water could initiate and accelerate internal MIC (Borenstein and Lindsay, 2002) once the appropriate conditions such as temperature, pH, and nutrient supply are met. MIC both during and after hydrotesting can cause severe pinhole leaks in equipment, and can clog gas lines as a result of so called “black powder” (Baldwin, 1998). This decreases efficiency of facilities and, once started, is not easily eliminated.

MIC research on hydrotesting is a comprehensive, complicated and challenging study involving various aspects, but there has been no systemic study on this area. Existing MIC research on hydrotesting has been confined to field operation, which is costly, time consuming and even more unfortunately, unable to easily control and monitor the process, leading to failure. In this research, well designed lab-scale testing was undertaken as a means of providing a guideline for real situations.

In this project, seawater from the Gulf of Mexico and the Persian Gulf as well as Wasia aquifer water-all with different degrees of salinity, sulfate concentration and total organic carbon (TOC), were used as water sources to investigate MIC behavior in a laboratory setting. Experiments were also conducted using both untreated waters and treated waters inoculated with SRB and additional key nutrients in order to simulate a worse case scenario and to accelerate the MIC process. The technique of polymerase chain reaction (PCR) was used in the MIC study to detect trace amounts of targeted organisms in the test media.

MIC mitigation during hydrotesting responds best to biocide use (Prasad, 2004). Two popular green biocides, THPS (TetrakisHydroxymethylPhosphonium Sulfate) and glutaraldehyde, have been used in combination with the metal chelator EDTA (EthyleneDiamineTetraAcetic acid) as a novel approach to inhibit SRB growth (Zhao et al., 2005). However, because of the degradability of the biocide THPS, a method is needed to predict residual THPS concentrations to assure an adequate minimum necessary to suppress planktonic cell growth and to prevent biofilm establishment. As part of this research, a mechanistic THPS degradation modeling is desired to provide an

accurate guideline for proper dosing to minimize THPS and prevent inadequate dosing during hydrotesting.

MIC modeling is unsophisticated compared to the quantitative and mechanistic H_2S or CO_2 modeling. Since the leading cathodic polarization theory (CDT) was first proposed in 1934, MIC mechanism has been a subject of controversy, and the prevailing MIC models were mostly based upon risk factors and applied to estimate MIC likelihood (Chexal et al., 1997; Maxwell and Campbell, 2006; Sooknah et al., 2007). From the view of electrochemistry and biology, a mechanistic MIC modeling based on biocatalytic cathodic sulfate reduction was developed to establish a more comprehensive mechanistic MIC modeling. In addition, the spatial location of biofilm and its distribution in a flow system is an ongoing challenge in MIC research. To date, the existing methods (Hoffmann et al., 2007) for monitoring biofilm are inadequate. An effective biomarker was proposed in this study.

CHAPTER 2: LITERATURE REVIEW

MIC problems resulting from operations using salt water is an important subject in gas and oil industries. The involvement of microorganisms in the corrosion process during specific hydrotesting operations distinguishes the study of MIC from other types of corrosion. To better understand the MIC process, a mechanistic model for MIC and a more powerful biomarker for locating biofilms are also desired.

2.1 Microbiologically influenced corrosion (MIC)

2.1.1 Characteristics of MIC

Microbiologically influenced corrosion (MIC) is the deterioration process of materials caused directly or indirectly by bacteria, fungi, algae, moulds or in consortia. Videla (1996) defined MIC as "An electrochemical process in which the presence of microorganisms is able to initiate, facilitate or accelerate the corrosion reaction without changing its electrochemical nature." Materials deteriorated by microorganisms can be either metallic or non-metallic materials. Recently, an MIC panel at the NACE 2003 International Conference limited the definition of MIC to the corrosion of metals and alloys (Lewandowski et al., 2003).

The relevance of microorganisms in corrosion of metals was known as early as 1934 by von Volzogen Kuhr and van der Vlught. Yet, MIC has increasingly become a significant concern to corrosion engineers because of severe damage to materials in many industries including the oil and gas industries, water utilities, nuclear power plants, and

chemical manufacturing facilities. MIC may result in corrosion of pipes and equipment, plugging of injection or disposal wells and souring of fluids and reservoirs, all of which will present major economic and safety concerns (Bibb, 1986; Brennenstuhl et al., 1990; Flemming, 1996). According to the report of Koch et al. (2001), an annual cost estimation of all forms of corrosion to the gas and oil industries is about $13.4 billion, with MIC, alone, costing $2 billion. Corrosion could lead to severe consequences. For example, the 2006 BP Alaska pipeline leak due to corrosion affected 8% of US oil production, and drew highened attentions to MIC by oil companies. The exact cause is still under investigation (Jacobson, 2007).

The main species of microbes associated with MIC on metals are sulfate-reducing bacteria (SRB), metal-reducing bacteria (MRB), metal-depositing bacteria (MDB), slime-producing bacteria and acid-producing bacteria (APB) (Beech and Gaylarde, 1999). In nature, it is difficult to find single bacterial species existing in isolation, and commonly, bacterial communities act synergistically in the MIC process. Among the bacterial communities, SRB are known to be the major culprit frequently implicated in MIC of iron, copper and ferrous alloys (Fonseca et al., 1998; Kuang et al., 2007).

2.1.2 Sulfate-reducing bacteria (SRB)

Generally, SRB are those bacterial species that can cause dissimilatory reduction of sulfur compounds, such as sulfate, thiosulfate, sulfite, and even sulfur to sulfide (Lovley and Philips, 1994), using sulfate as the terminal electron acceptor. Mohanty et al. (2000) narrowed the SRB definition to include all unicellular bacteria capable of reducing

sulfate to sulfide. Based on the analysis of 16S rRNA sequence, SRB, as a diverse group of prokaryotes, are classified into four sub-groups: gram-negative mesophilic bateria, thermophilic sulfate reducers, gram-positive spore-forming sulfate reducers, and thermophilic archaeal sulfate reducers (Castro et al., 2000). According to Bahr et al. (2005), the key enzyme involved in SRB respiration pathway is dissimilatory sulfite reductase (DSR) which is able to carry out the dissimilatory sulfate reduction process, and most of α and β subunits of DSR can be encoded in a 1.9-kb DNA region.

Although SRB are usually thought to be strictly anaerobic microbes, it has been demonstrated that SRB could still remain alive for hours or even days at low concentrations of dissolved oxygen (Hardy and Hamilton, 1981; Fukui and Takii, 1990). Marschall et al. (1993) studied the effect of oxygen on the growth of 10 SRB strains and found that three of the strains could reduce sulfate (thiosulfate/sulfite) to sulfide at a low rate when oxygen concentration was below 15 μM (6% air saturation). They concluded that oxygen could serve as an electron acceptor for SRB as well as create a toxic environment for SRB growth. Some thermophilic species like SRB can grow well around 100°C (Tatnall, 1995), while SRB species *Desulfovibrio* can grow well within the temperature range between 5 °C and 50 °C (best between 25°C and 45°C), and the pH range from 5.0 to 10 (optimum pH around 7.2) (Javaherdashi, 1999).

SRB can be found everywhere. Dzierzewicz et al. (2003) found that the most common genera of SRB is *Desulfovibrio,* belonging to the *Desulfovibrionaceae* family in the big group gram-negative mesophilic bacteria. They also found that *Desulfovibrio desulfuricans* is the most frequently found species of the genus in anaerobic regions of

mud, soils, marine and estuarine sediments. An image from Hu (2004) showed that the strain *Desulfovibrio desulfuricans* was observed to be rod shape under an epifluorescent microscope.

SRB caused corrosion can impact a variety of materials, e.g. alloys (Li et al., 2005), stainless steel (Duan et al., 2006), and mild steel (Zhao et al., 2007) by the production of H_2S or biofilm. The produced H_2S and subsequent corrosion products are the main factors of the plugging of pipelines (Baldwin, 1998), and the souring of fluid (Eckford and Fedorak, 2002a). SRB biofilm has been responsible for localized corrosion and is recognized as a major corrosion problem due to the severity of its damages and unpredictability.

2.1.3 Biofilm, extracellular polymeric substances (EPS) and localized corrosion

Microorganisms attach themselves to solid surfaces, embed themselves in the sticky secretion of extracellular polymeric substances (EPS) and form microbial layers, which are called "biofilm," sometimes called biofouling. Biofilms provide a colonization environment for bacteria to protect them from external attack once they are established. Immobilized microorganisms are called sessile microbes while those living in bulk solutions are called planktonic microbes. Donlan (2002) indicated that sessile cells and their counterpart planktonic cells are bio-functionally different with respect to the different gene transcription process.

Biofilm is a thin slimy film composed of EPS and bacteria with a gel-like matrix. Escher and Characklis (1990) demonstrated the biofilm formation process as having six

steps: adsorption of molecules on the surface to form conditioning form; transportation of microorganisms to the surface; initial adhesion of microbes; strengthened attachment of microorganisms through EPS; growth of biofilms and localized detachment of biofilms by outside forces. Surface roughness and material composition as well as thermodynamic shear stress play a major role in the process of biofilm formation. Microorganisms tend to colonize at some locations, such as welding zones, grain boundaries, and crevices.

According to Jahn and Nielsen (1998), bacterial EPS consist mostly of polysaccharides, proteins, nucleic acids, phospholipids and humic substances. Bacterial EPS also account for 50% to 90% (wt) of the organic matters in a biofilm (Wingender et al., 1999). EPS alone in seawater was found to accelerate coupon pit depth formation five times larger than those in EPS free medium (Chan et al., 2002). Apart from the EPS corrosive effect on metal directly, EPS can help biofilm thrive in an anaerobic situation due to its adhesive and complex matrix structure, which facilitates the growth and colonization of anaerobic bacteria like SRB.

Beech and Gaylarde (1991) found that EPS together with one cultured SRB strain (*Desulfovibrio desulfuricans*) can result in more severe corrosion than that of EPS with *Pseudomonas fluorescences* or a mixture culture of both. Some studies (White et al., 1985; Ford et al., 1987; Beech and Sunner, 2004; Braissant et al, 2007) also found that EPS has the capacity to bind metal ions to form metal concentration cells, which will result in galvanic coupling. It was found that EPS can be applied as a biomarker to detect and locate biofilm, aiming to mitigate MIC damages.

Corrosion occurring in specific locations while the remaining surface area is not severely attacked is often called localized corrosion. Usually, localized corrosion develops when a seemingly continuous film on the surface is discrete for some reason. MIC-caused localized corrosion can lead to pinhole leaks. Such corrosion may be due to the rupture of the protective film FeS produced in the presence of SRB. Another possibility may be the results from the characteristics of bacteria. It is well known that biofilm plays a key role in microbiologically induced localized corrosion, because the biofilm accumulation on the material surface may change such aspects as the near-surface water chemistry and transportation of species, which enhances the local electrochemistry reactions and causes severe corrosion in those specific positions. SRB induced localized corrosion can occur on many types of metals, even stainless steel (Shams El Din et al., 1996; Mattila et al., 1997; Xu et al., 2007).

2.1.4 Mechanisms

In principle, MIC occurs at the material interface where sessile cells influence the corrosion kinetics of anodic and/or cathodic reactions. MIC does not invoke any new electrochemical reactions, but the involvement of microorganisms does change the physiochemical environment at the interface. Examples of this include concentration of nutrition, pH, redox potential and water chemistry. A number of MIC mechanisms of metal corrosion by SRB has been proposed since the first cathodic depolarization theory (CDT) was suggested by von Wolzogen Kuhr and van der Vlugt (1934) and confirmed by Bryant et al. (1991). Apart from CDT, Efird (1988) found that iron sulfides might be the

corrosive substances by the way of galvanic corrosion, and Edyvean et al. (1998) proposed a MIC process caused by sulfide-induced stress corrosion cracking and hydrogen-induced cracking/blistering. The relevant reactions and end products generally occur simultaneously or successively during MIC process, making it difficult to determine which mechanism is the influencing one. Among the various MIC mechanisms, CDT is the most prevalent explanation whereby SRB's hydrogenase enzyme is involved in the removal of hydrogen from the cathodic area on the metal surface, leading to cathodic depolarization. Thus, coupled with sulfate reduction to sulfide, CDT explained the severe MIC pitting of metal.

2.2 Hydrotesting associated with MIC

Hydrotesting is a common practice to assess pipeline integrity before service. Different from pneumatic testing which is used only for leak testing, hydrotesting is applied to test for both leaks and strength. During hydrotesting, a pipeline is filled with a liquid and pressurized to a pressure greater (usually 10% higher) than the anticipated future operating pressure. In general, hydrotesting itself lasts only eight to ten hours. However, in the oil and gas industry, it is often the case that water is left in the system afterwards for many months before the system is actually commissioned. During this holding time or when the pipeline is first exposed to an aqueous environment like wet lay-up, corrosion due to MIC can commence (Borenstein, 2002). When the system makes contact with the ground (Videla, 1996) or is even exposed to air (Parra et at., 1996), there is further possibility of microbial contamination. Reuse of water also increases chances for MIC. Incomplete or improper hydrotesting practices can result in MIC causing pitting

attacks and also the so-called “black powder” problem (Baldwin, 1998). The common example is when the water used in the hydrotesting cannot be thoroughly eliminated at the end of the test, and the residual microorganisms, such as sulfate-reducing bacteria (SRB), can initiate or enhance the MIC. The biofilms left behind by the hydrotesting process pose a long-term threat during pipeline operations.

Seawater is routinely used in the hydrotesting of sub-sea pipelines. Other water sources mainly come from aquifer water and produced water. Any water source for hydrotesting can contain microorganisms. Natural seawater contains viruses, prokaryotes, protists (mainly flagellates) and algae (Weinbauer and Wenderoth, 2002). Water used in hydrotesting is usually treated with biocides. However, even treated water can be a source of SRB inoculum according to Sanders (1998). Two other methods to treat the test water were by adjusting pH and using water sources without sulfate (Prasad, 2004). However, pH adjustment (within a basic range) could increase the possibility of mineral scale formation on the surface, and using large amount of water without sulfate is usually costly and inconvenient when hydrotesting takes place off shore.

Rossmoore (1995) found that a variety of bacteria have the capability to reduce in size; decreasing energy consumption during starvation and reside in smaller pores. These bacteria can then wait to thrive when the appropriate environmental conditions are met. This unique feature of bacteria makes predicting and preventing the MIC in hydrotesting difficult. Steel corrosion in seawater sometimes has been misdiagnosed as attack induced only by conventional chloride corrosion. However, Borenstein (2002) found that microorganisms contained in stagnant chloride bearing-medium can result in steel failure

much faster than in conventional chloride crevice corrosion alone. This increased corrosion rate may result from sulfate and other nutrients in the seawater which cause souring and pipeline corrosion due to SRB activities.

In the field, oxygen scavengers are usually added to the water of hydrotesting to prevent oxygen caused corrosion. This provides an anaerobic environment for anaerobic bacteria such as SRB. MIC occurs when several favorable factors are present simultaneously, such as water chemistry, temperature, nutrients (organic and inorganic), microorganisms, and pressure. The majority of SRB can thrive at pH ranges from 5-9, and except for thermopiles, are unable to grow well at temperatures above 45^{o}C. Availability of a carbon source is usually considered to be the most important factor for SRB growth, and SRB growth will be severally restricted if utilizable carbon in organic nutrients such as formate, acetate and propionate, is below 20 ppm (Pots et al., 2002). Pots et al. (2002) also indicated that SRB growth would be the most prominent if the ratio of carbon to utilizable nitrogen was 10:1. Synergistic microorganisms can enrich the nutrients (such as carbon) in the local environment and thus promote SRB growth and accelerate the MIC process even though the initial environmental conditions are not appropriate for SRB growth. In a lab, however, it is difficult to simulate the complicated ecosystem to study the MIC process. To better simulate and accelerate the MIC process, well-controlled spiking tests using lab strains of SRB are needed.

2.3 Factors related to MIC in hydrotesting

2.3.1 Test temperature

Fluid temperature is affected by a variety of factors such as weather, pipe location, and water sources. For example, if seawater is used as the flush fluid, temperature varies depending on such factors as location, climate change, and season switch, in a range from below zero to above 30 °C. And inevitably, the testing pipelines laid under the sea are subject to the impact of different temperatures in a seawater environment−in deep seabed or shallow seashore. Geographically, seawater temperatures in places like Saudi Arabia are much higher than other locations. It was found that fluid temperatures during a hydrotesting for marine facility piping vary from 15^{o}C-30^{o}C (CSLC-MFD, 2003).

2.3.2 Test pressure

High pressure will adversely affect bacteria growth, especially above 10,000 psi, where even native pressure loving barophiles do not grow well (Evans and Dunsmore, 2006). However, reproducing a high-pressure environment is cost prohibitive and impractical. On the other hand, if the seawater used in hydrotesting comes from deep sea sources, native bacteria in the seawater may die or not grow at a lower operating pressure. Therefore, under lab conditions, atmosphere pressure is used as the cell growth environment.

2.3.3 Time period

In the field, the average lifespan of pipelines is predicted to be around 20 years. However, it is not economical or practical to spend such a long period to test pipeline life in a real situation. Borenstein (2002) reported on a nine-month test where there was MIC failure of steel piping in the hydrotesting process. A test up to 11 months is considered a reasonable test time period in the current research. Coupon samples were analyzed regularly. For tests in enriched media, the test period might be shortened since the MIC process is accelerated.

2.3.4 Water sources

As mentioned, water sources play an important role in hydrotesting, since there are different chemical compositions and bacterial consortia in each solution (Borenstein and Lindsay, 2002; Javaherdashi, 2003). To better simulate real situations, different types of culture media for bacteria growth should be used. In this research, natural seawater from the Gulf of Mexico and the Persian Gulf, Wasia aquifer water from Saudi Arabia and artificial seawater were used and in some cases, some essential nutrients were added to promote SRB growth and to accelerate the MIC process.

2.3.5 Nutrients

All organisms need energy to survive. Besides energy, bacteria also need to assimilate carbon source for the synthesis of their cell wall. SRB is able to obtain energy/carbon from organic matters as well as from inorganic substances (Badziong et al.,

1979; Mudryk et al., 2000). In natural seawater, the total organic concentration (TOC) may be considered as an indicator of how the nutrients in the seawater could support the bacterial growth. For water sources with poor nutrient supply, additional energy/carbon sources are critical for bacterial growth. A medium with additional nutrition supplements is called enriched medium.

Badziong et al. (1979) indicated that the SRB strain *Desulfovibrio vulgaris* can utilize hydrogen plus sulfate as an energy source and acetate plus CO_2 as a carbon source. Odom (1993) found that SRB could also obtain its carbon source from oil, and according to Mudryk et al. (2000), lactate is a versatile organic substrate that acts as carbon and energy source as well as an electron donor. Experimental tests proved that the lab strain *Desulfovibrio desulfuricans* could not grow well without lactate.

Fe^{2+} as suggested by Postgate (1984) is required for SRB growth because Fe^{2+} affects the biosynthesis of the iron-cytochromes in the respiratory chain. Sulfate also is identified as a limiting nutrient ion for SRB growth. Fonseca et al. (1998), when testing coupon corrosion under culture media with/without sulfate, found that MIC initiation due to SRB only occurred when sulfate ions were present. Higher sulfate concentration, however, could also hinder SRB growth (Mohanty et al., 2000). According to Hu's (2004) experimental results, typical sulfate concentration (2700 ppm) in natural seawater is not high enough to inhibit SRB growth.

2.4 Analytical methods

2.4.1 Planktonic and sessile cells quantification

MIC occurs where bacteria are present, in the form of either planktonic or sessile cells. The quantitative enumeration of planktonic cells can be obtained under optical microscopy using a hemocytometer, with serial dilutions if necessary (Penn, 1991). Although this method can provide viable cell counts directly, it cannot distinguish specific bacteria like SRB from other bacterial species and is limited to lab tests with pure strains. Based on the culture methods, the most-probable-number (MPN) technique is extensively used to numerate SRB in oil or gas systems (Vester and Ingvorsen, 1998). With reference to a standard chart, SRB concentration is assessed by the formation of black precipitate (FeS) in MPN tubes (with liquid culture medium). The MPN method is suitable to planktonic cell counts as well as sessile cell enumeration.

Usually, sessile bacteria are removed from material surfaces by scraping the surface with a sterile scalpel or by using mild sonication. The sessile cells can be inoculated in MPN tubes or plated on solid media. The solid plate counting to obtain colony forming units (CFU) is a popular way to count viable bacteria in the field of biological science (Hu, 2004). Although bacterial culture in artificial growth media is accepted as a standard method to estimate cell numbers, it must be noted that only a small percentage of bacterial samples can be recovered by using this method and that some bacteria cannot grow even under that condition. The methods cited above for assaying bacteria or corrosion, to some extent, disturb the test systems due to sampling needs.

Under this situation, there is a need for developing better online monitoring techniques of bacteria and MIC.

2.4.2 Online monitoring

A flow-through device with three or more channels is designed to monitor MIC procession online. Microbial activity in biofilm and during corrosion can be observed under microscopy such as in confocal laser microscopy (CLM) with the aid of computer analysis, which can provide a 3D image of the biofilm (Caldwell et al., 1992). Bacterial activity can also be measured by an electrochemical sensor (Andrade et al., 2006). Chemical conditions, such as pH, dissolved oxygen, and redox potential within biofilms can be obtained by applying the technique of micro-electrodes according to Li and Bishop (2004). The above online monitoring methods, to some extent, can only be limited to applications in laboratary operations because field conditions are very complicated and biofilms are difficult to locate.

With the development of biological science, more and more advanced molecular methods involved in the study of MIC are being used in field detection of microbes. Most of the molecular detection methods are based on assay of nucleic acid sequence, generally in combination with subsequent amplification by polymerase chain reaction (PCR) (Zhu et al., 2005). The nucleic acid sequence is then applied in the FISH (fluorescence *in situ* hybridization), DGGE (denaturing gradient gel electrophoresis) to construct so-called DNA probes to detect microbial community in the oil or gas systems (Larsen et al., 2006). DNA probes can detect specific microbes which may be responsible

for MIC and provide microbial profiles. However, existing DNA probes cannot distinguish planktonic and sessile cells.

2.4.3 Surface analysis

Currently, material surface observation of microorganism morphology and distribution, corrosion products and micro-structure change after film removal is routinely assessed with atomic force microscopy (AFM), environmental scanning electron microscopy (ESEM) and scanning electron microscopy (SEM). AFM is a powerful analytical tool used in MIC studies (Beech et al., 1996; Xu et al., 2002). It provides physicochemical and mechanical characterization of material surface at molecule resolution. AFM also can demonstrate quantitatively surface feature information. ESEM has the advantage of scanning fresh biological samples directly. In contrast, application of SEM on biofilm observation is often employed if devices like a critical point dryer are available to pre-treat the biological samples. A confocal scanning laser microscopy (CSLM) has also been used to study biofilm/metal surface interaction (Walker et al., 1998).

To analyze the chemical composition of corrosion products and biological deposits on the material surface, energy dispersive X-ray analysis (EDX), X-ray diffraction (XRD) and X-ray photoelectron spectroscopy (XPS) have been widely applied to obtain the elemental information. EXD and XPS can even help to determine possible chemical (not elemental) identity of products on the surface. Fourier transform infrared spectroscopy (FTIR) is primarily used for analysis of organic matters qualitatively and

quantitatively and is a very useful analytical tool for the study of EPS composition (Beech et al., 1999). These analytical tools used in MIC study provide a clear picture not only of progression on the surface, but also an understanding of the possible MIC process.

2.5 Mitigation of MIC

The best scenario for preventing MIC occurrence is to have no bacteria present in the system. Mitigation of MIC is always expensive and difficult.

Currently, mitigation of MIC relies mostly on biocides and biostats. Both methods are used to inhibit MIC by better control of microbial activity. Biocide can be any chemical that can kill or inhibit the growth and reproductive cycle of bacteria. Examples of some common biocides are glutaraldehyde, formalaldehyde, acrolein, Tetrakis-HydroxymethylPhosphonium Sulfate (THPS), diamines, polyamines, organochlorine compounds, dibromonitrilopropionamide (DNBPA), biguanide, methylene bisthiocynates and alkyl dithiocarbamates. Chlorine, bromine and ozone have also proved to be effective biocides according to Viera et al. (1999). Application of the same biocides, however, could induce biocide-resistant bacteria. More importantly, growing environmental concerns are making their use more restricted. Lower concentrations and longer effectiveness are desired.

THPS and glutaraldehyde are two biocides that provide better degradation and have less environmental impact. THPS, compared with glutaraldehyde, is more biodegradable and our preliminary results have shown that its inhibitive effect is better

than that of the glutaraldehyde (Zhao et al., 2005). THPS has a strong inhibitive effect on bacteria growth, especially on SRB by causing rapid and severe damage to cell membranes.

As an effective degradable biocide, THPS degradation can result from biodegradation, hydrolysis, oxidation and photo degradation. It was reported that within two hours THPS exposure to UV would completely degrade to THPO (Trihydroxymethyl phosphine oxide) when the initial concentration is low (20 ppm) (WHO, 2000). Lloyd (1994) and O'Connor (1992) concluded that pH also affects THPS photo-degradation and hydrolysis. A few other studies on THPS degradation rate can be found in the literature (McWilliam, 1994; Gorman, 1997). Unfortunately, almost all the THPS degradation data in the literatures are for acidic or neutral pH, and to date, there are no THPS degradation prediction models.

Other alternative chemical methods to mitigate MIC include pH adjustment and the introduction of nitrate and nitrite. The adjustment of pH in bulk solution can restrain harmful bacteria by promoting the growth of less aggressive microbes like fungi. The addition of nitrate/nitrite acts as an inhibitor on SRB growth and MIC in the following two ways: (1) the competition of SRB with nitrate- or nitrite- reducing bacteria (NRB) for electron donors (Eckford and Fedorak, 2002b); (2) nitrate- or nitrite-reducing sulfide-oxidizing bacteria (NR-SOB) use of nitrate or nitrite to reduce sulfide to sulfur or sulfate to remove produced sulfide and mitigate the sour situation caused by H_2S (Hubert et al., 2003). A mechanical method used predominantly in the oil industry is to run a "smart pig." Smart pig is a high-tech device designed to root around inside pipelines with liquid

in the systems as a driving force to eliminate solid or biofilm deposits on the internal surface (Jacobson, 2007).

2.6 Modeling

Prevention is always better than serious consequences. A prediction model can be an effective tool to assess corrosion before it occurs. Currently, modeling and prediction of MIC are unsophisticated compared to CO_2 and H_2S modeling.

During the past decades, some mathematical models have been proposed to assess MIC process mechanistically or empirically. Picioreanu and van Loosdrecht (2002) used a three-dimensional mathematical model to study biofilm development and investigate the initiation of microorganisms causing localized corrosion. The model was established based on the principles of transport of seven chemical species between interface of biofilm and metal surface. Although the study modeled aerobic biofilm interaction with metal, it also provided an insight for future anaerobic biofilm study. This mechanistic model, however, indicated that it is difficult to predict overall MIC behavior and is limited to a simple chemical system.

It is widely accepted that MIC prediction models rely on nutrient conditions, environmental conditions (pH, temperature, synergistic microbes, redox potential), and inoculum sources (SRB from water or pipe wall). Due to the uncertainty of whether a system has a sufficient SRB inoculum source, prediction of MIC is highly speculative with the exception of reservoir souring progression prediction for already soured wells. Accurate modeling of other systems with uncertain inoculum is still premature. So far,

"fault-tree" types of models prevail: (1) Checkworks predictive model (CW) (EPRI, 1994), (2) Union Electric Callaway MIC Index (UE) (Chexal et al., 1997; Schultz et al., 1997), and (3) Lutey/Stein MIC Index (L/S) (Lutey et al., 1997).

Recently, Maxwell and Campbell (2006) and Sooknah et al., (2007) explored the same empirical models and made them more practical, but they are all simple fault-tree like probability models weighing various factors such as pH, nutrient conditions, temperature, or planktonic cell count, providing only likelihood for MIC attacks in a pipeline system. Gu (2007) at a Calgary MIC Workshop mentioned two promising tools to mechanistically model MIC process: plume modeling, a concept from environmental engineering, and modeling based on a biomarker. To achieve those two goals, extensive interdisciplinary knowledge is required. Using mechanistic modeling to predict MIC in hydrotesting is extremely limited because of the many uncertainties involved as stated above.

CHAPTER 3: MIC IN HYDROTESTING USING SEAWATER FROM THE GULF OF MEXICO (GOM)

3.1 Introduction

Water used in hydrotesting may be left in test systems from a couple of days to years. The system, therefore, is vulnerable to MIC when harmful bacteria are present on the pipe surface or introduced by the water source. A leak found in the oil transit pipeline on March 2, 2006, at Prudehoe Bay was suspected to be partially a result of MIC although the exact cause in still under investigation (Jacobson, 2007). The pipeline failure resulted in a 1.9-acre oil spill and more serious environmental concerns afterwards. This accident has heightened the attention to MIC studies, especially in hydrotesting operations when bacteria may first have been introduced. In the near future, BP America intends to build a new oil pipeline off shore in the Gulf of Mexico (GoM), and for convenience, seawater at hand may be employed as the hydrotesting fluid to test pipeline integrity. This chapter will focus on the study of MIC during hydrotesting using seawater from the GoM, to provide a preliminary understanding of potential MIC occurrence during hydrotesting operations.

3.2 Objectives

- To investigate MIC in untreated Gulf of Mexico (GoM) seawater used in hydrotesting, and to study the accelerated MIC process by using contaminated GoM seawater.

- To study the effects of biocides (THPS and glutaraldehyde) on the MIC process in the untreated GoM seawater

3.3 Instrumentation and analytical methods

100 ml anaerobic vials (Figure 3-1) were used for the experiments. Use of a glove box deoxygenated with N_2 gas (Figure 3-2) provided an anaerobic environment. X65 (from a pipeline section supplied by BP) and C1018 coupons were used. These chewing gum shaped coupons with dimensions of 4.76cm×1.09cm×0.16cm (Figure 3-1) were made from the two types of carbon steel. Prior to use, the coupon surfaces were polished successively with 200 and 400 grit SiC abrasive papers, rinsed with alcohol, and then sonicated in a beaker filled with alcohol. Figure 3-3 shows a freshly polished coupon surface. The ratio of coupon surface to medium volume is close to that in 0.30m (12″) ID pipes. All liquids in the tests were deoxygenated using N_2 sparging before use. Planktonic SRB bacterial count was determined by manual counting under an optical microscope at 400X using a hemacytometer. If needed, a Rodine HCl solution was applied to remove any films on the coupon surfaces. Scanning Electron Microscopy (SEM) and Energy Dispersive Spectrometry (EDS) were employed to perform surface analyses. A CHEMets® kit (www.chemetrics.com, product code: K-7540) was used to test the oxygen concentration in the experimental vials.

For biofilm observations under SEM, unless mentioned specifically, coupons were pretreated according to the following procedures: coupons were removed from vials and were immediately treated with 4% w/w glutaraldehyde for around 1 hour (to

immobilize the biofilm), and then were dehydrated with 30% (v/v), 50%, 75% and 100% alcohol in sequence. Before observing the biofilm, the coupons were first treated using a critical point dryer (BAL-TEC, CPD 030) then coated with a gold film.

Unless indicated specifically, the method of weight loss together with corrosion rate (CR) was used to demonstrate uniform corrosion, while pitting rate (PT) was employed to indicate MIC caused pitting corrosion. It was found all the pitting areas were quite small compared to the whole sample surface area, and in this study, pitting area was taken as 1/100 of sample surface area.

Figure 3-1: X65 coupon in an actual experimental vial

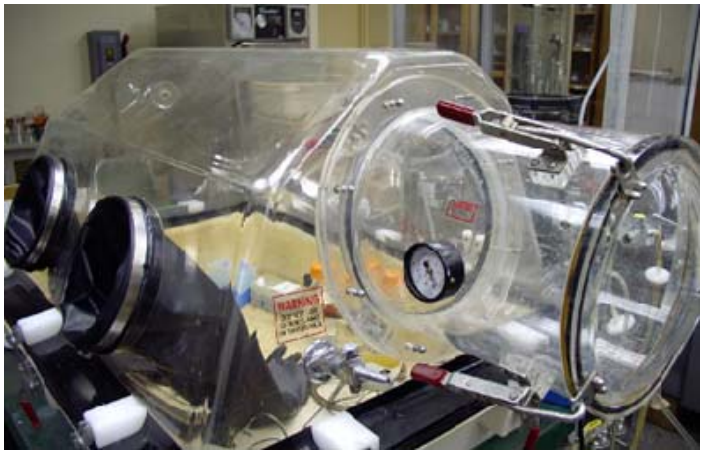

Figure 3-2: Chamber for anaerobic operations

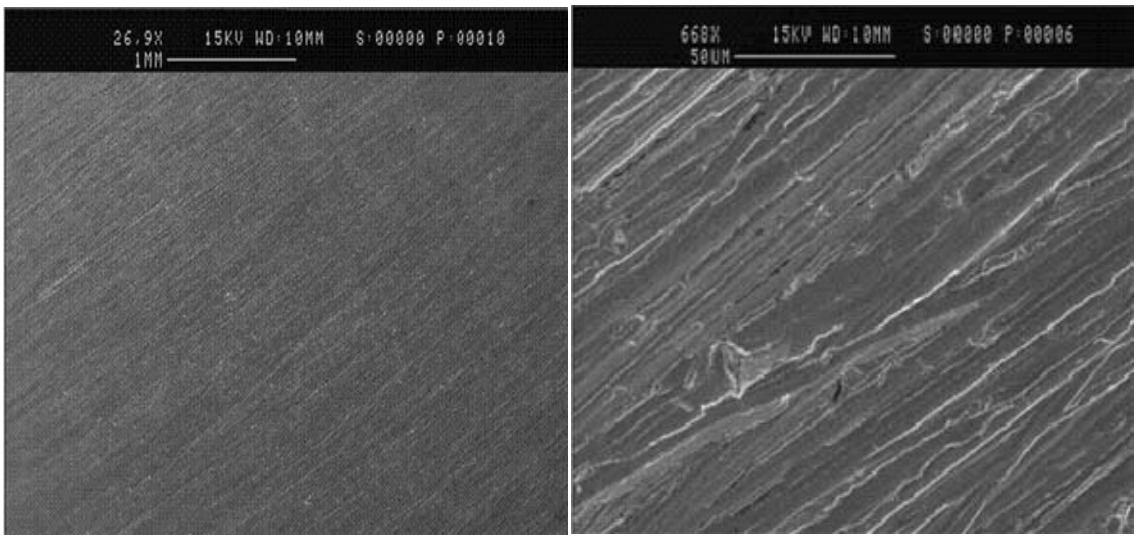

(a) SEM at 27X (b) SEM at 668X

Figure 3-3: SEM images of a polished X65 specimen before use

3.4 Results and discussion

3.4.1 Test using untreated GoM seawater

3.4.1.1 Test conditions

Two GoM seawater samples were supplied by BP. Unless mentioned specifically, data given for this experiment are for the first GoM sample. Table 3-1 shows the test matrix. Both the chemical and microbial analyses of GoM seawater were performed by outside labs (ENC Labs and Gas Technology Institute, respectively). Table 3-2 indicates that the GoM seawater has a similar chemical composition to that of typical natural seawater. The total organic carbon (TOC) in the first GoM sample was less than 1 ppm compared to TOC < 1 to 2 ppm for typical seawater while the TOC of the second GoM sample was 4.6 ppm. The GoM seawater samples from BP were actually very clean in terms of total bacteria concentrations, and the SRB cell count was below the detection limit of 1 to 3 SRB cells per liter using PCR. When Hardy (1981) measured seven

samples from two similar locations of the North Sea, he obtained SRB numbers from 0 to 90 cells/ml, the average was 22 SRB/ml. Lee et al. (2007), using the MPN method, detected around 10^1 SRB/ml and 10^2 SRB/ml in Persian Gulf and Florida Key West seawaters, respectively. These two water samples came from 1.2 to 1.5 meters deep and near-shore (within 100 meters) locations that could be contaminated by wastes. Table 3-3 shows the quantitative PCR analysis (Zhu et al., 2005) of the microbes in the GoM seawater.

Table 3-1: Test matrix using GoM seawater

Test conditions	
Temperature (°C)	4, 10, 25, 37
Time	1 month (using the second GoM seawater), 3 months, 6 months, 11 months
Culture media	Untreated GoM seawater. (Sterilized GoM seawater was used for 6-month and 11-month tests only).

Table 3-2: Major element comparison between typical natural seawater and GoM seawater

	Ca^{2+} (ppm)	Na^{+} (ppm)	Cl^{-} (ppm)	F^{-} (ppm)	SO_4^{2-} (ppm)	K^{+} (ppm)	Total organic carbon (TOC)
Typical natural seawater	400 to 412	10,500 to 10,770	18,800 to 19,300	1.2 to 1.3	2,655 to 2,715	380 to 390	<1 to 2
GoM seawater	421	10,800	19,700	1.41	2,655	398	Not detected <1

Table 3-3: Quantitative PCR analysis of GoM seawater

	GoM seawater
Total bacteria concentration	13.3 cells/ml
Sulfate-reducing bacteria (SRB) concentration	None detected

3.4.1.2 Test results

Figure 3-4 and Figure 3-5 show, after six months, no biofilms on the coupon surfaces, but both showed crystal substances on the surface which may be mineral deposits. It is unlikely that this is a biofilm due to its highly organized structure. The elements on the coupon surfaces using EDS analyses suggested there was no elemental S, an indicator of SRB presence. In the one-month test, weight loss increased as the temperature increased while pH increased as the temperature decreased (see Figure 3-6), after acid cleaning, no pits were detected for this test (see Figure 3-7 ~ Figure 3-10).

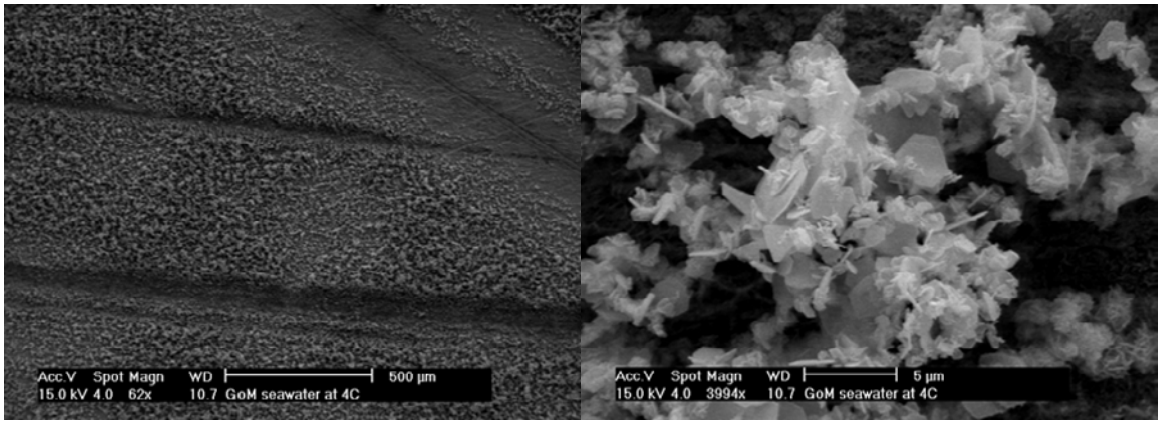

(a) SEM at 62X (b) SEM at 3994X

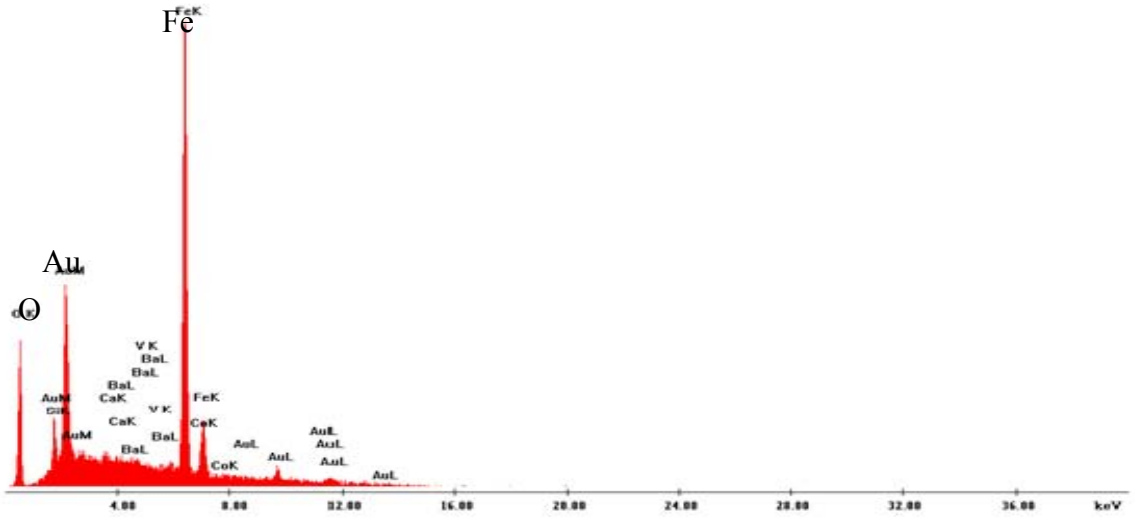

(c) Composition on the coupon surface

Figure 3-4: 6-month test in untreated GoM seawater at 4ºC (SEM and EDS analysis of coupon surface before acid cleaning)

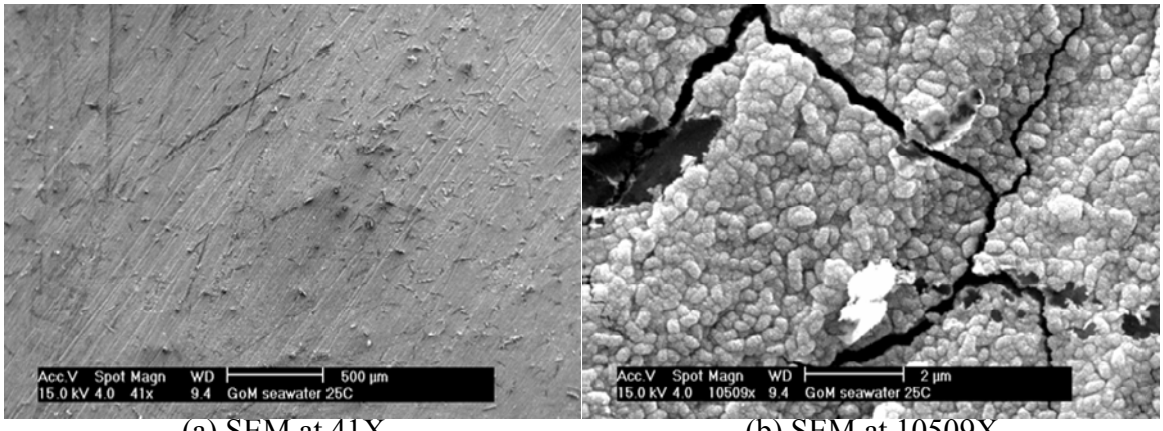

(a) SEM at 41X (b) SEM at 10509X

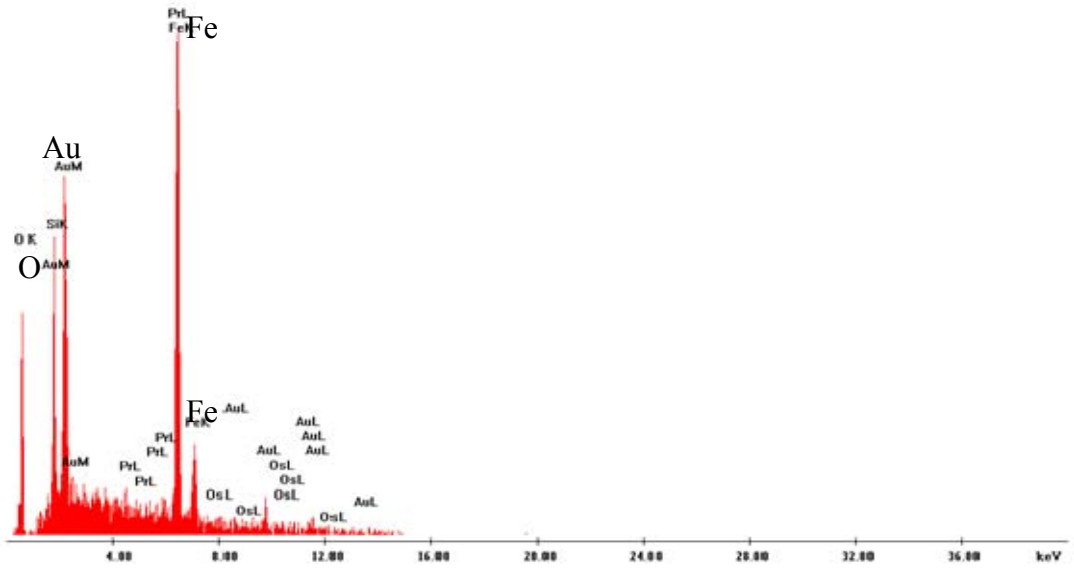

(c) Composition on the coupon surface

Figure 3-5: 6-month test in untreated GoM seawater at 25ºC (SEM and EDS analysis of coupon surface before acid cleaning)

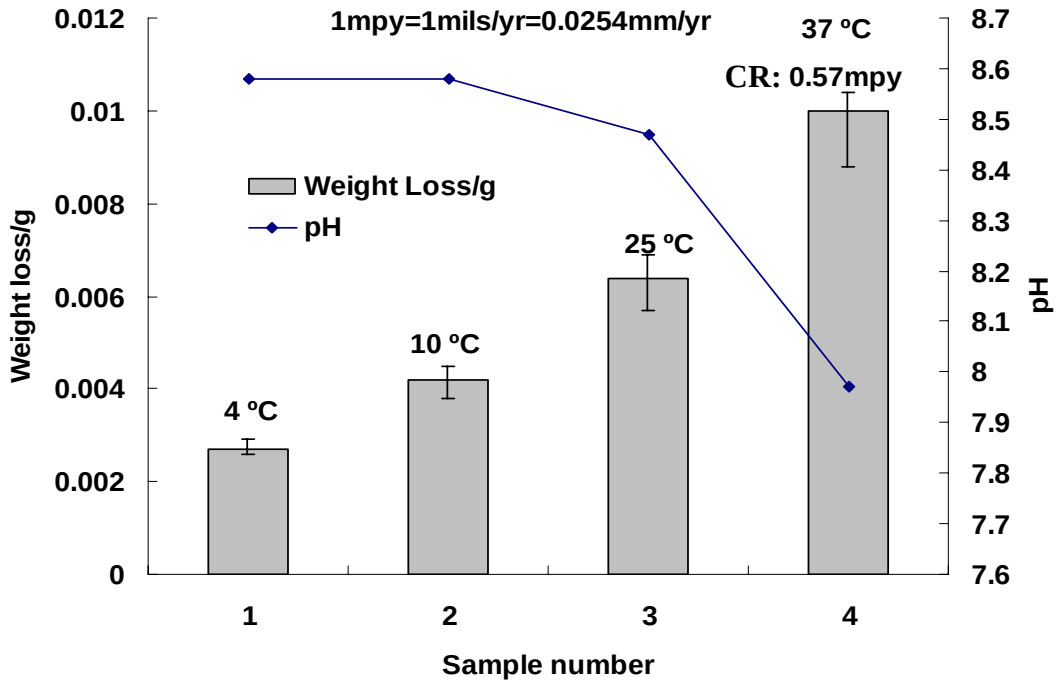

Figure 3-6: X65 coupon weight loss in the second untreated GoM seawater after the 1-month test

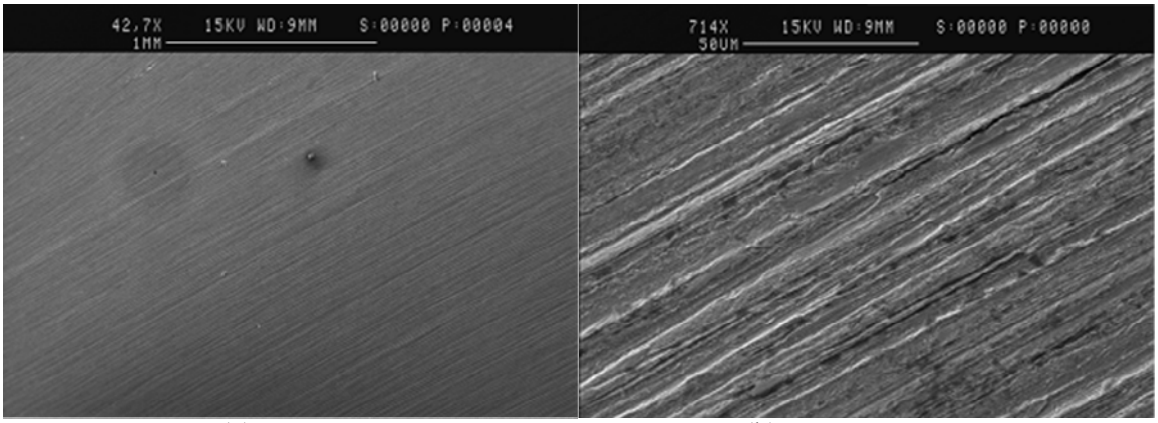

(a) SEM at 43X (b) SEM at 714X

Figure 3-7: 1-month test in the untreated second shipment of GoM seawater at 4ºC (SEM analysis of coupon surface after acid cleaning)

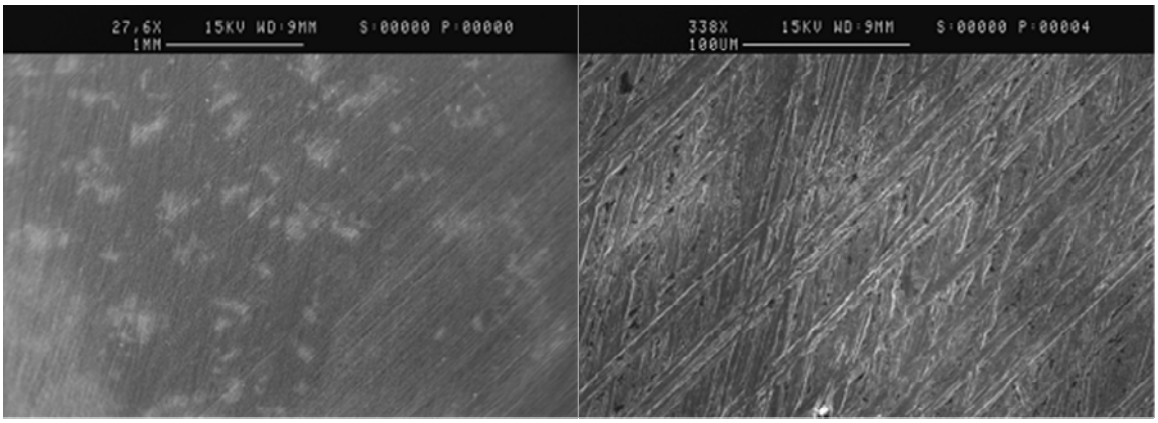

(a) SEM at 28X (b) SEM at 338X

Figure 3-8: 1-month test in the untreated second shipment of GoM seawater at 10ºC (SEM analysis of coupon surface after acid cleaning)

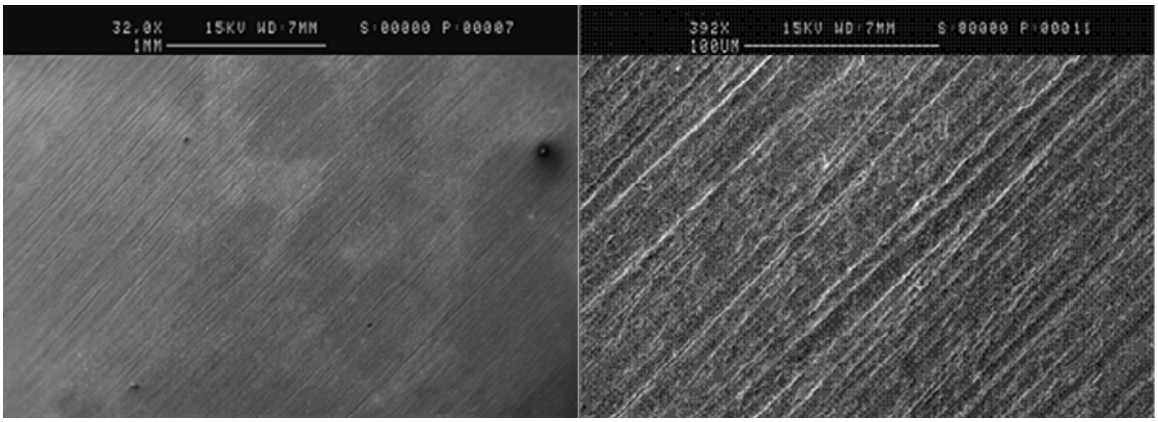

(a) SEM at 32X (b) SEM at 392X

Figure 3-9: 1-month test in the untreated second shipment of GoM seawater at 25ºC (SEM analysis of coupon surface after acid cleaning)

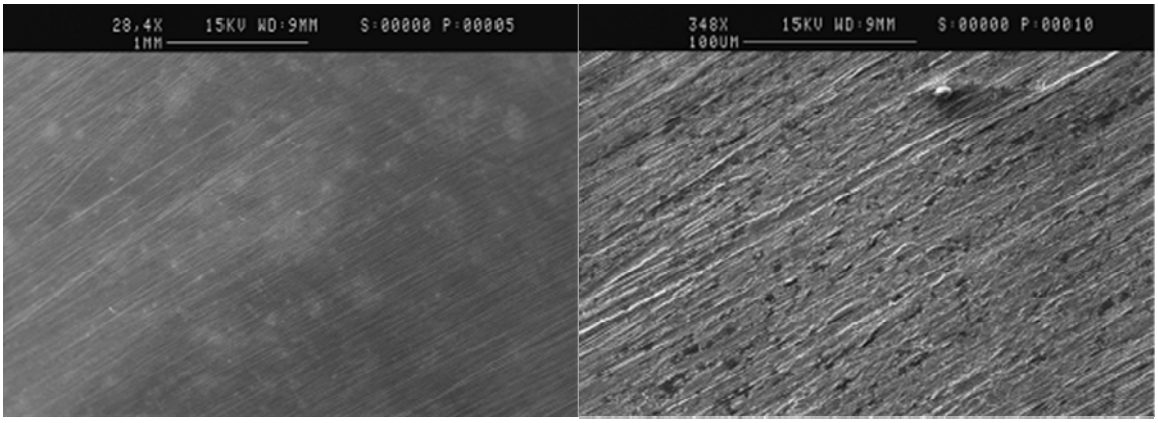

(a) SEM at 28X (b) SEM at 348X

Figure 3-10: 1-month test in the untreated second shipment of GoM seawater at 37ºC (SEM analysis of coupon surface after acid cleaning)

The 3-month test results showed the same weight loss and pH trends as the one-month test (see Figure 3-11). The difference, however, was that corrosion was more serious and small pits could be observed, especially at 4ºC and 10ºC (see Figure 3-12 and Figure 3-13).

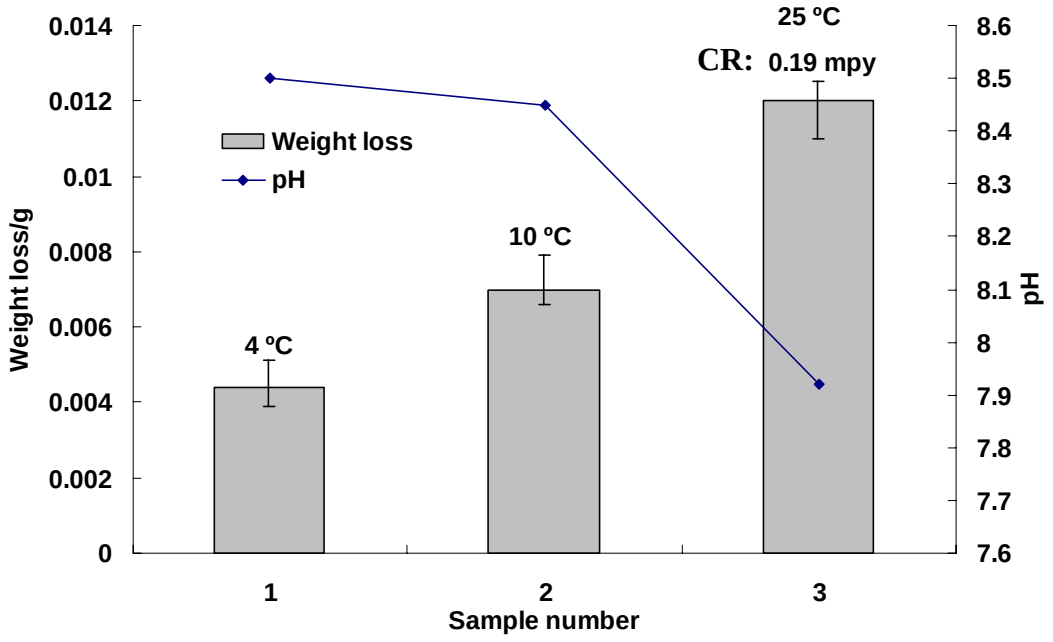

Figure 3-11: X65 coupon weight loss in untreated GoM seawater after the 3-month test

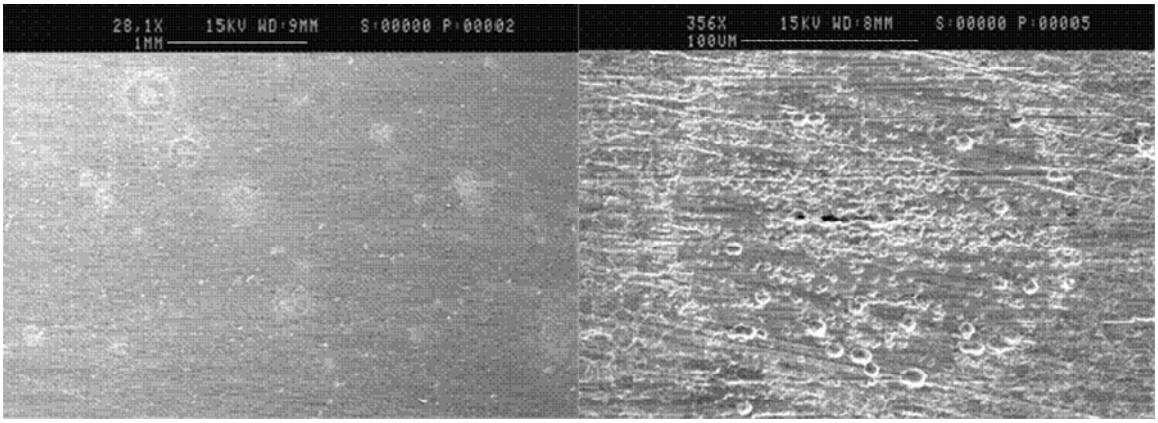

(a) SEM at 28X (b) SEM at 356X

Figure 3-12: 3-month test in untreated GoM seawater at 4ºC (SEM analysis of coupon surface after acid cleaning)

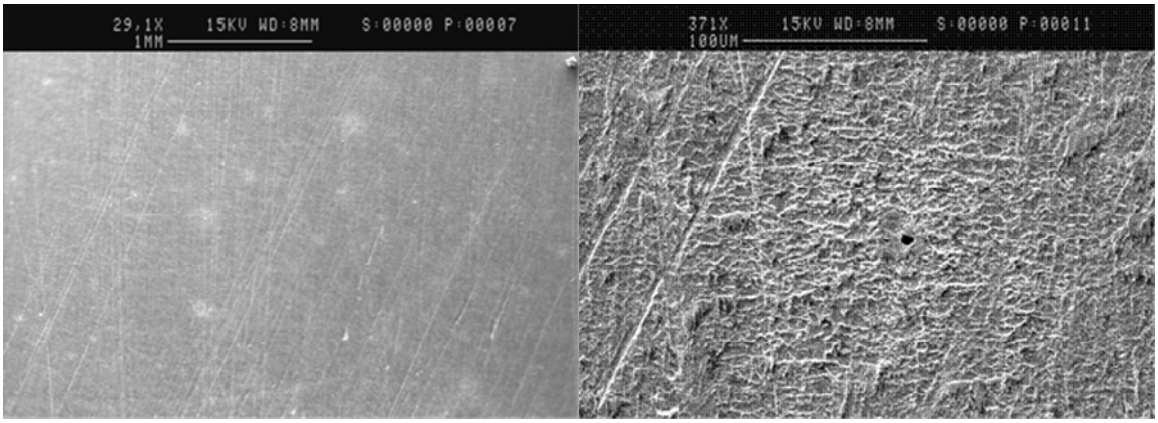

(a) SEM at 29X (b) SEM at 371X

Figure 3-13: 3-month test in untreated GoM seawater at 10ºC (SEM analysis of coupon surface after acid cleaning)

In the six-month test, weight loss also increased with the increase of temperature. However, there was no significant weight loss difference between the samples in the untreated and the sterilized GoM seawater. Figure 3-14 shows that the pH dropped for the 25ºC samples compared to those at 4^{o}C and 10ºC. This was due to the fact that trace amount of O_2 at higher temperature speeds up the oxidation of $Fe(OH)_2$, which tends to make the test medium neutral. Coupon surfaces showed some patterns that resemble

pitting at 4ºC and 10ºC, (see Figure 3-15 ~ Figure 3-17) while the coupons for the control samples (sterilized GoM seawater) and the samples at 25ºC showed no pitting (see Figure 3-18 ~ Figure 3-20).

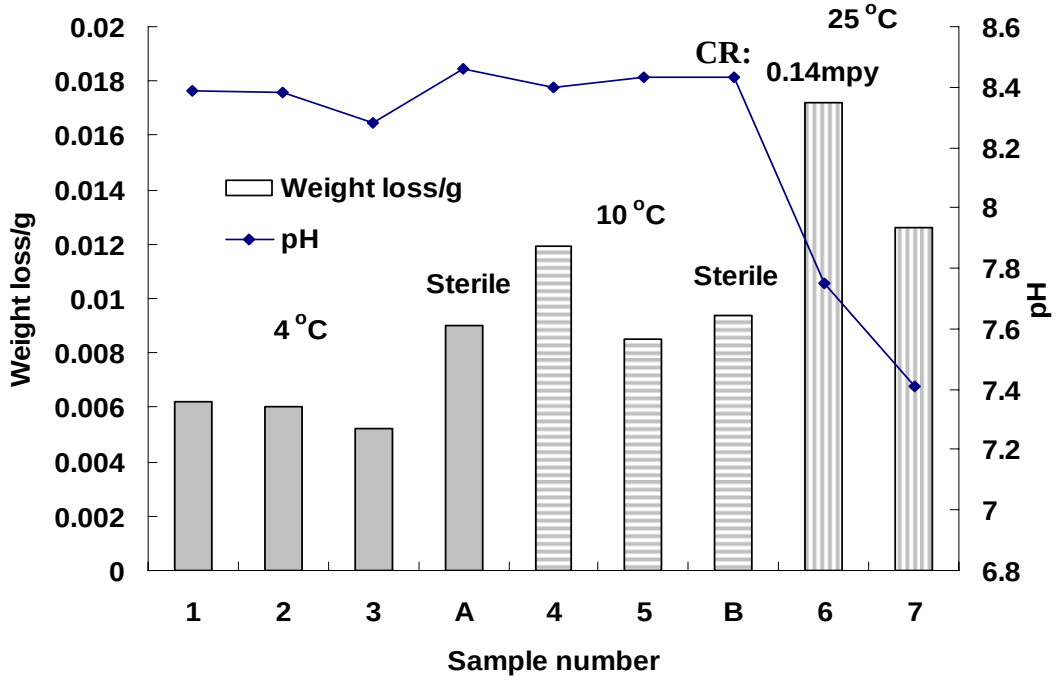

Figure 3-14: X65 coupon weight loss in untreated and sterilized GoM seawater after the 6-month test (#1, #2 and #3 are duplicate samples and #A is a control sample at 4ºC; #4 and #5 are duplicate samples and #B is a control sample at 10ºC; #6 and #7 are duplicate samples at 25ºC)

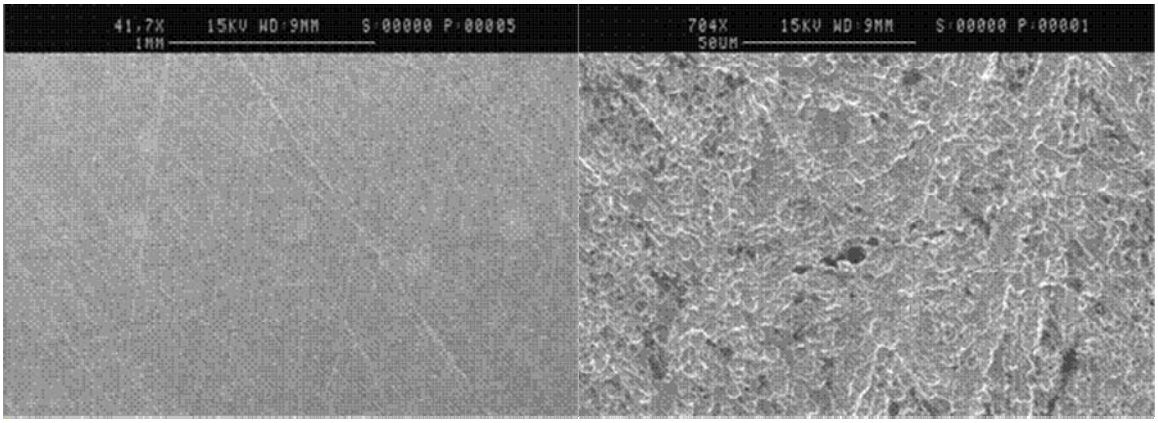

(a) SEM at 42X (b) SEM at 704X

Figure 3-15: 6-month test in untreated GoM seawater at 4ºC (SEM analysis of coupon surface after acid cleaning)

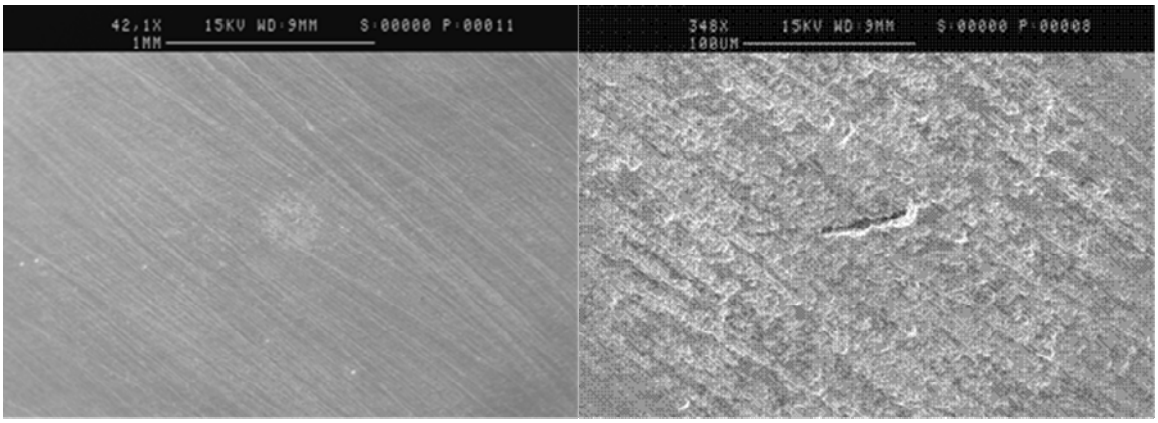

(a) SEM at 42X (b) SEM at 704X

Figure 3-16: 6-month test in untreated GoM seawater at 4ºC (SEM analysis of coupon surface after acid cleaning; duplicate sample as in Figure 3-15)

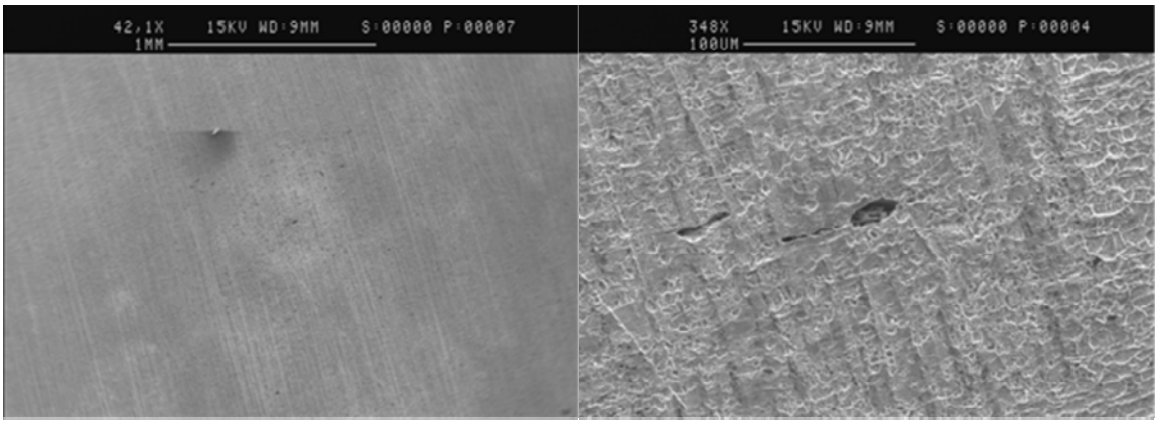

(a) SEM at 42X (b) SEM at 348X

Figure 3-17: 6-month test in untreated GoM seawater at 10ºC (SEM analysis of coupon surface after acid cleaning)

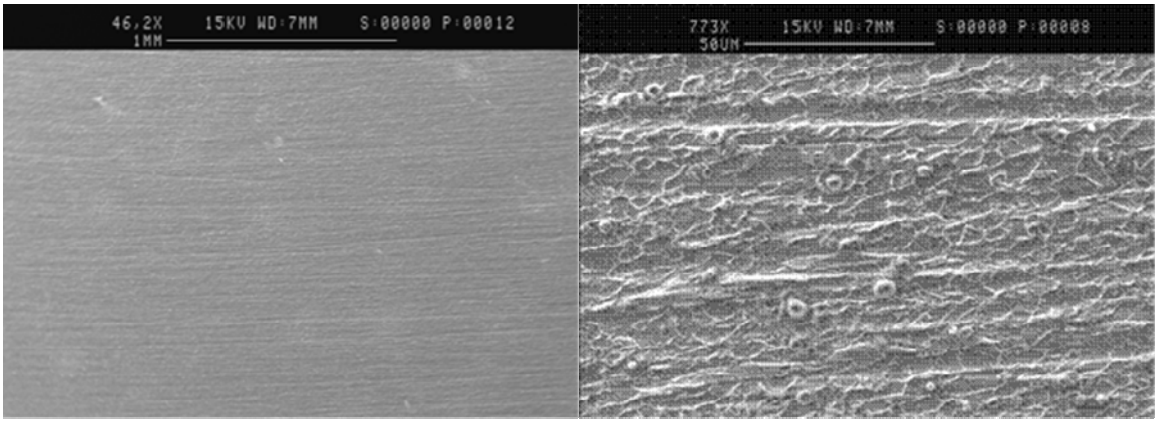

(a) SEM at 46X (b) SEM at 773X

Figure 3-18: 6-month test in sterilized GoM seawater at 4ºC (SEM analysis of coupon surface after acid cleaning)

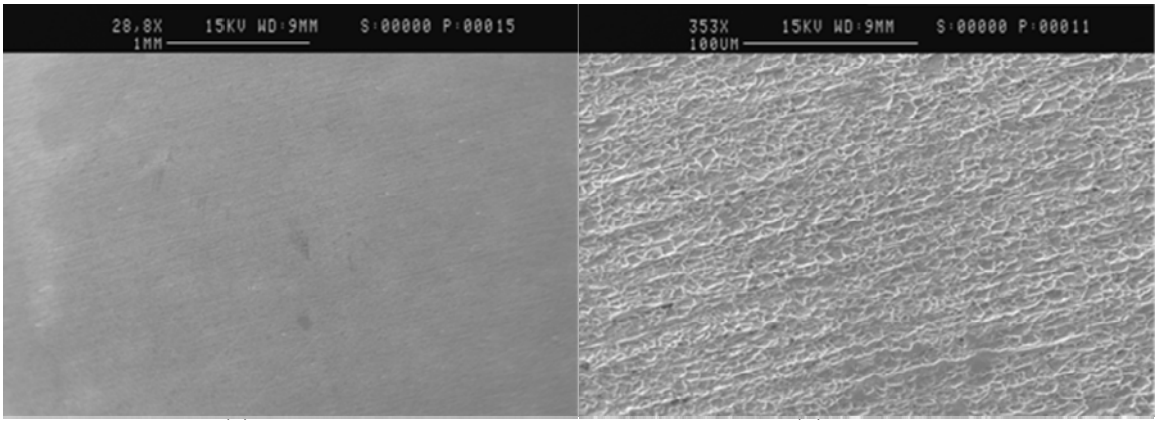

Figure 3-19: 6-month test in untreated GoM seawater at 25ºC (SEM analysis of coupon surface after acid cleaning)

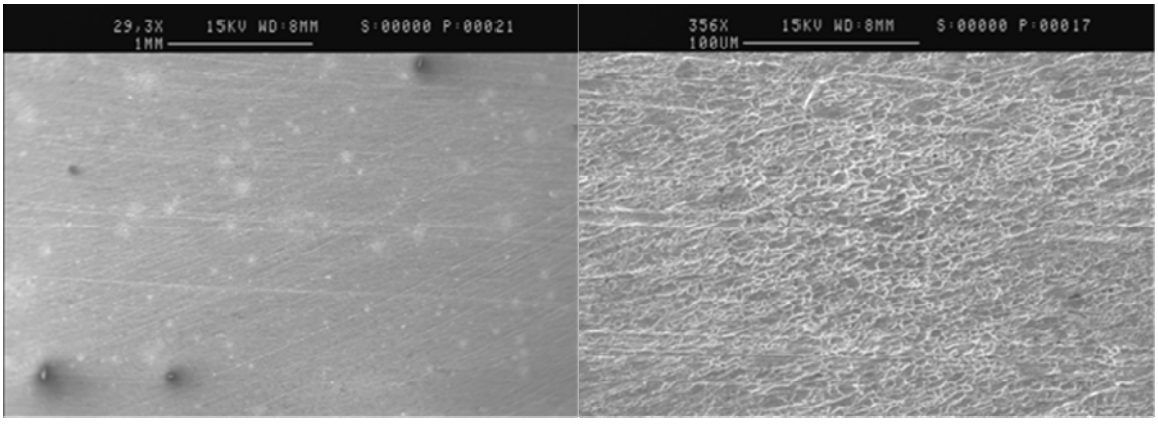

(a) SEM at 29X (b) SEM at 356X

Figure 3-20: 6-month test in untreated GoM seawater at 25ºC (SEM analysis of coupon surface after acid cleaning; a duplicate sample as in Figure-19)

In the eleven-month test, weight loss increased slightly with the increase of temperatures (see Figure 3-21) and the coupon surfaces turned coarser with the temperature increase. This might have resulted from the uniform corrosion (non-MIC related). All the coupon surfaces showed pits, from 4ºC to 25ºC including the sterilized control samples. Considering the pit morphology (long and narrow), dissolved oxygen (albeit low) and existence of aggressive chloride ions, the pitting probably resulted from under-deposit corrosion (Jones, 1996) (see Figure 3-22 ~ Figure 3-26).

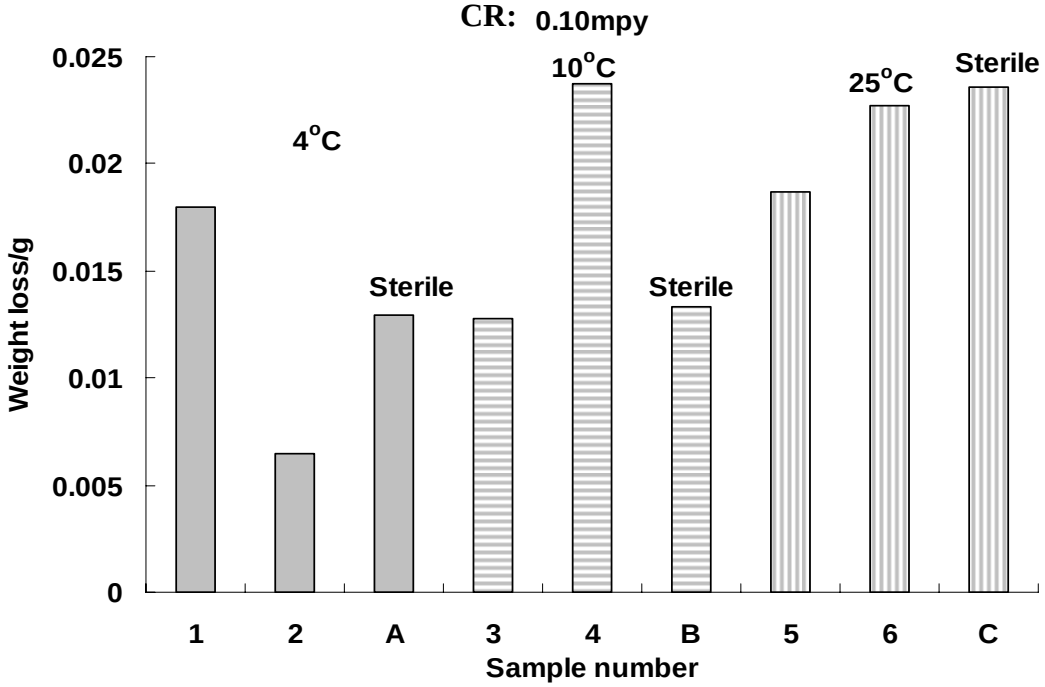

Figure 3-21: X65 coupon weight loss in untreated GoM seawater after the 11-month test (#1 and #2 are duplicate samples and #A is a control sample at 4ºC; #3 and #4 are duplicate samples and #B is a control sample at 10ºC; #5 and #6 are duplicate samples and #C is a control sample at 25ºC)

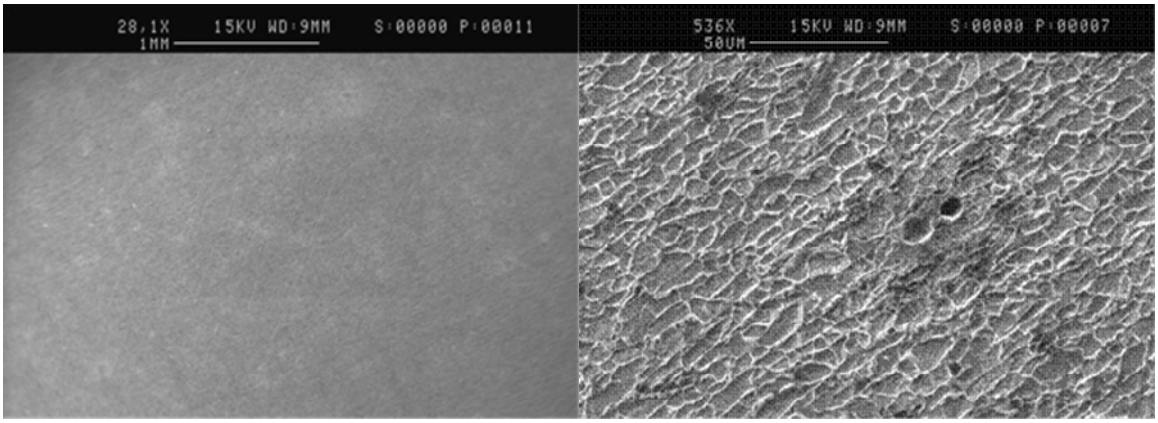

(a) SEM at 28X (b) SEM at 536X

Figure 3-22: 11-month test in untreated GoM seawater at 4ºC (SEM analysis of coupon surface after acid cleaning)

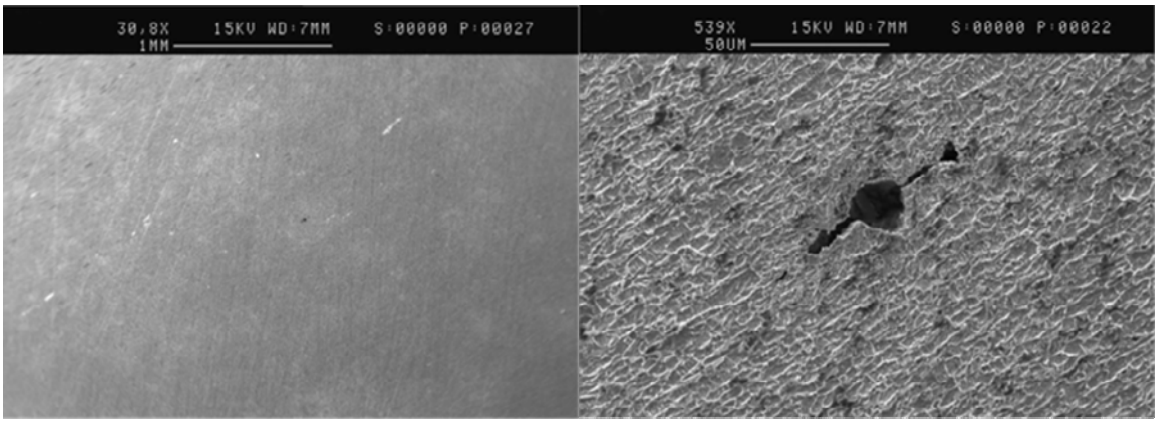

(a) SEM at 31X (b) SEM at 539X

Figure 3-23: 11-month test in sterilized GoM seawater at 4ºC (SEM analysis of coupon surface after acid cleaning)

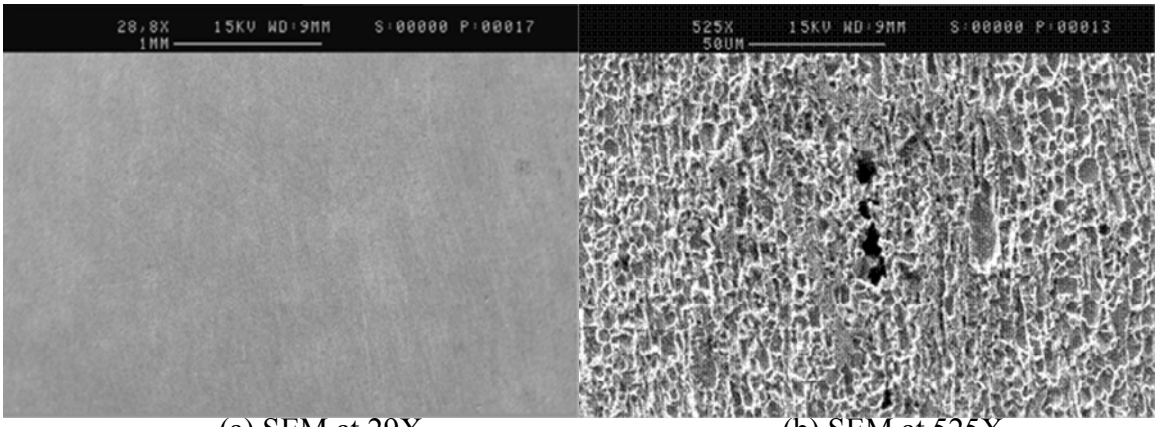

(a) SEM at 29X (b) SEM at 525X

Figure 3-24: 11-month test in untreated GoM seawater at 10ºC (SEM analysis of coupon surface after acid cleaning)

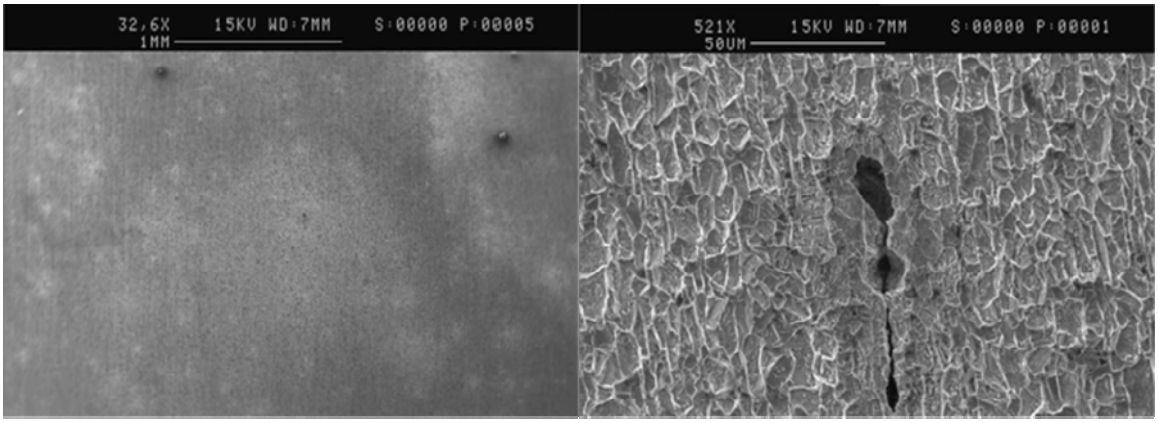

(a) SEM at 33X (b) SEM at 521X

Figure 3-25: 11-month test in sterilized GoM seawater at 10ºC (SEM analysis of coupon surface after acid cleaning)

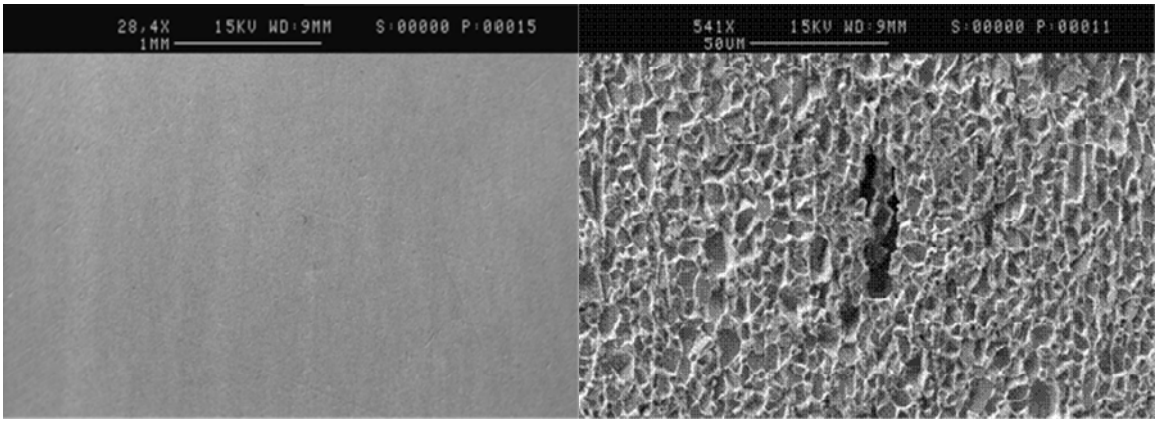

(a) SEM at 28X (b) SEM at 541X

Figure 3-26: 11-month test in sterilized GoM seawater at 25ºC (SEM analysis of coupon surface after acid cleaning)

In comparing the one-month, three-month, six-month and eleven-month results, it is evident that weight loss increased with time (see Figure 3-27). It should be pointed out that all the weight-loss rates were quite small. The data also showed that the corrosion rates due to salt-water corrosion in deoxygenated seawater were quite small. To date, there are no published systematic studies on marine corrosion in deoxygenated seawater.

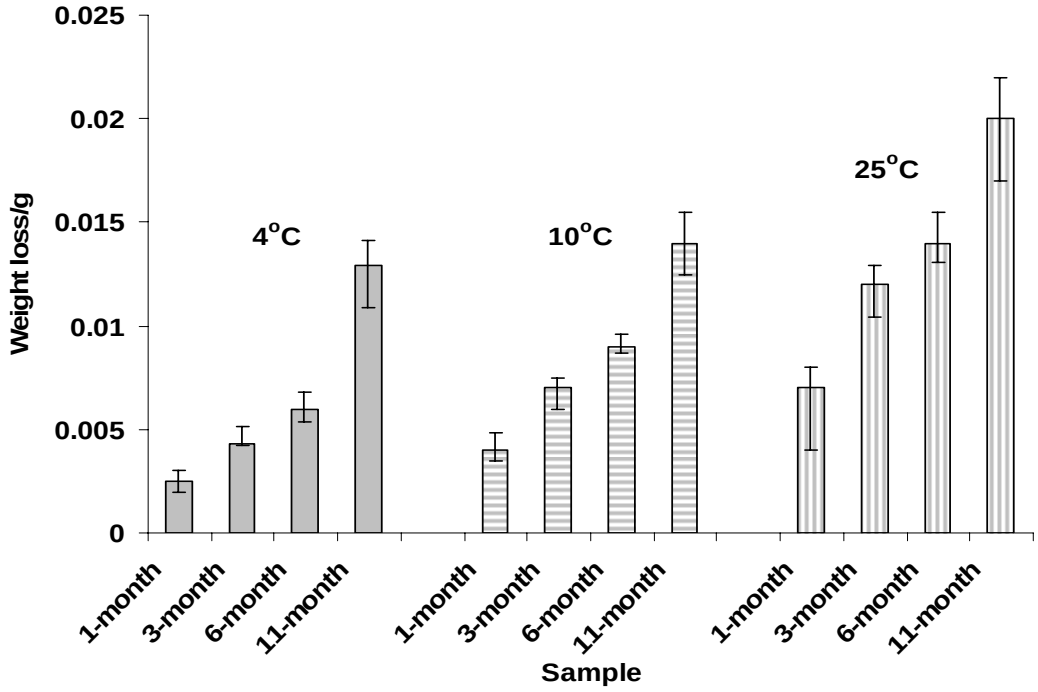

Figure 3-27: X65 coupon weight loss with time in untreated GoM seawater

3.4.2 Tests using GoM seawater treated with glutaraldehyde (G) or THPS (T)

Table 3-4 shows the test matrix of GoM seawater treated with both glutaraldehyde (G) and THPS (T). In the 3-month test, there was little weight loss with the increase of temperature when the biocide glutaraldehyde was added to the water. However, weight loss did increase with the increase of temperature when the biocide THPS was added (see Figure 3-28). Figure 3-28 also shows that at the same temperature, the addition of THPS caused more weight loss than did the addition of glutaraldehyde. No pits were detected on the coupon surfaces in this test (see Figure 3-29 ~ Figure 3-32).

Table 3-4: Test matrix using GoM seawater with biocides under dark conditions

Biocides	Culture medium	Initial concentration (ppm)	Temperature (ºC)	Time (months)
Glutaraldehyde	GoM seawater	50	4, 10, 25	3, 5, 11
THPS	GoM seawater	50	4, 10, 25	3, 5, 11

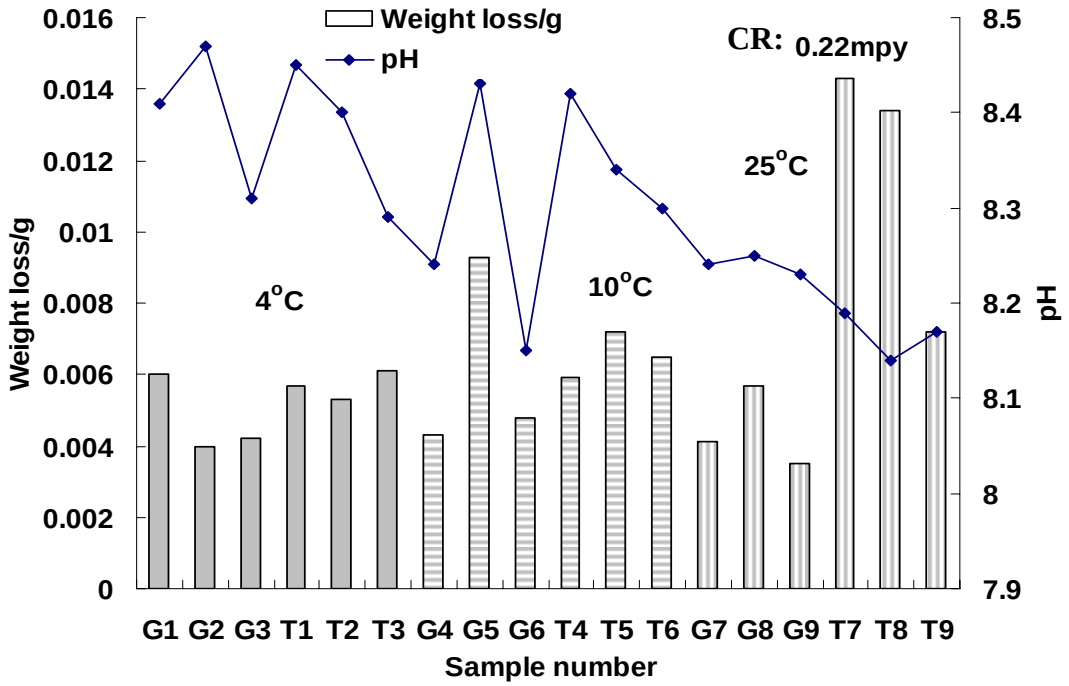

Figure 3-28: X65 coupon weight loss in GoM seawater with biocides after the 3-month test (G-glutaraldehyde, T-THPS. G1, G2 and G3 are duplicate samples and T1, T2 and T3 are duplicate samples at 4ºC; G4, G5 and G6 are duplicate samples and T4, T5 and T6 are duplicate samples at 10ºC; G7, G8 and G9 are duplicate samples and T7, T8 and T9 are duplicate samples at 25ºC)

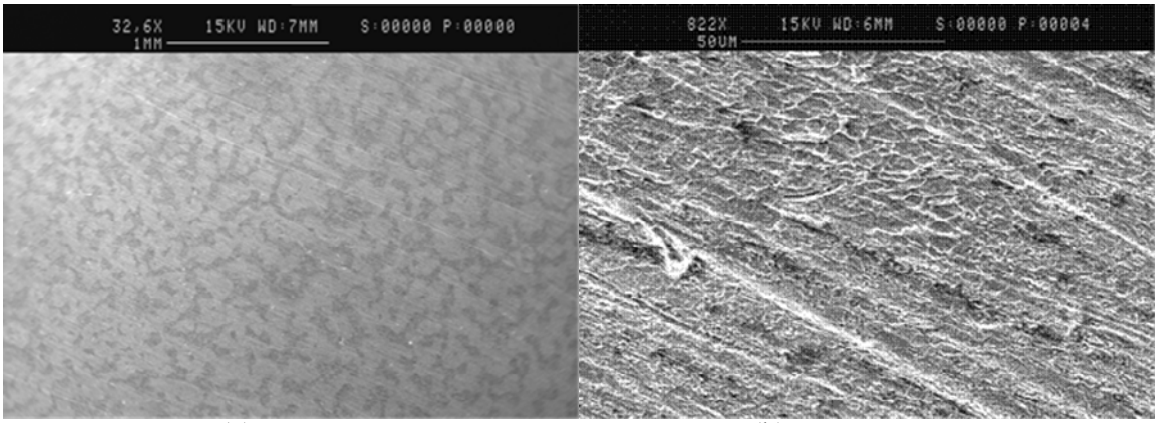

(a) SEM at 33X (b) SEM at 822X

Figure 3-29: 3-month test in GoM seawater with biocide glutaraldehyde at 4ºC (SEM analysis of coupon surface after acid cleaning)

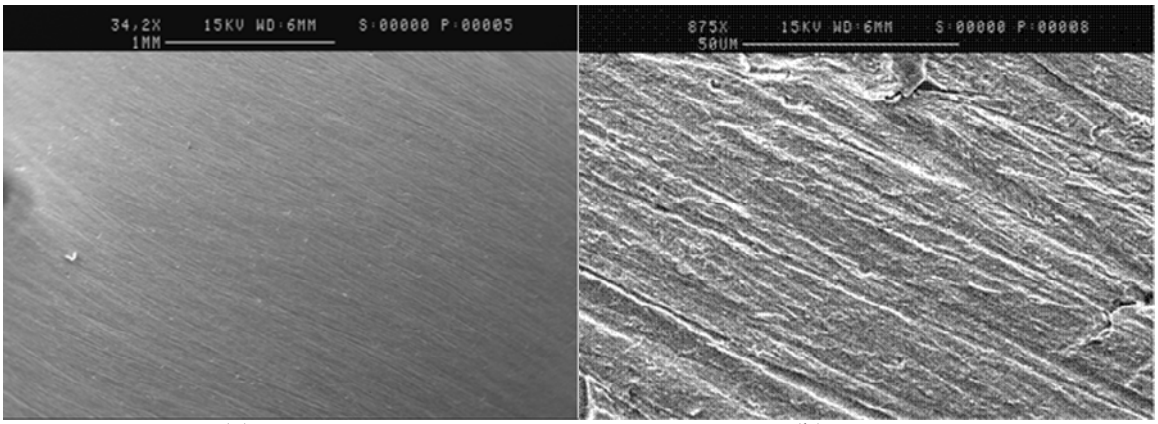

(a) SEM at 34X (b) SEM at 875X

Figure 3-30: 3-month test in GoM seawater with biocide THPS at 4ºC (SEM analysis of coupon surface after acid cleaning)

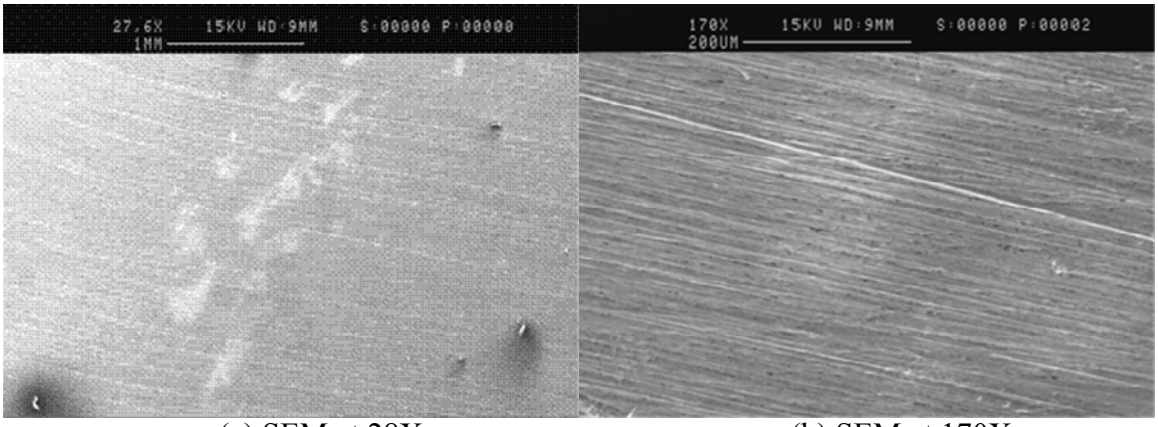

(a) SEM at 28X (b) SEM at 170X

Figure 3-31: 3-month test in GoM seawater with biocide glutaraldehyde at 25ºC (SEM analysis of coupon surface after acid cleaning)

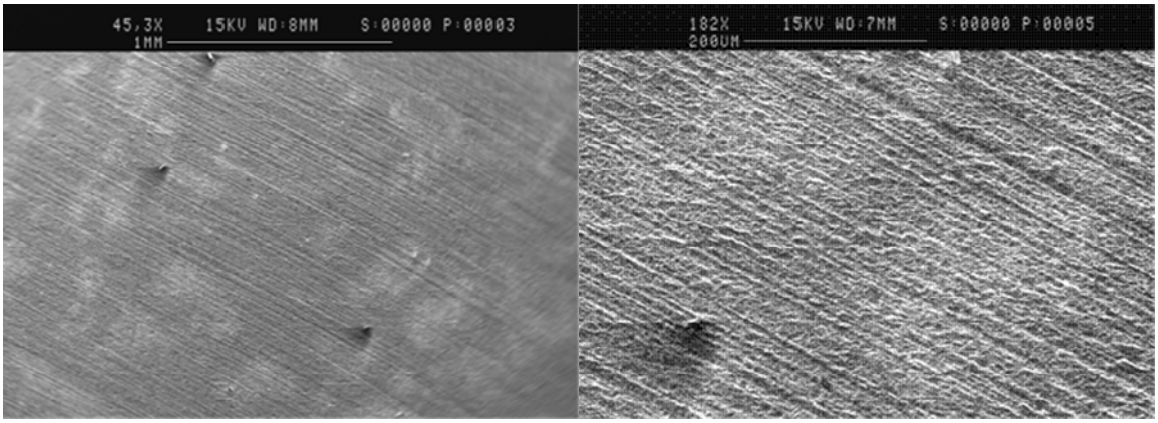

(a) SEM at 45X (b) SEM at 182X

Figure 3-32: 3-month test in GoM seawater with biocide THPS at 25ºC (SEM analysis of coupon surface after acid cleaning)

In the five-month test, there was almost no weight loss increase from 4^{o}C to 10ºC for either biocide. There was only a slight increase at 25ºC (see Figure 3-33). However, there were densely populated tiny pits (invisible to the naked eye) on coupons at the three temperatures with both the THPS and glutaraldehyde treatment (see Figure 3-34 ~ Figure 3-39). Such pitting patterns were not present when no biocide was used. This was likely due to chemical attacks from the biocide or a synergistic effect between the biocide and seawater salts.

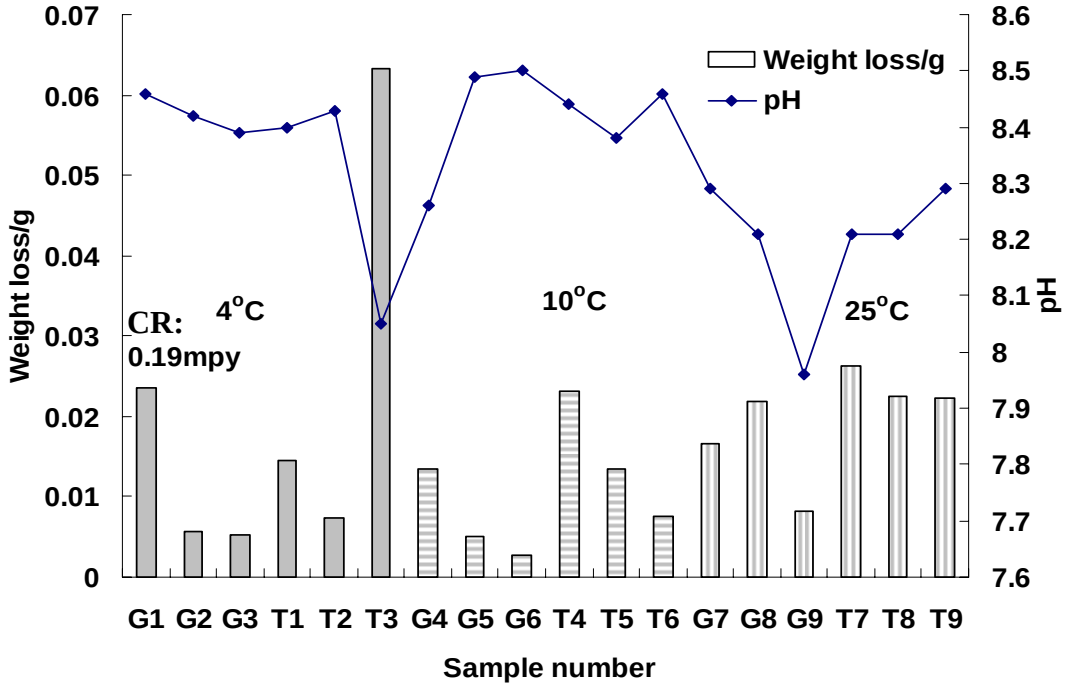

Figure 3-33: X65 coupon weight loss in GoM seawater with biocides after the 5-month test (G-glutaraldehyde, T-THPS. G1, G2 and G3 are duplicate samples and T1, T2 and T3 are duplicate samples at 4ºC; G4, G5 and G6 are duplicate samples and T4, T5 and T6 are duplicate samples at 10ºC; G7, G8 and G9 are duplicate samples and T7, T8 and T9 are duplicate samples at 25ºC. T3 appeared to be O_2 contamination)

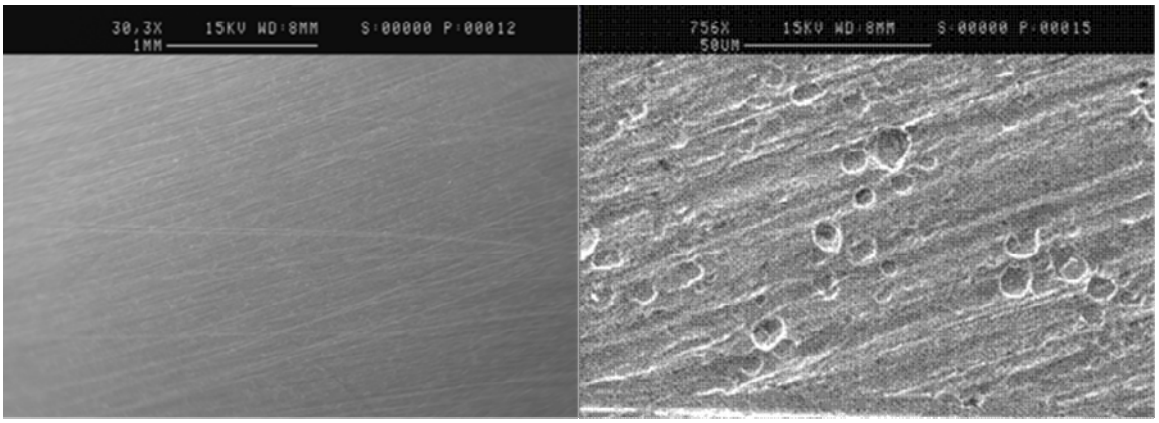

(a) SEM at 30X (b) SEM at 756X

Figure 3-34: 5-month test in GoM seawater with biocide glutaraldehyde at 4ºC (SEM analysis of coupon surface after acid cleaning)

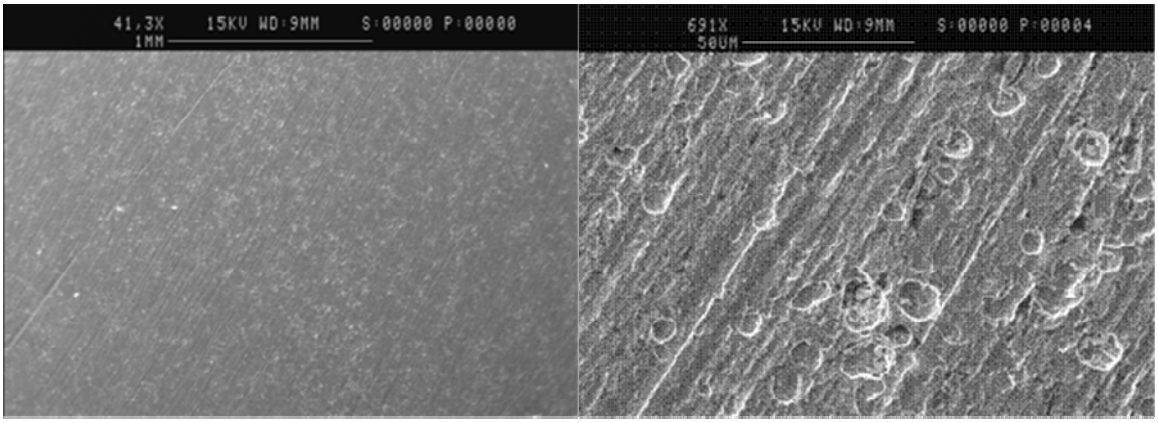

(a) SEM at 41X (b) SEM at 691X

Figure 3-35: 5-month test in GoM seawater with biocide THPS at 4ºC (SEM analysis of coupon surface after acid cleaning)

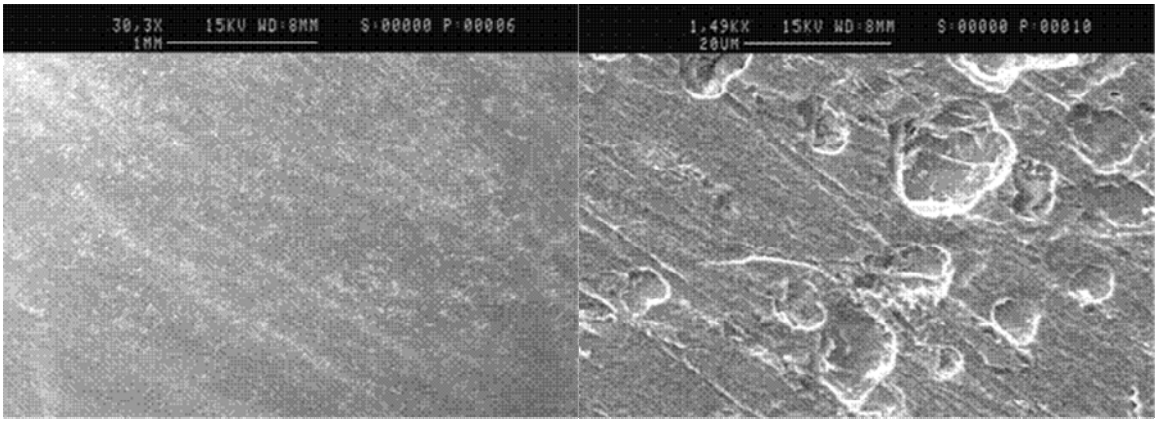

(a) SEM at 30X (b) SEM at 1490X

Figure 3-36: 5-month test in GoM seawater with biocide glutaraldehyde at 10ºC (SEM analysis of coupon surface after acid cleaning)

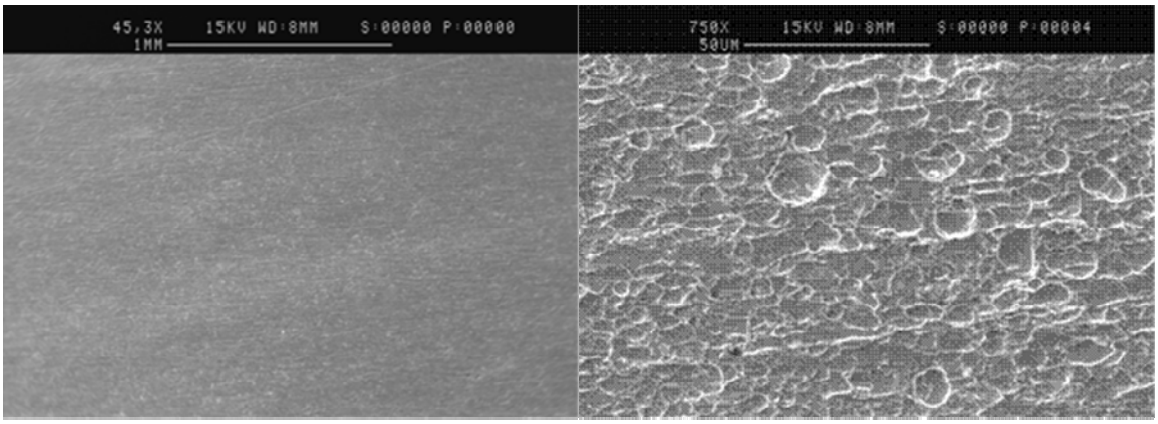

(a) SEM at 45X (b) SEM at 750X

Figure 3-37: 5-month test in GoM seawater with biocide THPS at 10ºC (SEM analysis of coupon surface after acid cleaning)

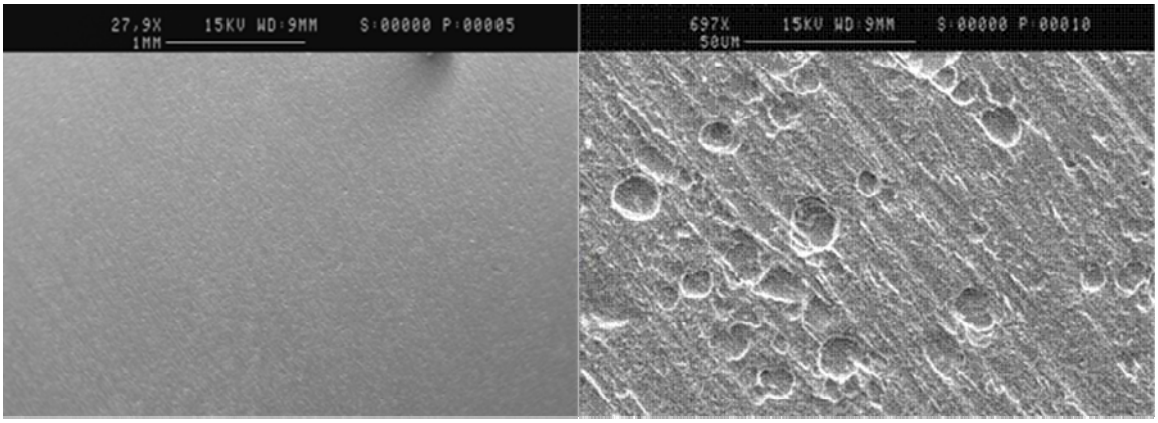

(a) SEM at 28X (b) SEM at 697X

Figure 3-38: 5-month test in GoM seawater with biocide glutaraldehyde at 25ºC (SEM analysis of coupon surface after acid cleaning)

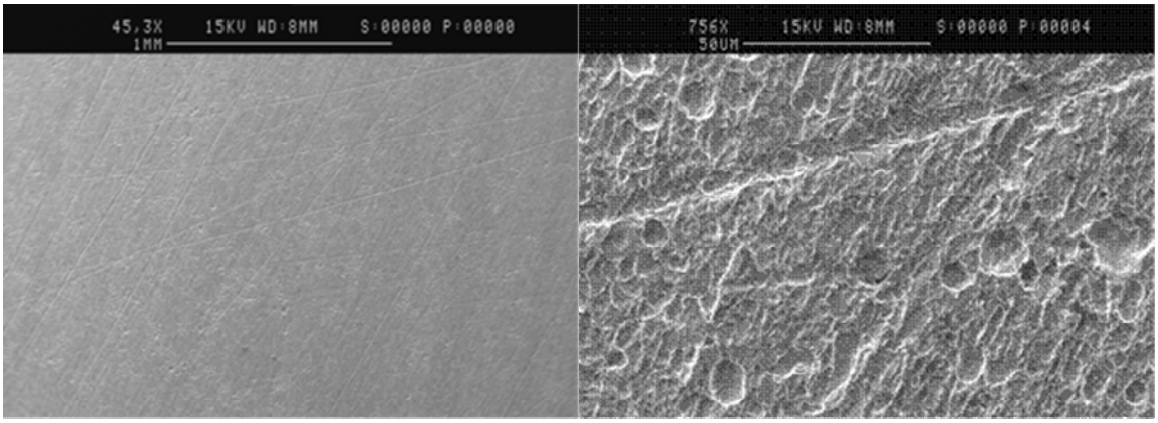

(a) SEM at 45X (b) SEM at 756X

Figure 3-39: 5-month test in GoM seawater with biocide THPS at 25ºC (SEM analysis of coupon surface after acid cleaning)

In the eleven-month test, weight loss vs. temperature showed the same trend as with the five-month test samples (see Figure 3-40). However, compared to the five-month test, there were fewer pits on the coupons at the three temperatures with both THPS and glutaraldehyde treatment (see Figure 3-41~ Figure 3-46). This may have been due to the merging of smaller pits resulting in a more uniform corrosion. This merging is supported by the higher weight loss in the eleven-month test (see Figure 3-47 and Figure 3-48).

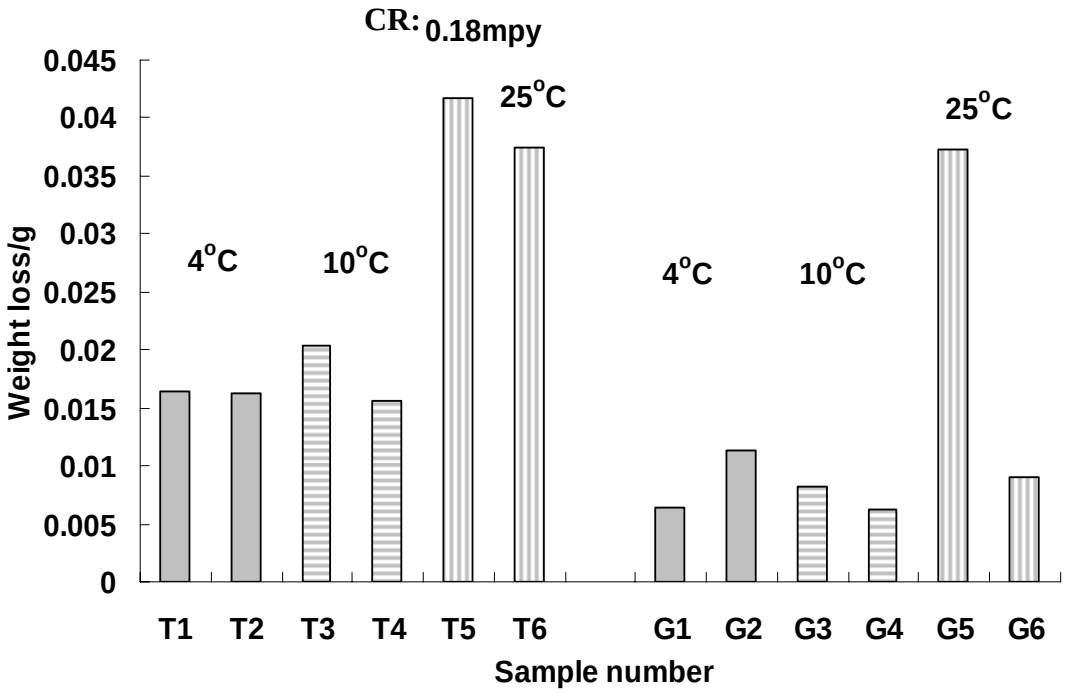

Figure 3-40: X65 coupon weight loss in GoM seawater with biocides after the 11-month test (G-glutaraldehyde, T-THPS. T1 and T2 are duplicate samples and G1 and G2 are duplicate samples at 4ºC; T3 and T4 are duplicate samples and G3 and G4 are duplicate samples at 10ºC; T5 and T6 are duplicate samples and G5 and G6 are duplicate samples at 25ºC)

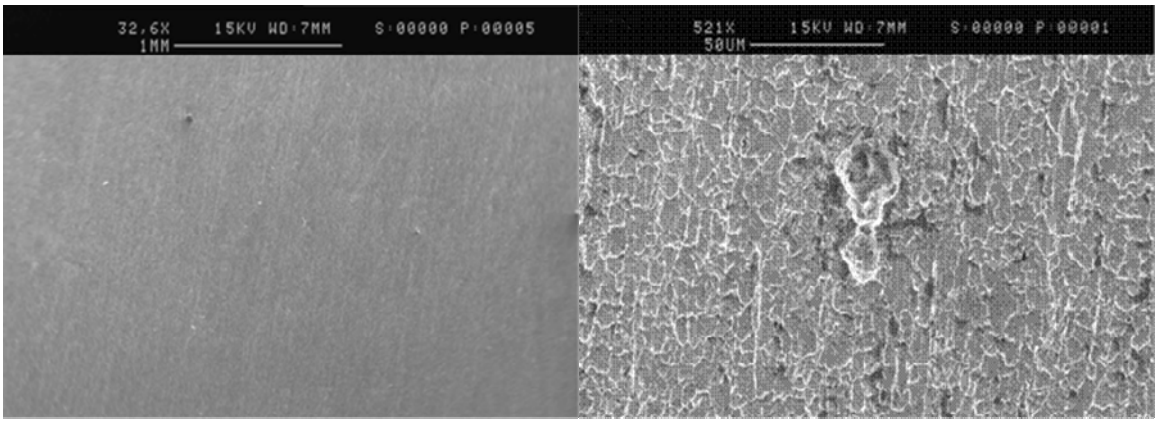

(a) SEM at 33X (b) SEM at 521X

Figure 3-41: 11-month test in GoM seawater with biocide THPS at 4ºC (SEM analysis of coupon surface after acid cleaning)

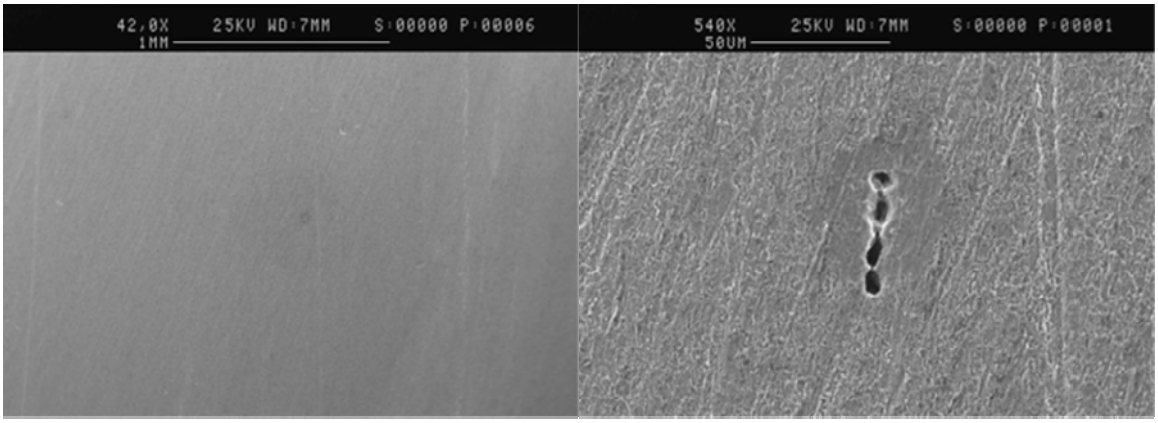

(a) SEM at 42X (b) SEM at 540X

Figure 3-42: 11-month test in GoM seawater with biocide glutaraldehyde at 4ºC (SEM analysis of coupon surface after acid cleaning)

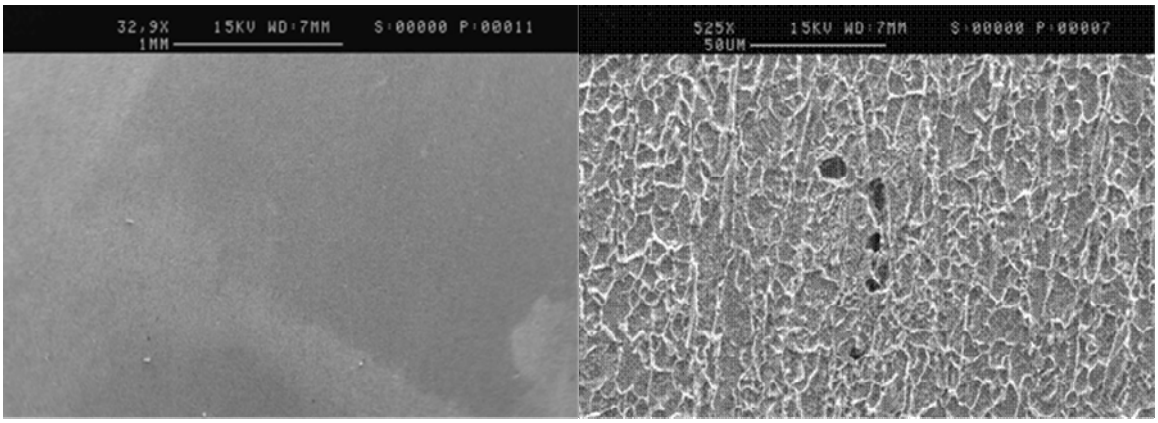

(a) SEM at 33X (b) SEM at 525X

Figure 3-43: 11-month test in GoM seawater with biocide THPS at 10ºC (SEM analysis of coupon surface after acid cleaning)

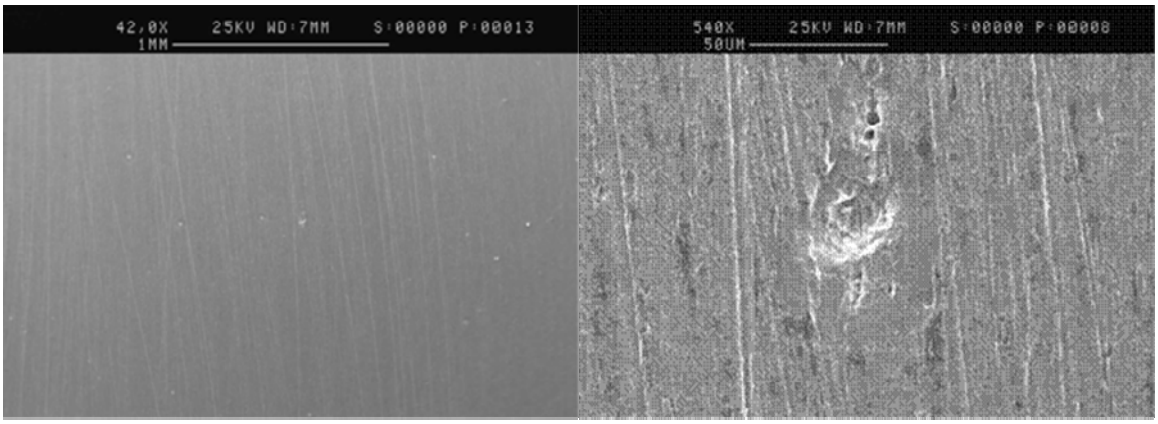

(a) SEM at 42X (b) SEM at 540X

Figure 3-44: 11-month test in GoM seawater with biocide glutaraldehyde at 10ºC (SEM analysis of coupon surface after acid cleaning)

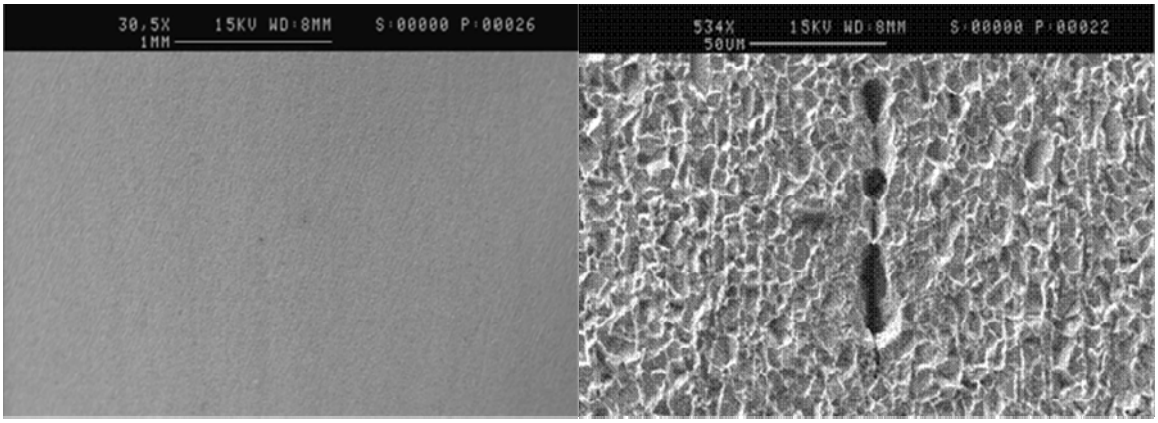

(a) SEM at 31X (b) SEM at 534X

Figure 3-45: 11-month test in GoM seawater with biocide THPS at 25ºC (SEM analysis of coupon surface after acid cleaning)

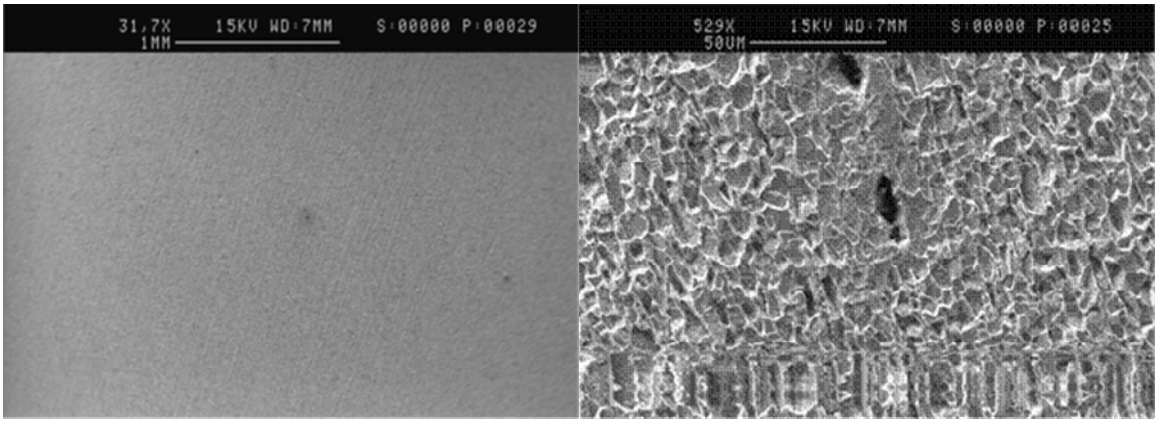

(a) SEM at 32X (b) SEM at 529X

Figure 3-46: 11-month test in GoM seawater with biocide glutaraldehyde at 25ºC (SEM analysis of coupon surface after acid cleaning)

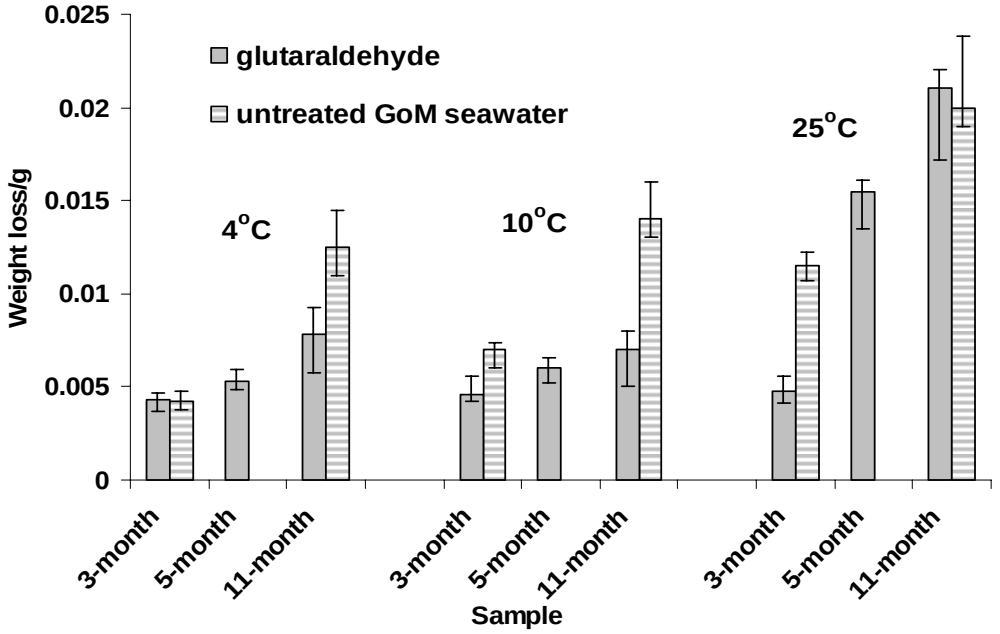

Figure 3-47: Weight loss with time under different temperatures in GoM seawater with and without glutaraldehyde

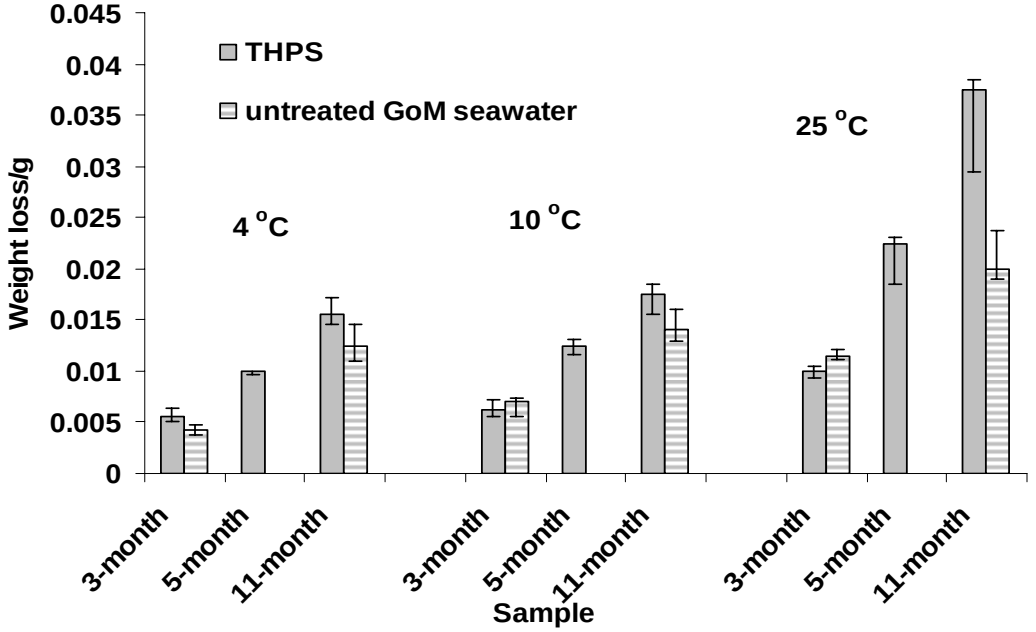

Figure 3-48: Weight loss with time under different temperatures in GoM seawater with and without THPS

Unlike the 3-month and five-month test results, the pit morphology in treated water was longer and narrower, similar to those shown in the eleven-month test using untreated GoM seawater. Compared to the untreated GoM seawater test results, THPS use showed increased weight loss (refer to Figure 3-48), while glutaraldehyde use showed slightly reduced weight loss (see Figure 3-47). While THPS resulted in more weight loss than glutaraldehyde under the same test conditions (see Figure 3-49 ~ Figure 3-51), it should be pointed out that all the weight losses in this project are quite small (all below 0.23 mpy).

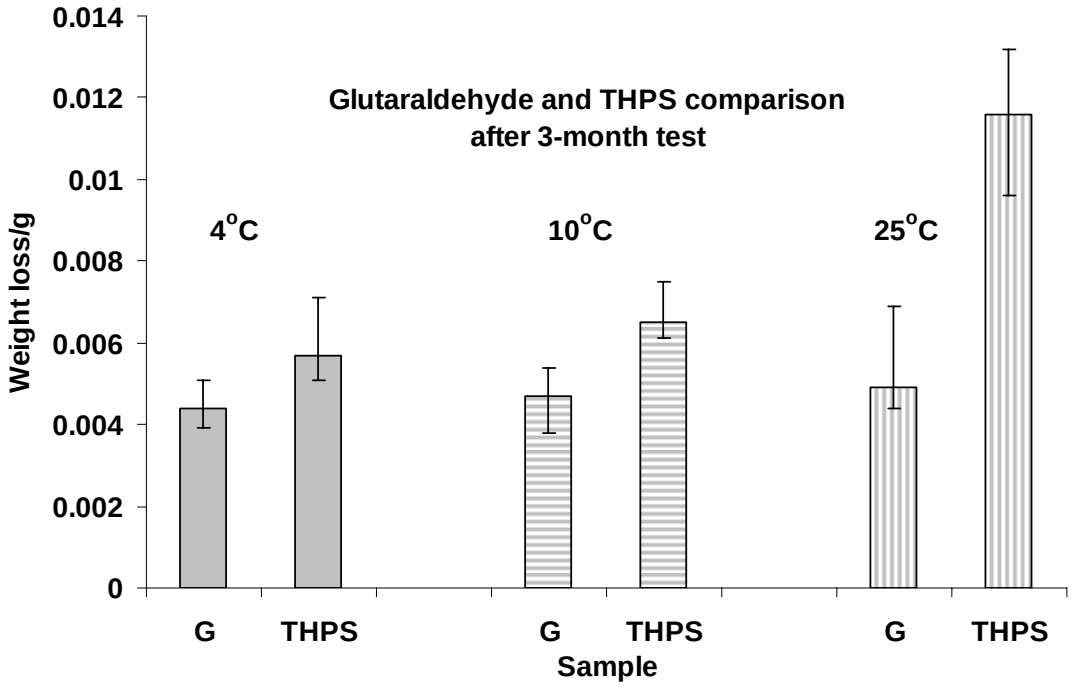

Figure 3-49: Weight loss comparison between glutaraldehyde (G) and THPS use in GoM seawater after the 3-month test

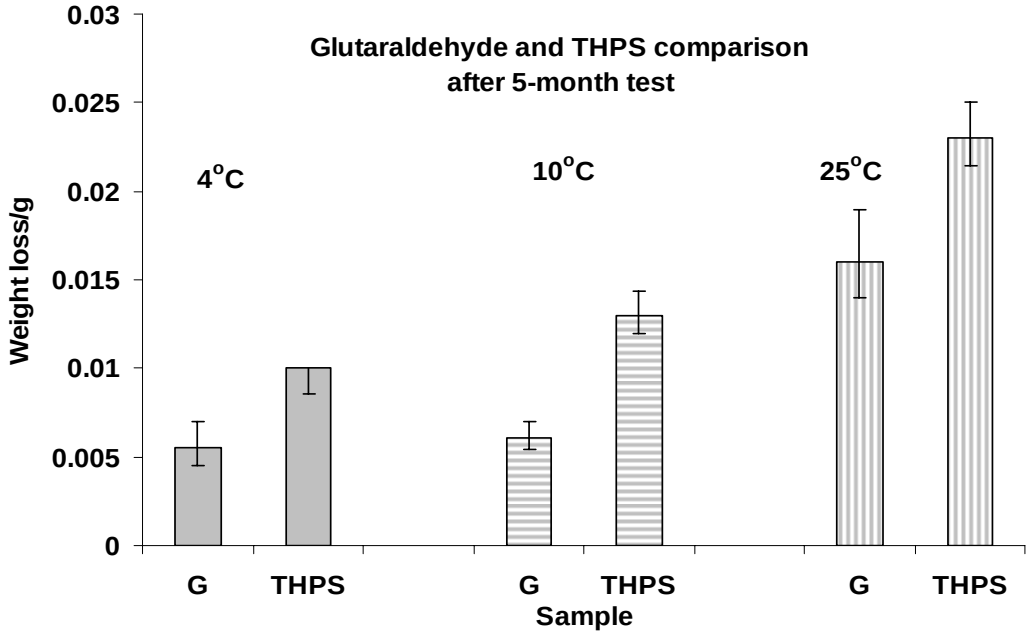

Figure 3-50: Weight loss comparison between glutaraldehyde (G) and THPS use in GoM seawater after the 5-month test

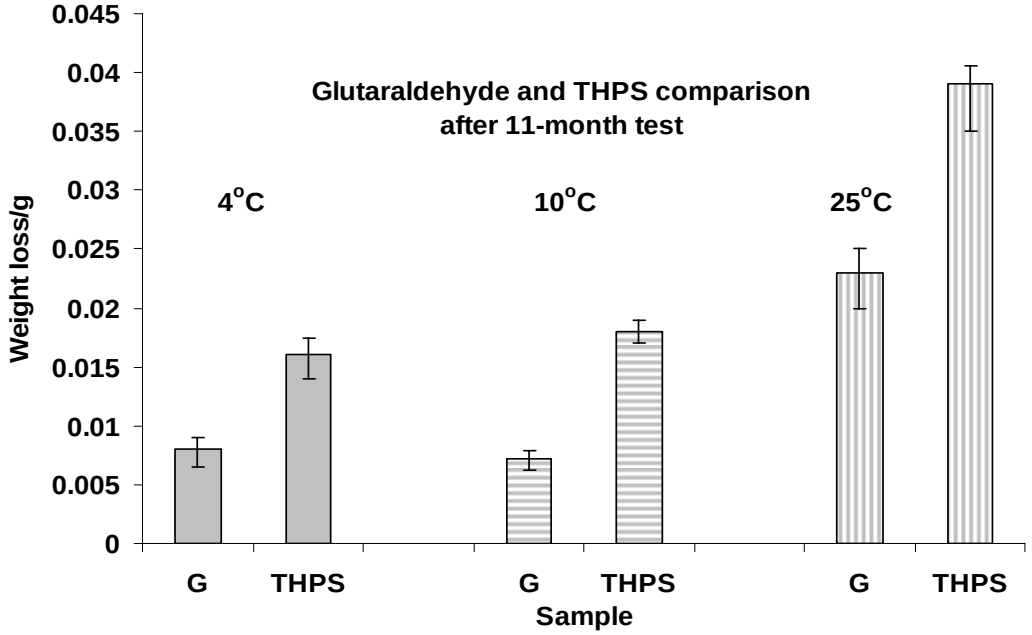

Figure 3-51: Weight loss comparison between glutaraldehyde (G) and THPS use in GoM seawater after the 11-month test

3.4.3 Tests using GoM seawater spiked with sulfate-reducing bacteria

Tests were also performed to simulate hydrotesting cases using water spiked with SRB. Table 3-5 shows the test matrix.

Table 3-5: Test matrix using GoM seawater spiked with marine SRB stain

Test conditions	
Culture medium	GoM seawater
SRB strain	*Desulfovibrio desulfuricans subsp. aestuarii* - ATCC 14563 (marine SRB)
Initial bacteria concentration	10^6 cells/ml
Test temperature (ºC)	17, 37
Test time	2 weeks

Individual SRB cells as well as colonies were detected using SEM on the coupon surfaces (see Figure 3-52 ~ Figure 3-55). The individual cells may have been planktonic cells deposited on the surfaces or sessile cells that attached to the surfaces, but had not yet formed colonies. EDS images also indicated elements on the coupon surfaces (see Figure 3-53 and Figure 3-55).

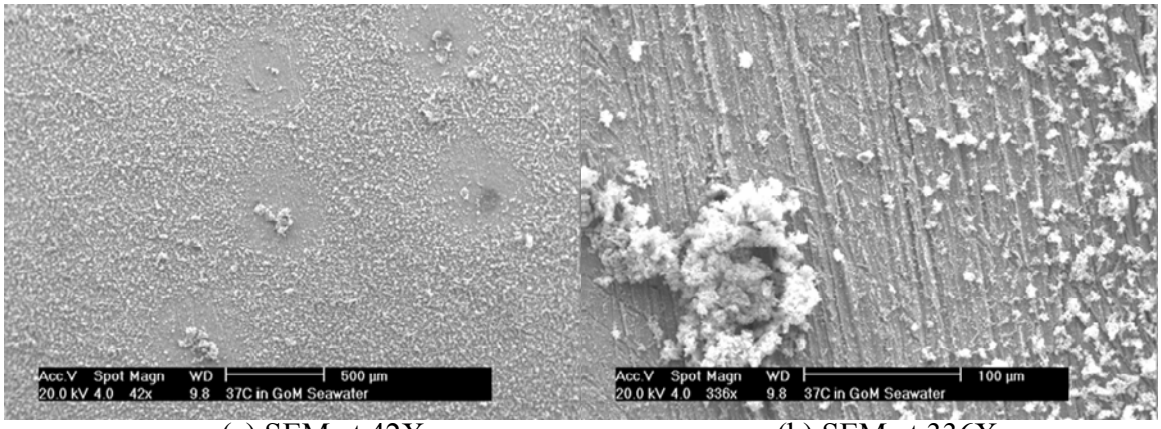

(a) SEM at 42X (b) SEM at 336X

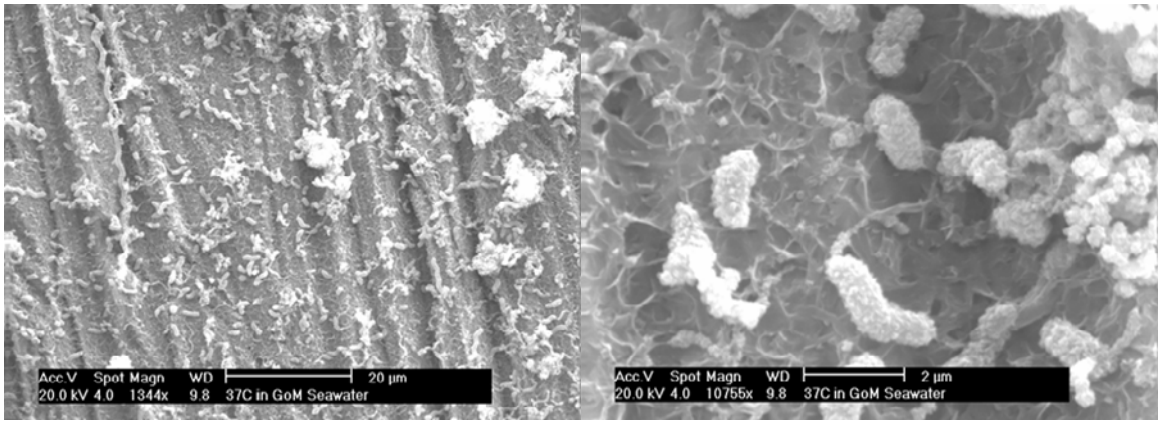

(c) SEM at 1334X (d) SEM at 10755X

Figure 3-52: 2-week test in GoM seawater spiked with SRB at 37ºC (SEM analysis of coupon surface before acid cleaning shows individual bacteria on the coupon surface)

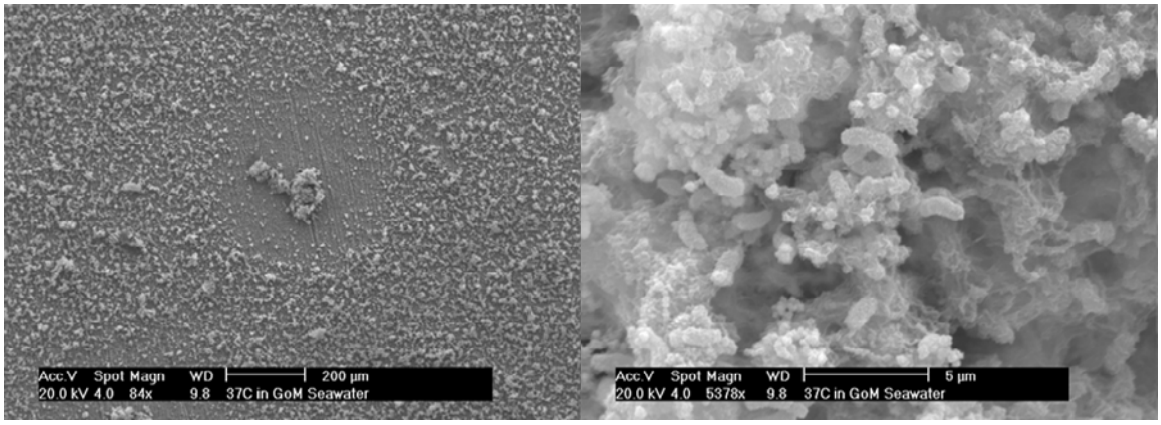

(a) SEM at 84X (b) SEM at 5378X

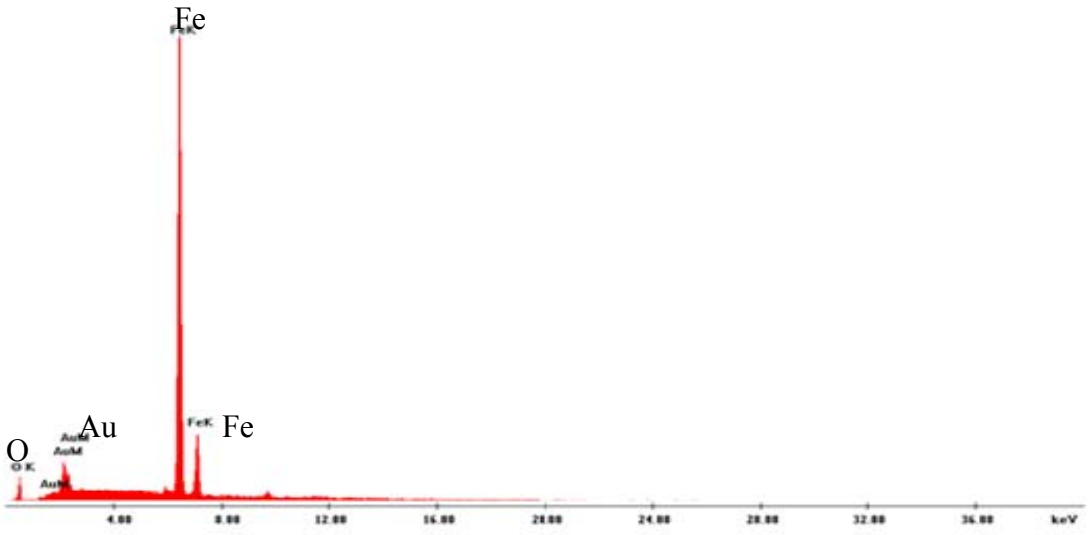

(c) Composition on the coupon surface

Figure 3-53: 2-week test in GoM seawater spiked with SRB at 37ºC (SEM and EDS analysis of coupon surface before acid cleaning show colonies of bacteria on the coupon surface)

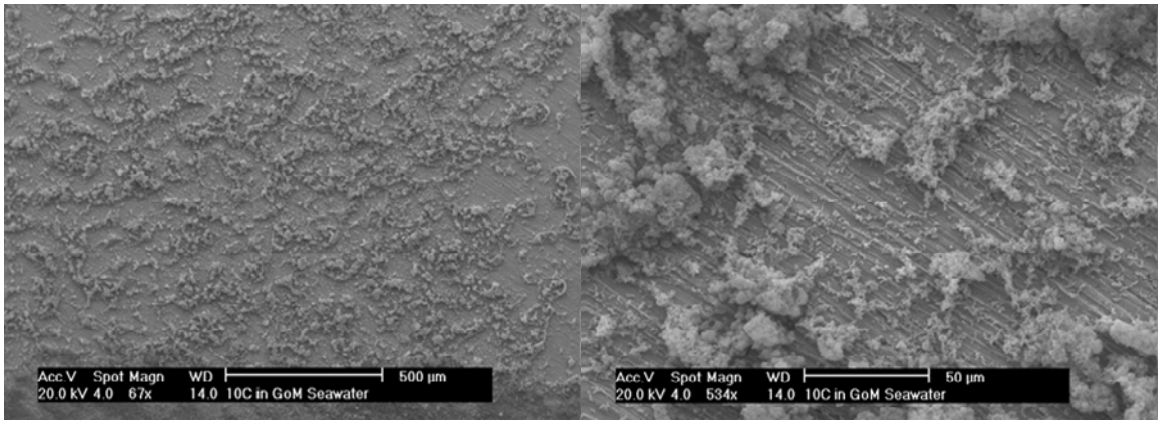

(a) SEM at 67X (b) SEM at 534X

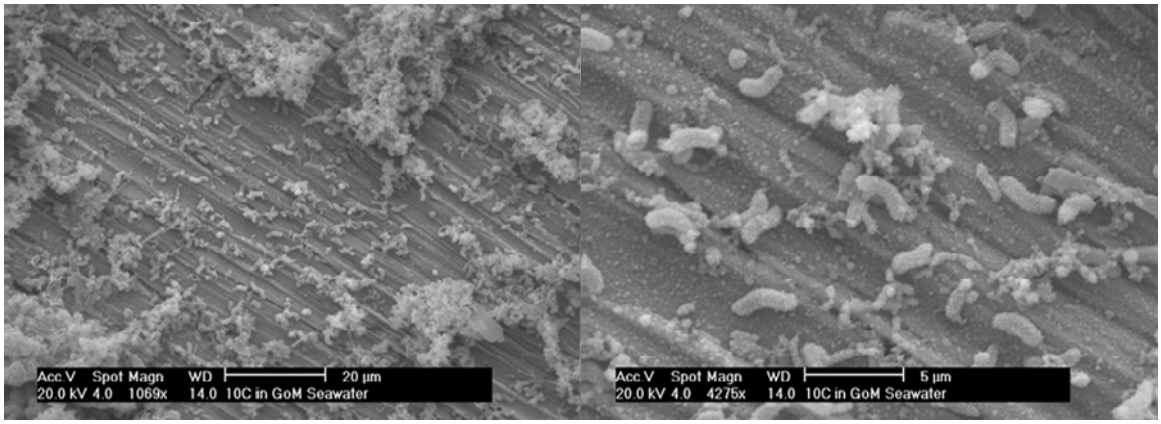

(c) SEM at 1069X (d) SEM at 4275X

Figure 3-54: 2 week test in GoM seawater spiked with SRB at 17ºC (SEM analysis of coupon surface before acid cleaning shows individual bacteria on the coupon surface)

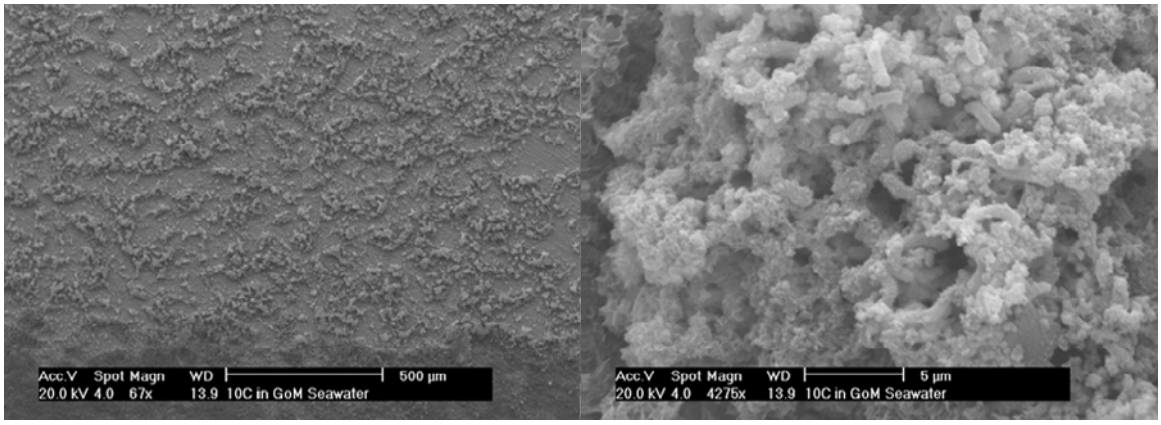

(a) SEM at 67X (b) SEM at 4275X

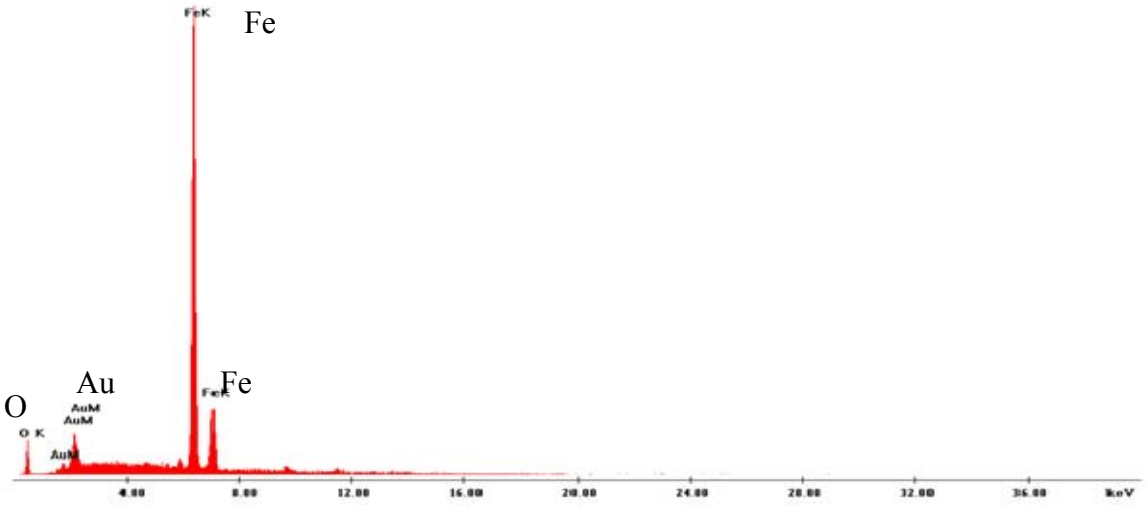

(c) Composition on the coupon surface

Figure 3-55: 2-week test in GoM seawater spiked with SRB at 17ºC (SEM and EDS analysis of coupon surface before acid cleaning show colonies of bacteria on the coupon surface)

From the EDS spectra, elemental S was evident at the black dot location only under 37 ºC (see Figure 3-56 and Figure 3-57). Figure 3-56 indicates that all black dots were in the center of specific areas surrounded by granules; however, in the other similar areas (see Figure 3-53 (a)), bacteria colonies rather than black dots were found. The colonies might have covered these black dot areas that were accidentally removed during

coupon handling. The circular-shaped relatively clean areas around the colonies indicated the possibility that the colonies may have changed the local environment, thus preventing mineral deposits from forming. Figure 3-58 shows some small pits on the coupon surface after removal of the biofilm. The morphology of these pits is consistent with what was typically found in other tests when SRB biofilms were grown on coupons in vials. These pits are quite different from the pits seen earlier when SRB were not involved.

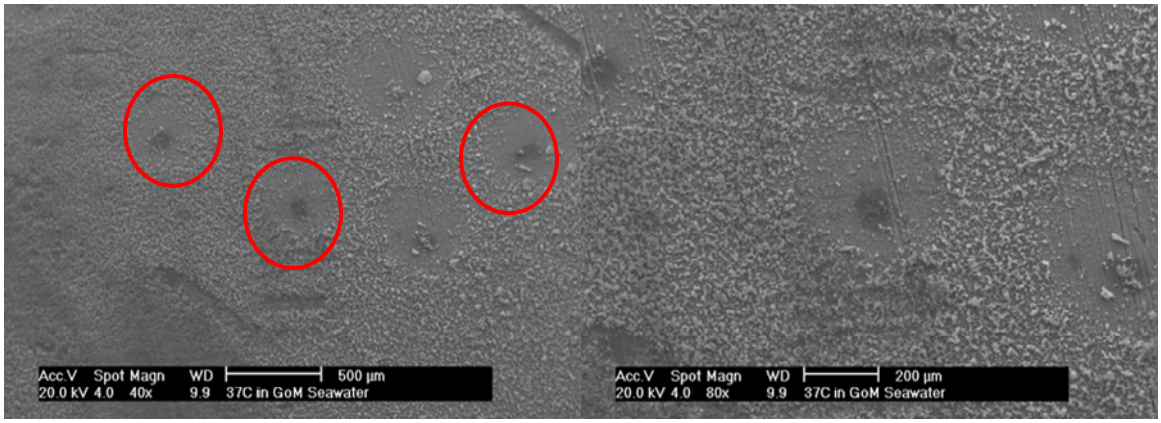

(a) SEM at 40X (b) SEM at 80X

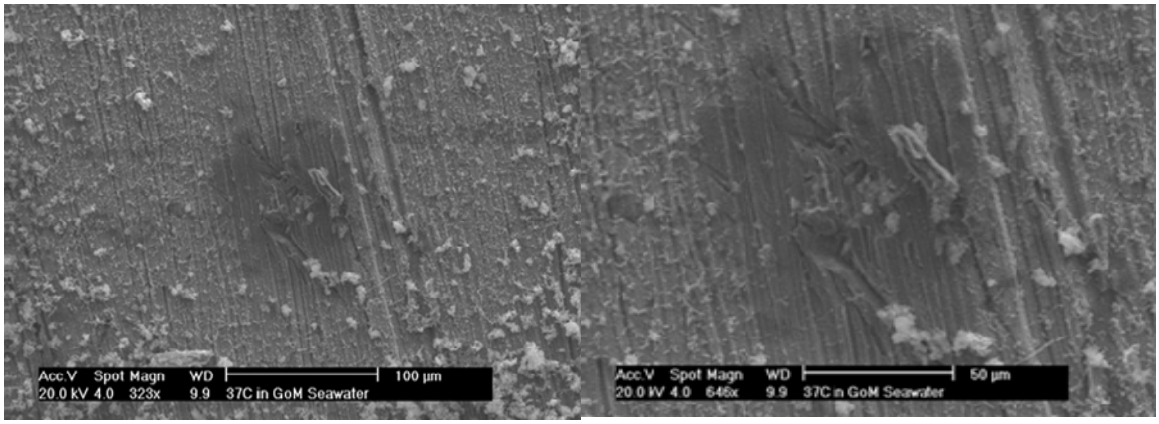

(c) SEM at 323X (d) SEM at 646X

Figure 3-56: 2-week test in GoM seawater spiked with SRB at 37ºC (SEM analysis of coupon surface before acid cleaning; Black dots were evident on the coupon surface)

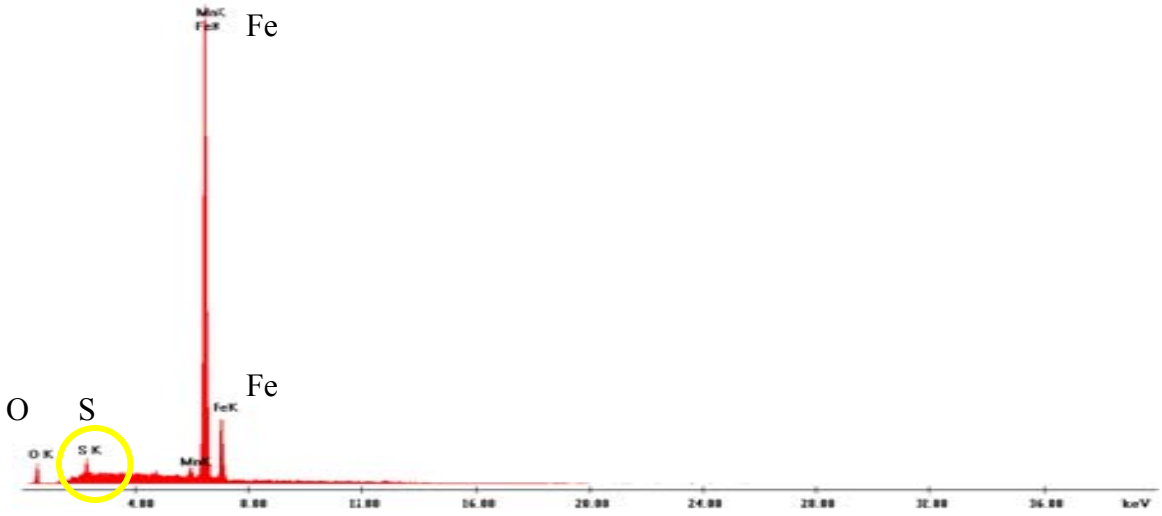

Figure 3-57: Composition on the coupon surface (EDS analysis of black dots shown in Figure 3-56; 2-week test in GoM seawater spiked with SRB at 37ºC.)

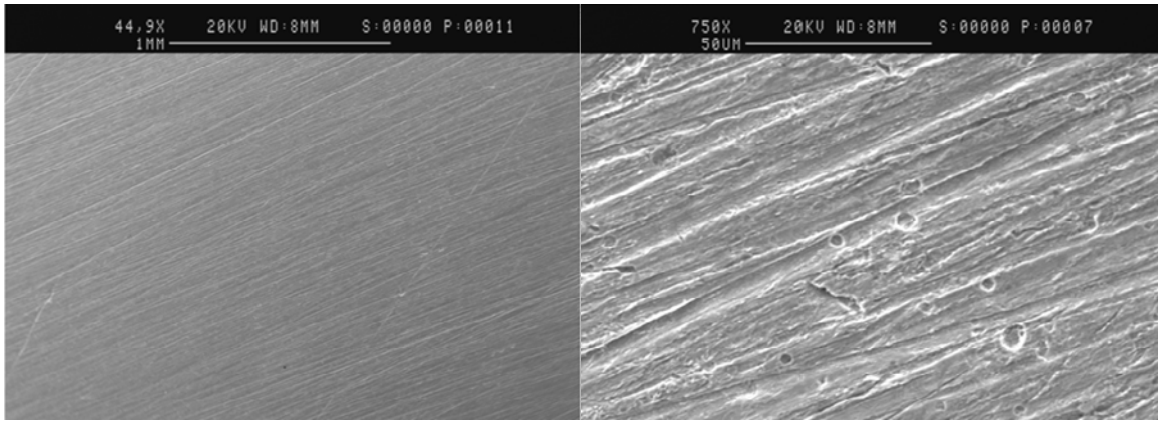

(a) SEM at 45X (b) SEM at 750X

Figure 3-58: 2-week test in GoM seawater spiked with SRB at 37ºC (SEM analysis of coupon surface after acid cleaning)

3.5 Conclusions:

- With the supplied untreated GoM seawater, no MIC was observed in any tests up to 11 months in duration at temperatures up to 37°C. The supplied GoM seawater contained a very low level of SRB that was undetectable using quantitative PCR

capable of detecting 1 to 3 SRB cells per liter. There was a very low total organic carbon content (4.6 ppm). Organic carbons are necessary for SRB growth.

- No biofilm was found in the tests using untreated GoM seawater. Corrosion in deoxygenated (less than 40 ppb) GoM seawater without MIC was negligible (< 0.6 mpy). However, long narrow pits (with length up to 70 μm, width 15 μm depth 13 μm) were evident after 11 months. Weight loss increased with time and temperature.
- The tests with THPS and glutaraldehyde resulted in numerous tiny pits (depth less than 10 μm) after five months, but this type of isolated pits was not observed in tests at 11 months. The pits appeared to have coalesced. The eleven-month tests showed higher weight losses with a few long and narrow pits similar to those in the untreated GoM seawater tests. The higher corrosion rate was caused by THPS (around 0.23mpy). Glutaraldehyde caused less weight loss than THPS.
- When GoM seawater was deliberately spiked with 10^6 SRB cells per ml, biofilms formed on the coupon surface. Some pits (typically seen in other tests involving SRB) were observed after biofilm removal. S and Fe were found by EDS beneath the biofilms indicating the presence of FeS.

CHAPTER 4: MIC IN HYDROTESTING USING QURRAYAH AND WASIA WATER FROM SAUDI ARABIA (SA)

4.1 Introduction

MIC occurrence in a system during and after hydrotesting depends on various factors. Among those factors, the water sources used and their point of origin are the most important because the water provides an environment for microbial growth. Typically, the composition of natural seawater used as hydrotesting fluid is almost the same around the world (refer to the composition comparison between typical seawater and seawater from the Gulf of Mexico in Table 3-2). However, water from some specific locations may show significant differences. Table 4-1 shows Na^+, SO_4^{2-} and total organic carbon (TOC) in a comparison between typical seawater and Qurrayah water (seawater) in Saudi Arabia (SA). It is clear that Na^+ and SO_4^{2-} concentrations in Qurrayah water (seawater) are almost 1.6 times higher than in typical seawater, and TOC concentration, which is very important for microbial growth, can be 500 times higher. For convenience, other available water sources like well/river water may also be used in hydrotesting. The major elemental composition of Wasia water (well water) from SA is presented in Table 4-1. The Na^+ and SO_4^{2-}concentrations in Wasia water are much lower than that in seawater. The significant composition difference between various water sources will definitely affect the MIC process. This chapter will focus on studying MIC in hydrotesting using waters (Qurrayah water and Wasia water) from SA.

Table 4-1: Major element comparison between typical natural seawater and SA waters*

	Na^+ (ppm)	SO_4^{2-} (ppm)	Total organic carbon (TOC) (ppm)
Typical natural seawater	10,500~10,770	2,655~2,715	<1 to 2
Qurrayah water (seawater)	16,580	4,330	498
Wasia water (well water)	406	320	20.2

*The Na^+ and SO_4^{2-} assay of SA waters was done by ENC Labs, and TOC was assayed by San Antonio Testing Laboratory, Inc.

4.2 Objectives

- Investigate MIC behavior in untreated Wasia water and Qurrayah water from Saudi Arabia (SA), and study accelerated MIC process by using a lab strain of SRB and enriched SA waters
- Study SRB growth dependence on key nutrients: sodium lactate and Fe^{2+}
- Investigate the "black powder" problem to provide a guideline about how it is produced under a certain situation
- Develop a PCR technique to detect bacteria in unknown samples

4.3 Instrumentation and analytical methods

The instrumentation and methods predominantly listed in this study are the same as stated in Section 3.3. Apart from SEM and EDS, Infinite Focus Microscope (IFM) was used to perform surface analysis. PCR device-Eppendorf Mastercycler® gradient thermal cycler was employed to do the DNA amplification. SRB DNA was extracted using a FastDNA®SPIN For Soil Kit (www.mpbio.com, Cat #6560-200).

4.4 Results and discussion

4.4.1 Tests using untreated SA waters

4.4.1.1 Test conditions

Two water samples (Wasia well water and Qurrayah seawater) were supplied by Saudi Aramco. Table 4-2 shows the test matrix. The Na^+ and SO_4^{2-} assays of SA waters were done by ENC Labs, and the total organic carbon (TOC) analyses of SA waters were performed by San Antonio Testing Laboratory, Inc. (seeTable 4-1).

After deoxygenation, L(+)−cysteine was used as an oxygen scavenger. The oxygen concentration in the experimental vials after the completion of each test was determined to be below 40 ppb. Without the oxygen scavenger, over a long time some oxygen can penetrate the vial septum causing the coupon to rust, presenting as a yellowish rust color.

Table 4-2: Test matrix using untreated SA waters

Test conditions	
Test media	Wasia water (well water) & Qurrayah water (seawater)
Oxygen scavenger	500 ppm in each medium
Initial pH	6.86 (Wasia) & 7.14 (Qurrayah)
Specimen	X65 gum-shaped carbon steel
Test temperature (°C)	25, 31, 37
Test period	2 weeks, 1 month, 3 months

4.4.1.2 Test results

Part I: Tests using untreated Wasia water (well water)

In this two-week test, no biofilms or bacteria were found on the coupon surface (Figure 4-1 ~ Figure 4-3). Figure 4-4 shows that weight loss increased with the increase of temperature while the pH showed little change. No pits were detected for this test (Figure 4-5 and Figure 4-6).

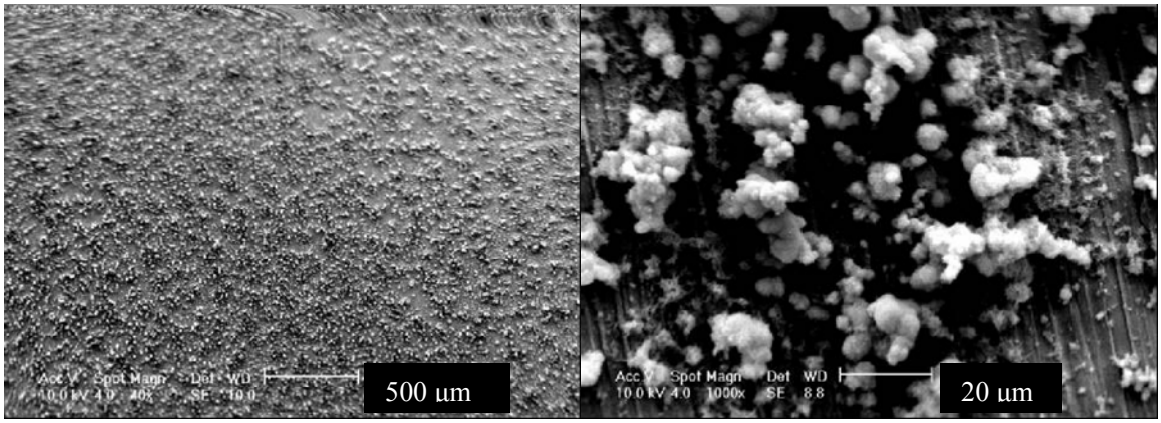

(a) SEM at 40X (b) SEM at 1000X

Figure 4-1: 2-week test in the untreated Wasia water at 25ºC (SEM analysis of coupon surface before acid cleaning)

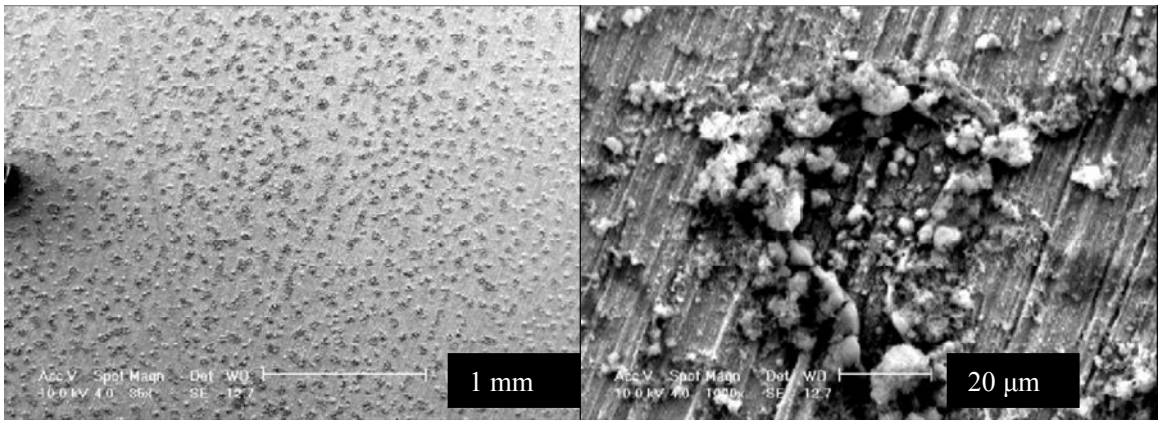

(a) SEM at 35X (b) SEM at 1000X

Figure 4-2: 2-week test in the untreated Wasia water at 31ºC (SEM analysis of coupon surface before acid cleaning)

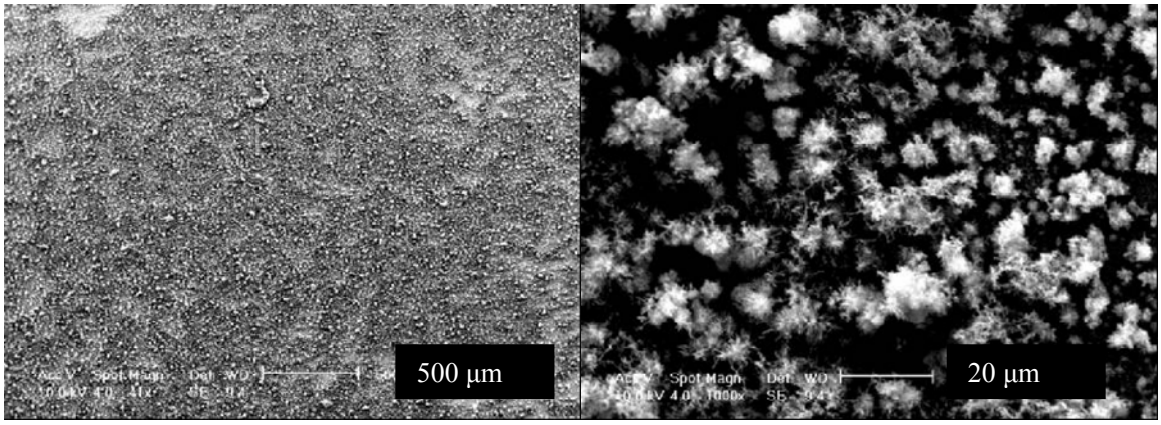

(a) SEM at 41X (b) SEM at 1000X

Figure 4-3: 2-week test in the untreated Wasia water at 37ºC (SEM analysis of coupon surface before acid cleaning)

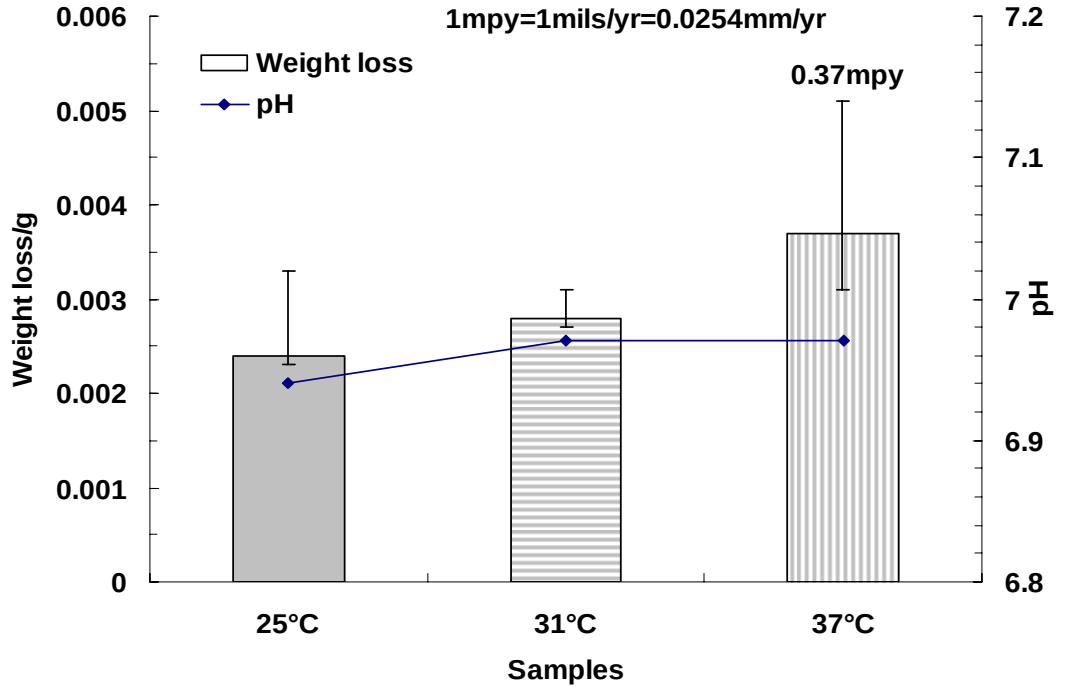

Figure 4-4: X65 coupon weight loss in untreated Wasia water (well water) after 2-week test

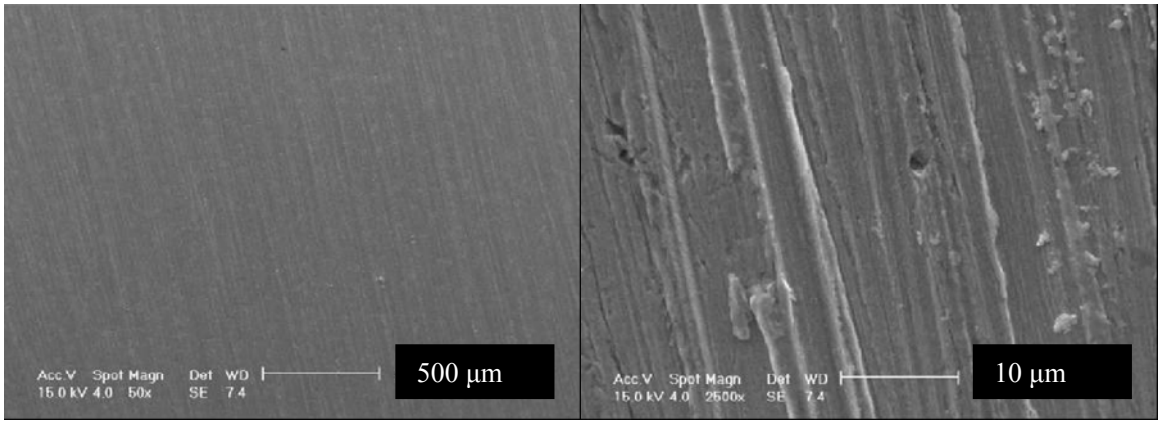

(a) SEM at 50X (b) SEM at 2500X

Figure 4-5: 2-week test in the untreated Wasia water at 25ºC (SEM analysis of coupon surface after acid cleaning)

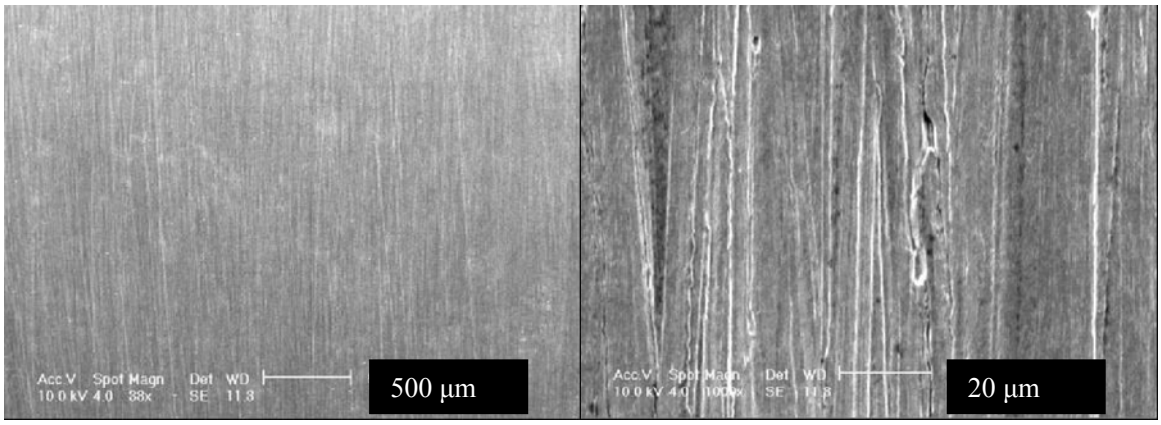

(a) SEM at 38X (b) SEM at 1000X

Figure 4-6: 2-week test in the untreated Wasia water at 37ºC (SEM analysis of coupon surface after acid cleaning)

In the one-month test, again, there were no biofilms or bacteria on the coupon surface at 37ºC (Figure 4-7). Element S from FeS that can be produced by SRB could not be found in the EDS image (Figure 4-7 (d)). The SEM image did show some particulate matters and patchy films that were also evident in the 2-week test and other longer tests.

The one-month test results showed the same weight loss and pH trends as the two-week test (Figure 4-8). Again, no pits were detected (Figure 4-9 and Figure 4-10).

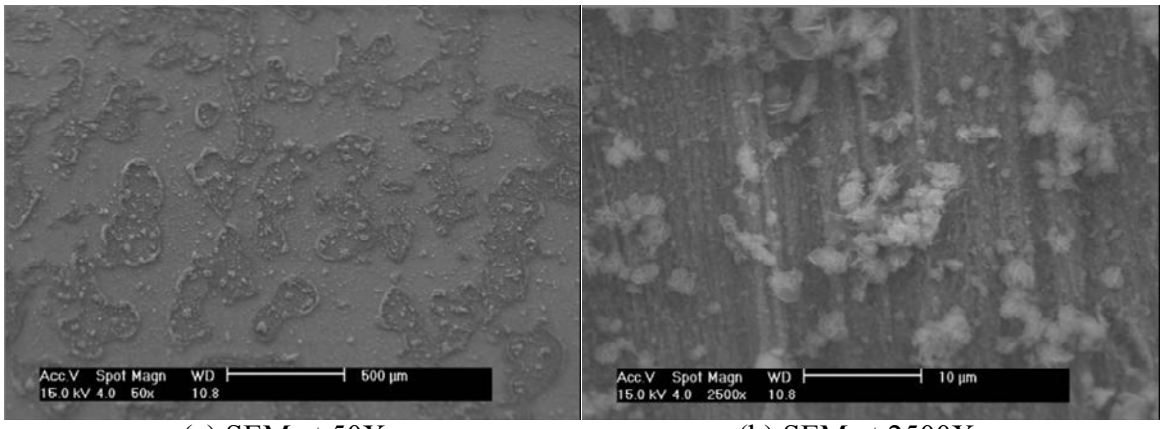

(a) SEM at 50X (b) SEM at 2500X

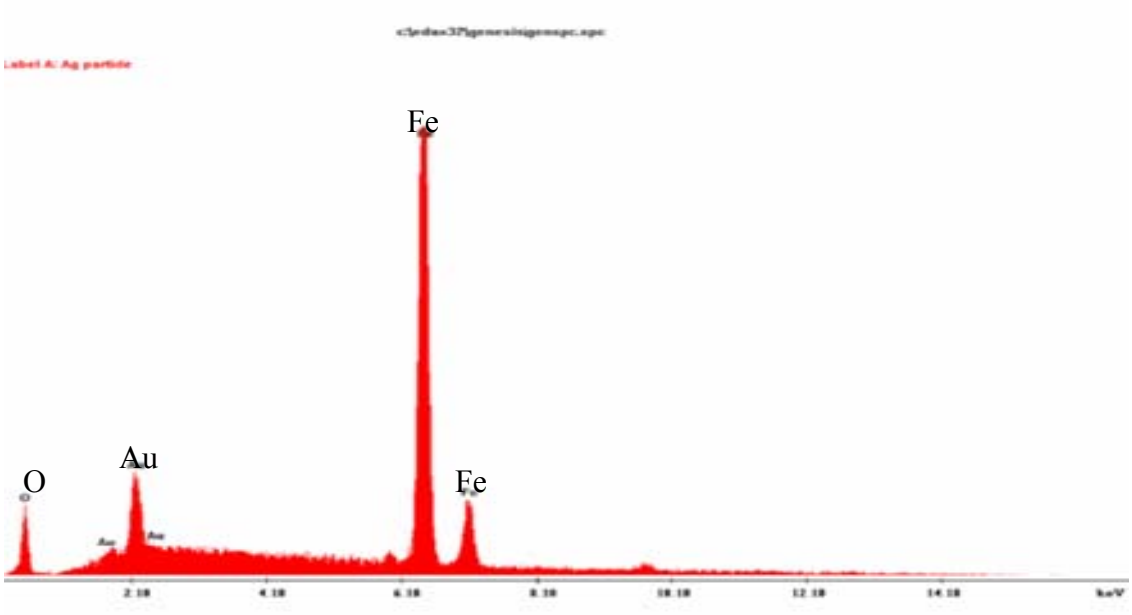

(d) Composition on the coupon surface

Figure 4-7: 1-month test in the untreated Wasia water at 37ºC (SEM analysis of coupon surface before acid cleaning)

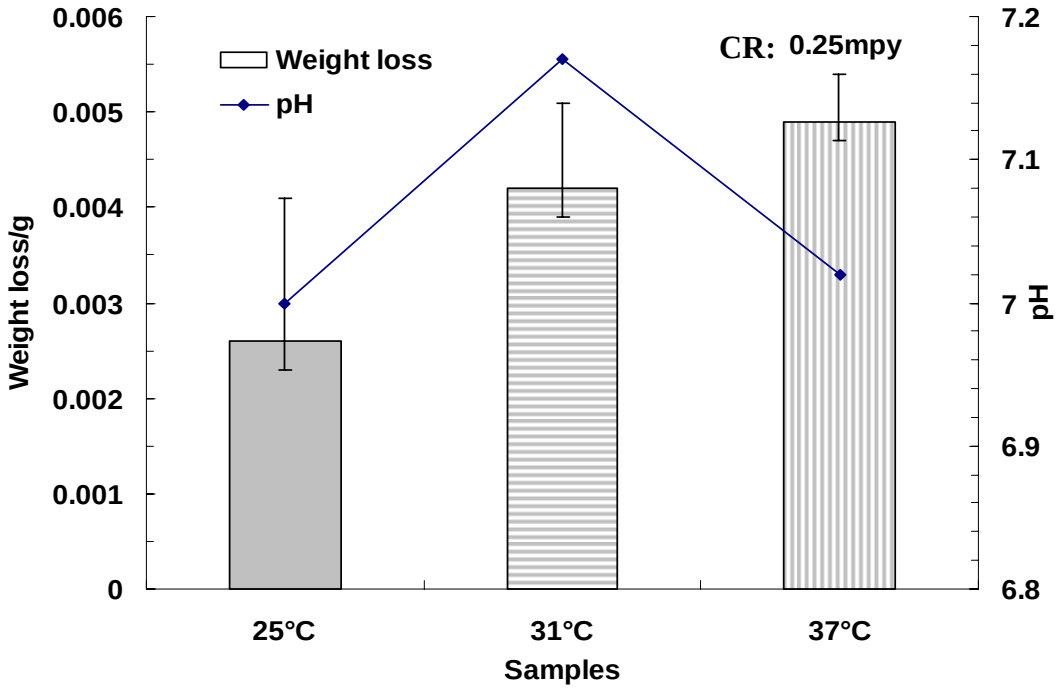

Figure 4-8: X65 coupon weight loss in the untreated Wasia water (well water) after 1-month test

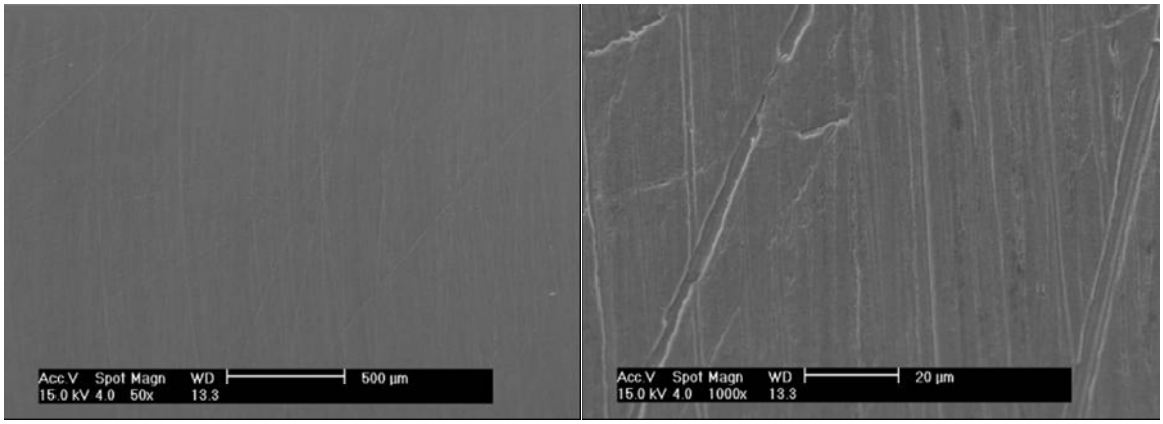

(a) SEM at 50X (b) SEM at 1000X

Figure 4-9: 1-month test in the untreated Wasia water at 25ºC (SEM analysis of coupon surface after acid cleaning)

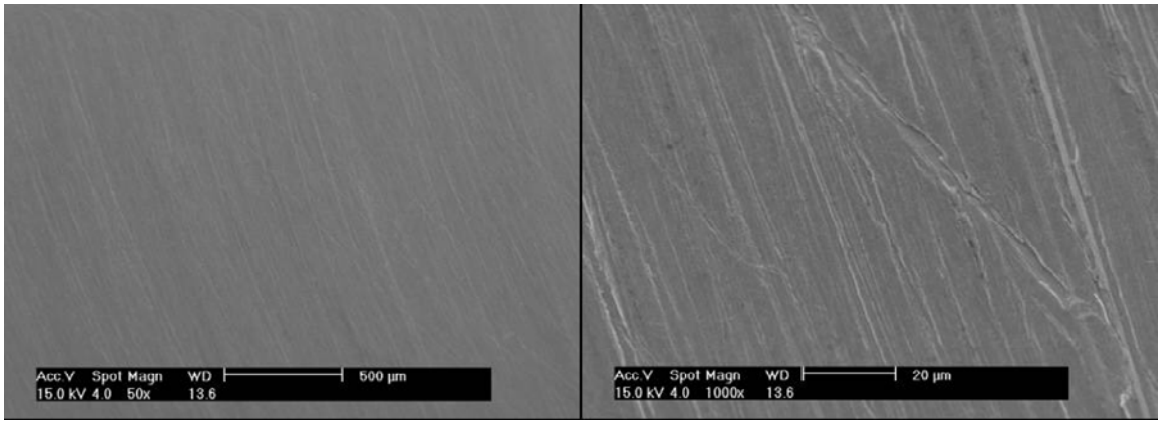

(a) SEM at 50X (b) SEM at 1000X

Figure 4-10: 1-month test in the untreated Wasia water at 37ºC (SEM analysis of coupon surface after acid cleaning)

In this three-month test, no biofilms or bacteria were found on the coupon surface (Figure 4-11~Figure 4-13, and no elemental S was found by EDS for test temperatures 25ºC, 31ºC and 37ºC (Figure 4-11 (c), Figure 4-12 (c) and Figure 4-13 (c), respectively). Figure 4-11 and Figure 4-12 show many particles on the coupon surface and the following EDS images (Figure 4-11 (c) and Figure 4-12 (c)) show elemental O. In comparison, the coupon surface (Figure 13) is much smoother when elemental O is absent (Figure 13 (c)). Thus, the particles in this test were probably due to the presence of oxygen. Even though the oxygen level in vials was kept low (< 40 ppb), there was still some oxygen that could have reacted with the coupon.

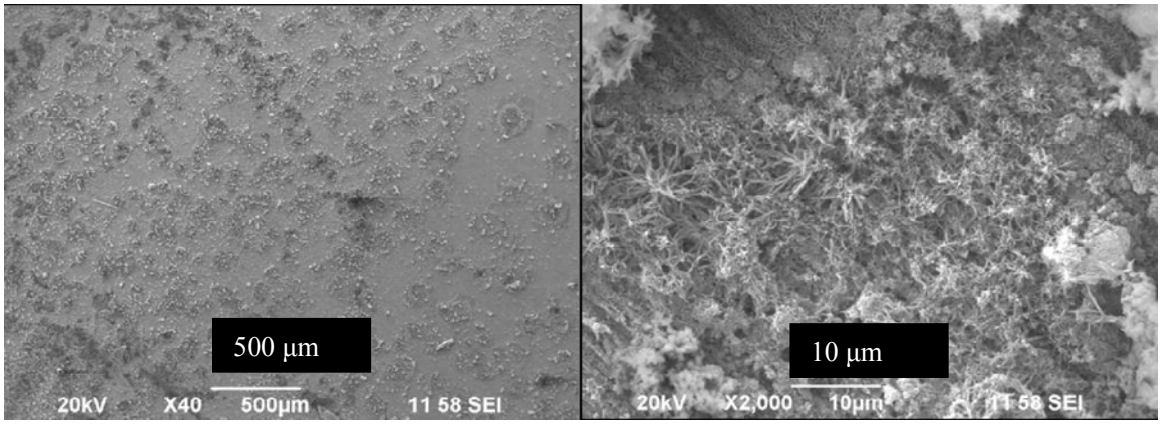

(a) SEM at 40X (b) SEM at 2000X

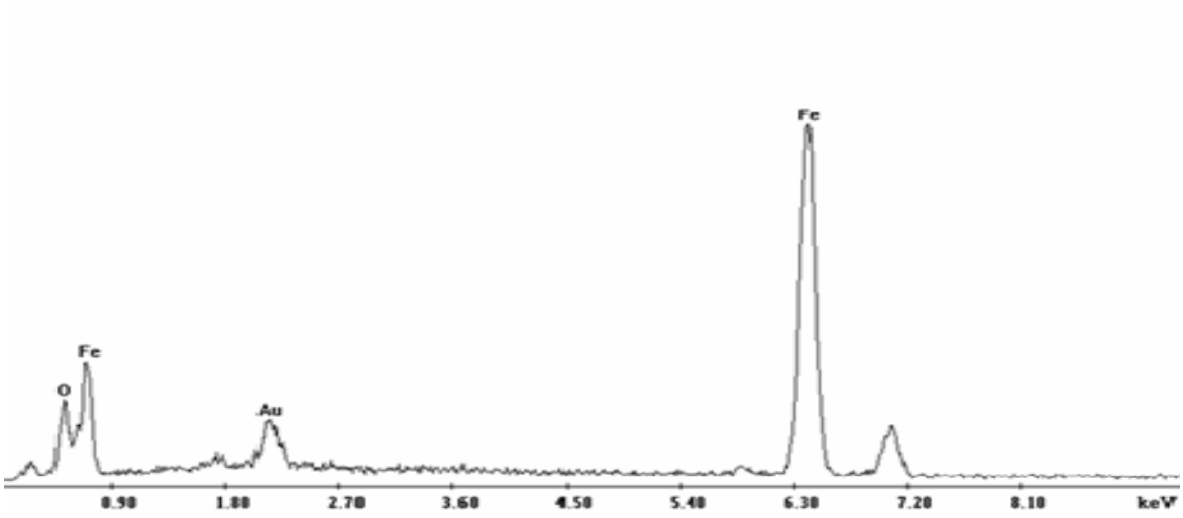

(d) Composition on the coupon surface

Figure 4-11: 3-month test in the untreated Wasia water at 25ºC (SEM and EDS analysis of coupon surface before acid cleaning)

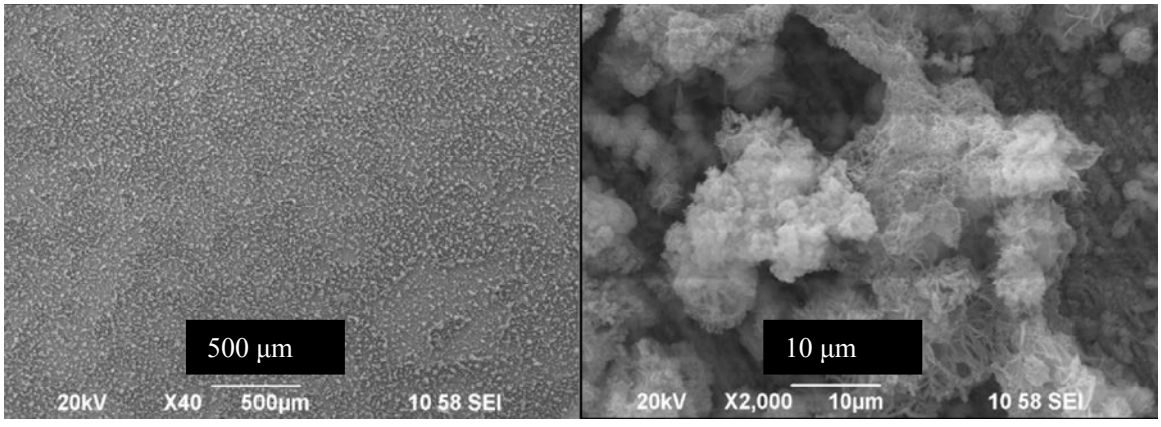

(a) SEM at 40X (b) SEM at 2000X

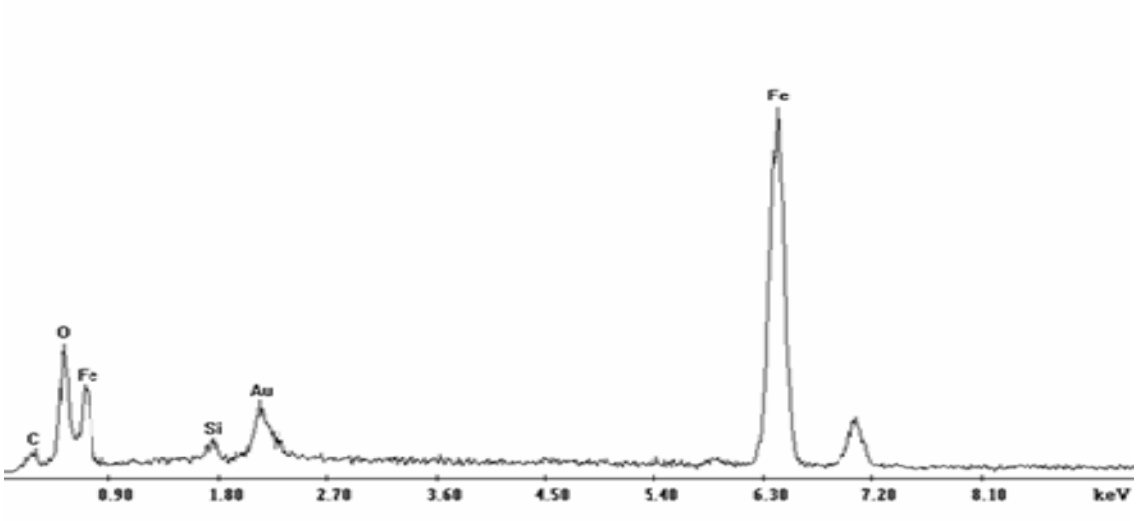

(c) Composition on the coupon surface

Figure 4-12: 3-month test in the untreated Wasia water at 31ºC (SEM and EDS analysis of coupon surface before acid cleaning)

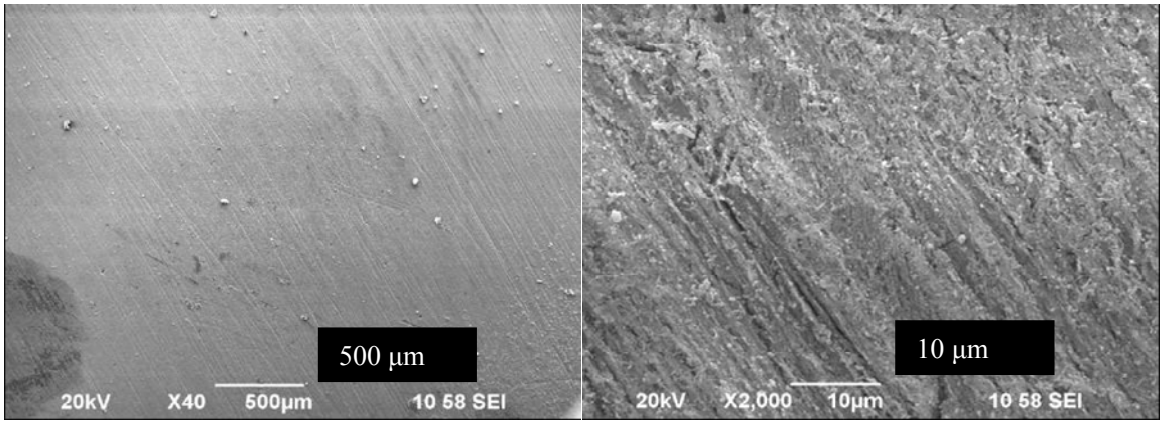

(a) SEM at 40X

(b) SEM at 300X

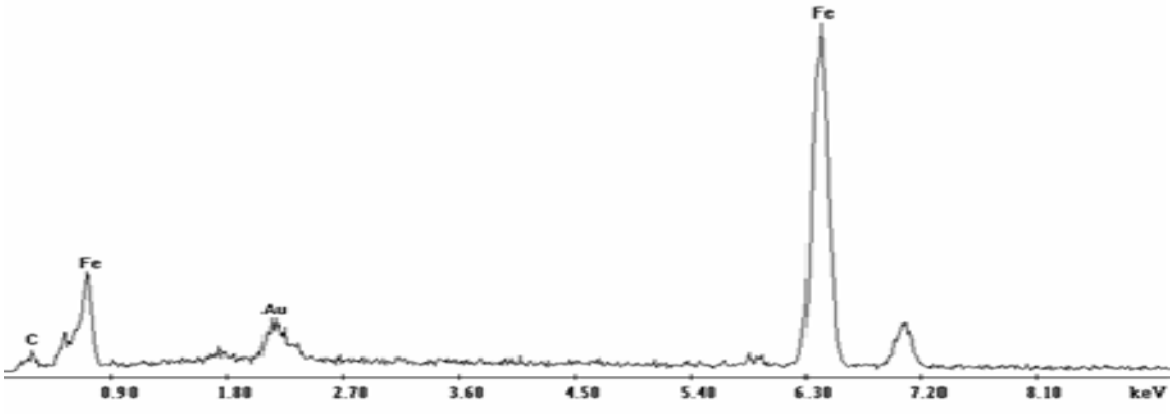

(c) Composition on the coupon surface

Figure 4-13: 3-month test in the untreated Wasia water at 37ºC (SEM and EDS analysis of coupon surface before acid cleaning)

The three-month test shows a slightly increased weight loss with the increase of temperatures (Figure 4-14) and compared to the previous two-week and one-month test, the coupon surfaces turned coarser (Figure 4-15 and Figure 4-16), and showed some pitting (Figure 4-17). This might have resulted from the background corrosion (probably non-MIC related under- deposit corrosion,). The typical MIC causes either isolated larger and deeper pits or smaller pits in groups while background corrosion generally results in rather evenly distributed smaller pits. It should be pointed out that the weight changes were quite small, and that the corrosion rates due to background corrosion in deoxygenated Wasia water were quite small (below 0.4 mpy).

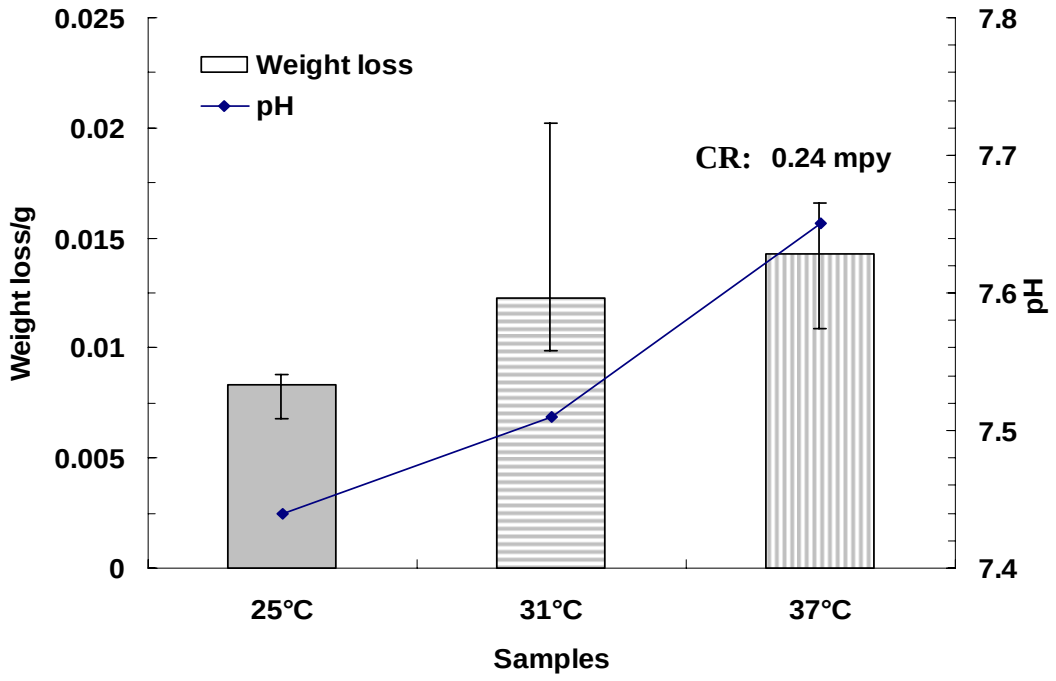

Figure 4-14: X65 coupon weight loss in the untreated Wasia water (well water) after 3-month test

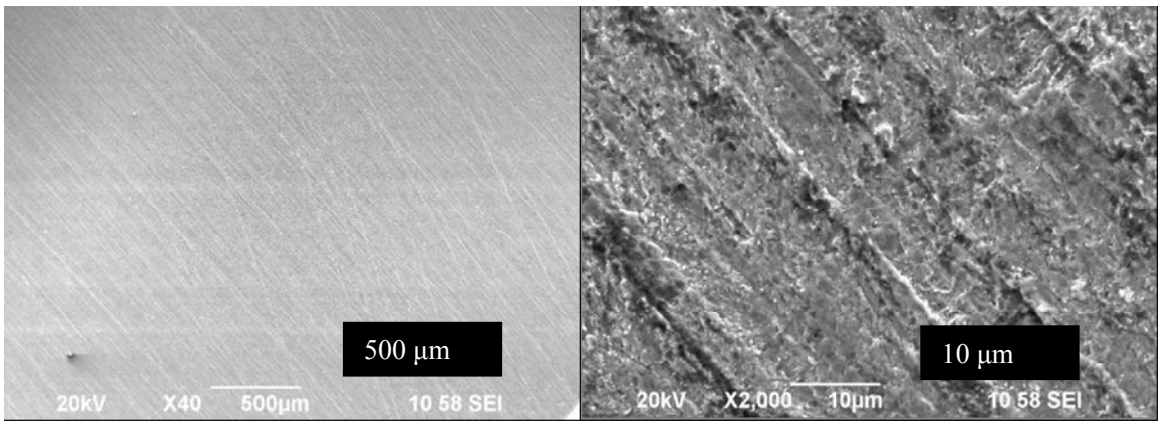

(a) SEM at 40X (b) SEM at 2000X

Figure 4-15: 3-month test in the untreated Wasia water at 25ºC (SEM analysis of coupon surface after acid cleaning)

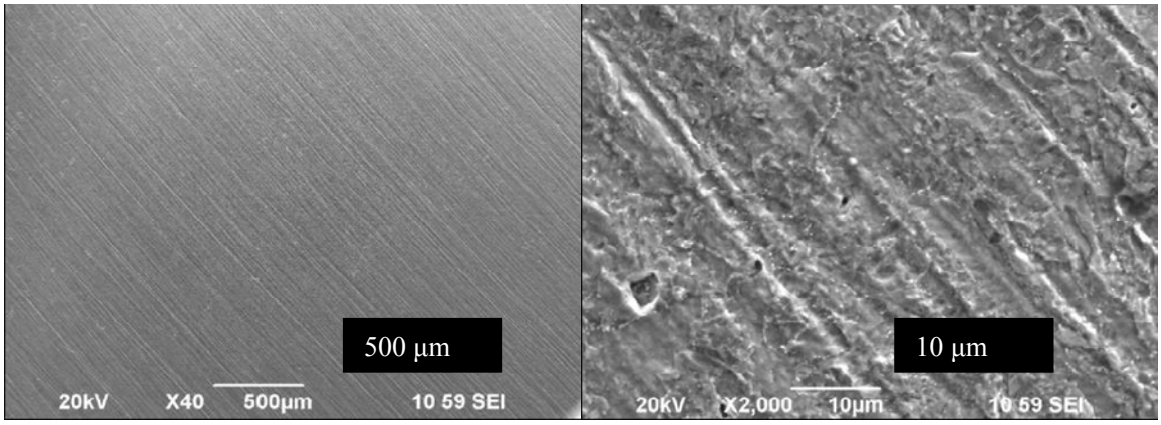

(a) SEM at 40X (b) SEM at 2000X

Figure 4-16: 3-month test in the untreated Wasia water at 31ºC (SEM analysis of coupon surface after acid cleaning)

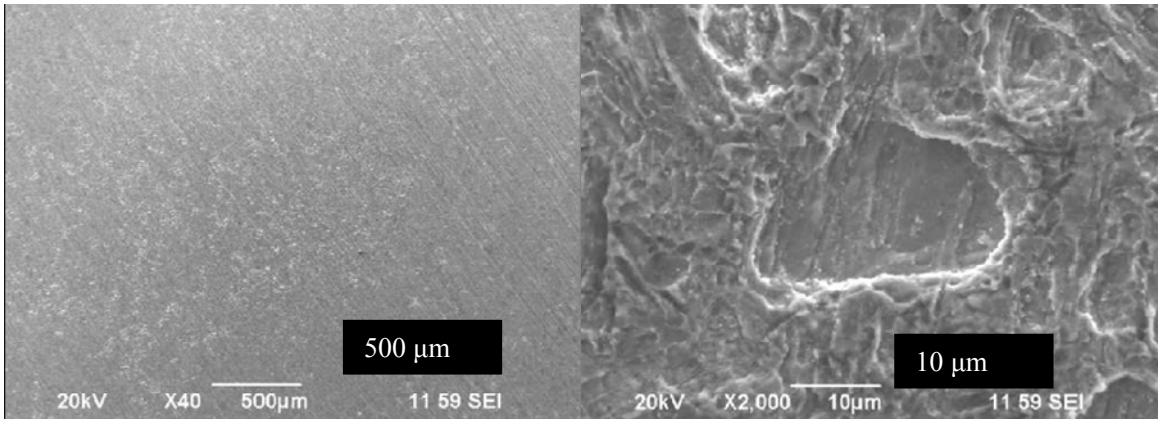

(a) SEM at 40X (b) SEM at 2000X

Figure 4-17: 3-month test in the untreated Wasia water at 37ºC (SEM analysis of coupon surface after acid cleaning)

Part II: Tests using untreated Qurrayah water (seawater)

In the two-week test, no biofilms or bacteria were found on the coupon surface (Figure 4-18, Figure 4-19 and Figure 4-20). Both coupon surfaces and the EDS analysis (Figure 4-18 (c), Figure 4-19 (c) and Figure 4-20 (c)) looked similar. The effect of oxygen was also noted as in the tests of Part I. Figure 4-21 shows that weight loss

increased with the increase of temperature; however, no pits were observed on the coupon surface for this test (Figure 4-22 and Figure 4-23).

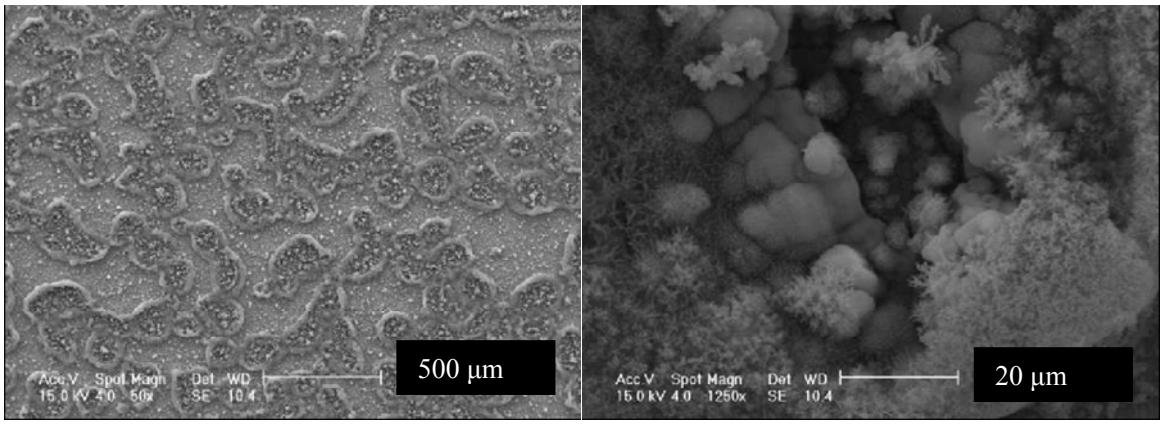

(a) SEM at 50X (b) SEM at 1250X

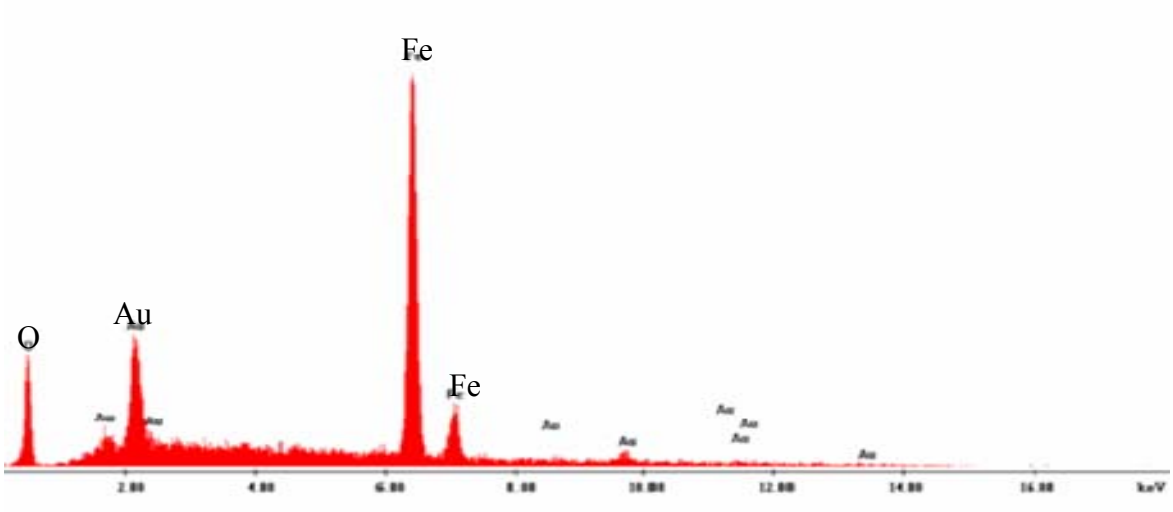

(c) Composition on the coupon surface

Figure 4-18: 2-week test in the untreated Qurrayah water at 25 ºC (SEM and EDS analysis of coupon surface before acid cleaning)

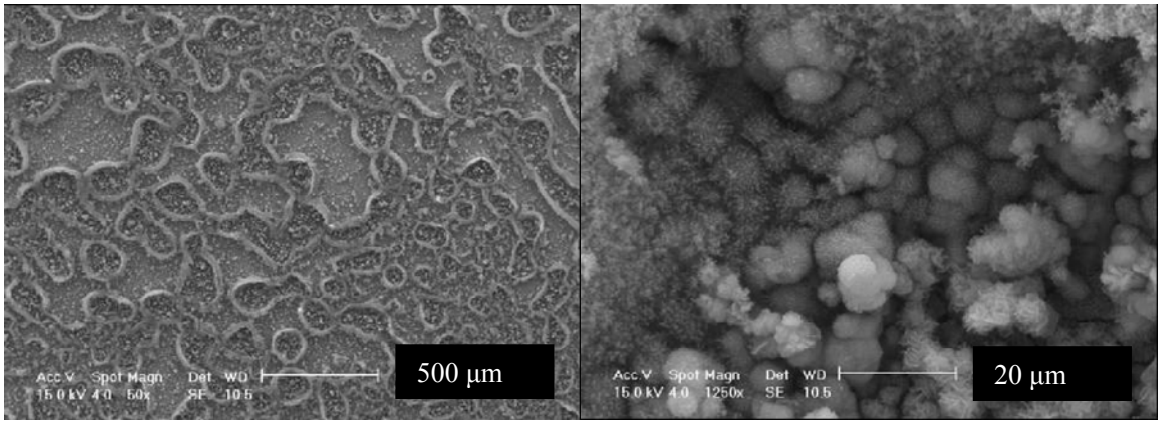

(a) SEM at 50X (b) SEM at 1250X

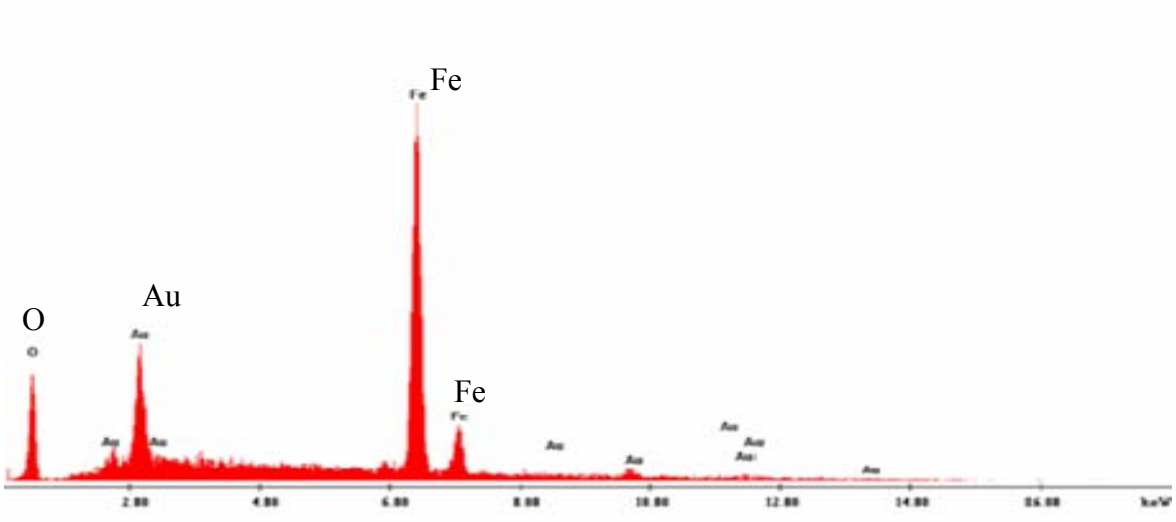

(c) Composition on the coupon surface

Figure 4-19: 2-week test in the untreated Qurrayah water at 31 ºC (SEM and EDS analysis of coupon surface before acid cleaning)

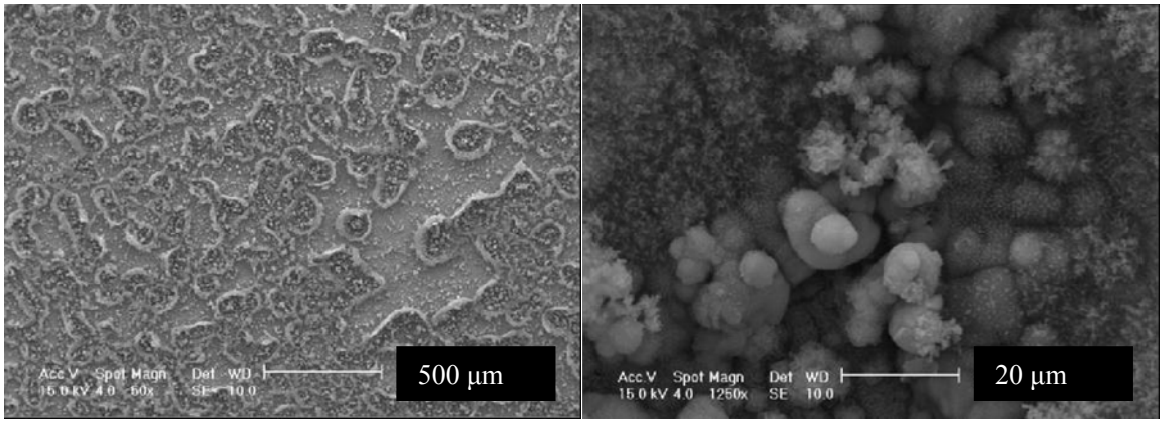

(a) SEM at 50X (b) SEM at 1250X

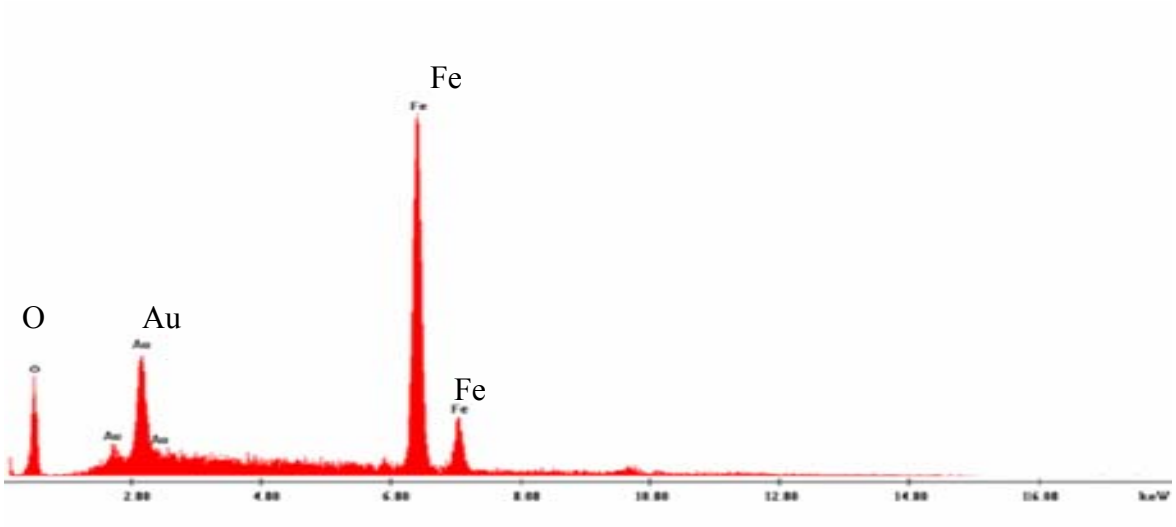

(c) Composition on the coupon surface

Figure 4-20: 2-week test in the untreated Qurrayah water at 37 ºC (SEM and EDS analysis of coupon surface before acid cleaning)

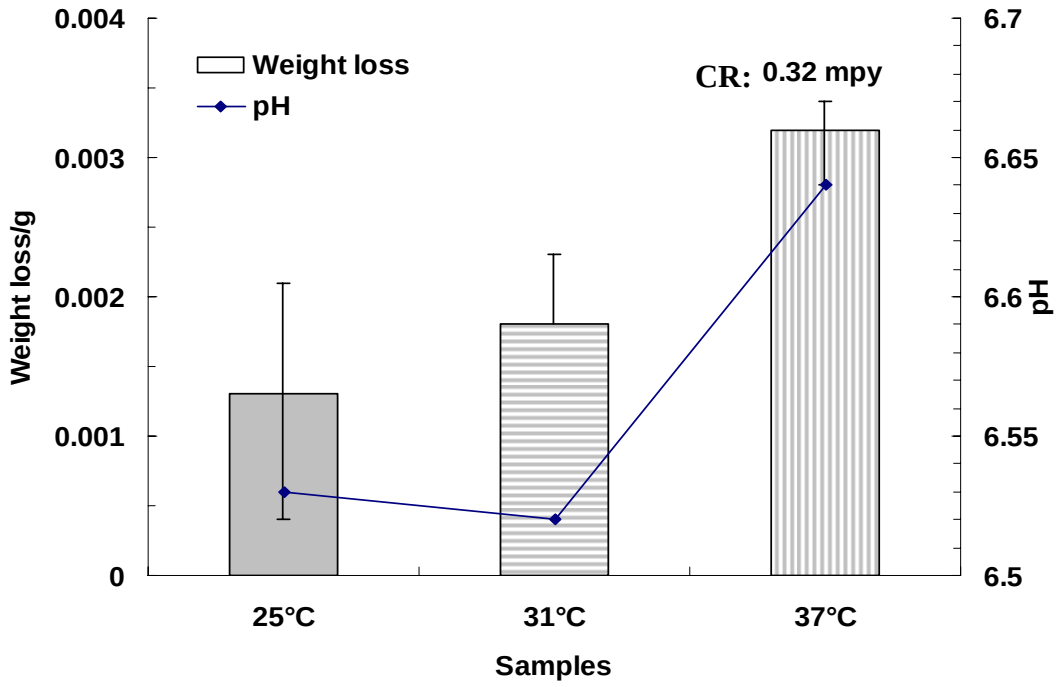

Figure 4-21: X65 coupon weight loss in the untreated Qurrayah water (seawater) after 2-week test

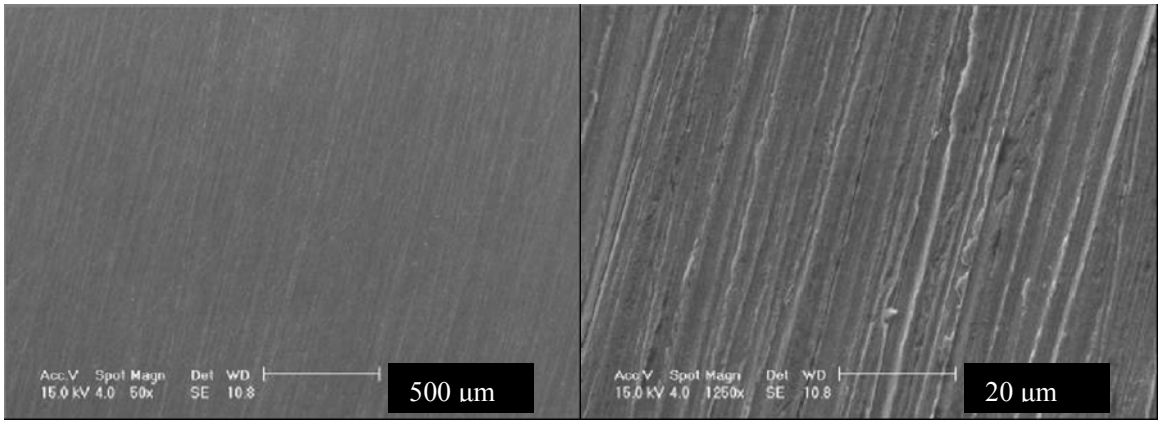

(a) SEM at 50X (b) SEM at 1250X

Figure 4-22: 2-week test in the untreated Qurrayah water at 25 ºC (SEM analysis of coupon surface after acid cleaning)

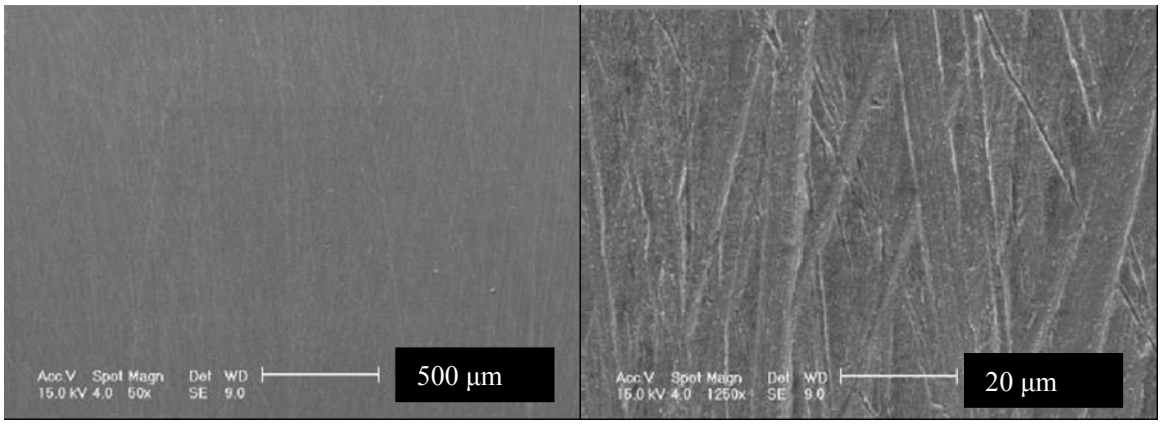

(a) SEM at 50X (b) SEM at 1250X

Figure 4-23: 2-week test in the untreated Qurrayah water at 37 ºC (SEM analysis of coupon surface after acid cleaning)

In the one-month test, after the test coupons were removed from the untreated Qurrayah water, in order to reduce the time the coupons were exposed to air, the coupons were not treated with glutaraldehyde. The resulting smoother surfaces (Figure 4-24, Figure 4-25 and Figure 4-26) were noted as being different from the patchy surfaces in the two-week test. This indicated that oxygen affected the appearance of the coupon

surface. In the test of 25ºC, evenly distributed crystals were found on the coupon surface (Figure 4-24), and EDS images (Figure 4-24 (c)) showed they are probably NaCl. For tests at 31ºC and 37ºC, there were no crystals and the percentage of the Cl was decreasing with the increase of temperature (see Figure 4-25 (c) and Figure 4-26 (c)). With increased temperature, cracks also appeared on the mineral film on the coupon surface (see Figure 4-25 and Figure 4-26).

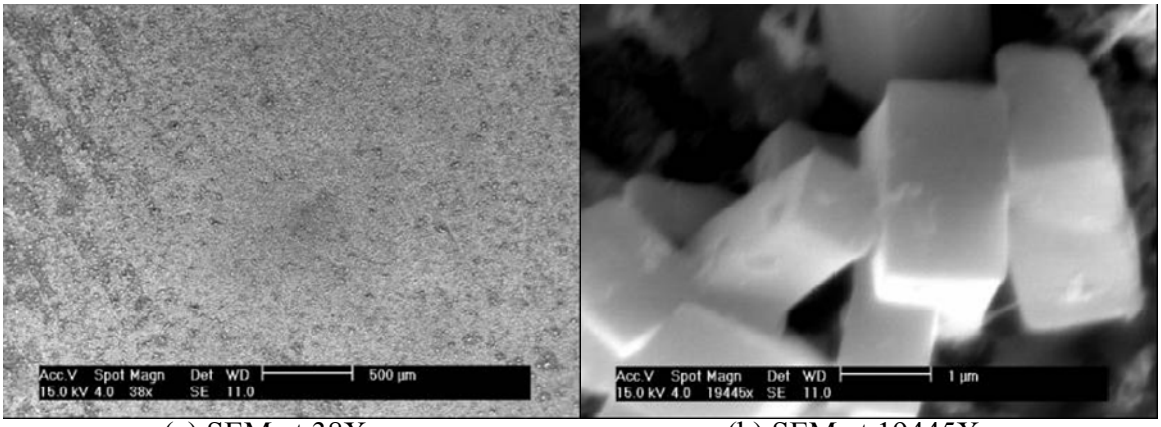

(a) SEM at 38X (b) SEM at 19445X

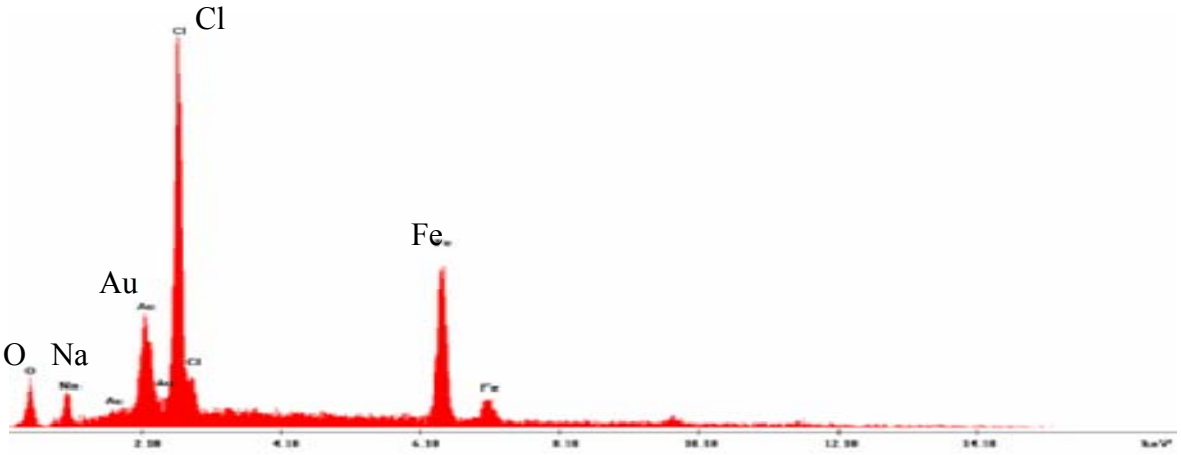

(d) Composition on the coupon surface

Figure 4-24: 1-month test in the untreated Qurrayah water at 25 ºC (SEM and EDS analysis of coupon surface before acid cleaning; Coupons were immediately dehydrated with 100% alcohol, and then coated with gold in order to reduce the exposure to the air.)

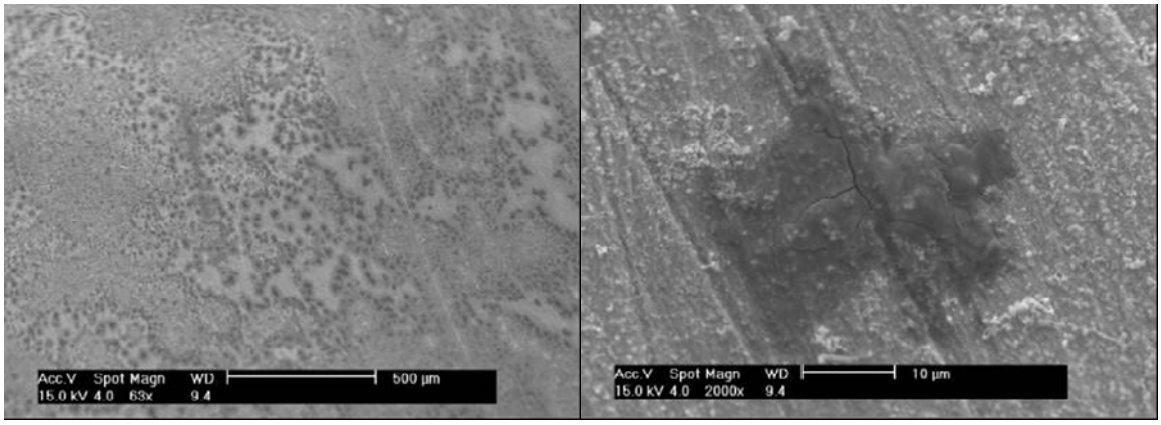

(a) SEM at 63X (b) SEM at 2000X

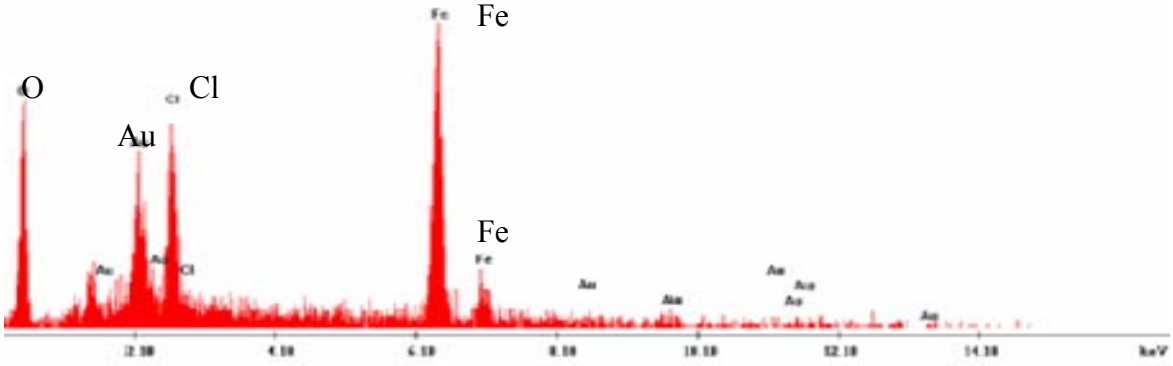

(c) Composition on the coupon surface

Figure 4-25: 1-month test in the untreated Qurrayah water at 31 ºC (SEM and EDS analysis of coupon surface before acid cleaning; Coupons were immediately dehydrated with 100% alcohol, and then coated with gold in order to reduce the exposure to the air.)

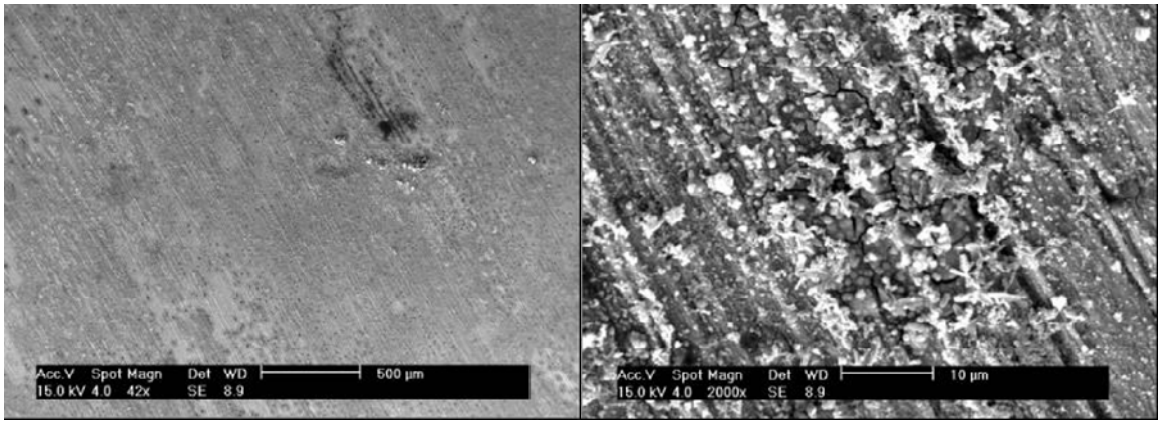

(a) SEM at 42X (b) SEM at 2000X

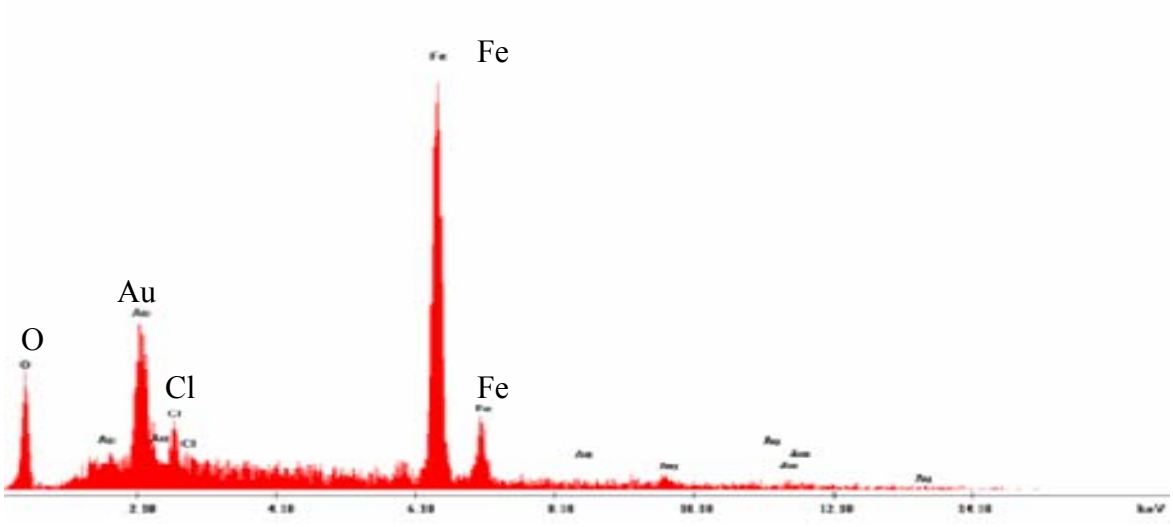

(c) Composition on the coupon surface

Figure 4-26: 1-month test in the untreated Qurrayah water at 37 ºC (SEM and EDS analysis of coupon surface before acid cleaning; Coupons were immediately dehydrated with 100% alcohol, and then coated with gold in order to reduce the exposure to the air.)

Figure 4-27 shows a slight increase of weight loss with the increase of temperature. No pits were observed on the coupon surface for this test (Figure 4-28 ~ Figure 4-30)

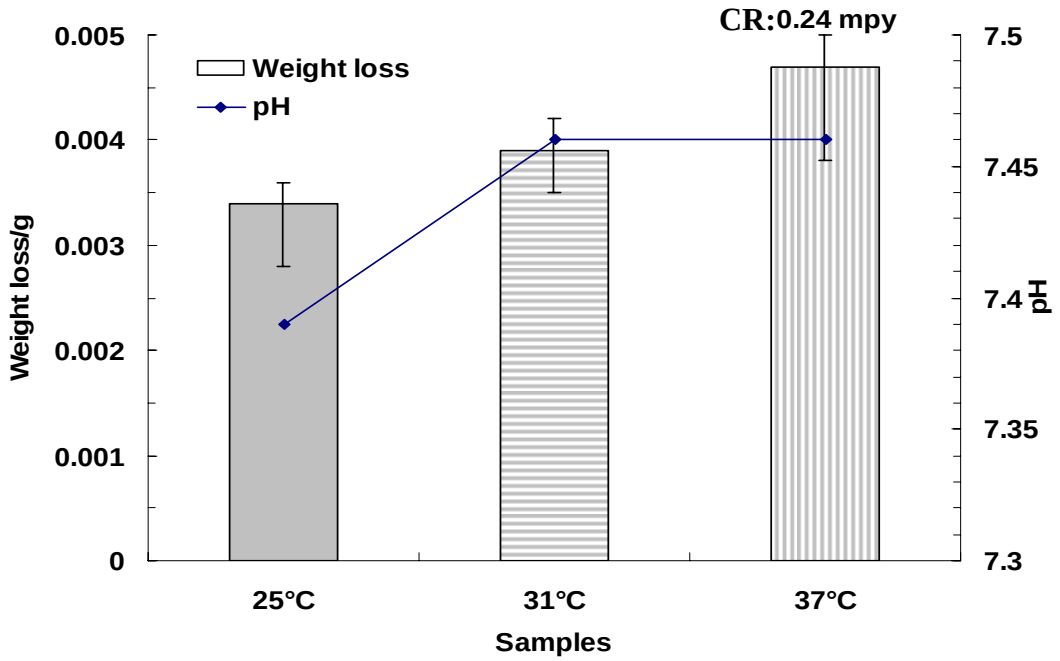

Figure 4-27: X65 coupon weight loss in the untreated Qurrayah water (seawater) after 1-month test

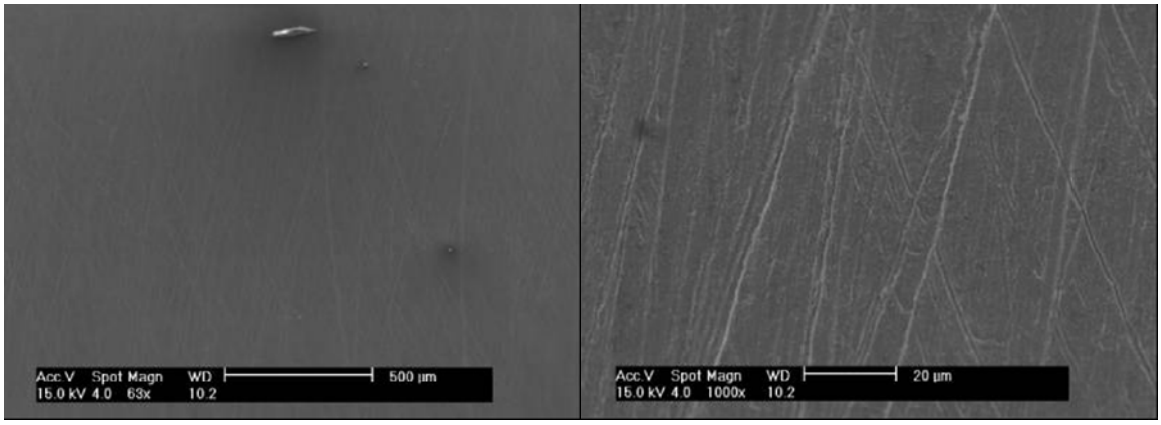

(a) SEM at 63X (b) SEM at 1000X

Figure 4-28: 1-month test in the untreated Qurrayah water at 25 ºC (SEM analysis of coupon surface after acid cleaning)

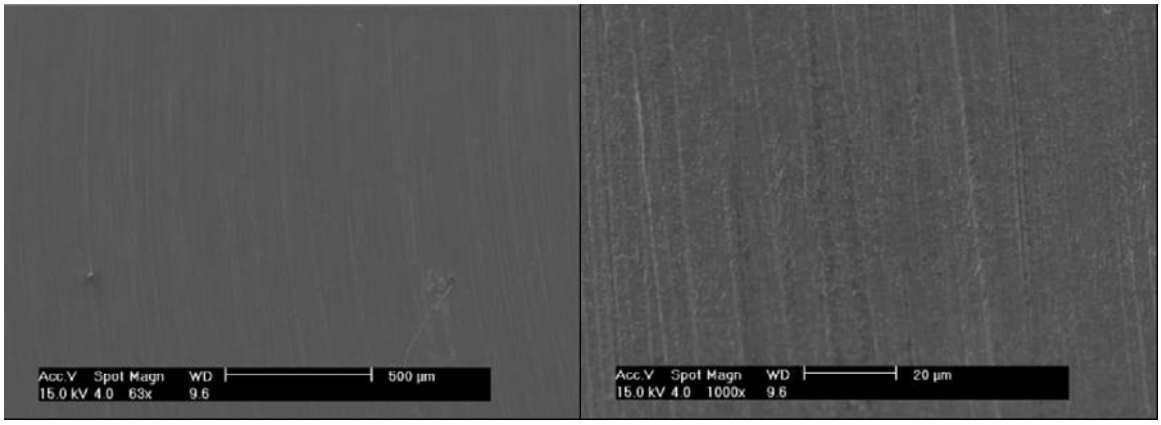

(a) SEM at 63X (b) SEM at 1000X

Figure 4-29: 1-month test in the untreated Qurrayah water at 31 ºC (SEM analysis of coupon surface after acid cleaning)

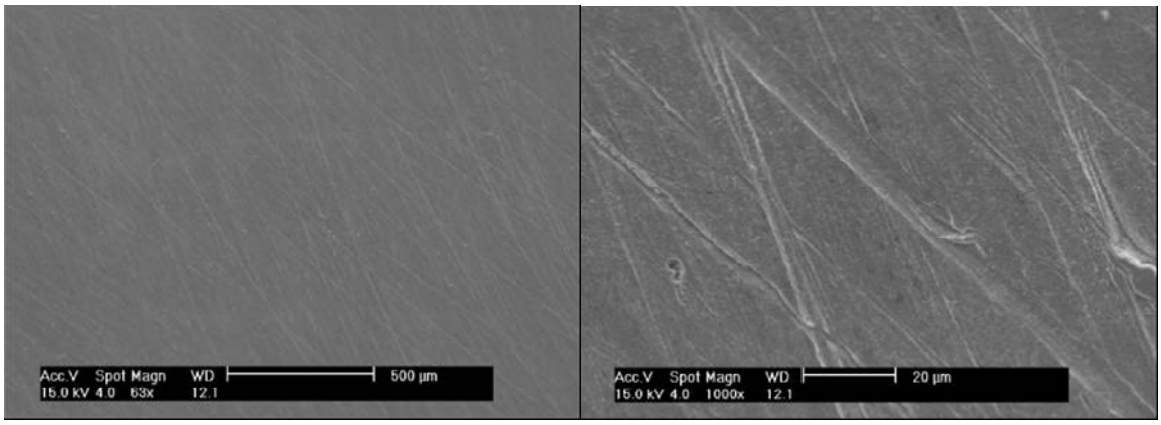

(a) SEM at 63X (b) SEM at 1000X

Figure 4-30: 1-month test in the untreated Qurrayah water at 37 ºC (SEM analysis of coupon surface after acid cleaning)

In this three-month test, the coupon surfaces were the same as those found in the 2-week test. No bacteria or elemental S was found on coupon surfaces (see Figure 4-31 ~ Figure 4-33). Figure 4-34 shows that weight loss increased slightly with the increase of temperature. Pits were found on the coupon surface at all the three test temperatures (25^oC, 31^oC and 37^oC) (Figure 4-35 ~ Figure 4-37). The pits resembled those typically

caused by MIC. Microorganisms in the Qurrayah water at the given conditions may favor MIC when there is a longer period of time. SEM showed no microbes. More sensitive methods such as quantitative PCR may need to be used to detect bacteria. The data showed that the corrosion rates in deoxygenated Qurrayah water were quite small (Max. 0.32mpy).

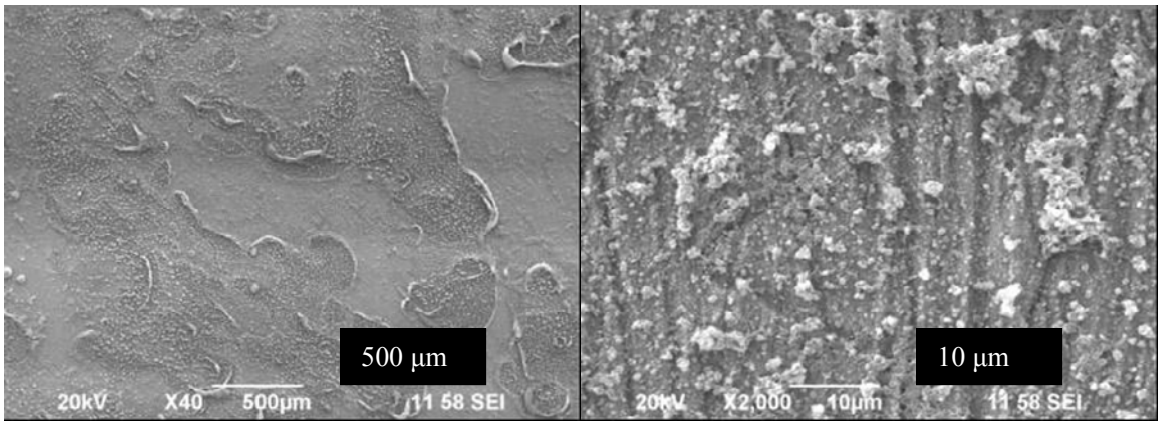

(a) SEM at 40X (b) SEM at 2000X

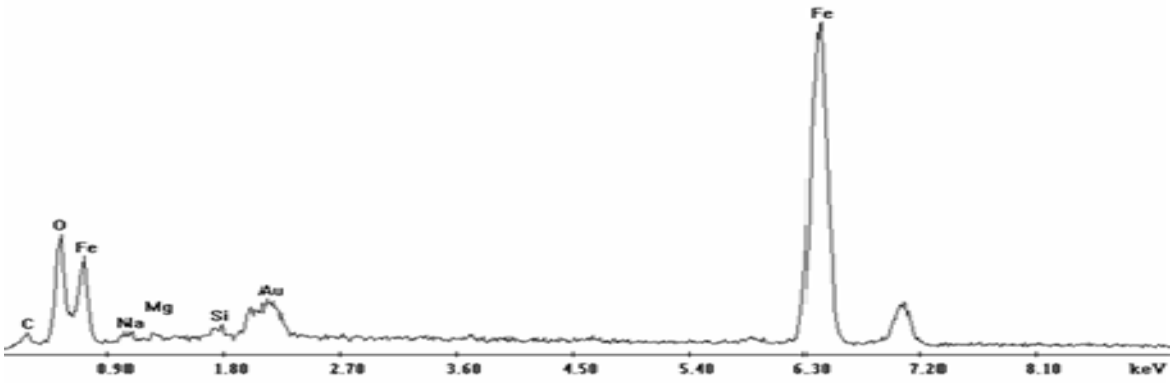

(c) Composition on the coupon surface

Figure 4-31: 3-month test in the untreated Qurrayah water at 25 ºC (SEM and EDS analysis of coupon surface before acid cleaning)

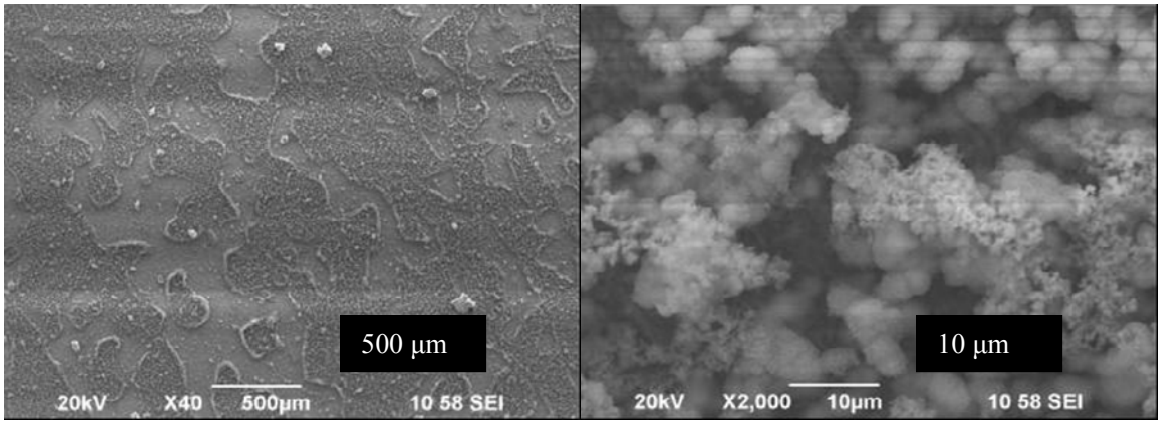

(a) SEM at 40X (b) SEM at 2000X

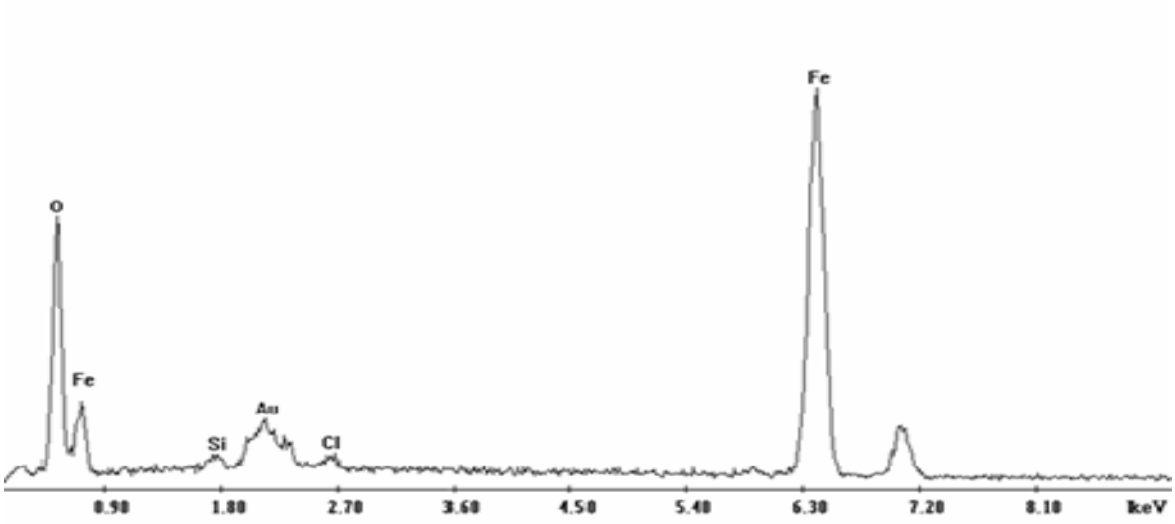

(c) Composition on the coupon surface

Figure 4-32: 3-month test in the untreated Qurrayah water at 31 ºC (SEM and EDS analysis of coupon surface before acid cleaning)

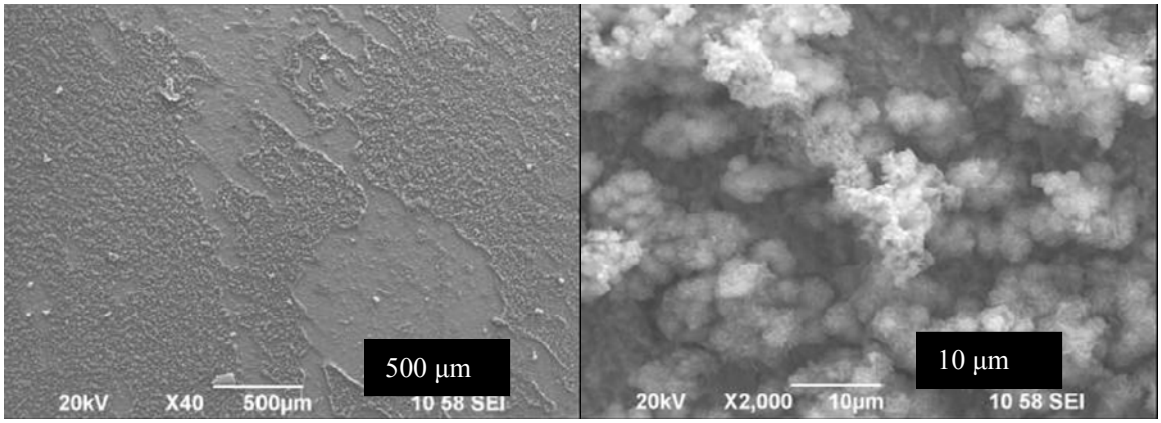

(a) SEM at 40X (b) SEM at 2000X

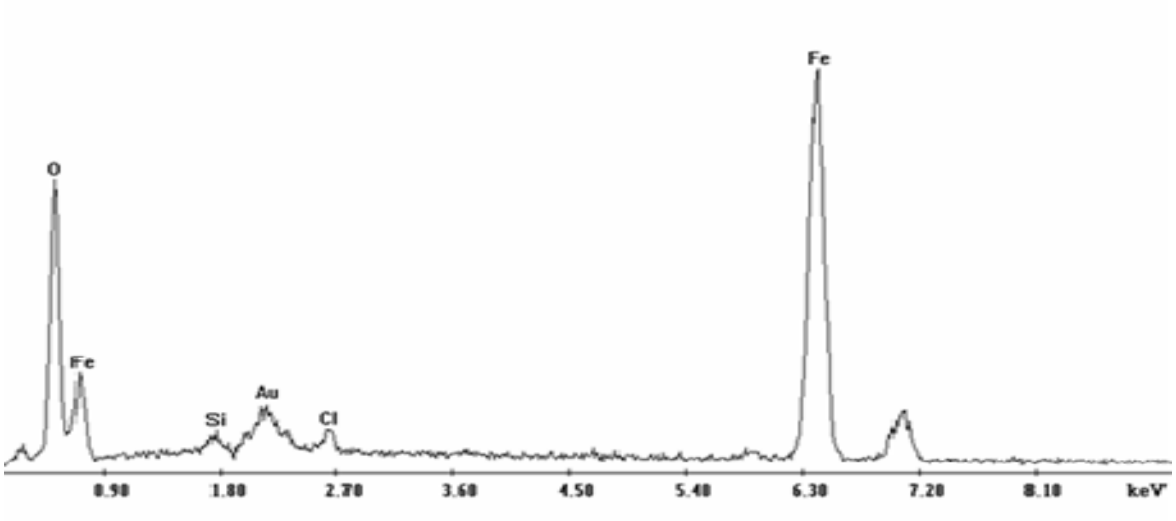

(c) Composition on the coupon surface

Figure 4-33: 3-month test in the untreated Qurrayah water at 37 ºC (SEM and EDS analysis of coupon surface before acid cleaning)

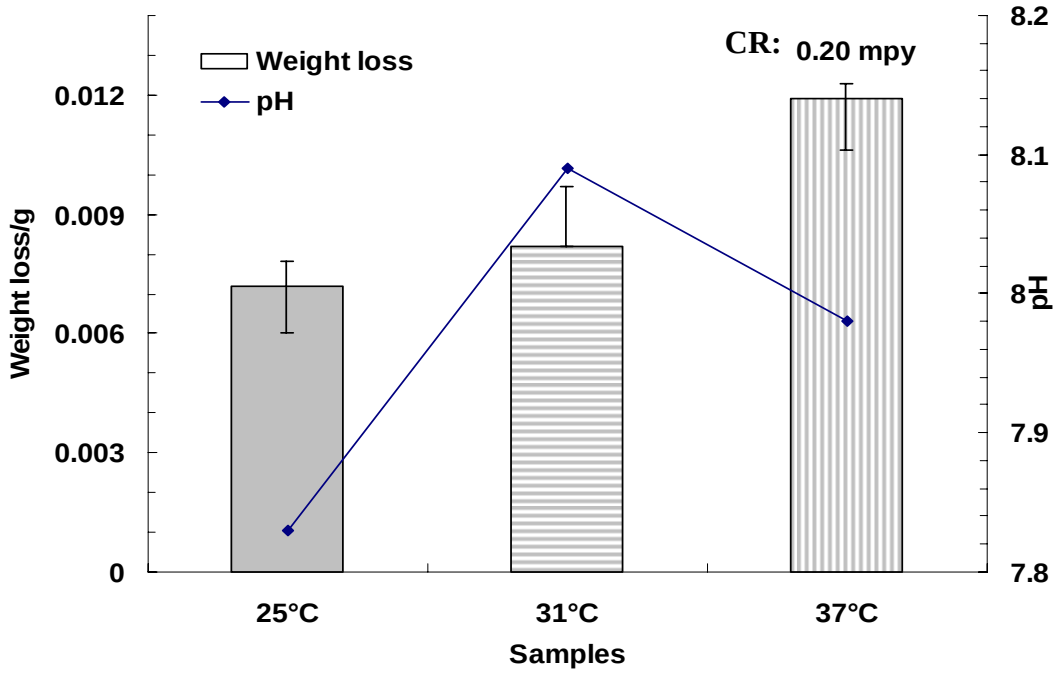

Figure 4-34: X65 coupon weight loss in the untreated Qurrayah water (seawater) after 3-month test

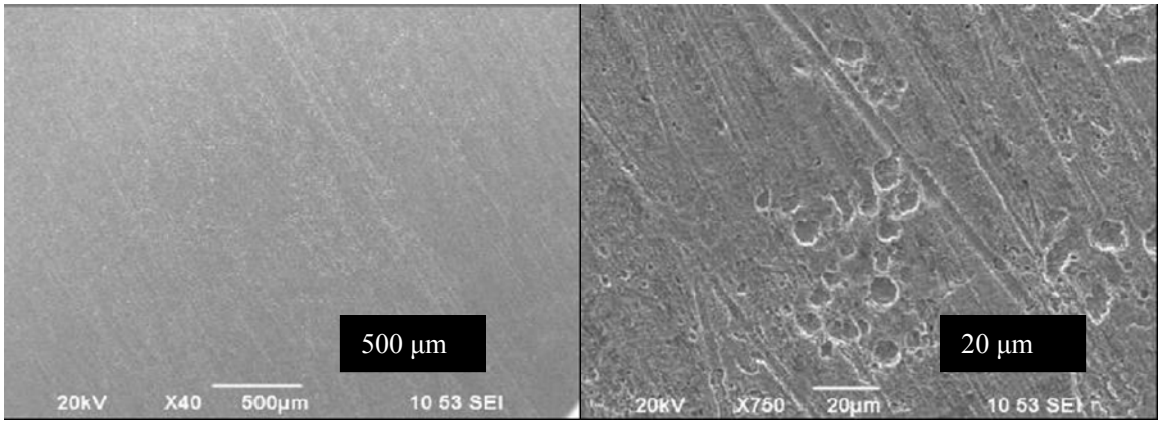

(a) SEM at 40X (b) SEM at 750X

Figure 4-35: 3-month test in the untreated Qurrayah water at 25 ºC (SEM analysis of coupon surface after acid cleaning)

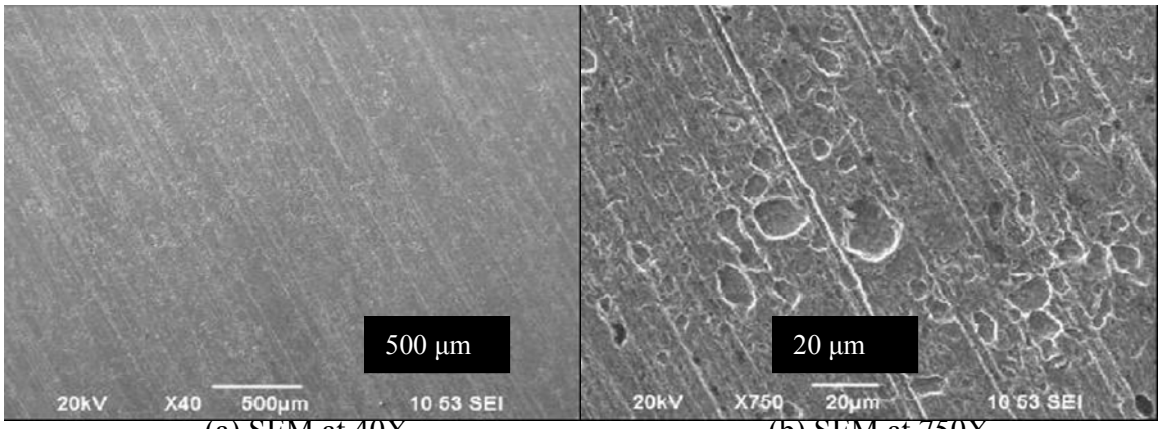

(a) SEM at 40X (b) SEM at 750X

Figure 4-36: 3-month test in the untreated Qurrayah water at 31 ºC (SEM analysis of coupon surface after acid cleaning)

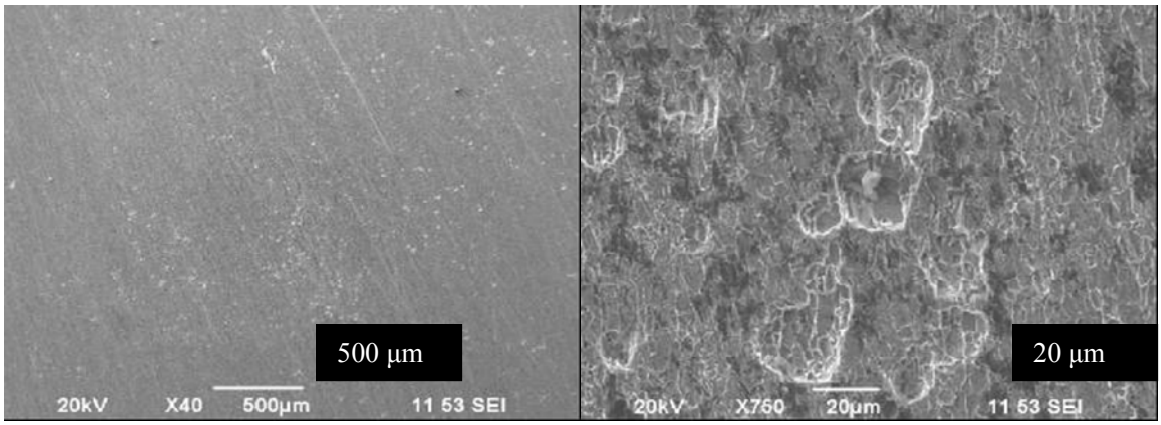

(a) SEM at 40X (b) SEM at 750X

Figure 4-37: 3-month test in the untreated Qurrayah water at 37 ºC (SEM analysis of coupon surface after acid cleaning)

By comparing the results of tests in the untreated Wasia water and untreated Qurrayah water, corrosion rates were comparable at the same temperature after the same test periods. In the tests with Qurrayah water, pits became evident with increased temperature and time. Besides the possibility of MIC occurrence, the pit appearance can be explained by the presence of high concentration of Cl and the mechanism of under-deposit corrosion, induced when the deposit formed on the coupon surface. While the available literature on marine corrosion always involves dissolved oxygen, to date there are no systematic studies in the literature on corrosion in deoxygenated well water or seawater.

4.4.2 SRB growth in enriched artificial seawater

Artificial seawater can be used to simulate natural seawater. The chemical composition of the artificial seawater (Instant Ocean) is similar to that of typical natural seawater (Table 4-3). Enriched artificial seawater (EASW) plays an important role for culturing microbies because it is easy to manipulate and control its chemical composition (Berges and Franklin, 2001). EASW has the advantage of simulating real conditions in mildly to heavily contaminated natural seawater. In the test using SA waters with SRB spiking, the planktonic SRB concentration remained constant and showed no growth. To promote SRB growth in artificial seawater, key nutrients were added to the artificial seawater. Table 4-4 shows the test matrix. For comparison, the same marine SRB strain was also cultured in full nutrient medium at 37ºC. The recipe for that culture medium is shown in Table 4-5. Figure 4-38 shows how temperature affects SRB growth, where 37ºC

is the optimum growth temperature for the lab strain used (*Desulfovibrio desulfuricans subsp. aestuarii*, ATCC 14563). Compared to the full nutrient medium (Table 4-5), the enriched artificial seawater with limited nutrients is an acceptable environment for SRB growth, especially at 37ºC, and those added chemicals provided adequate nutrients for SRB growth.

Table 4-3: Major element comparison between natural seawater and Instant Ocean®*

	Salinity (1000 ppm)	Na^+	Mg^{2+}	Ca^{2+}	K^+	Sr^{2+}	Cl^-	SO_4^{2-}	BO_3^{3-}	CO_3^{2-} HCO_3^-
Seawater	35	470	53	10.3	10.2	0.09	550	28	0.42	1.90
Instant Ocean®	29.65	462	52	9	9.4	0.19	521	23	0.44	1.90

*All in millimoles per kilogram, except salinity. (Instant Ocean® is a registered trademark of Aquarium Systems, Inc.)

Table 4-4: Test matrix for SRB growth in enriched artificial seawater

	Test conditions
SRB strain	*Desulfovibrio desulfuricans subsp. aestuarii* - ATCC 14563
Culture medium	Artificial seawater enriched with 1g/L yeast extract, 3.5g/L sodium lactate and 200ppm F^{2+}
Test temperature (ºC)	10, 25, 37

Table 4-5: 1250 modified Baar's medium used for cultivation of marine SRB

Component I		Component II		Component III		Component IV
$MgSO_4$	2.0g	K_2HPO_4	0.5g	Sodium Lactate	3.5g	See below*
Sodium Citrate	5.0g	Distilled water	200ml	Yeast Extract	1.0g	
$CaSO_4$	1.0g			Distilled water	400ml	
NH_4Cl	1.0g					
NaCl	25g					
Distilled water	400ml					

*Filter-sterilized 5%wt ferrous ammonium sulfate. Add 0.1 ml of this solution to 5.0 ml of medium prior to inoculation.

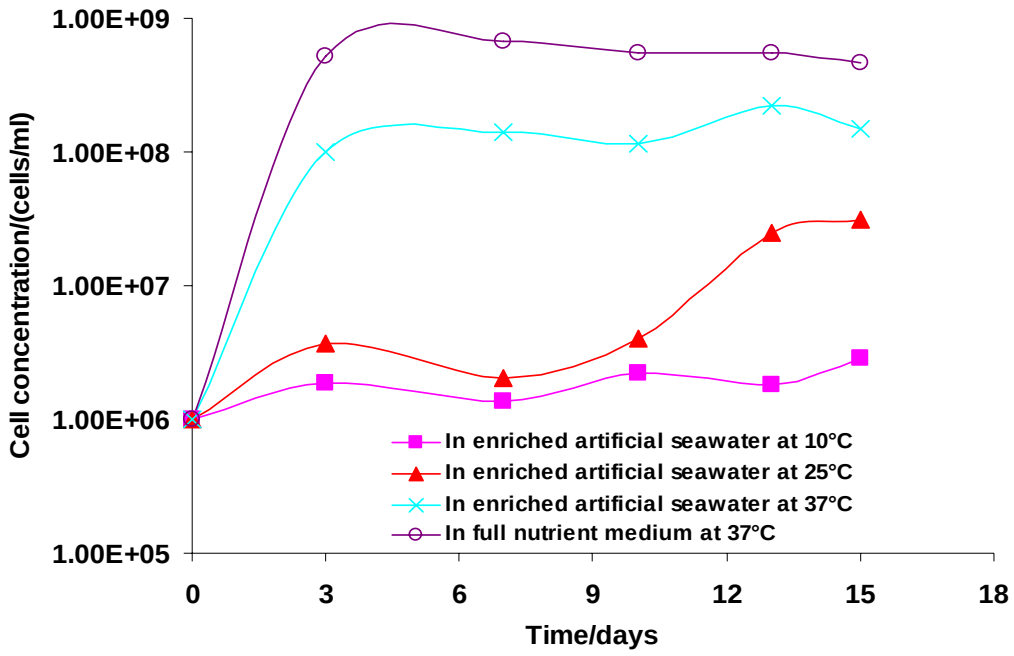

Figure 4-38: SRB growth in enriched artificial seawater and full nutrient medium at different temperatures

4.4.3 Tests using enriched SA waters spiked with SRB

4.4.3.1 Tests conditions and analytical methods

These tests were performed to simulate hydrotesting cases using contaminated water containing SRB. These tests present the worst-case scenario. Two water samples (Wasia well water and Qurrayah seawater) were from SA. Table 4-6 and Table 4-7 show the test matrix. L(+)−cysteine was used as the oxygen scavenger causing the oxygen concentration in the anaerobic vials to be below 40 ppb when the test was completed. Cysteine was used to eliminate the small amount of oxygen that leaked into vials during longer periods.

Table 4-6: Test matrix using enriched SA waters

Test conditions	
Test media	Wasia water (well water) & Qurrayah water (seawater)
Oxygen scavenger	100 ppm in each medium
Nutrients	60% w/w Sodium lactate (1.5ml/L); Fe^{2+} (10ppm)
SRB strain	*Desulfovibrio desulfuricans subsp. aestuarii* - ATCC 14563 (marine SRB)
Initial SRB (marine strain) concentration (cells/ml)	1000
Specimen	X65 gum-shaped carbon steel
Test temperature (ºC)	25, 31, 37
Test period	2 weeks, 1 month, 3 months

Table 4-7: Test matrix using enriched Qurrayah water

Test conditions	
Test media	Qurrayah water (seawater)
Oxygen scavenger	100 ppm
Nutrients	60% w/w Sodium lactate (1.5ml/L); Fe^{2}+ (10ppm)
SRB strain	*Desulfovibrio desulfuricans subsp. aestuarii* - ATCC 14563 (marine SRB)
Initial SRB (marine strain) concentration (cells/ml)	1000
Specimen	X65 gum-shaped carbon steel
Test temperature (ºC)	25, 31, 37
Test period	1 week, 2 weeks, 1 month

4.4.3.2 Test results

Part I: Tests using enriched Wasia water (well water) spiked with SRB

In this two-week test, the test vials remained clear during the test period, which indicated that spiked SRB did not grow, and no biofilms or bacteria were found on the coupon surface (Figure 4-39 ~ Figure 4-41). Compared to the previous tests using untreated SA waters, the SEM and EDS analysis of coupon surfaces (see Figure 4-39) looked similar. Figure 4-42 shows that weight loss there was only slight weight loss with the increase of temperature and no pits were observed on the coupon surfaces for this test after cleaning (Figure 4-43 and Figure 4-44).

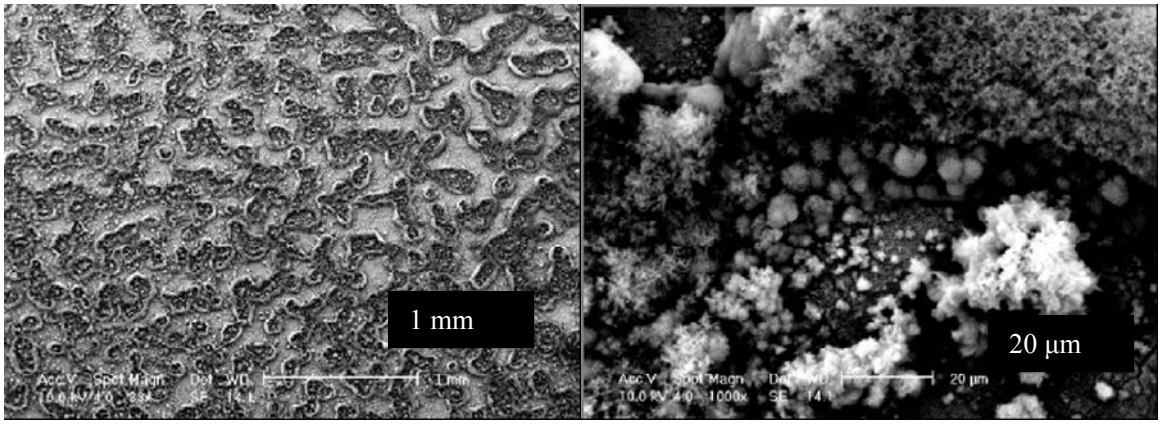

(a) SEM at 33X (b) SEM at 1000X

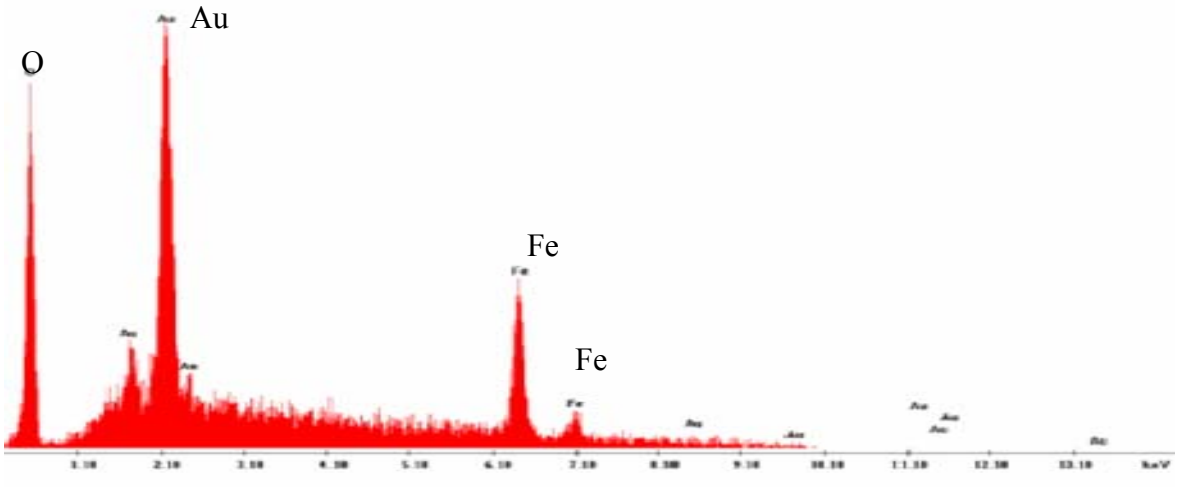

(c) Composition on the coupon surface

Figure 4-39: 2-week test in the enriched Wasia water spiked with SRB at 25 ºC (SEM and EDS analysis of coupon surface before acid cleaning)

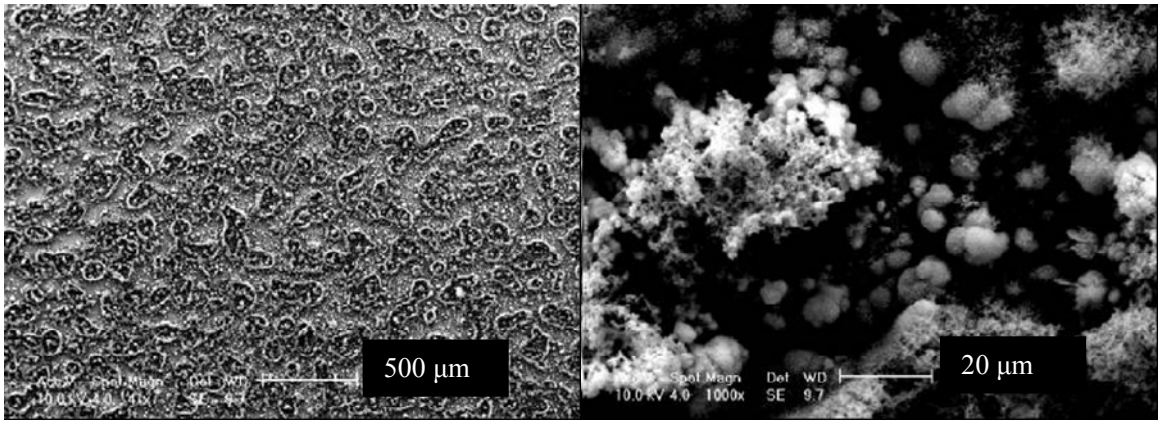

(a) SEM at 41X (b) SEM at 1000X

Figure 4-40: 2-week test in the enriched Wasia water spiked with SRB at 31 ºC (SEM analysis of coupon surface before acid cleaning)

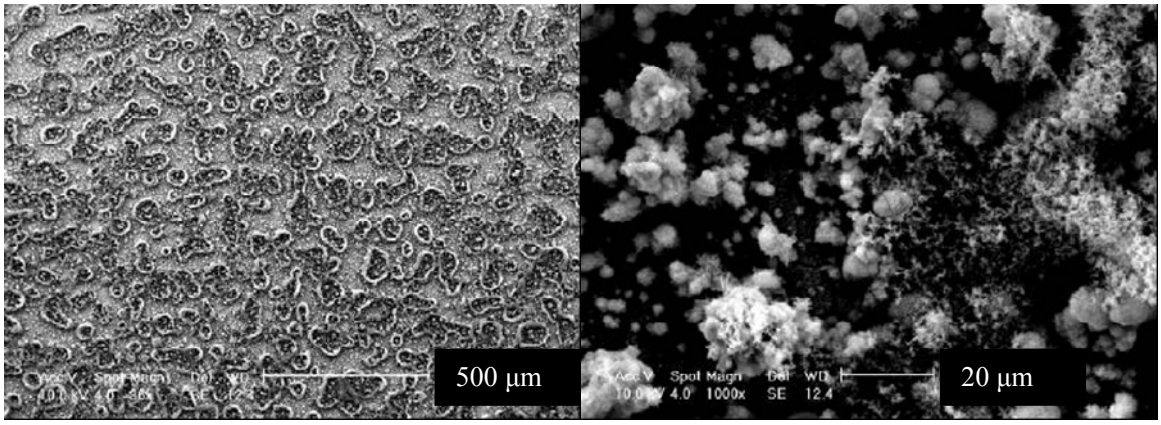

(a) SEM at 36X (b) SEM at 1000X

Figure 4-41: 2-week test in the enriched Wasia water spiked with SRB at 37 ºC (SEM analysis of coupon surface before acid cleaning)

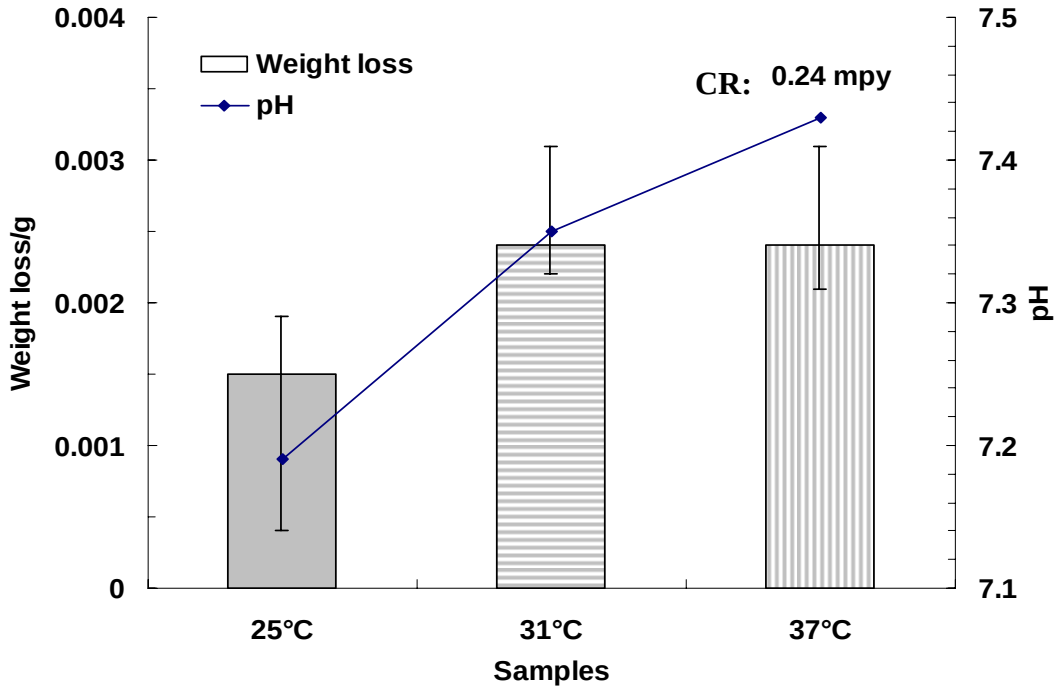

Figure 4-42: X65 coupon weight loss in the enriched Wasia water (well water) spiked with SRB after 2-week test

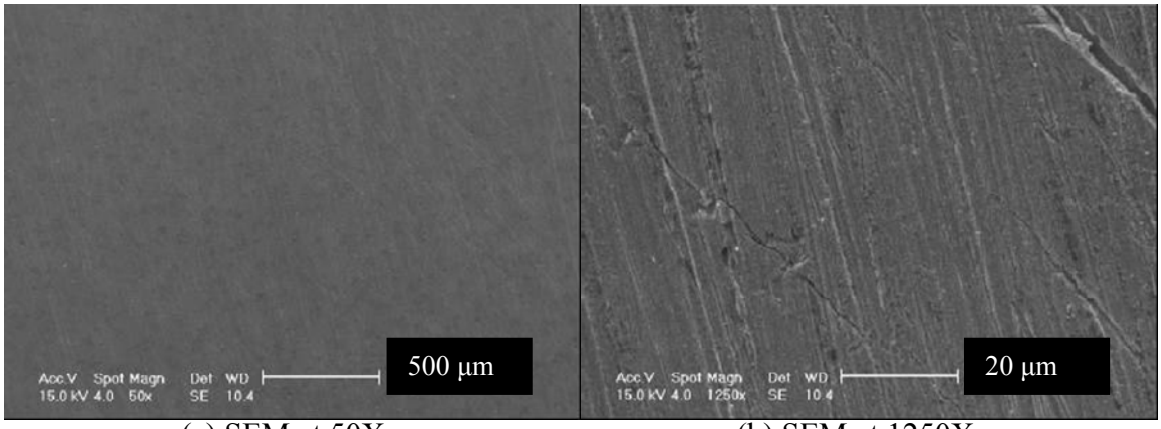

(a) SEM at 50X (b) SEM at 1250X

Figure 4-43: 2-week test in the enriched Wasia water spiked with SRB at 25 ºC (SEM analysis of coupon surface after acid cleaning)

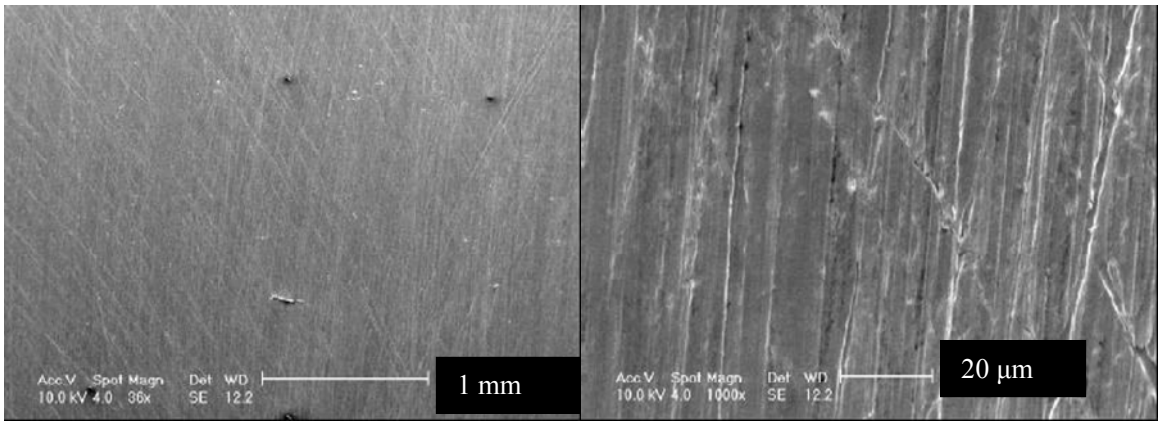

(a) SEM at 36X (b) SEM at 1000X

Figure 4-44: 2-week test in the enriched Wasia water spiked with SRB at 37 ºC (SEM analysis of coupon surface after acid cleaning)

In this one-month test, the coupon surfaces resembled those in the two-week test above. No bacteria or elemental S was found on the coupon surfaces (Figure 4-45 and Figure 4-46). Figure 4-47 shows an increase of weight loss with the increase of temperature, but no pits were detected in this test (Figure 4-48 and Figure 4-49).

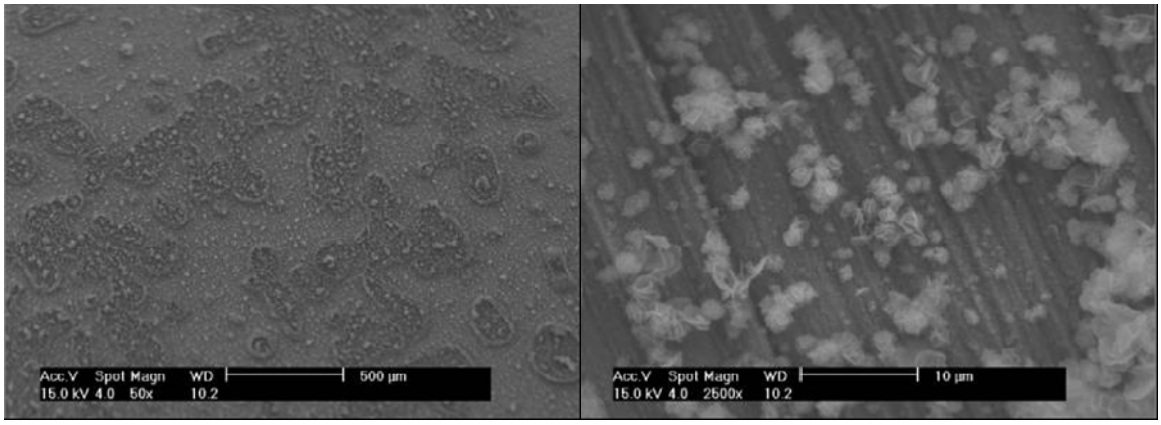

(a) SEM at 50X (b) SEM at 2500X

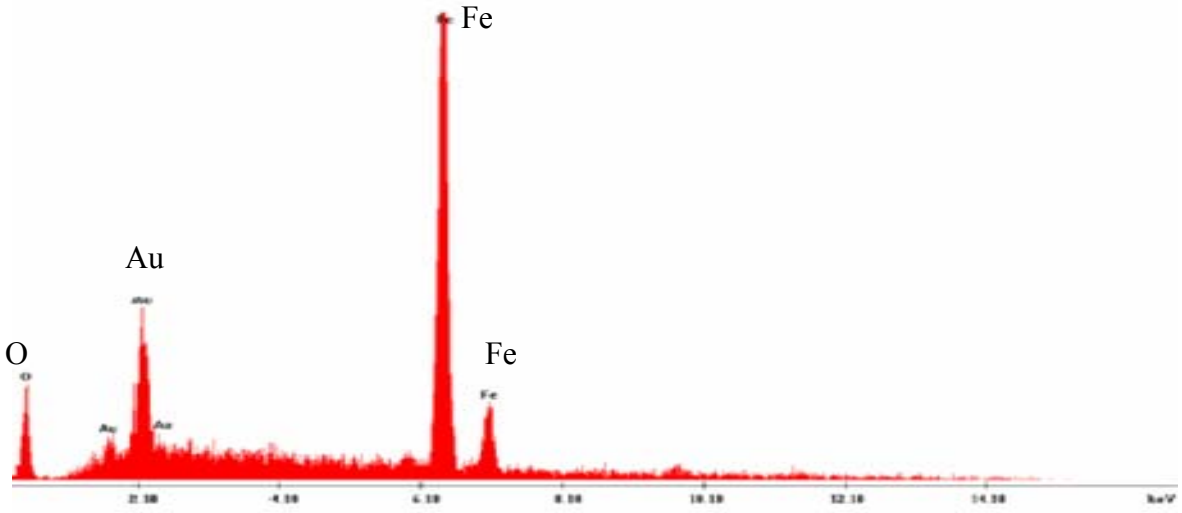

(c) Composition on the coupon surface

Figure 4-45: 1-month test in the enriched Wasia water spiked with SRB at 25 ºC (SEM and EDS analysis of coupon surface before acid cleaning)

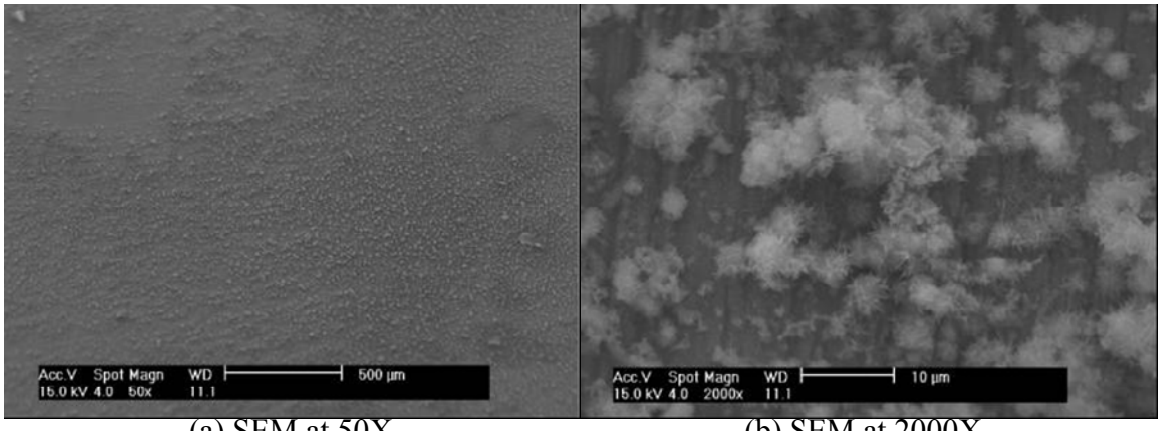

(a) SEM at 50X (b) SEM at 2000X

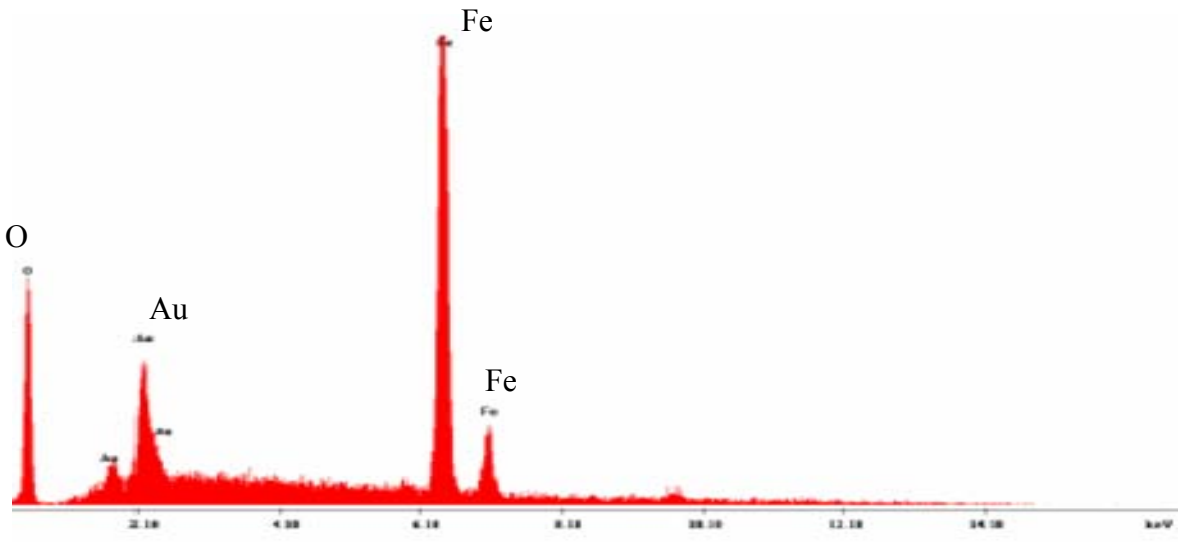

(c) Composition on the coupon surface

Figure 4-46: 1-month test in the enriched Wasia water spiked with SRB at 37 ºC (SEM and EDS analysis of coupon surface before acid cleaning)

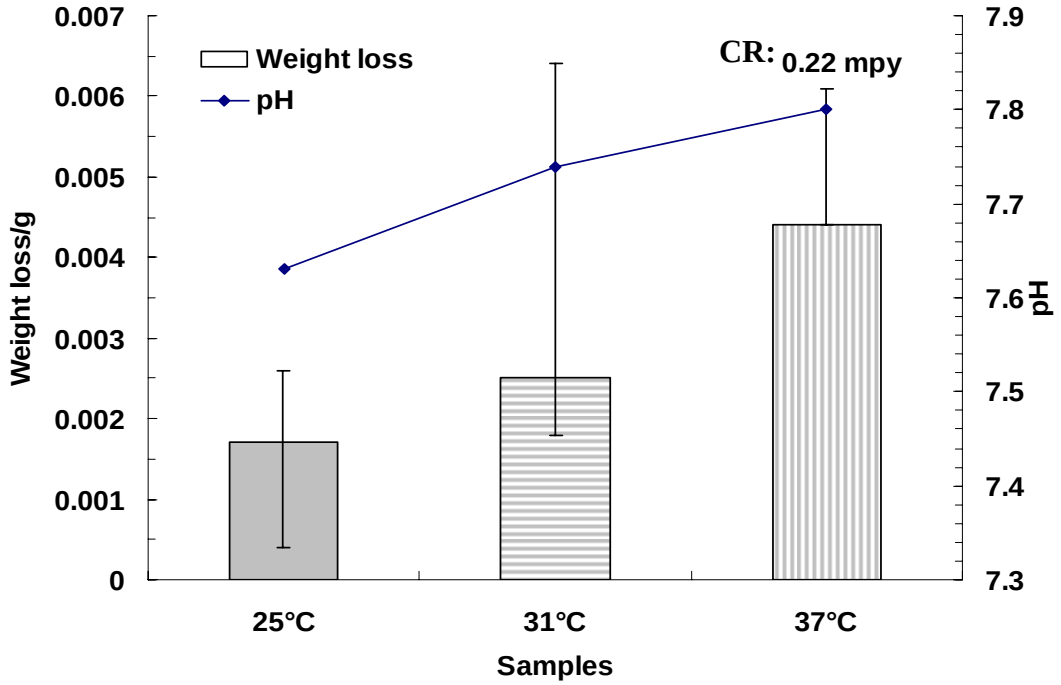

Figure 4-47: X65 coupon weight loss in the enriched Wasia water (well water) spiked with SRB after 1-month test

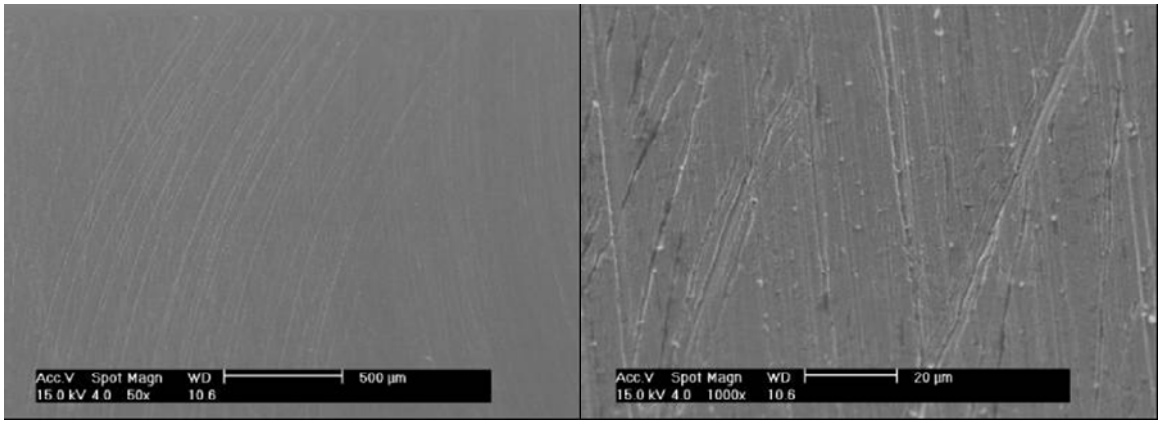

(a) SEM at 50X (b) SEM at 1000X

Figure 4-48: 1-month test in the enriched Wasia water spiked with SRB at 25 ºC (SEM analysis of coupon surface after acid cleaning)

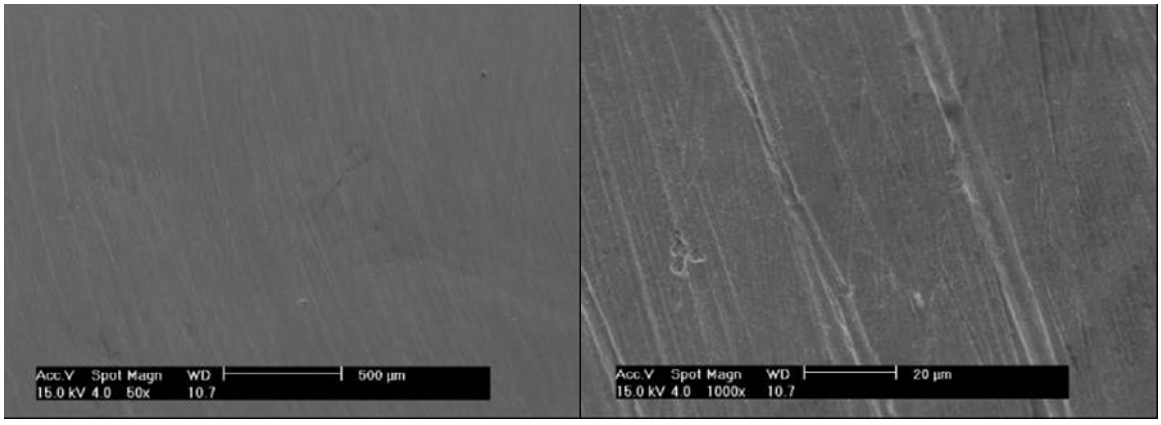

(a) SEM at 50X (b) SEM at 1000X

Figure 4-49: 1-month test in the enriched Wasia water spiked with SRB at 37 ºC (SEM analysis of coupon surface after acid cleaning)

In this three-month test, all the coupons were covered with a dense layer of film and SRB cells were observed individually embedded between the particulate matters (Figure 4-50, Figure 4-51 and Figure 4-53). There was one exception which was a duplicate test Sample #2 at 31ºC where the surface was covered with a patchy mineral film and without bacteria (Figure 4-52). Those individual cells seen in Figure 4-50,

Figure 4-51 and Figure 4-52 may be planktonic cells deposited on the surface or sessile cells that attached on the surface, but had not yet formed colonies. From the EDS spectra, elemental S was found in all the tests (Figure 4-50 (c), Figure 4-51 (c) and Figure 4-53 (c)) where SRB cells were also present except for the duplicate Sample #2 at 31ºC mentioned above (Figure 4-52 (c)). The results showed that the dense layer formed on the coupon surface may be FeS produced by SRB.

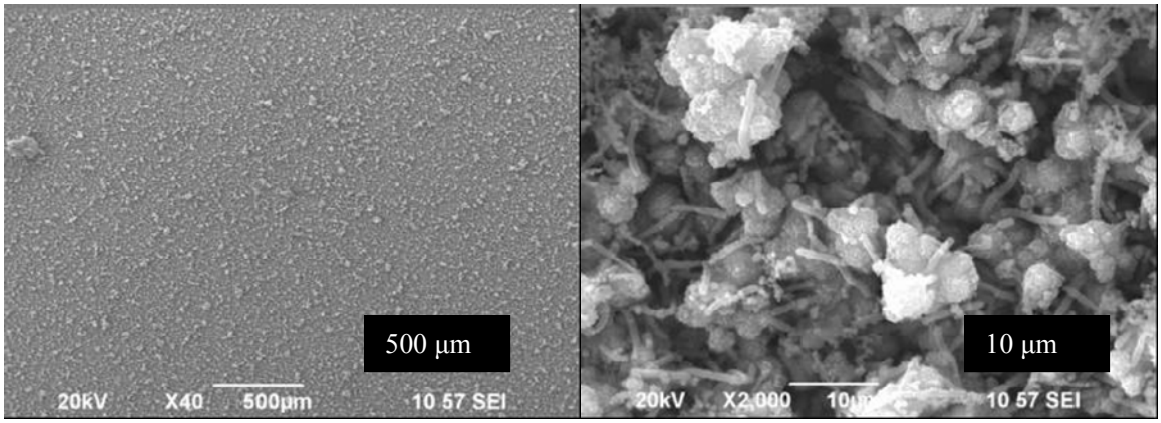

(a) SEM at 40X (b) SEM at 750X

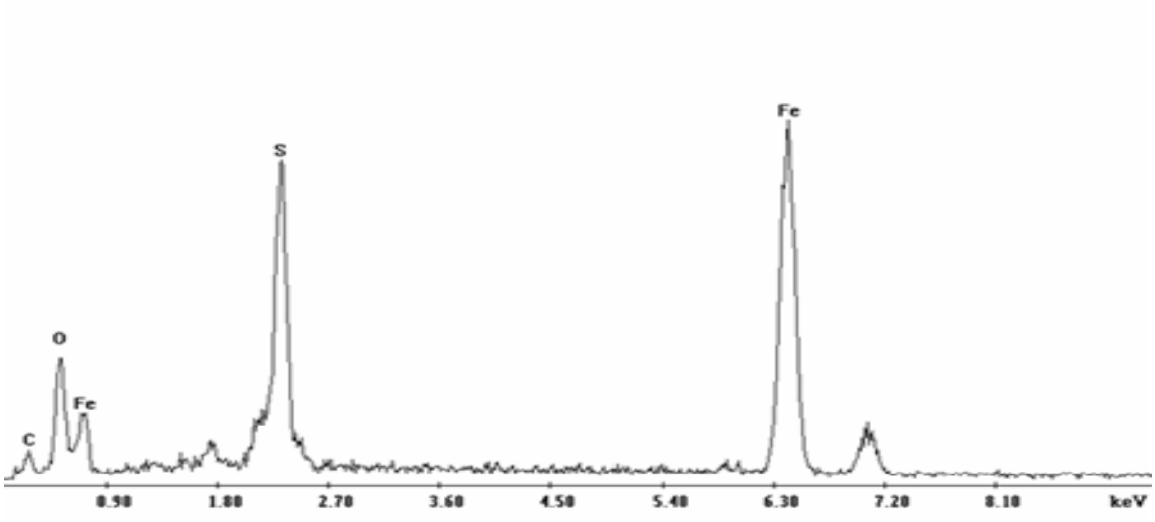

(c) Composition on the coupon surface

Figure 4-50: 3-month test in the enriched Wasia water spiked with SRB at 25 ºC (SEM and EDS analysis of coupon surface before acid cleaning)

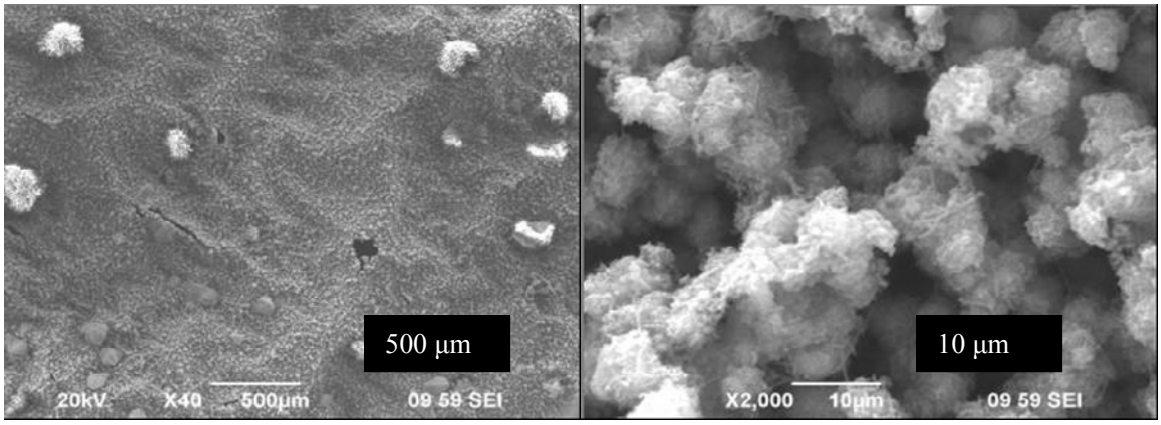

(a) SEM at 40X (b) SEM at 2000X

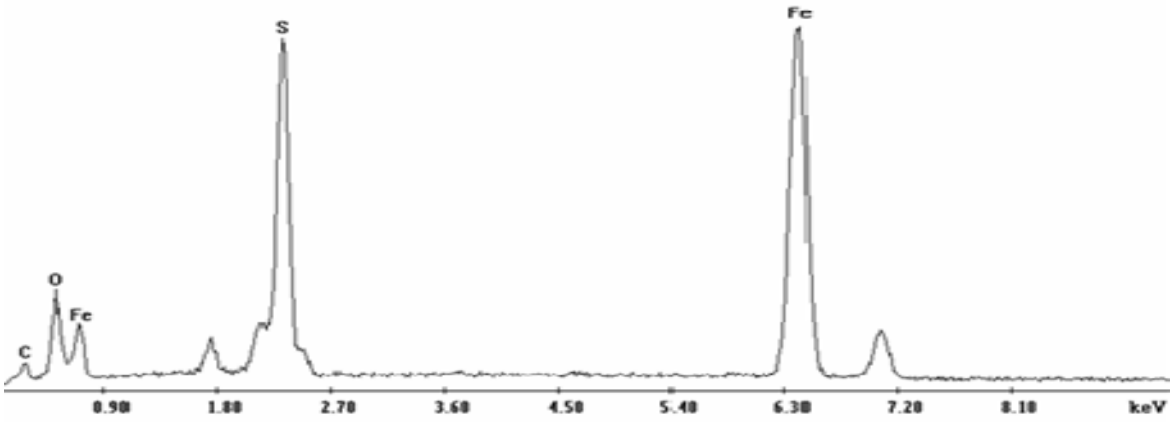

(c) Composition on the coupon surface

Figure 4-51: 3-month test in the enriched Wasia water spiked with SRB at 31 ºC (SEM and EDS analysis of coupon surface before acid cleaning; sample #1)

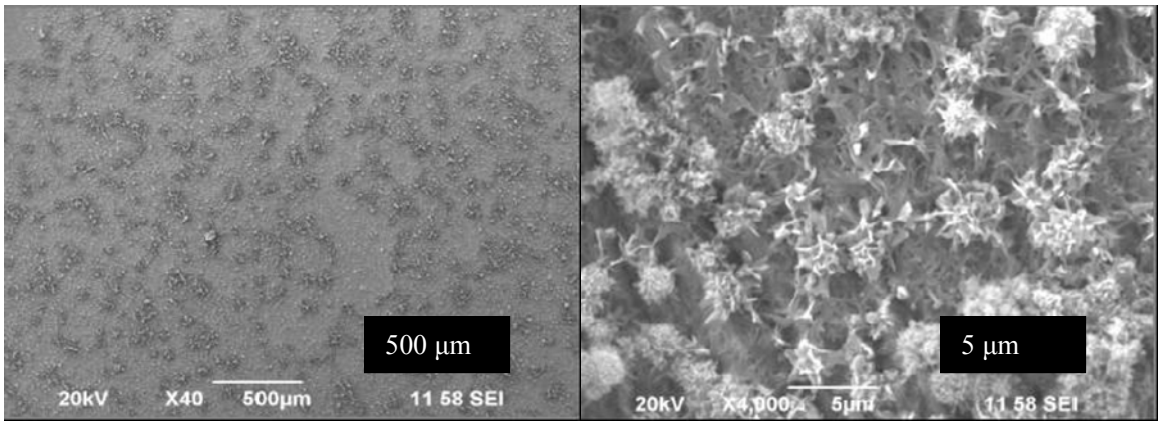

(a) SEM at 40X (b) SEM at 4000X

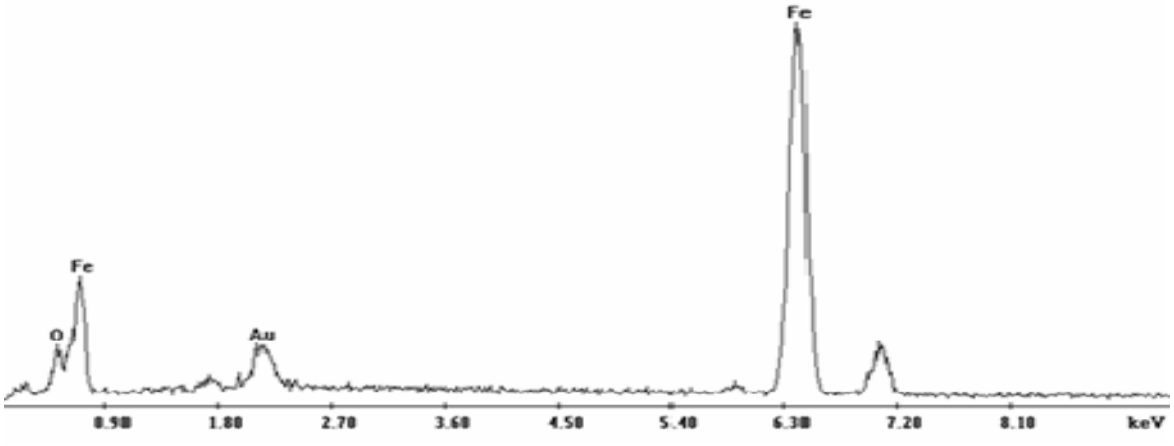

(c) Composition on the coupon surface

Figure 4-52: 3-month test in the enriched Wasia water spiked with SRB at 31 ºC (SEM and EDS analysis of coupon surface before acid cleaning; sample #2-duplicate sample as sample #1 in Figure 4-51)

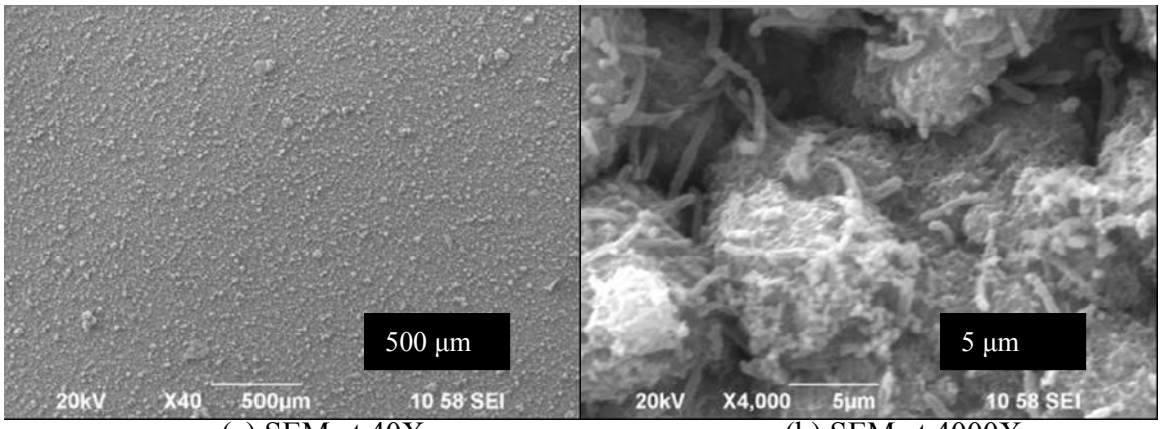

(a) SEM at 40X (b) SEM at 4000X

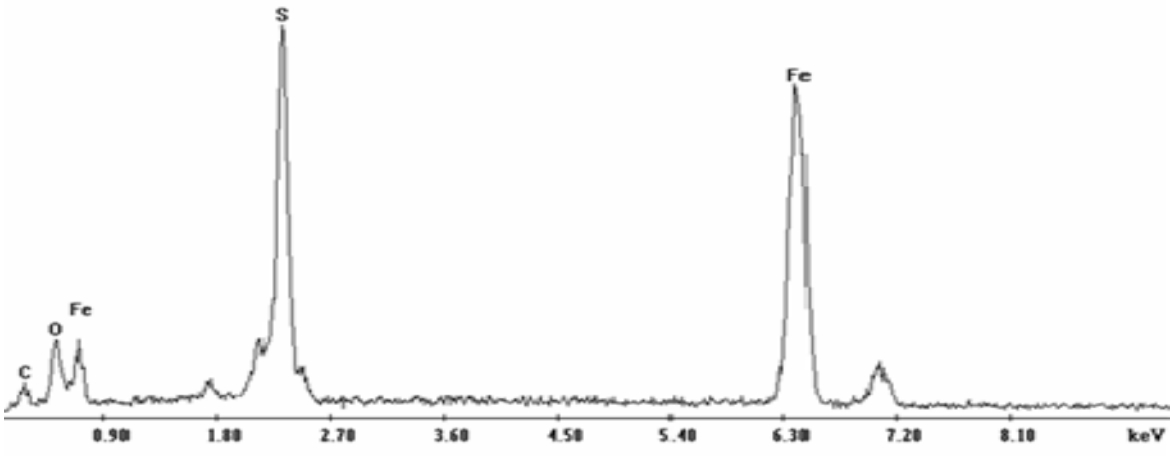

(c) Composition on the coupon surface

Figure 4-53: 3-month test in the enriched Wasia water spiked with SRB at 37 ºC (SEM and EDS analysis of coupon surface before acid cleaning)

Instead of corrosion rate, the pitting rates of all the samples were obtained in this test. Figure 4-54 shows there was no obvious trend in weight loss change with the increase of temperature, but with comparison to previous uniform corrosion rate (CR), MIC caused pitting rate (PR) is quite large (1.42 mm/yr). The coupon surfaces showed different corrosion patterns after cleaning: at 25ºC, deep pits were found (Figure 4-55); at 31ºC, a peculiar corrosion pattern was observed (Figure 4-56) while the Sample #2 surface appeared smoother (Figure 4-57); at 37ºC, a scattering of large round coarse spots were found (Figure 4-58).

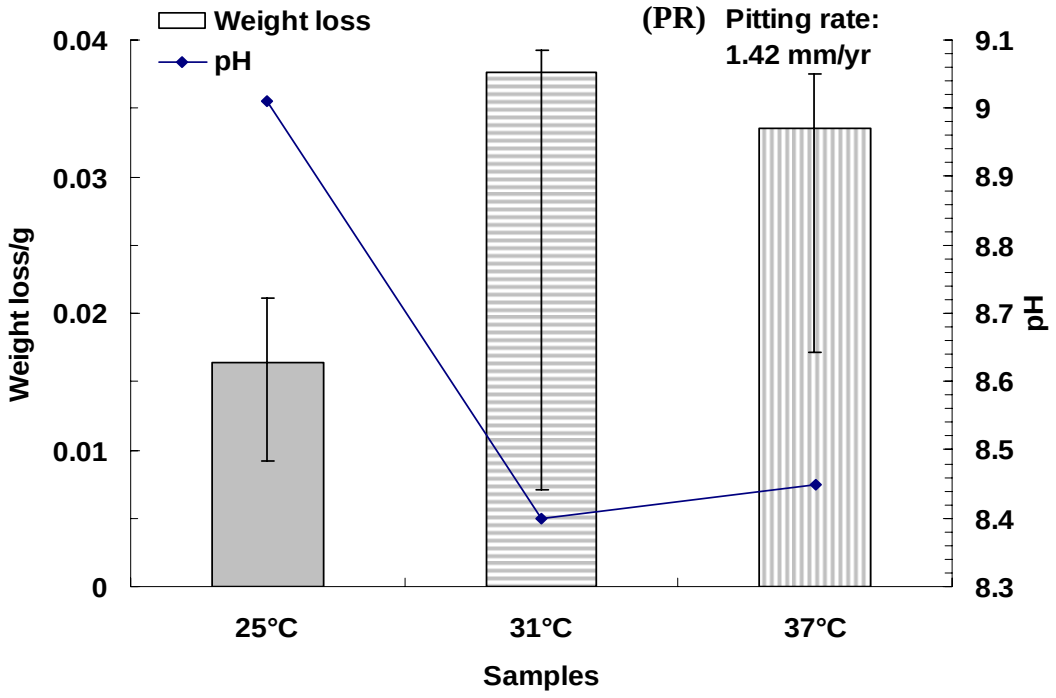

Figure 4-54: X65 coupon weight loss and pitting rate in the enriched Wasia water (well water) spiked with SRB after the 3-month test

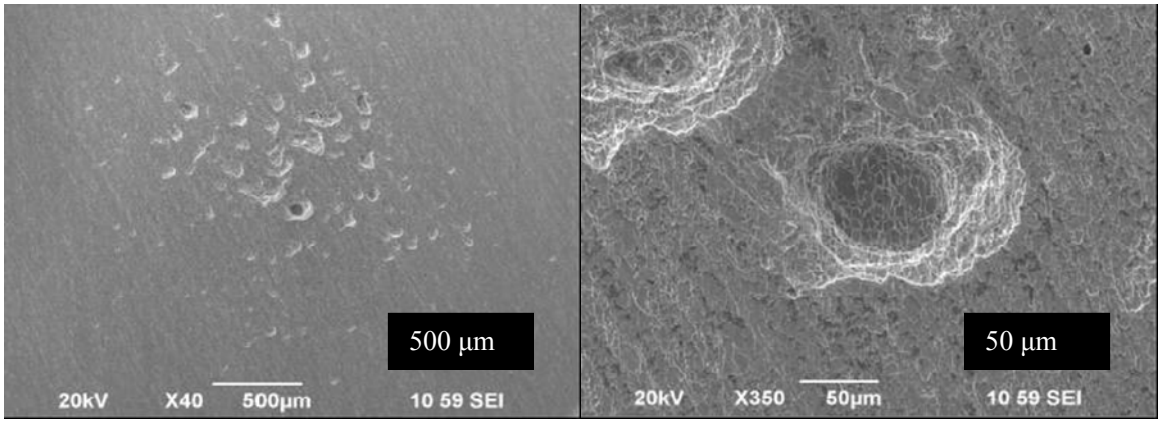

Figure 4-55: 3-month test in the enriched Wasia water spiked with SRB at 25 ºC (SEM analysis of coupon surface after acid cleaning)

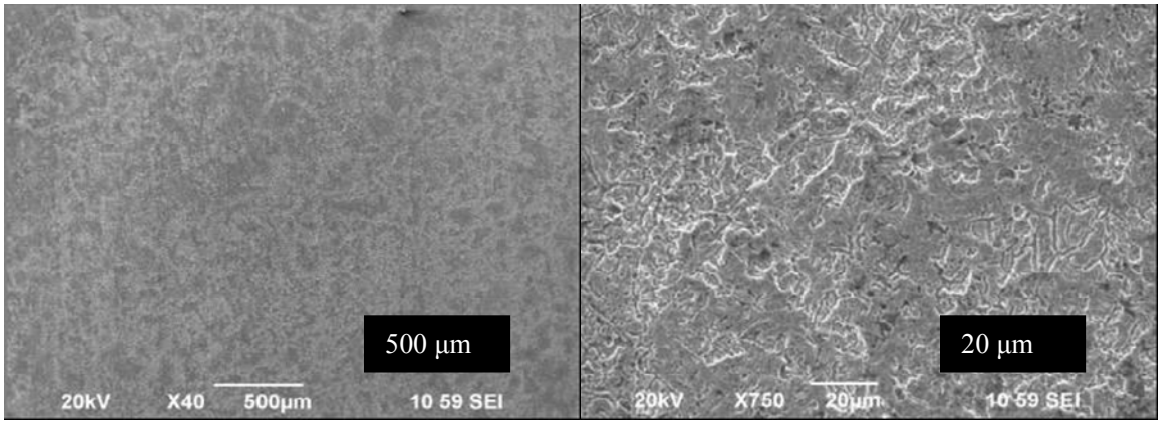

(a) SEM at 40X (b) SEM at 750X

Figure 4-56: 3-month test in the enriched Wasia water spiked with SRB at 31 ºC (SEM analysis of coupon surface after acid cleaning; sample #1)

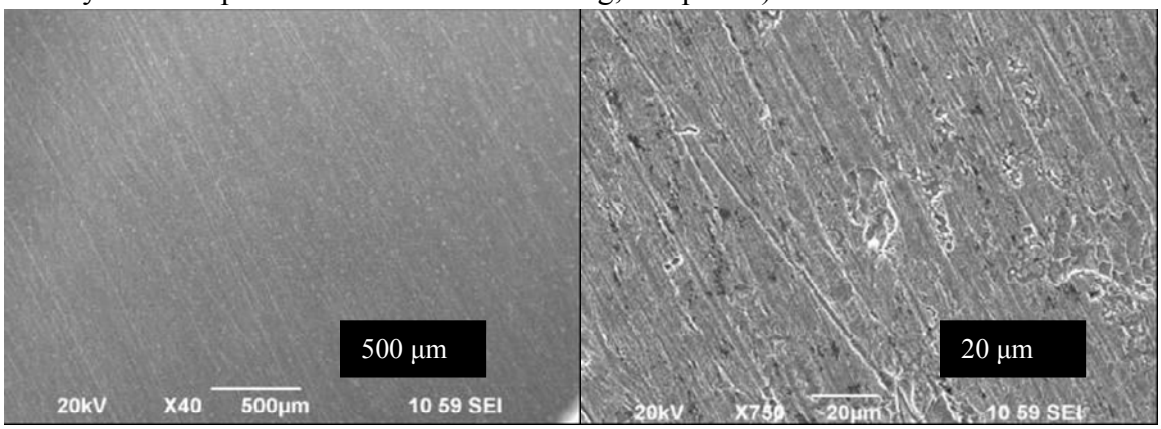

(a) SEM at 40X (b) SEM at 750X

Figure 4-57: 3-month test in the enriched Wasia water spiked with SRB at 31 ºC (SEM analysis of coupon surface after acid cleaning; sample #2–duplicate sample as sample #1 in Figure 4-56)

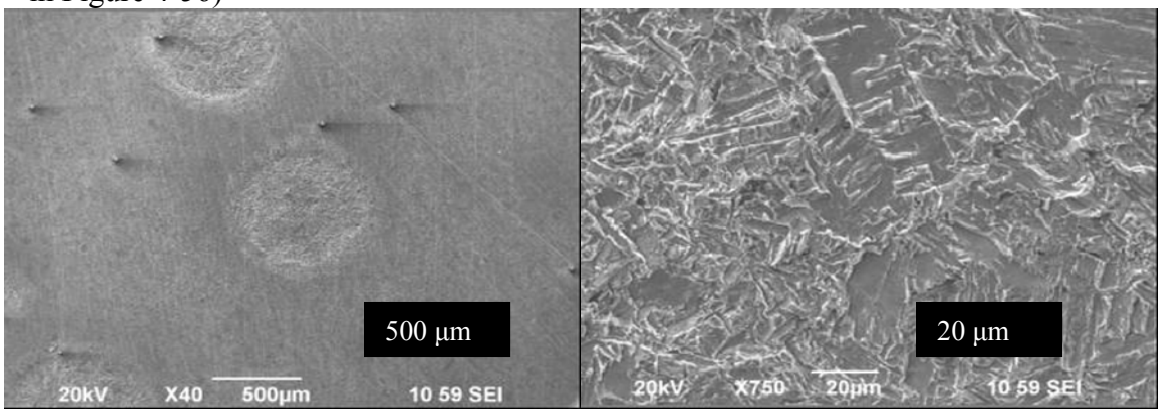

(a) SEM at 40X (b) SEM at 750X

Figure 4-58: 3-month test in the enriched Wasia water spiked with SRB at 37 ºC (SEM analysis of coupon surface after acid cleaning)

The morphology of these surfaces is consistent with what was typically seen in other tests when SRB biofilms were grown on coupons in vials. They were quite different from the pits shown earlier when SRB spiking was not used (refer to Figure 4-17 in Part I in Section 4.4.1.2). It was found that the corrosion rates in the tests using untreated and enriched Wasia water were all comparable with one exception−the three-month test when corrosion rates using enriched Wasia water with SRB spiking were roughly two times higher indicating that spiked SRB could facilitate corrosion over a long period.

Part II: Tests using enriched Qurrayah water (seawater) spiked with SRB

Figure 4-59 shows the vials in the tests using untreated (no nutrient supplement) and enriched Qurrayah water. The test vials using enriched Qurrayah water with SRB spiking turned black and had a strong H_2S smell when opened while the test using untreated Qurrayah water did not.

Figure 4-59: Test in the Qurrayah water (seawater) with and without SRB (2 clear vials are at the condition of untreated Qurrayah water without SRB, and 2 black vials are at the condition of enriched Qurrayah water with SRB.)

i: Tests in lasting two-week, one-month and three-month

In the two-week test, weight loss, corrosion rate (CR)/pitting rate (PR), pH and planktonic SRB concentration of each sample at three test temperatures were obtained after the test was terminated (see Figure 4-60). Corrosion rates were obtained from the samples #1-3, sample #5 and samples #8-9, and pitting rates were obtained from the samples #4, and samples #6-7. Figure 4-60 shows that pitting rate is extremely larger than uniform corrosion rate.

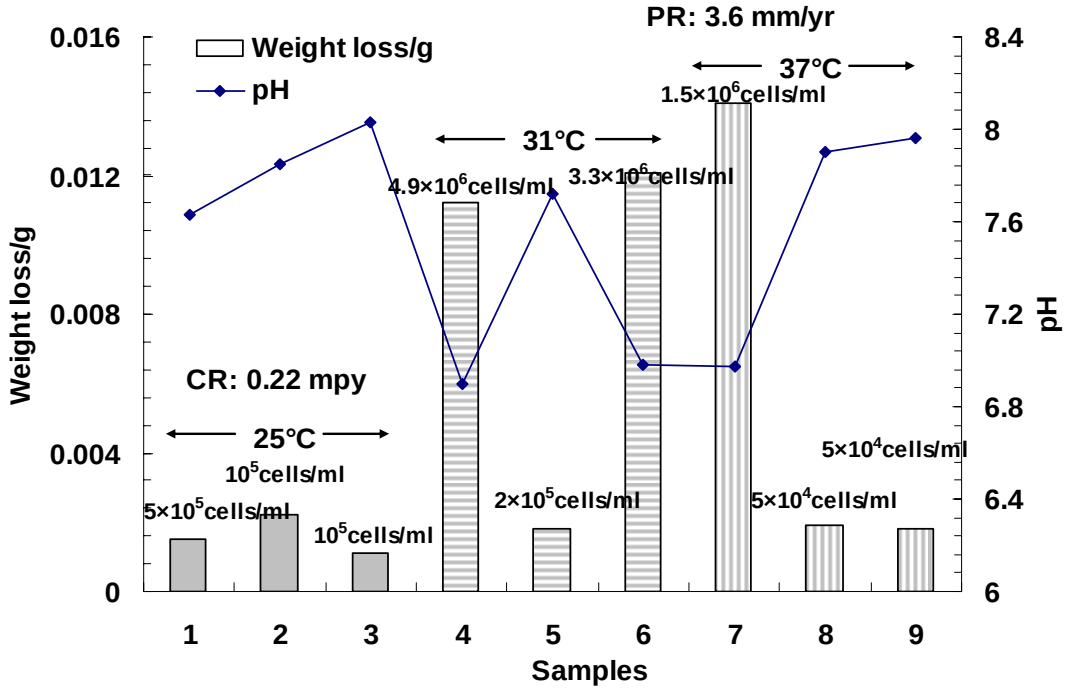

Figure 4-60: X65 coupon weight loss in the enriched Qurrayah water (seawater) spiked with SRB after the 2-week test (Planktonic SRB concentration was obtained when the test was terminated. #1-#3 are duplicate samples at 25°C. #4-#6 are duplicate samples at 31°C. #7-#9 are duplicate samples at 37°C.)

Figure 4-61 and Figure 4-62 show the coupon surfaces of duplicate samples #1 and #2 at 25ºC where no biofilms or bacteria were found. The EDS images show no elemental S (Figure 4-61 (c) and Figure 4-62 (c). At the test temperature 31ºC, no biofilms or bacteria were found on the coupon surfaces of duplicate samples #4 and #5 (Figure 4-63 and Figure 4-64). EDS detected S on sample #4 (Figure 4-63 (c)). However, S was not found on the surface of duplicate sample #5 (Figure 4-64 (c)). At the test temperature 37ºC, the same phenomenon occurred: no SRB were found on either sample surface (Figure 4-65 and Figure 4-66), and S was found on sample #7 (Figure 4-65 (c)) but not on the duplicate sample #8 (Figure 4-66 (c)).

The coupon surfaces of the three other samples at each test temperature after coupon surface cleaning show no pits or corrosion patterns (Figure 4-67 ~ Figure 4-69). In comparing the data shown in Figure 4-60 with the coupon surfaces before they were cleaned, it was found that the pH of the samples was lower when S was found on their surfaces (Samples #4 and #7, refer to Figure 4-63 and Figure 4-65, respectively), and consequently, the weight losses were larger than the other samples without S on the surfaces (refer to Samples #1, #2, #5 and #8). SRB are capable of reducing sulfate to sulfide, which can decrease pH by producing H_2S. The FeS formed on the coupon surface could have resulted from deposit or solid reaction of S^{2-} with Fe^{2+}.

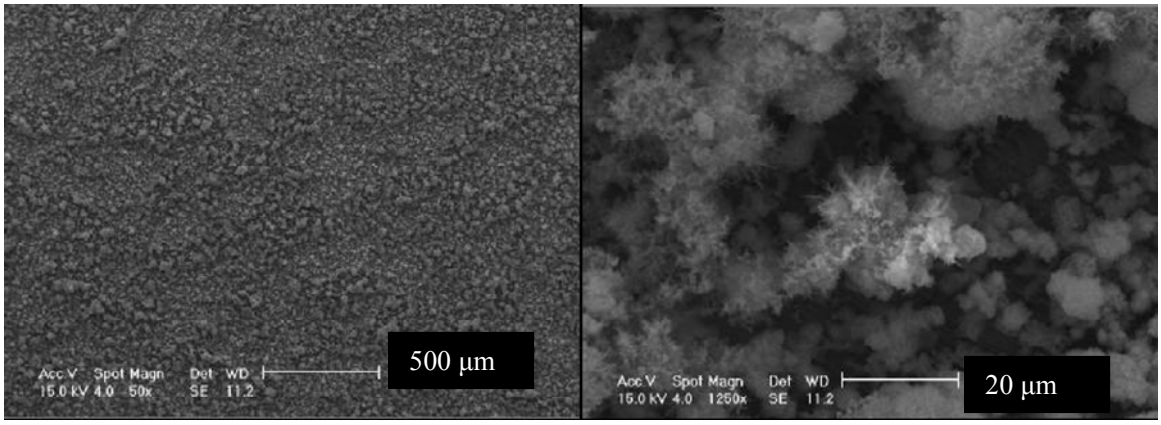

(a) SEM at 50X (b) SEM at 1250X

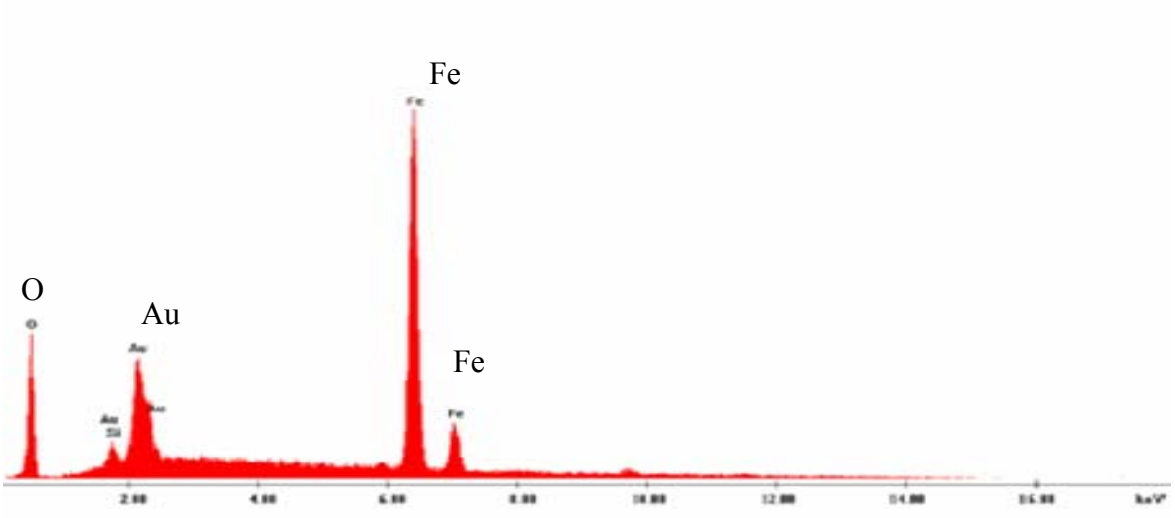

(c) Composition on the coupon surface

Figure 4-61: 2-week test in the enriched Qurrayah water spiked with SRB at 25 ºC (SEM and EDS analysis of coupon surface before acid cleaning; Sample #1 in Figure 4-60)

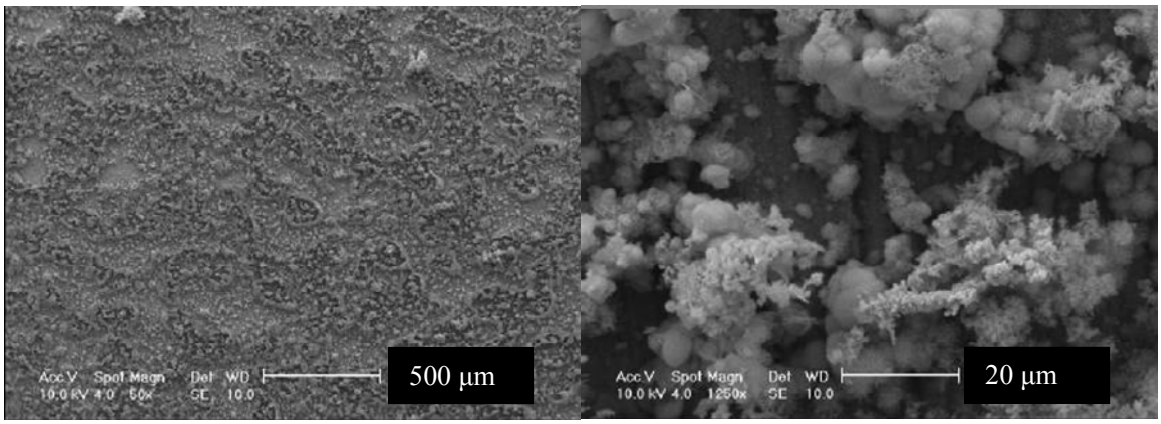

(a) SEM at 50X (b) SEM at 1250X

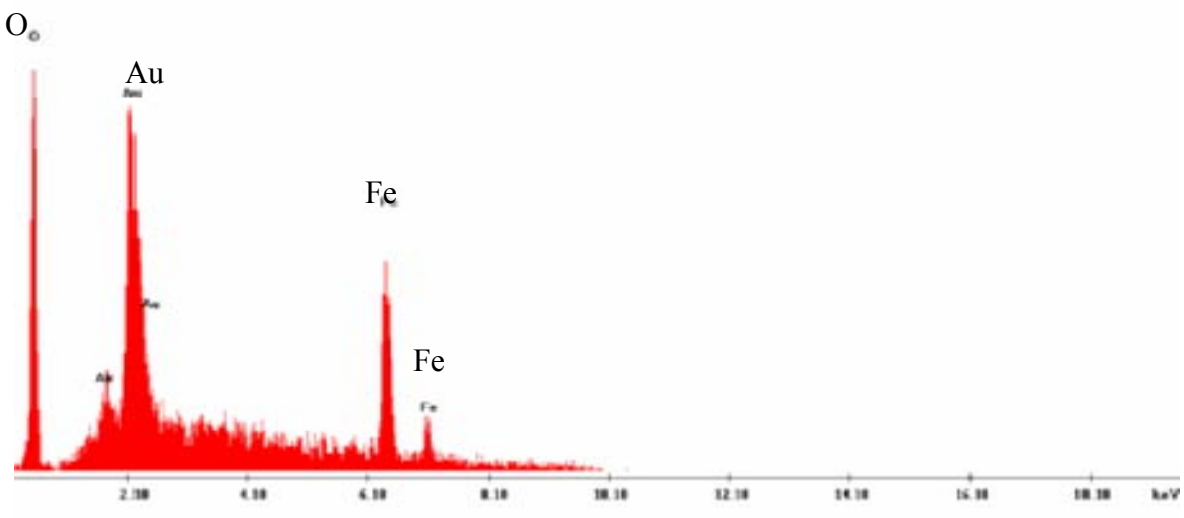

(c) Composition on the coupon surface

Figure 4-62: 2-week test in the enriched Qurrayah water spiked with SRB at 25 ºC (SEM and EDS analysis of coupon surface before acid cleaning; Sample #2 in Figure 4-60)

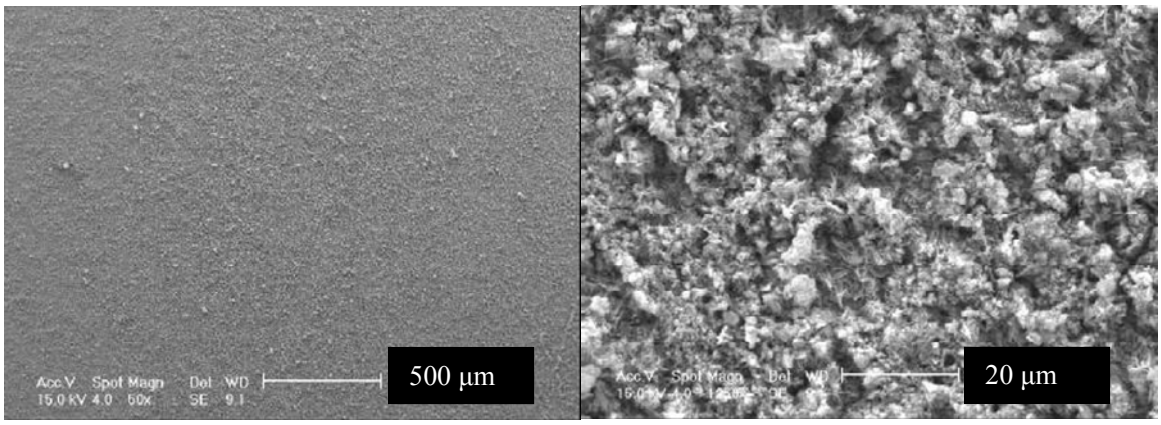

(a) SEM at 50X (b) SEM at 1250X

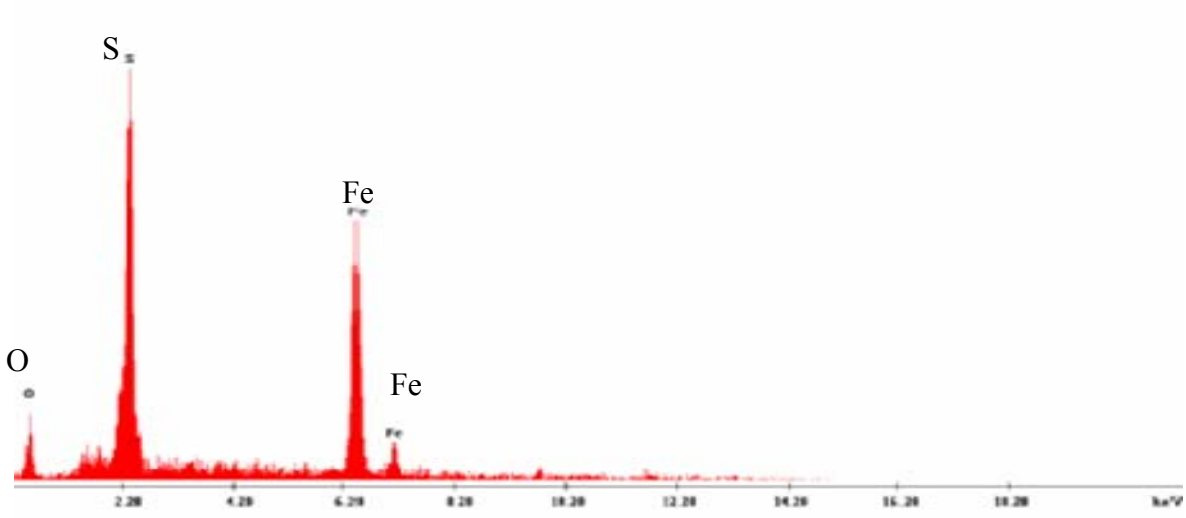

(c) Composition on the coupon surface

Figure 4-63: 2-week test in the enriched Qurrayah water spiked with SRB at 31 ºC (SEM and EDS analysis of coupon surface before acid cleaning; Sample #4 in Figure 4-60)

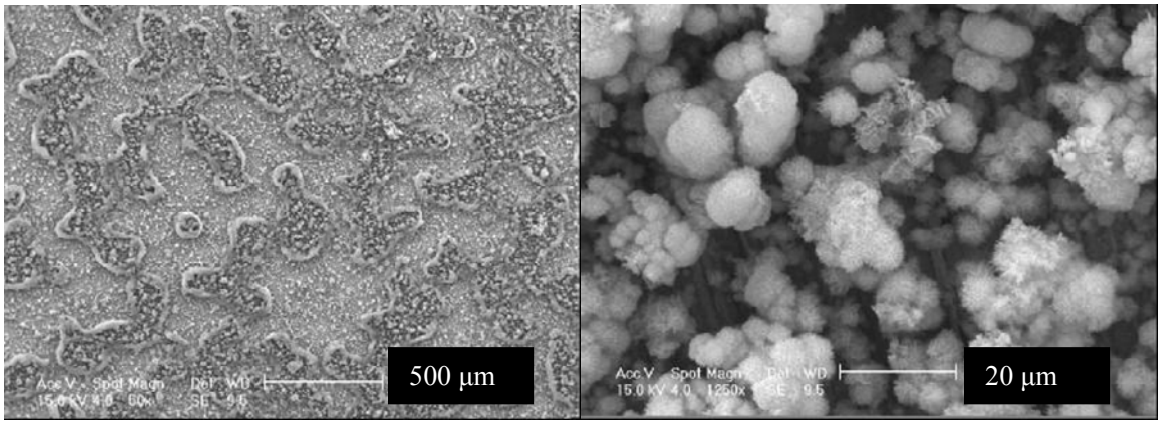

(a) SEM at 50X (b) SEM at 1250X

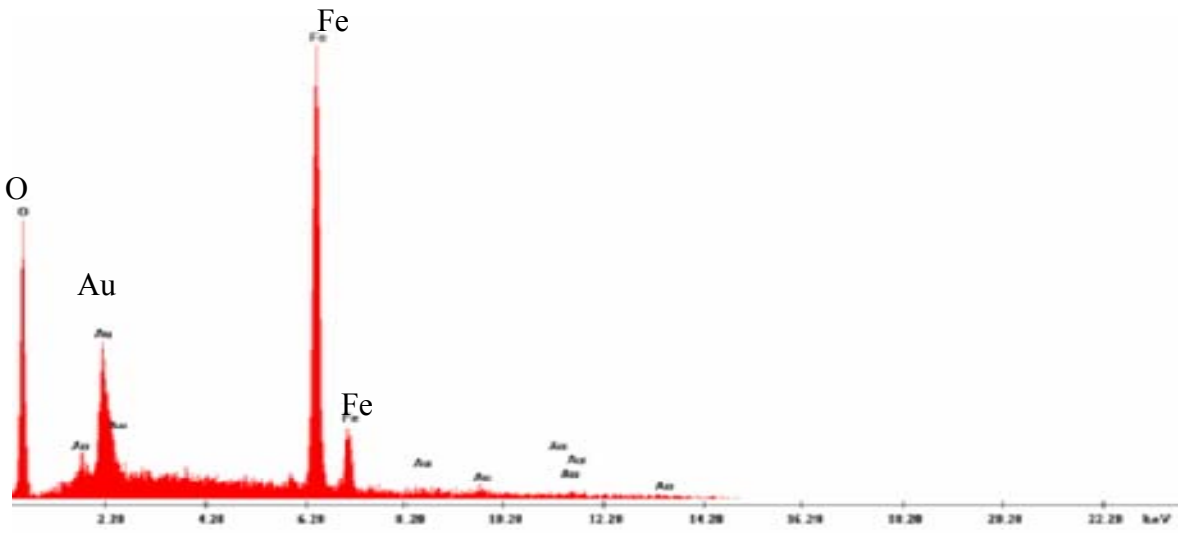

(c) Composition on the coupon surface

Figure 4-64: 2-week test in the enriched Qurrayah water spiked with SRB at 31 ºC (SEM and EDS analysis of coupon surface before acid cleaning; Sample #5 in Figure 4-60)

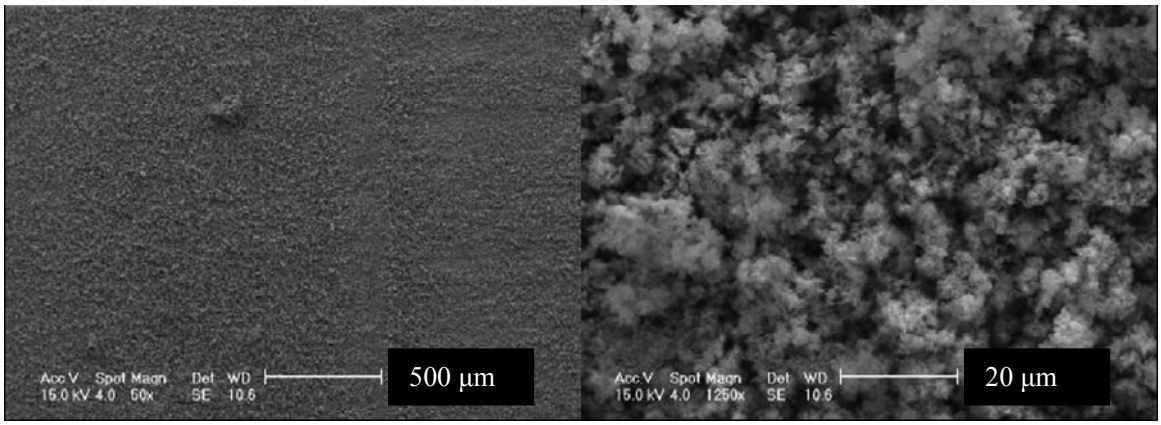

(a) SEM at 50X (b) SEM at 1250X

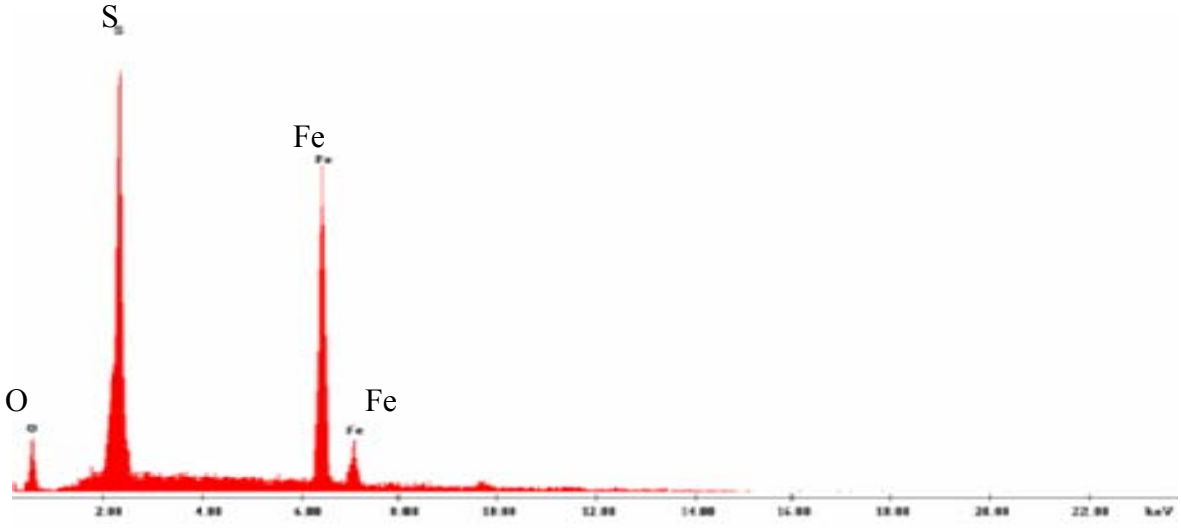

(c) Composition on the coupon surface

Figure 4-65: 2-week test in the enriched Qurrayah water spiked with SRB at 37 ºC (SEM and EDS analysis of coupon surface before acid cleaning; Sample #7 in Figure 4-60)

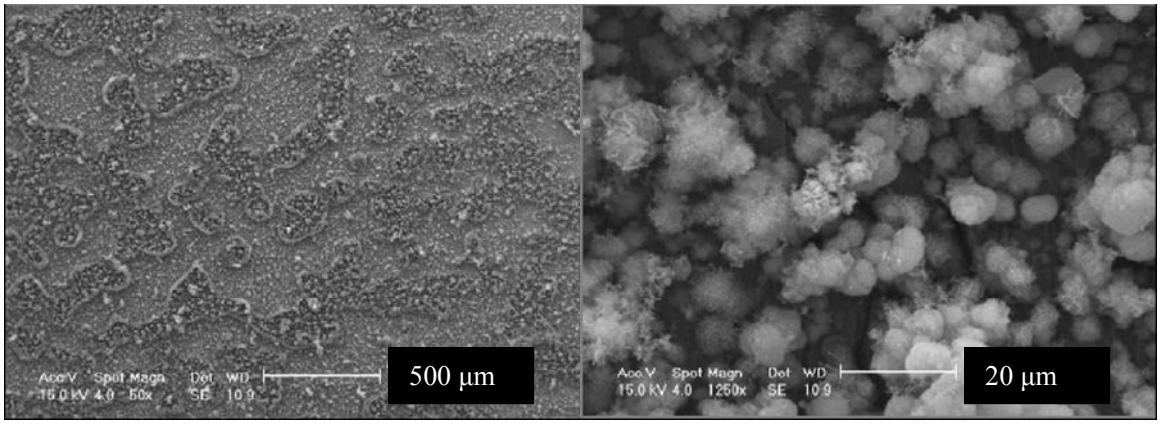

(a) SEM at 50X (b) SEM at 200X

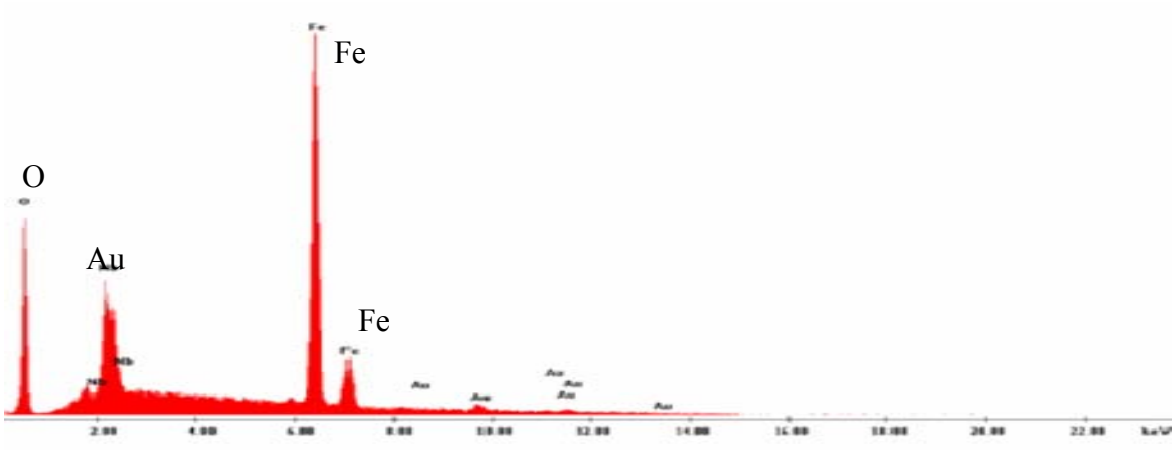

(c) Composition on the coupon surface

Figure 4-66: 2-week test in the enriched Qurrayah water spiked with SRB at 37 ºC (SEM and EDS analysis of coupon surface before acid cleaning; Sample #8 in Figure 4-60)

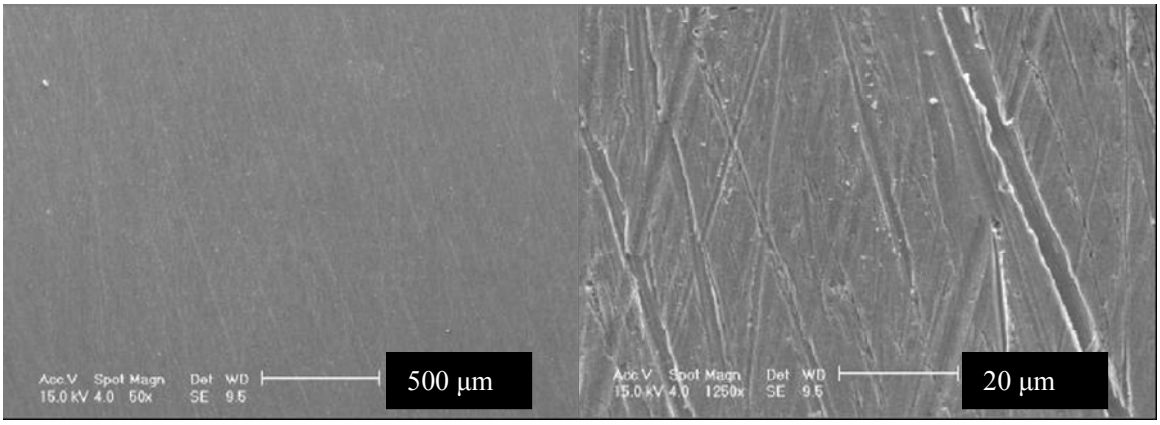

(a) SEM at 50X (b) SEM at 1250X

Figure 4-67: 2-week test in the enriched Qurrayah water spiked with SRB at 25 ºC (SEM analysis of coupon surface after acid cleaning; Sample #3 in Figure 4-60)

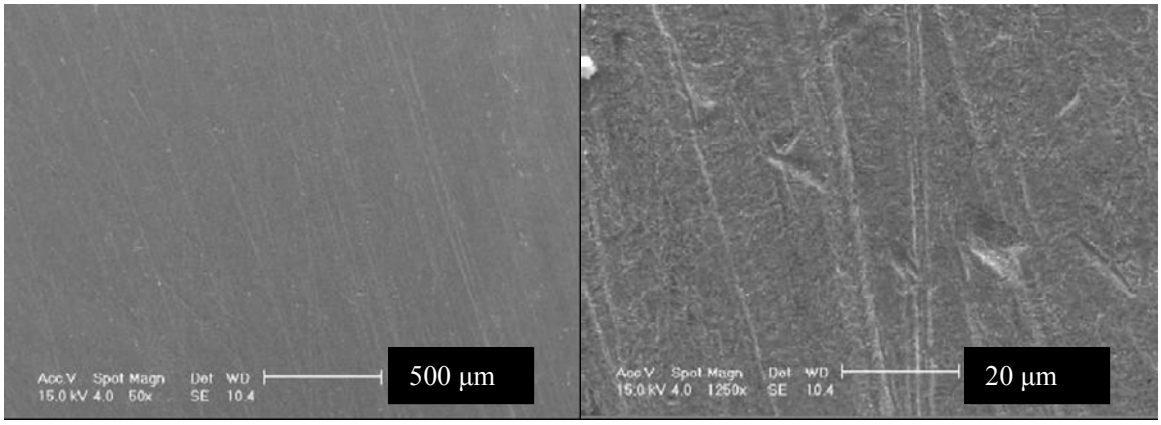

(a) SEM at 50X (b) SEM at 1250X

Figure 4-68: 2-week test in the enriched Qurrayah water spiked with SRB at 31 ºC (SEM analysis of coupon surface after acid cleaning; Sample #6 in Figure 4-60)

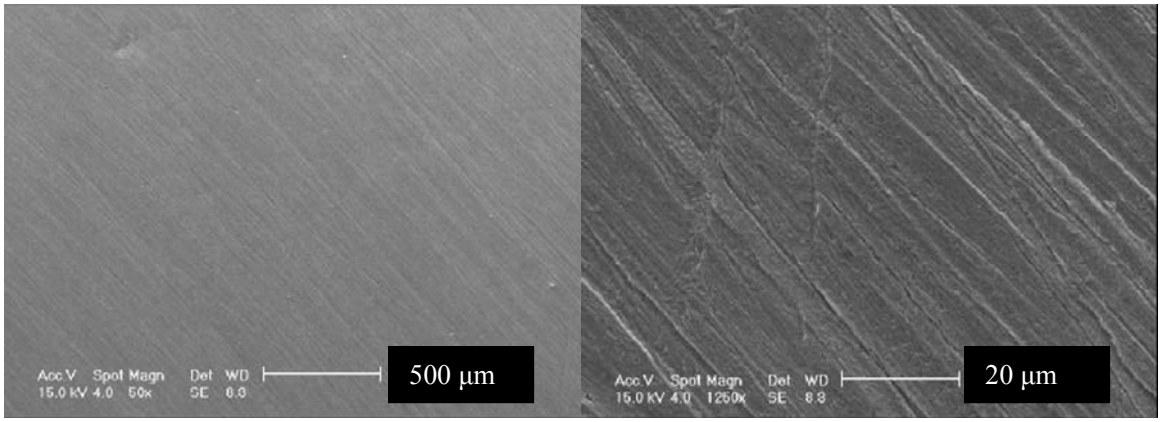

(a) SEM at 50X (b) SEM at 1250X

Figure 4-69: 2-week test in the enriched Qurrayah water spiked with SRB at 37 ºC (SEM analysis of coupon surface after acid cleaning; Sample #9 in Figure 4-60)

In this one-month test of Qurrayah water spiked with SRB, Figure 4-70 shows the weight loss, corrosion rate, pitting rate and pH of each sample at three test temperatures after the test was terminated. Samples #2, #4 and #8 run at temperatures 25ºC, 31ºC and 37ºC, respectively, were randomly selected to do the SEM and EDS. Corrosion rates were obtained from the samples #1 and #7, and pitting rates were obtained from the

samples #2~6, and samples #8-9. Figure 4-70 shows that pitting rate is extremely larger than uniform corrosion rate.

The results showed no biofilms or bacteria on the coupon surfaces (Figure 4-71 ~ Figure 4-73), but elemental S was detected by EDS on all the coupons (Figure 4-71 (c), Figure 4-72 (c) and Figure 4-73 (c)). Samples (#1 and #7 in Figure 4-70) while having less weight loss failed to obtain the surface appearance; thus, the assumption in the two-week test above in which there was a strong relationship between pH, FeS and weight loss could not be verified. The current data, however, is still consistent with the phenomena that the selected samples #2, #4 and #8 had lower pH and bigger weight losses with the element S presence.

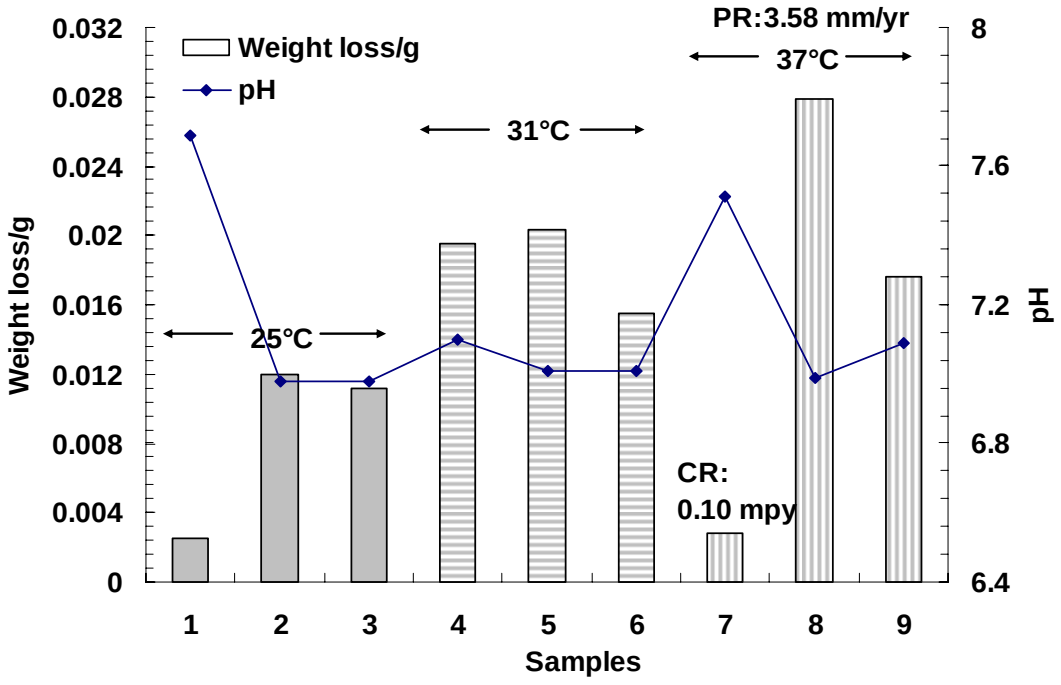

Figure 4-70: X65 coupon weight loss in the enriched Qurrayah water (seawater) spiked with SRB after the 1-month test (#1-#3 are duplicate samples at 25°C. #4-#6 are duplicate samples at 31°C. #7-#9 are duplicate samples at 37°C.)

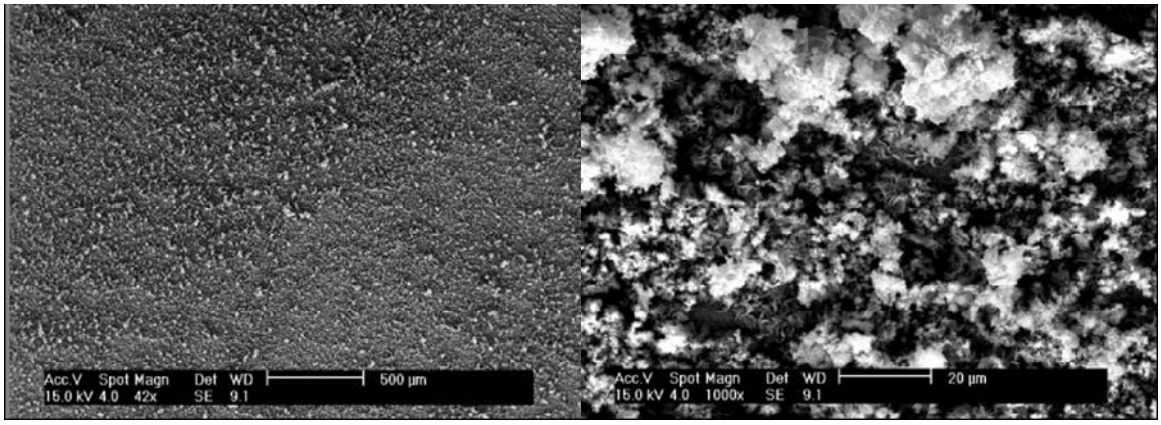

(a) SEM at 42X (b) SEM at 1000X

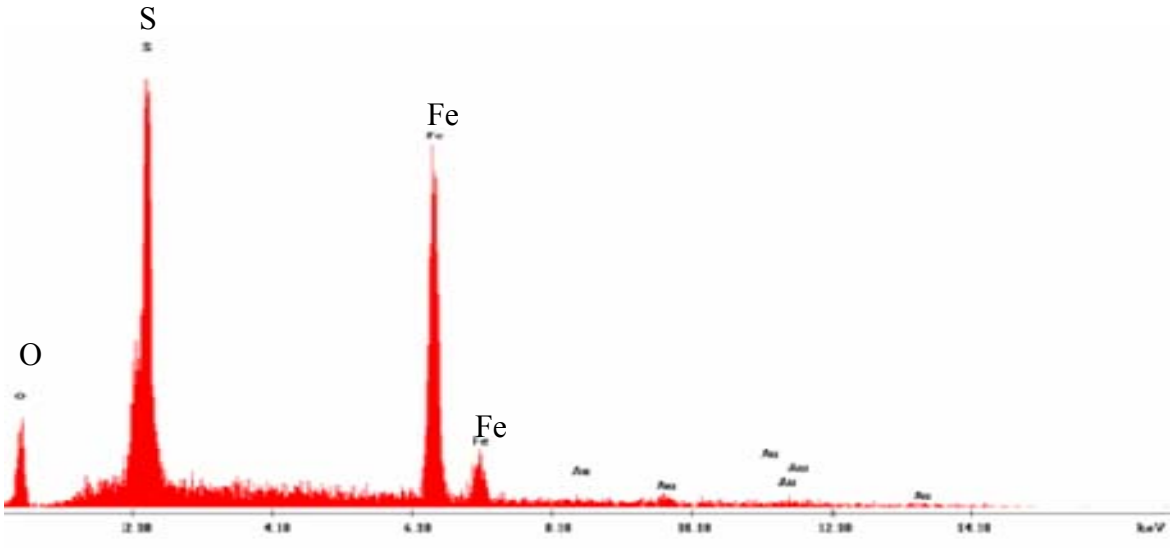

(c) Composition on the coupon surface

Figure 4-71: 1-month test in the enriched Qurrayah water spiked with SRB at 25 ºC (SEM and EDS analysis of coupon surface before acid cleaning; Sample #2 in Figure 4-70)

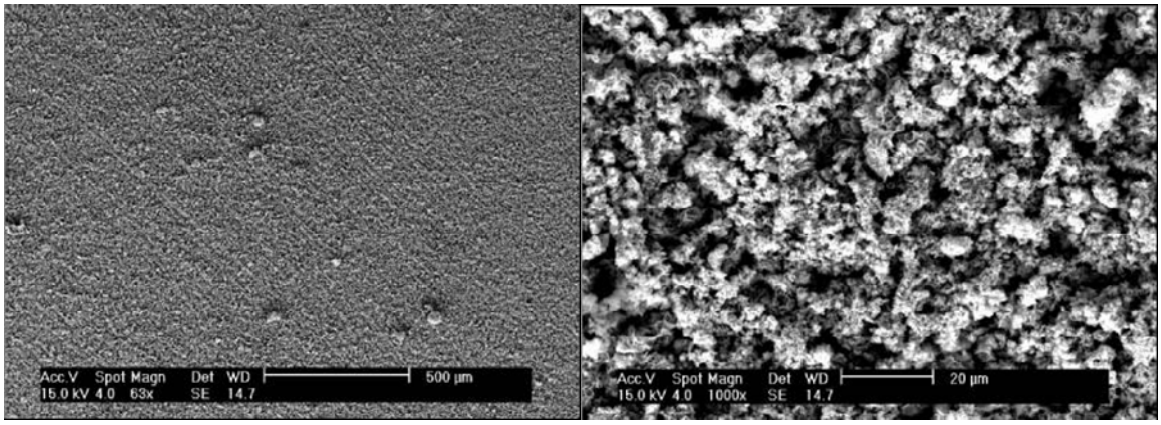

(a) SEM at 63X (b) SEM at 1000X

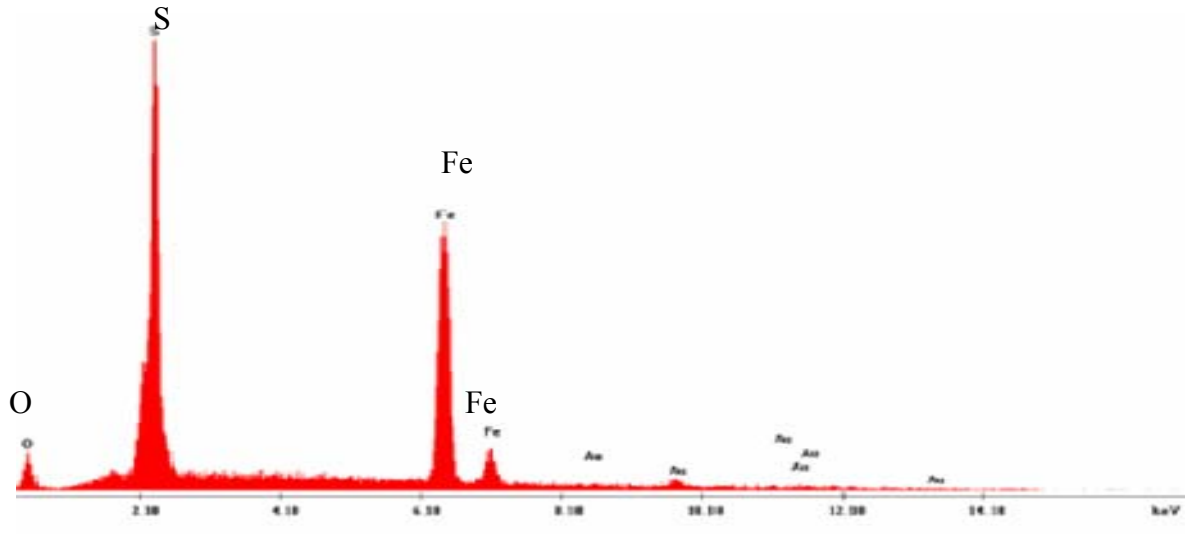

(c) Composition on the coupon surface

Figure 4-72: 1-month test in the enriched Qurrayah water spiked with SRB at 31 ºC (SEM and EDS analysis of coupon surface before acid cleaning; Sample #4 in Figure 4-70)

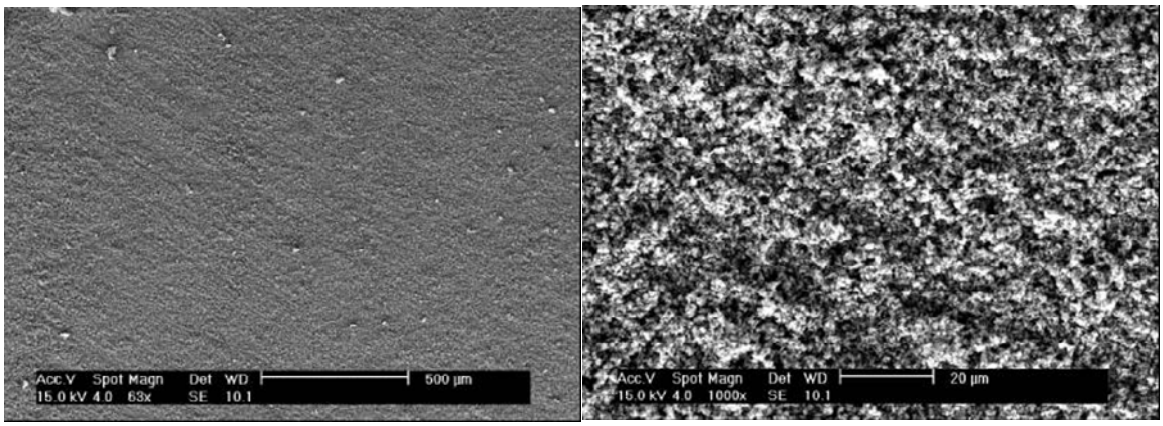

(a) SEM at 63X (b) SEM at 1000X

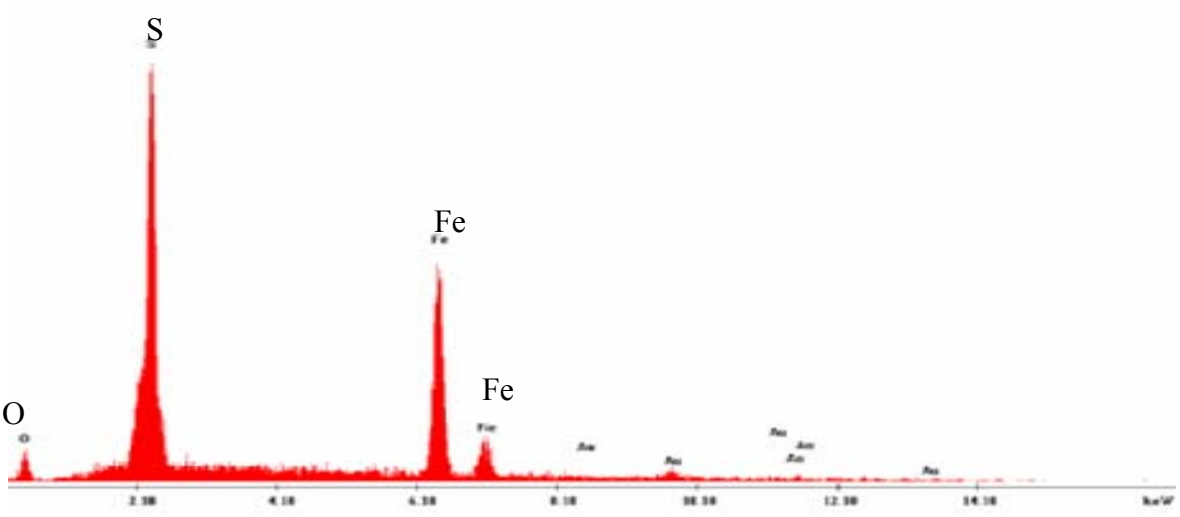

(c) Composition on the coupon surface

Figure 4-73: 1-month test in the enriched Qurrayah water spiked with SRB at 37 ºC (SEM and EDS analysis of coupon surface before acid cleaning; Sample #8 in Figure 4-70)

After the films were removed, the coupon surfaces showed no obvious corrosion on the surfaces of sample #2 and #4 (Figure 4-74 and Figure 4-75) while sample #8 had some pits at temperature 37ºC (Figure 4-76). Duplicate samples #7 and #9 of sample #8 also showed pits (Figure 4-77 and Figure 4-78), but the pits on the surface of sample #7

were not consistent with what was typically found in other tests when SRB biofilms were grown on coupons in vials. Rather, they were quite similar to the pits shown earlier when SRB were not involved (refer to Figure 4-17 in Part I in Chapter 4.4.1.2). Figure 4-70 shows Sample #7 had higher pH and smaller weight loss, which indicated there was no FeS formed on the coupon surface according to the previous assumption. This indicated that SRB in the test vial were not active enough to produce H_2S. From the tests above, it can be concluded that MIC is complicated because even with duplicate samples there were not consistent results in some cases.

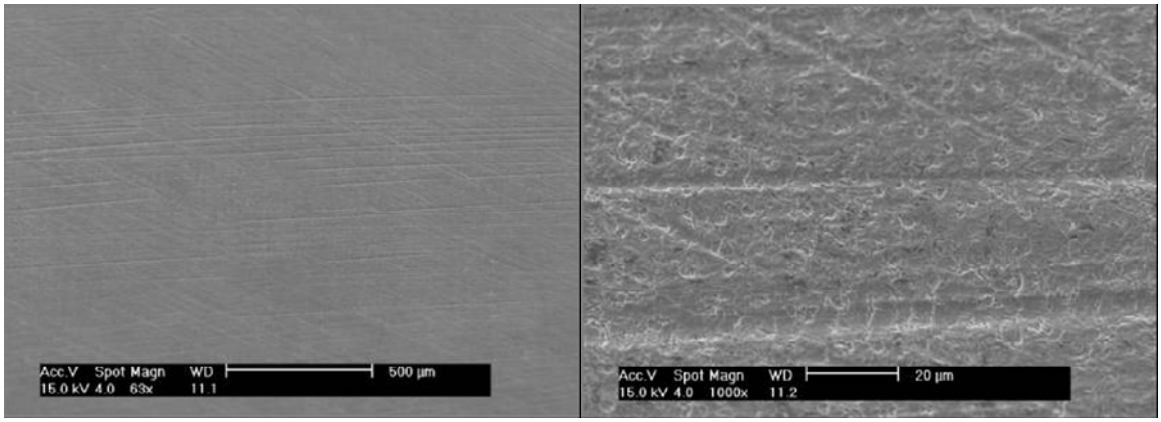

(a) SEM at 63X (b) SEM at 1000X

Figure 4-74: 2-week test in the enriched Qurrayah water spiked with SRB at 25 ºC (SEM analysis of coupon surface after acid cleaning; Sample #2 in Figure 4-70)

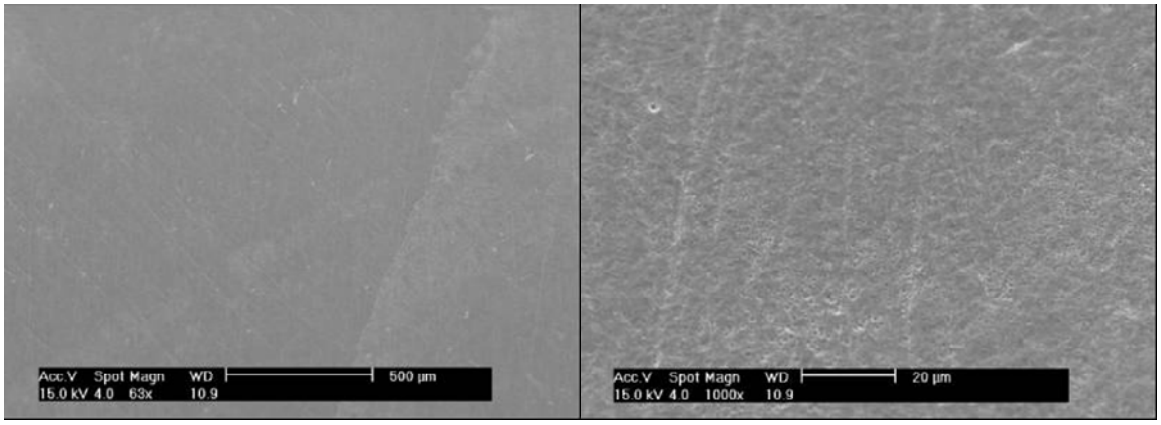

(a) SEM at 63X (b) SEM at 1000X

Figure 4-75: 2-week test in the enriched Qurrayah water spiked with SRB at 31 ºC (SEM analysis of coupon surface after acid cleaning; Sample #4 in Figure 4-70)

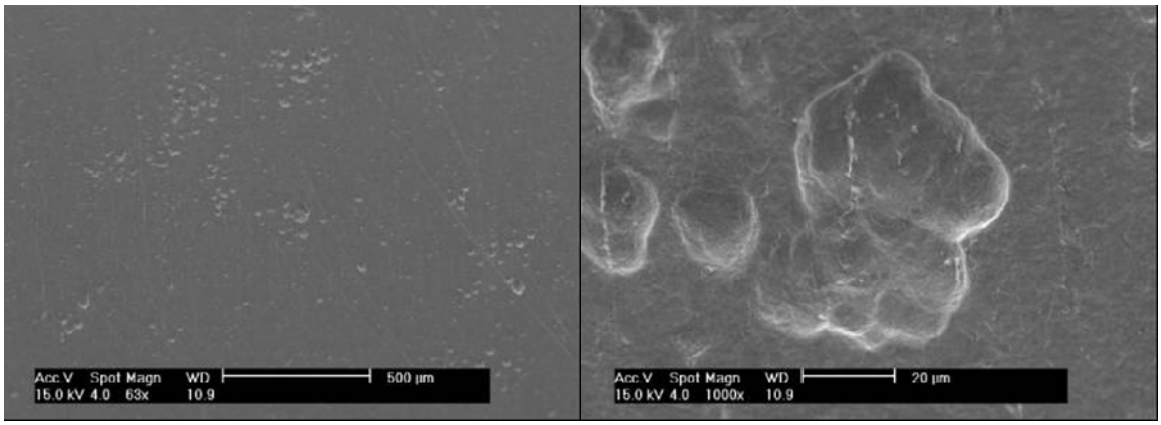

(a) SEM at 63X (b) SEM at 1000X

Figure 4-76: 2-week test in the enriched Qurrayah water spiked with SRB at 37 ºC (SEM analysis of coupon surface after acid cleaning; Sample #8 in Figure 4-70)

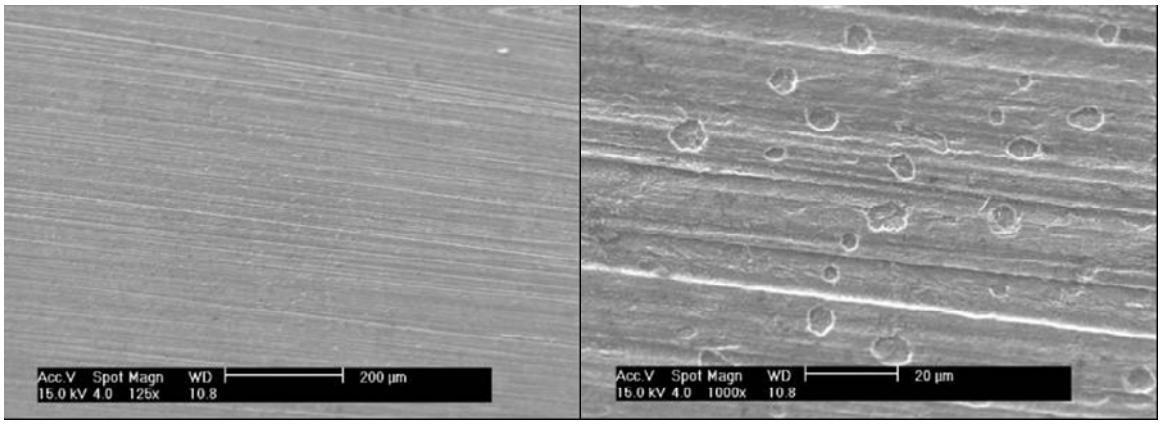

(a) SEM at 125X (b) SEM at 1000X

Figure 4-77: 2-week test in the enriched Qurrayah water spiked with SRB at 37 ºC (SEM analysis of coupon surface after acid cleaning; Sample #7 in Figure 4-70)

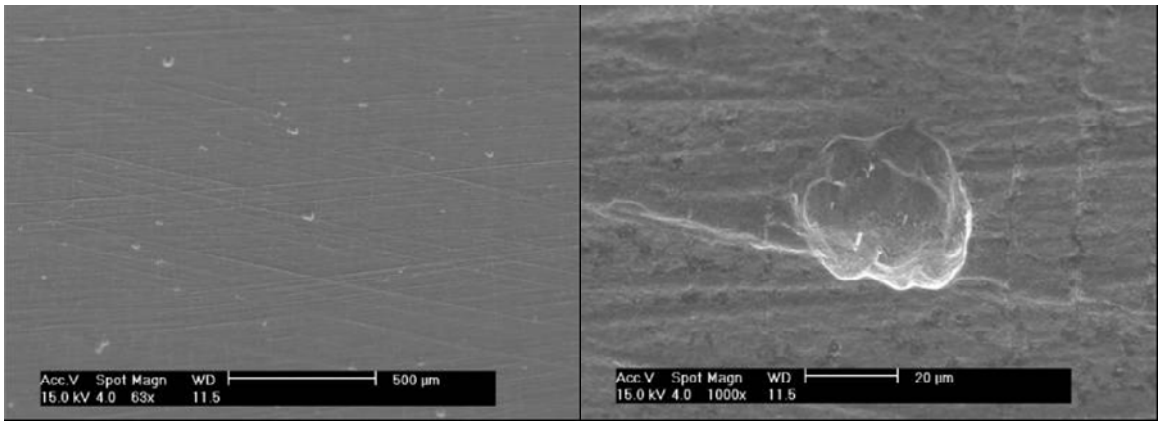

(a) SEM at 63X (b) SEM at 1000X

Figure 4-78: 2-week test in the enriched Qurrayah water spiked with SRB at 37 ºC (SEM analysis of coupon surface after acid cleaning; Sample #9 in Figure 4-70)

In this three-month test, no biofilms or loose bacteria were found on any test sample surfaces (Figure 4-79 ~ Figure 4-81) while elemental S was observed on the surfaces of all the samples by EDS (Figure 4-79 (c), Figure 4-80 (c), Figure 4-81 (c)). Weight loss and pitting rates of all samples were obtained as shown in Figure 82. Typical MIC pits were found on all the coupon surfaces (Figure 4-83 ~ Figure 4-86). Clusters of pits were observed (Figure 4-86). Over a long period, these pits may eventually lead to pinhole leaks.

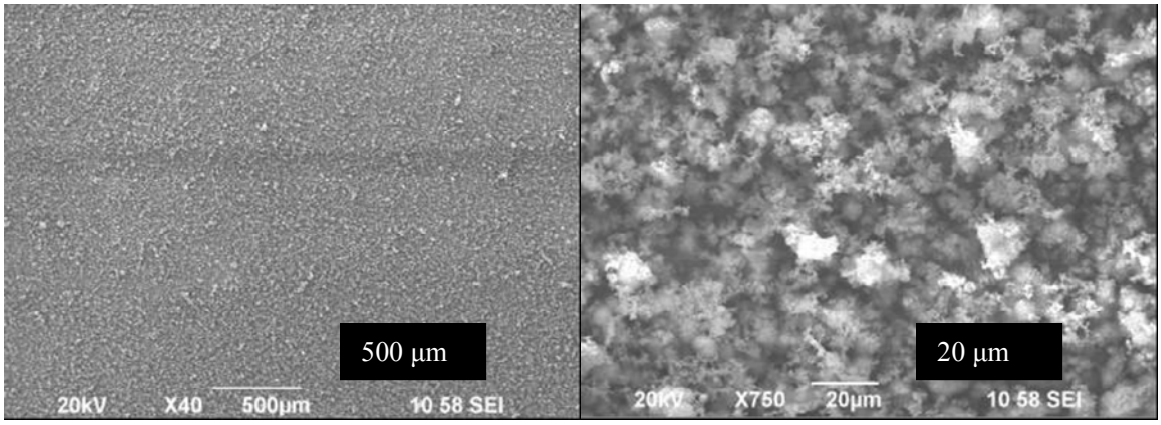

(a) SEM at 40X (b) SEM at 750X

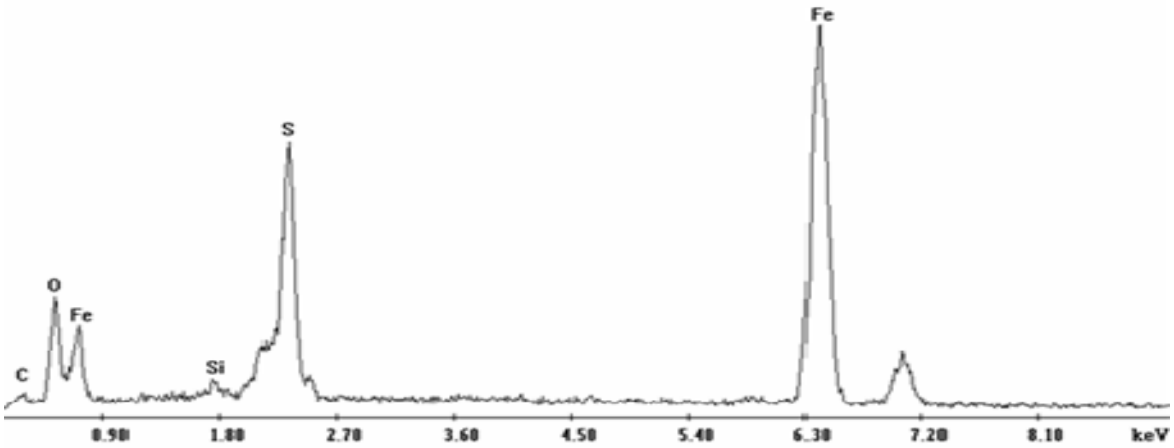

(c) Composition on the coupon surface

Figure 4-79: 3-month test in the enriched Qurrayah water spiked with SRB at 25 ºC (SEM and EDS analysis of coupon surface before acid cleaning)

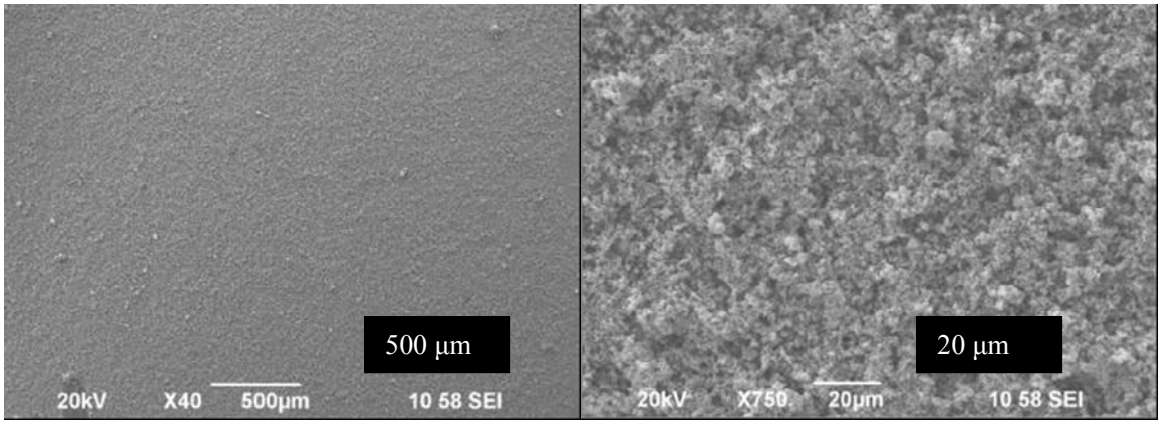

(a) SEM at 40X (b) SEM at 750X

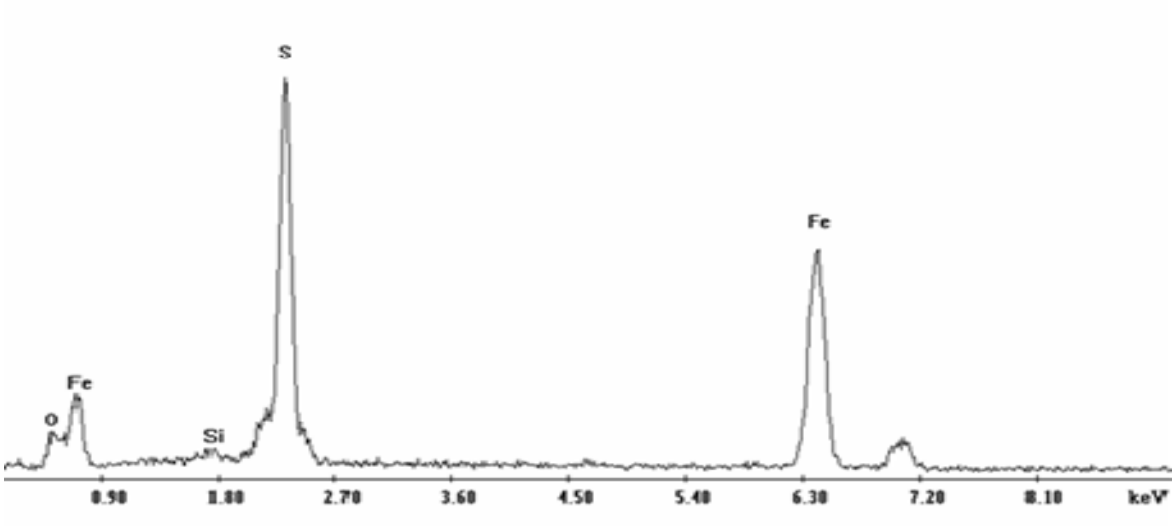

(c) Composition on the coupon surface

Figure 4-80: 3-month test in the enriched Qurrayah water spiked with SRB at 31 ºC (SEM and EDS analysis of coupon surface before acid cleaning)

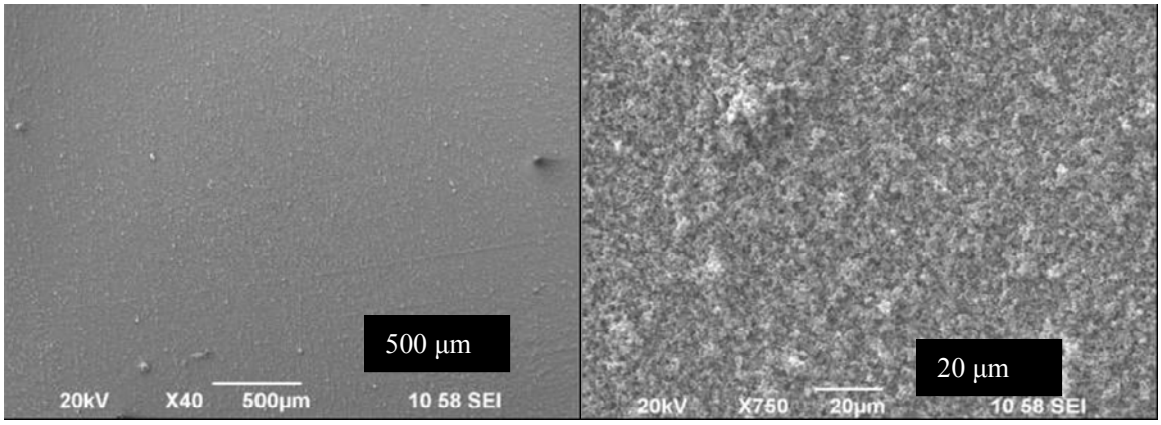

(a) SEM at 40X (b) SEM at 750X

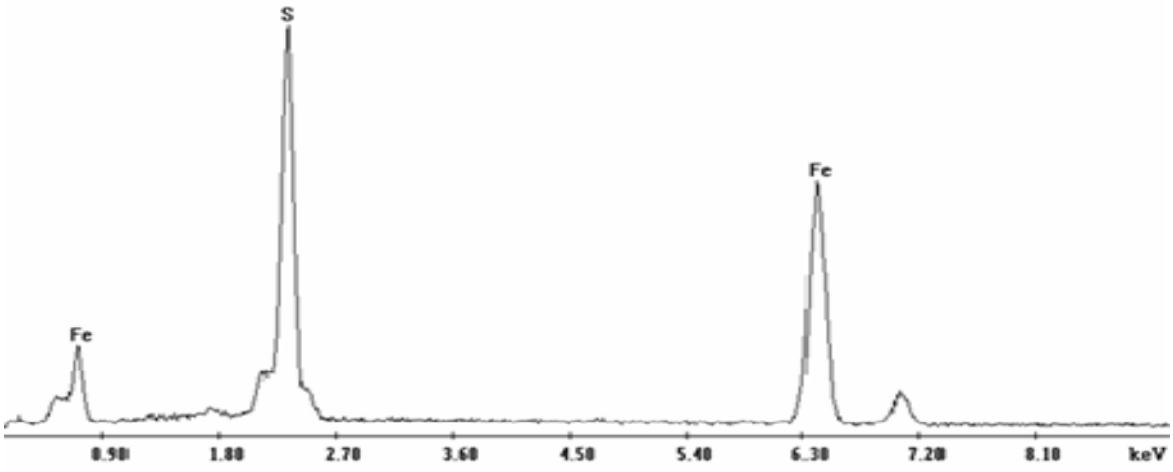

(c) Composition on the coupon surface

Figure 4-81: 3-month test in the enriched Qurrayah water spiked with SRB at 37 ºC (SEM and EDS analysis of coupon surface before acid cleaning)

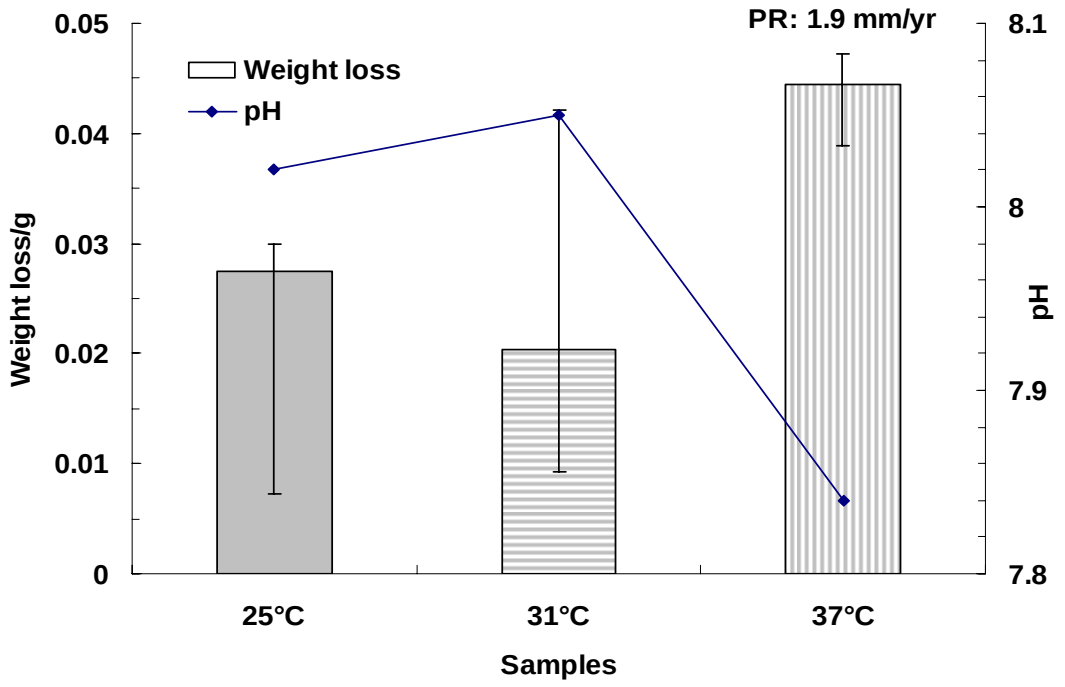

Figure 4-82: X65 coupon weight loss and pitting rate in the enriched Qurrayah water (seawater) spiked with SRB after 3-month test

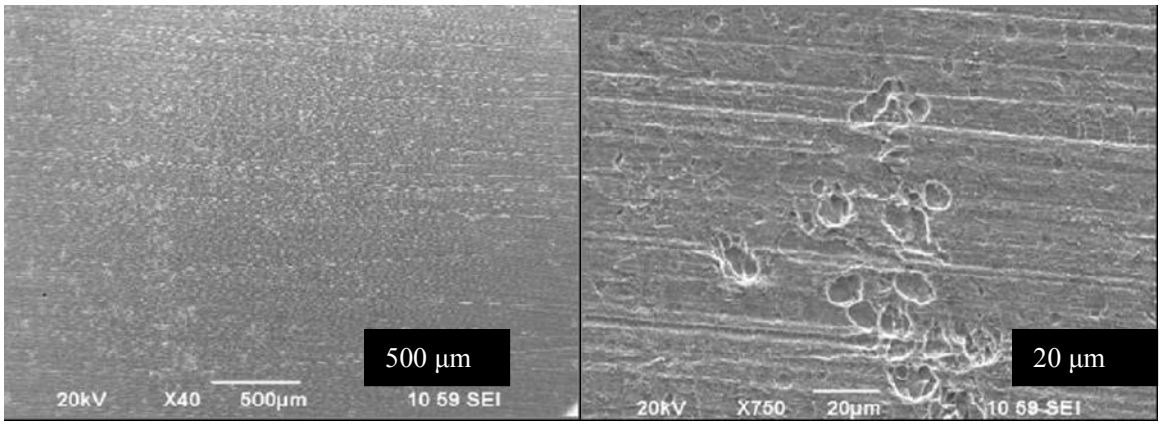

(a) SEM at 40X (b) SEM at 750X

Figure 4-83: 3-month test in the enriched Qurrayah water spiked with SRB at 25 ºC (SEM analysis of coupon surface after acid cleaning)

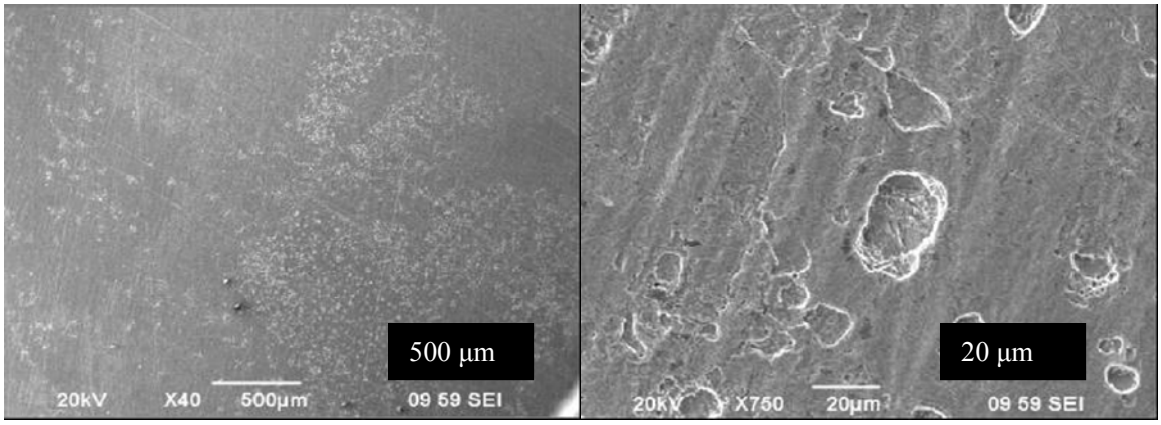

(a) SEM at 40X (b) SEM at 750X

Figure 4-84: 3-month test in the enriched Qurrayah water spiked with SRB at 31 ºC (SEM analysis of coupon surface after acid cleaning)

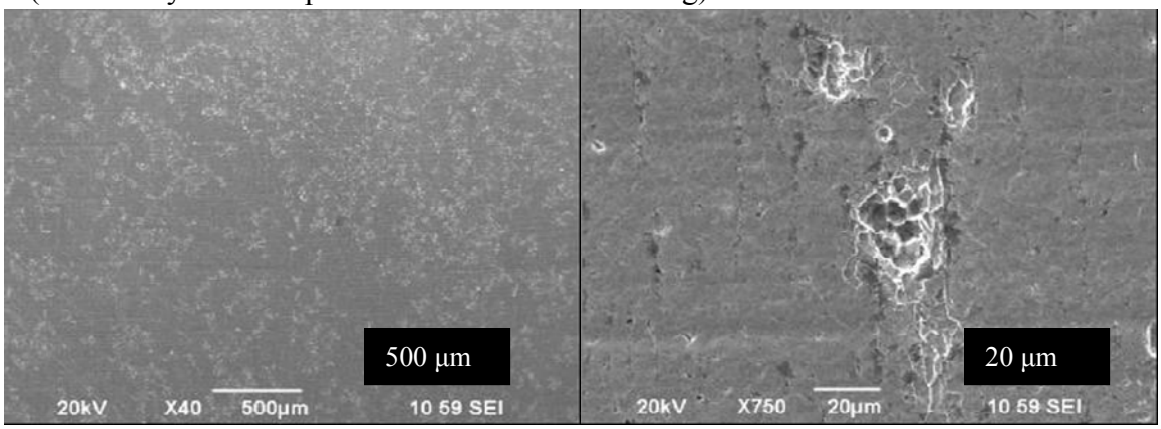

(a) SEM at 40X (b) SEM at 750X

Figure 4-85: 3-month test in the enriched Qurrayah water spiked with SRB at 37 ºC (SEM analysis of coupon surface after acid cleaning; Location #1)

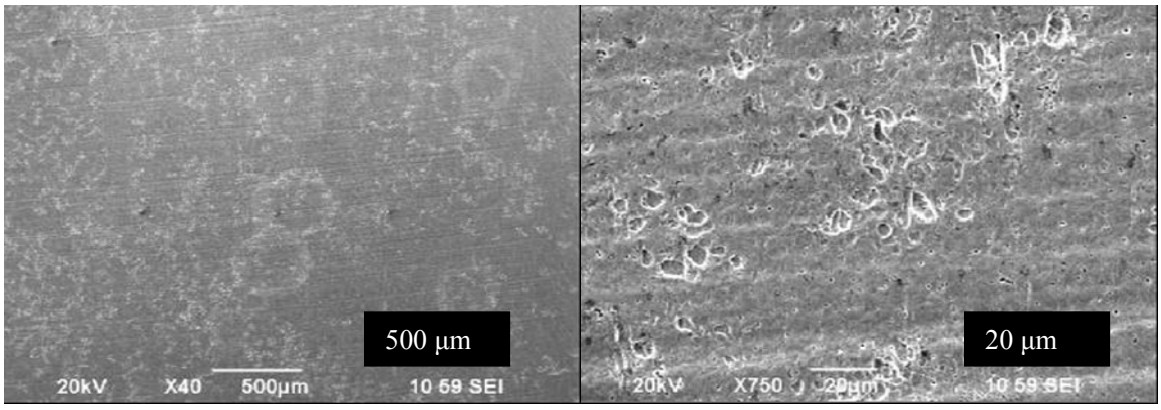

(a) SEM at 40X (b) SEM at 750X

Figure 4-86: 3-month test in the enriched Qurrayah water spiked with SRB at 37 ºC (SEM analysis of coupon surface after acid cleaning; Location #2 of the same sample in Figure 4-85)

It was found that the corrosion rates in the tests using enriched Qurrayah water were roughly four times higher than those using untreated Qurrayah water indicating that spiked SRB accelerated the corrosion process.

At the given test conditions, FeS formation and pitting patterns point to SRB involvement. However, neither sessile biofilms nor loose bacteria were found on coupon surfaces. Further investigation is warranted.

ii: Tests in lasting one-week, two-week and one-month

In the one-week test, neither biofilms (Figure 4-87 and Figure 4-88) nor elemental S (Figure 4-87 (c) and Figure 4-88 (c)) were found on the duplicate sample surfaces at 25ºC. At 31ºC, both biofilms (Figure 4-89) and S (Figure 4-89 (c)) were found on #1 sample surface. Figure 4-89 shows a small biofilm colony composed of a couple of rod bacteria. Biofilms, however, could not be found on the duplicate sample #2 surfaces (Figure 4-90) although S was observed (Figure 4-90 (c)). At 37ºC, duplicate sample #1 and #2 were both found to have the biofilms (Figure 4-91 and Figure 4-92) and S on the surface (Figure 4-91 (c) and Figure 4-92 (c)). The biofilms were typical of those found in MIC. Bacteria aggregate into clusters and stick to each other by extracellular polymeric substances (EPS) secreted by bacteria. Figure 4-93 shows increased weight loss with the increase of temperature while pH presented the opposite trend. Corrsion rates were obtained from the samples at 25^{o}C while pitting rates were obtained from the samples at 31^{o}C and 37^{o}C. Typical MIC pits were found on all the sample surfaces at the three test temperatures (Figure 4-94 ~ Figure 4-99). Figure 4-98 and Figure 4-99 show severe

pitting after only one week exposure to SRB. These pits may threaten pipeline integration if their progression is left unchecked.

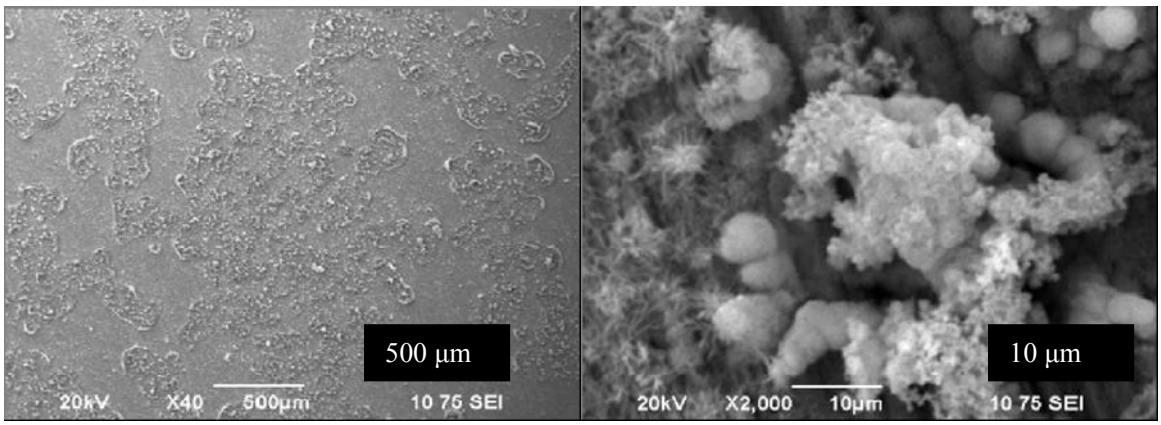

(a) SEM at 40X (b) SEM at 2000X

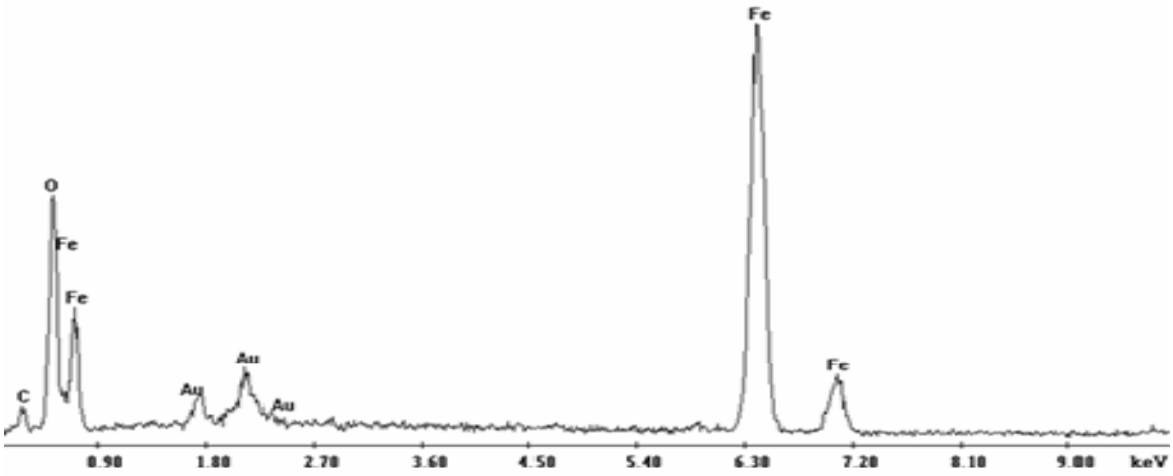

(c) Composition on the coupon surface

Figure 4-87: 1-week test in the enriched Qurrayah water spiked with SRB at 25 ºC (SEM and EDS analysis of coupon surface before acid cleaning; Sample #1)

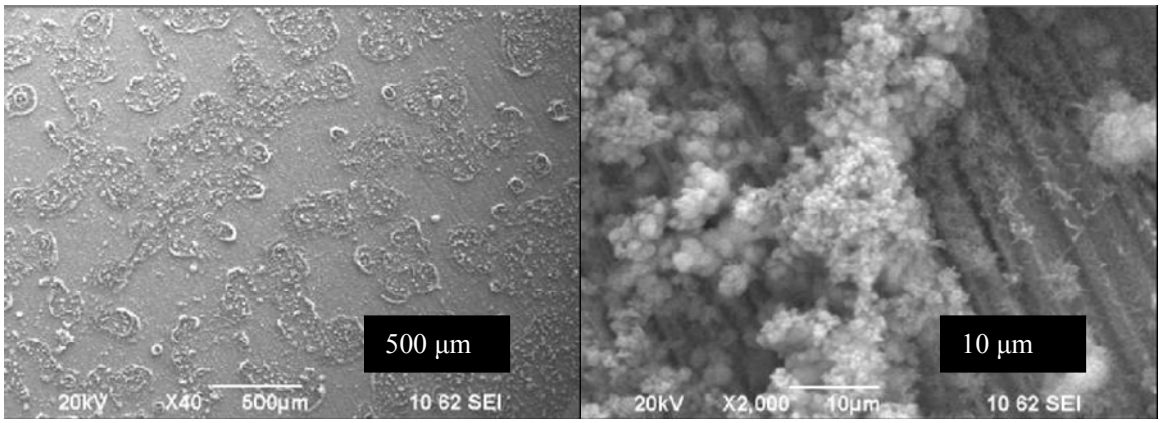

(a) SEM at 40X (b) SEM at 2000X

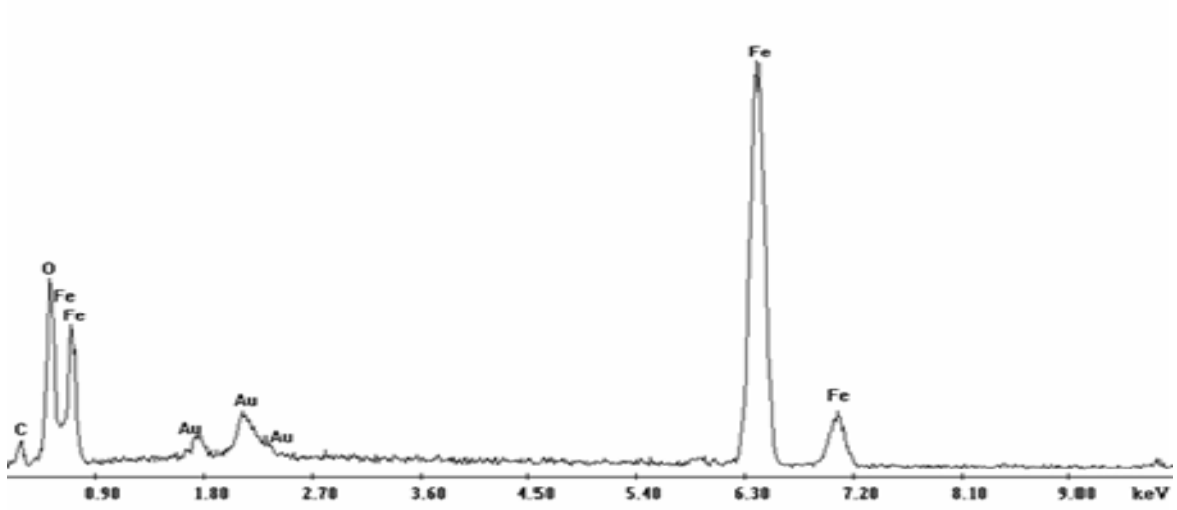

(c) Composition on the coupon surface

Figure 4-88: 1-week test in the enriched Qurrayah water spiked with SRB at 25 ºC (SEM and EDS analysis of coupon surface before acid cleaning; Sample #2 – duplicate sample as Sample #1in Figure 4-87)

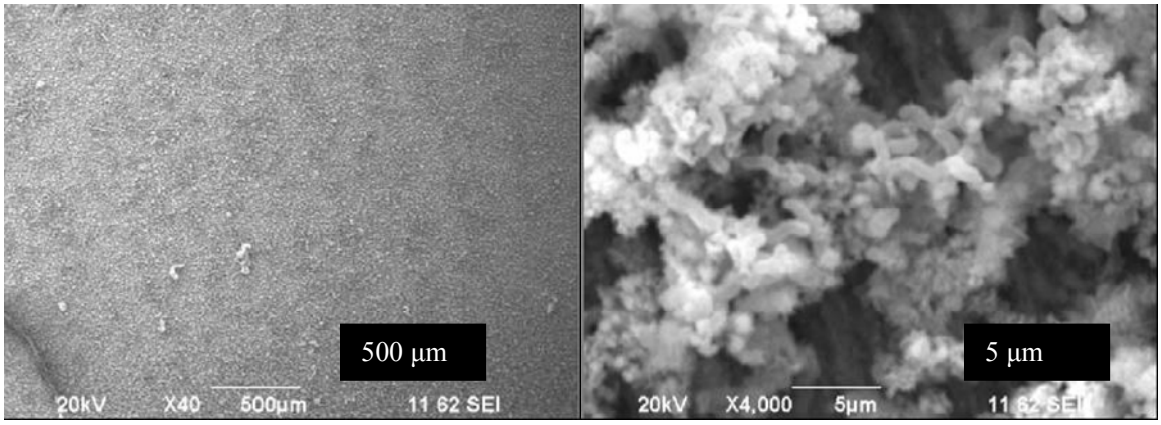

(a) SEM at 40X (b) SEM at 4000X

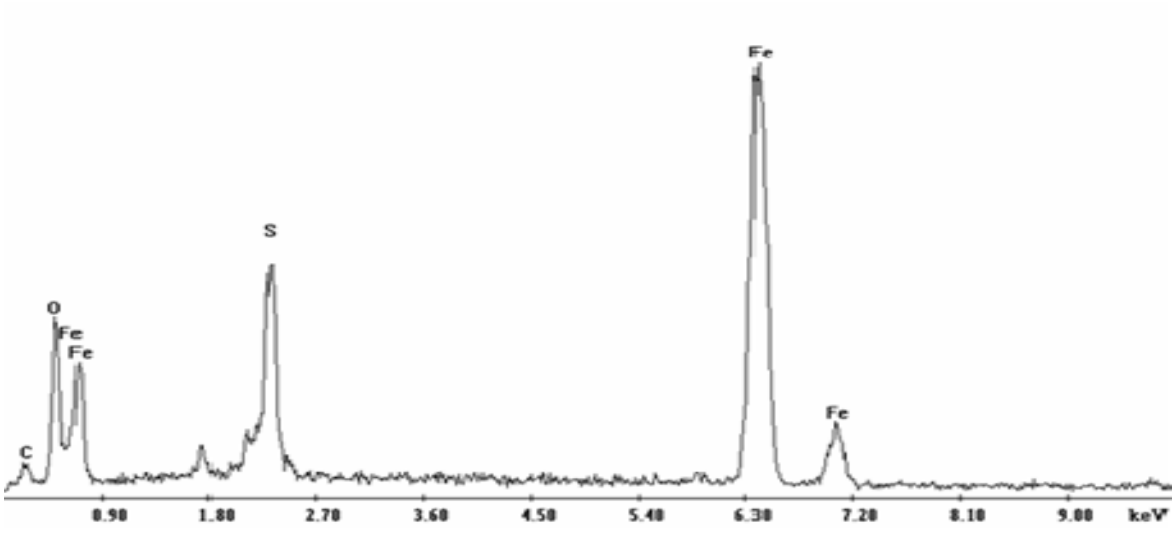

(c) Composition on the coupon surface

Figure 4-89: 1-week test in the enriched Qurrayah water spiked with SRB at 31 ºC (SEM and EDS analysis of coupon surface before acid cleaning; Sample #1)

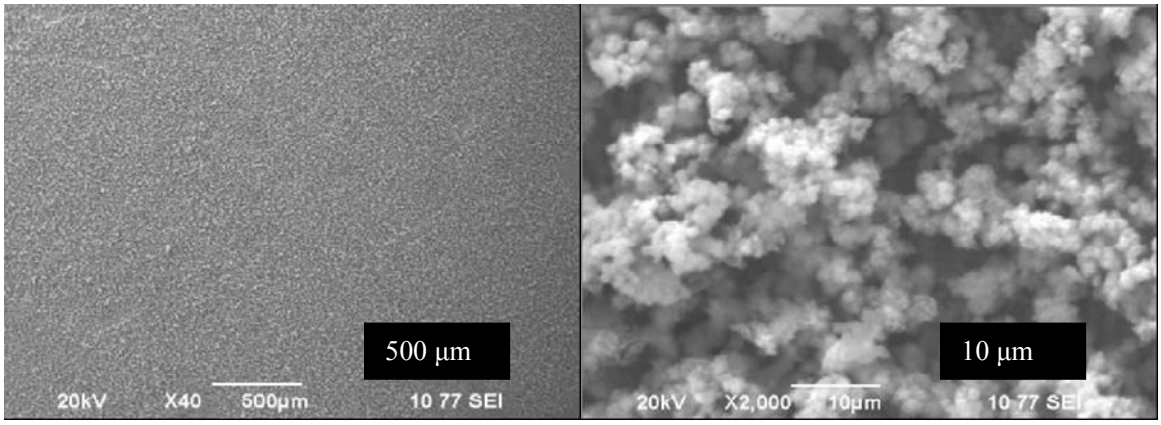

(a) SEM at 40X (b) SEM at 2000X

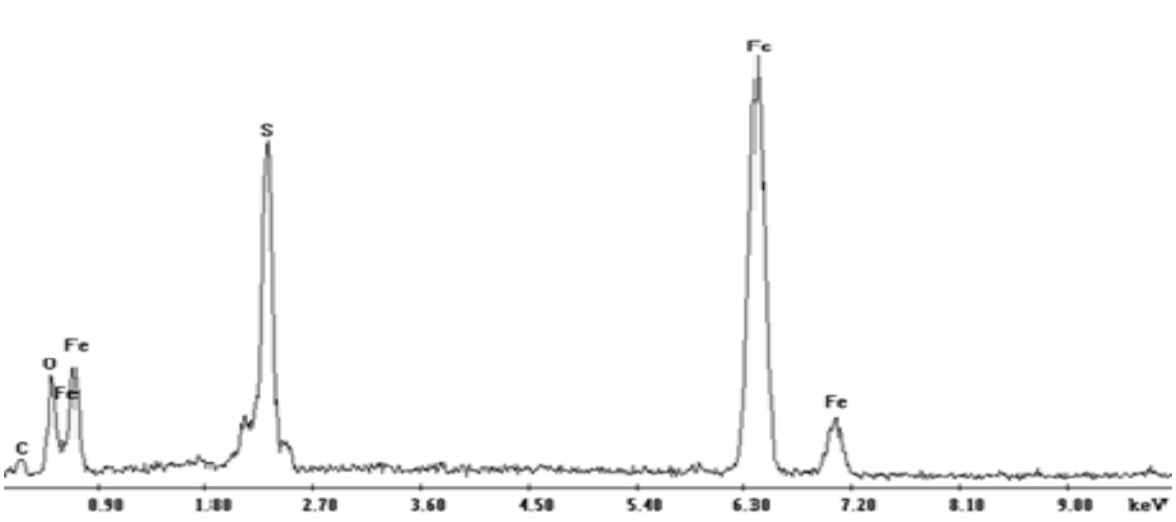

(c) Composition on the coupon surface

Figure 4-90: 1-week test in the enriched Qurrayah water spiked with SRB at 31 ºC (SEM and EDS analysis of coupon surface before acid cleaning; Sample #2 – duplicate sample as Sample #1 in Figure 4-89)

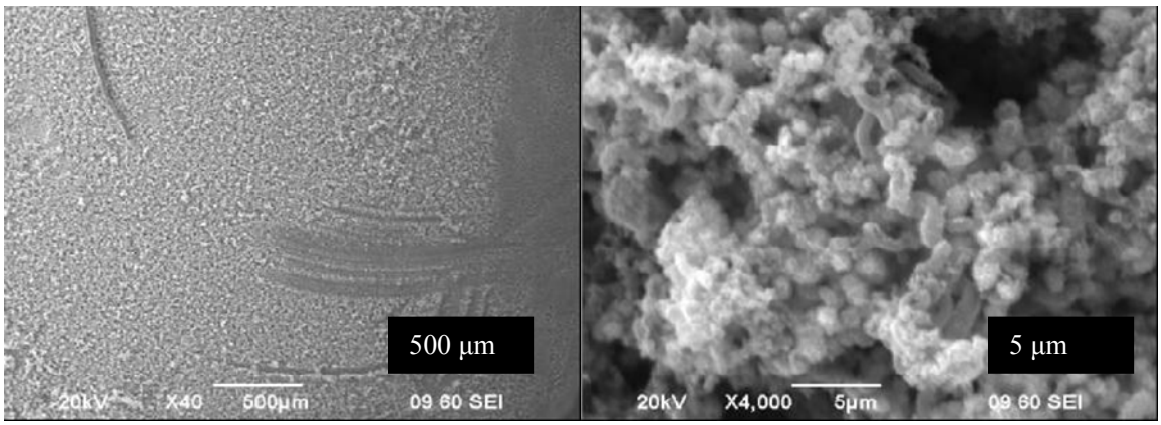

(a) SEM at 40X (b) SEM at 4000X

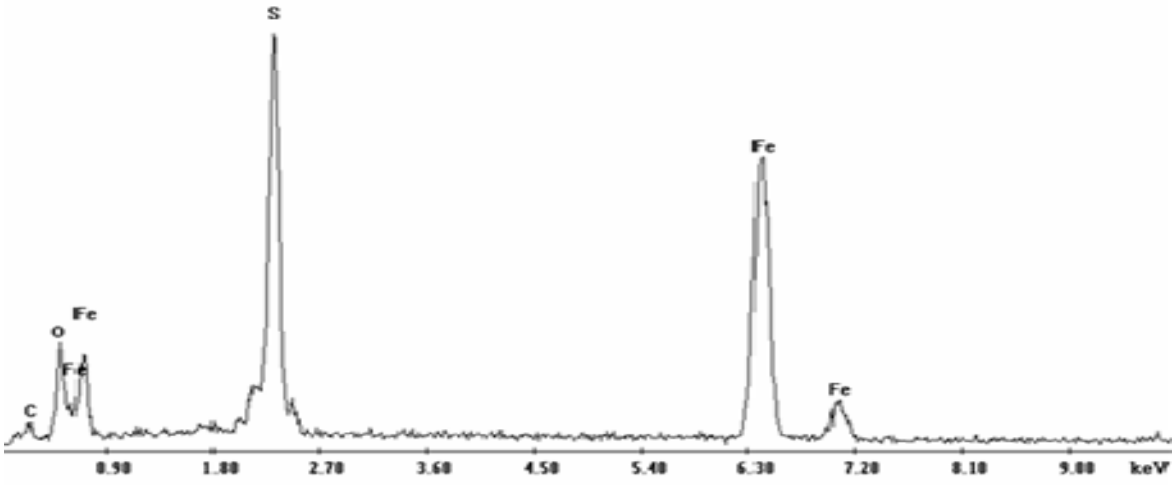

(c) Composition on the coupon surface

Figure 4-91: 1-week test in the enriched Qurrayah water spiked with SRB at 37 ºC (SEM and EDS analysis of coupon surface before acid cleaning; Sample #1)

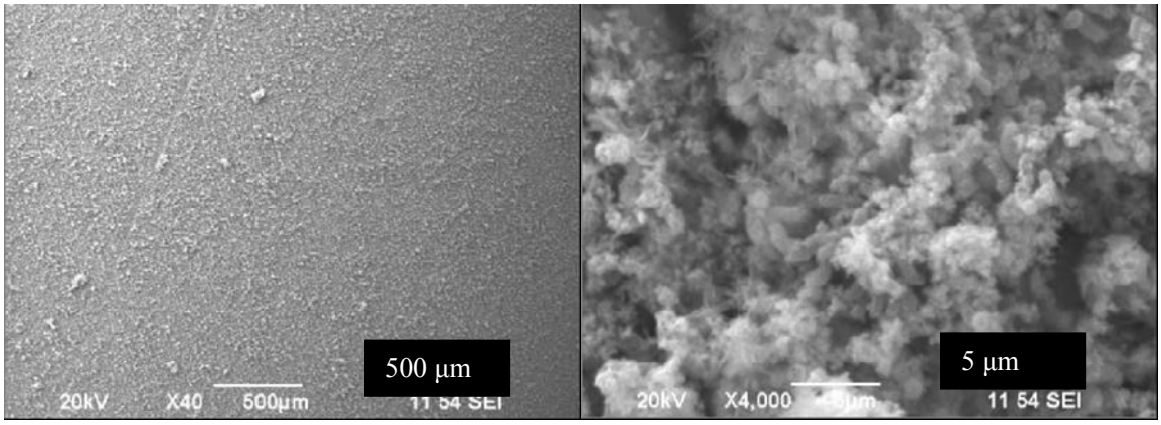

(a) SEM at 40X (b) SEM at 4000X

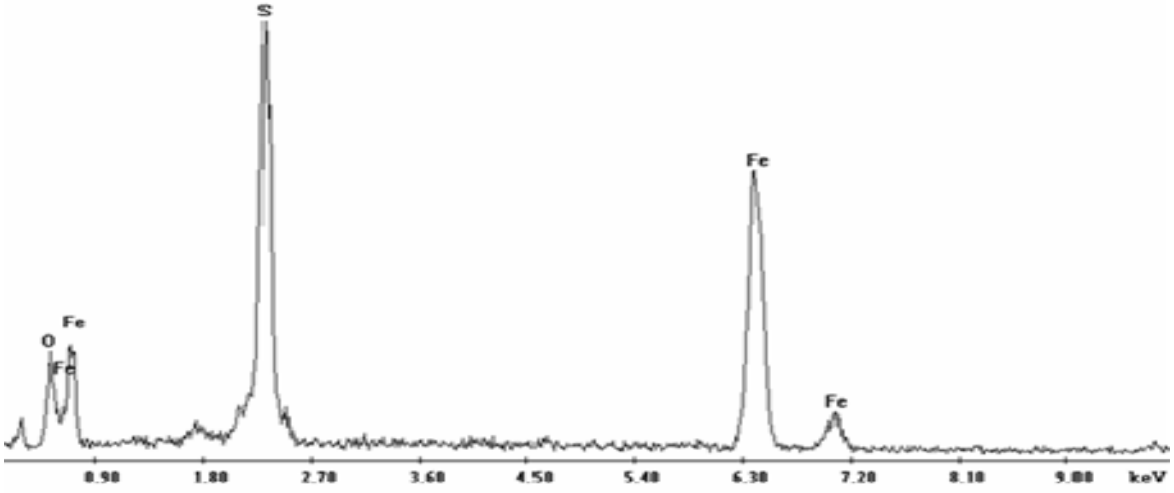

(c) Composition on the coupon surface

Figure 4-92: 1-week test in the enriched Qurrayah water spiked with SRB at 37 ºC (SEM and EDS analysis of coupon surface before acid cleaning; Sample #2– duplicate sample as Sample #1 in Figure 4-91)

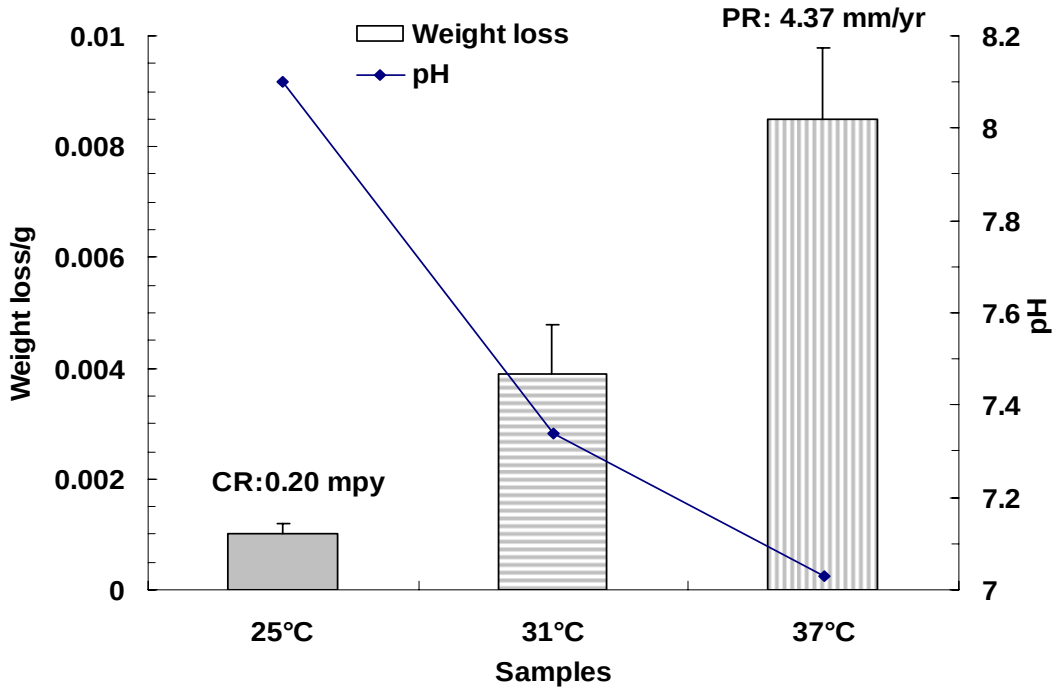

Figure 4-93: X65 coupon weight loss in the enriched Qurrayah water (seawater) spiked with SRB after the 1-week test

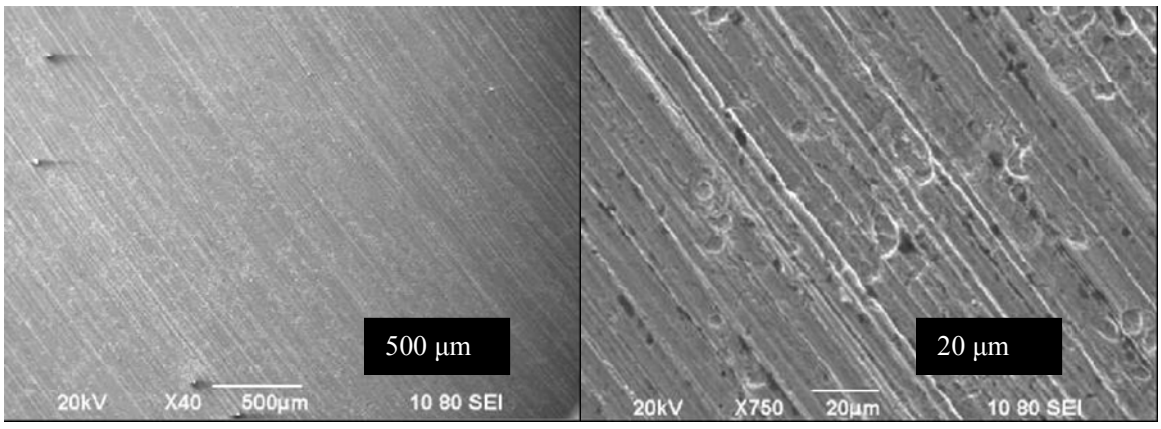

(a) SEM at 40X (b) SEM at 750X

Figure 4-94: 1-week test in the enriched Qurrayah water spiked with SRB at 25 ºC (SEM analysis of coupon surface after acid cleaning; Sample #1)

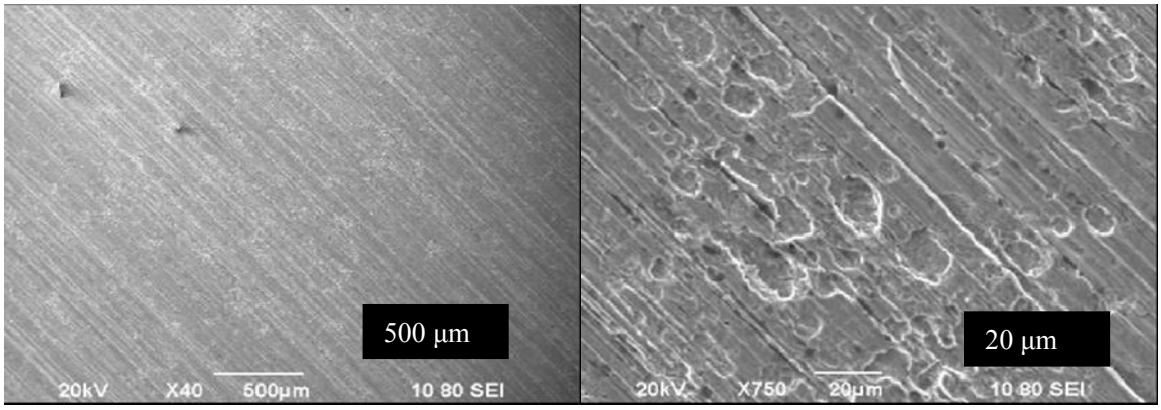

(a) SEM at 40X (b) SEM at 750X

Figure 4-95: 1-week test in the enriched Qurrayah water spiked with SRB at 25 ºC (SEM analysis of coupon surface after acid cleaning; Sample #2– duplicate sample as Sample #1 in Figure 4-94)

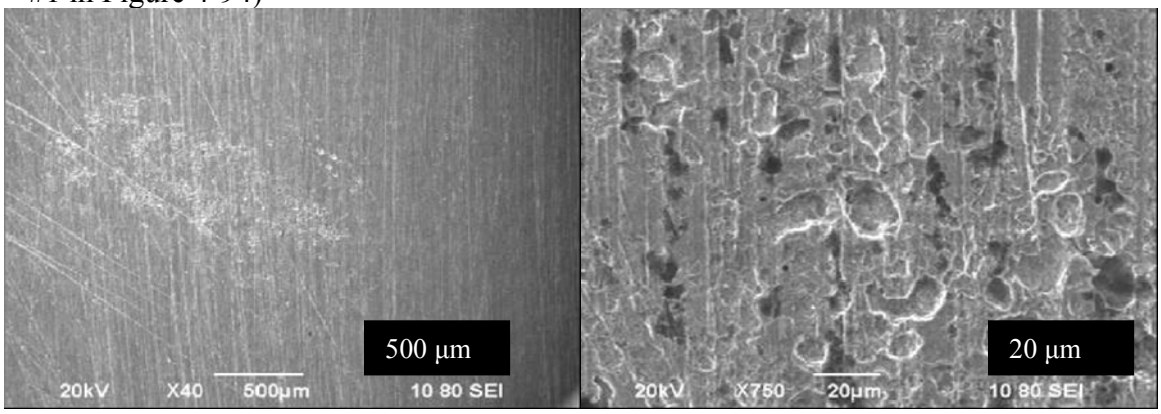

(a) SEM at 40X (b) SEM at 750X

Figure 4-96: 1-week test in the enriched Qurrayah water spiked with SRB at 31 ºC SEM analysis of coupon surface after acid cleaning; Sample #1)

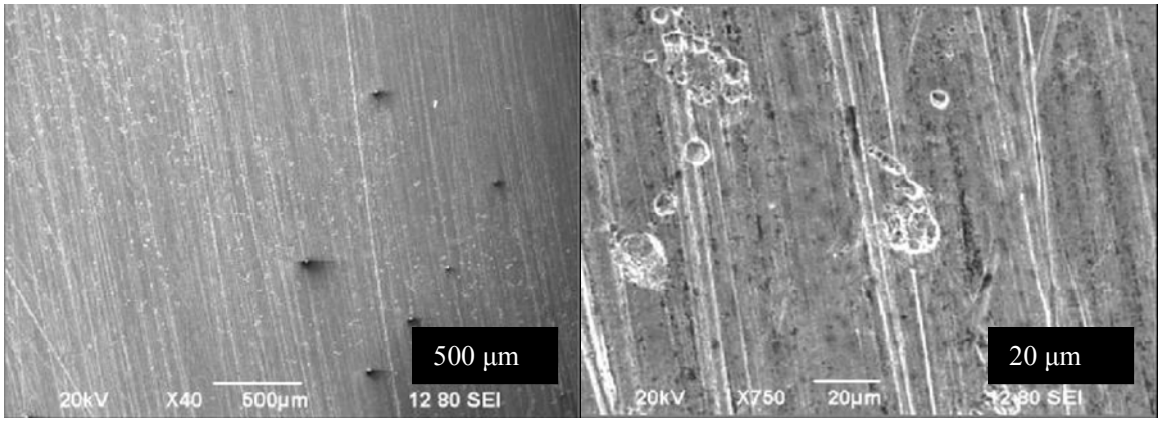

(a) SEM at 40X (b) SEM at 750X

Figure 4-97: 1-week test in the enriched Qurrayah water spiked with SRB at 31 ºC (SEM analysis of coupon surface after acid cleaning; Sample #2– duplicate sample as Sample #1 in Figure 4-96)

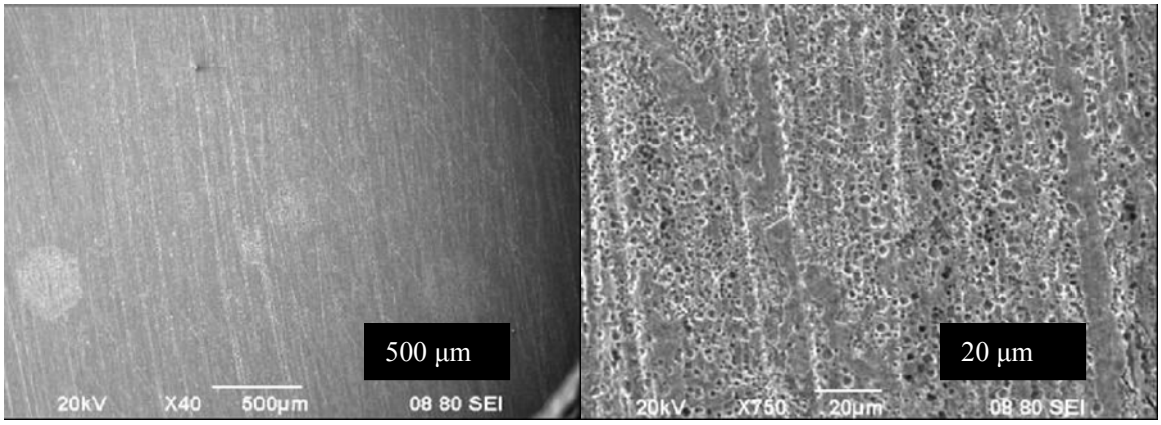

(a) SEM at 40X (b) SEM at 750X

Figure 4-98: 1-week test in the enriched Qurrayah water spiked with SRB at 37 ºC SEM analysis of coupon surface after acid cleaning; Sample #1)

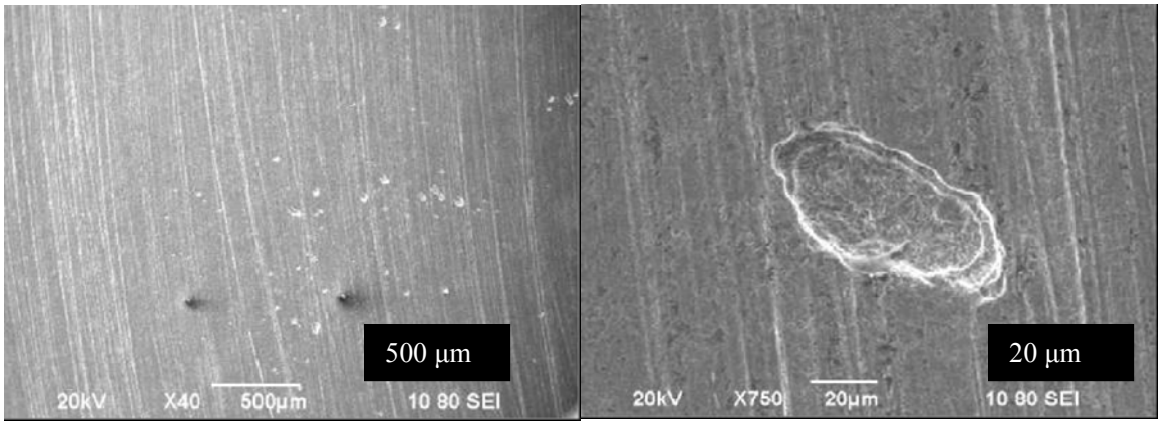

(a) SEM at 40X (b) SEM at 750X

Figure 4-99: 1-week test in the enriched Qurrayah water spiked with SRB at 37 ºC (SEM analysis of coupon surface after acid cleaning; Sample #2– duplicate sample as Sample #1 in Figure 4-98)

In the two-week test of enriched Qurrayah water spiked with SRB, elemental S was observed on all sample surfaces at all the three test temperatures (Figure 4-100 (c) ~ Figure 4-105 (c)). However, it became more difficult to find the biofilms on the sample surfaces at the increased temperature. At 25ºC, biofilms could be easily observed (Figure 4-100 and Figure 4-101). In contrast, at 31ºC, only sample #1 showed bacteria (Figure 4-

102) while no bacteria were found on duplicate sample #2 (Figure 4-103). At 37ºC, very few bacteria were found (Figure 4-104 and Figure 4-105).

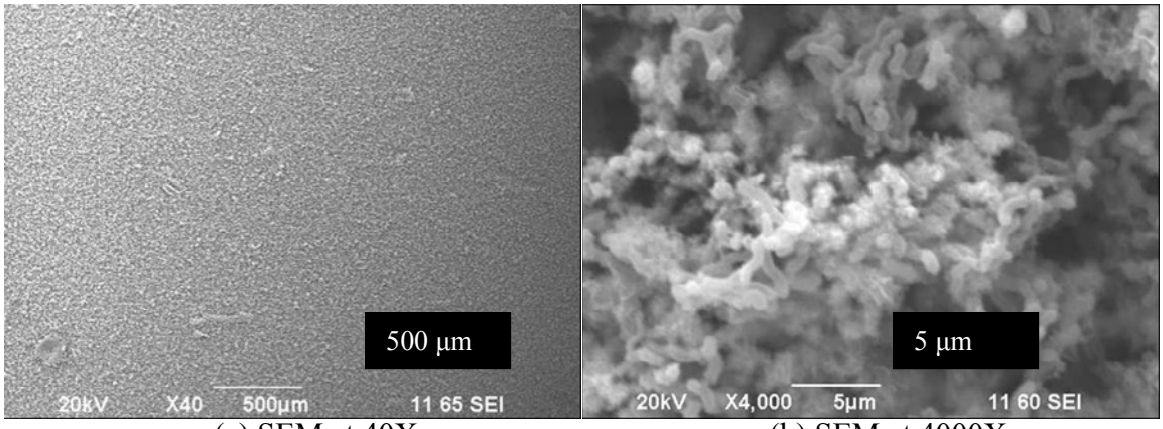

(a) SEM at 40X (b) SEM at 4000X

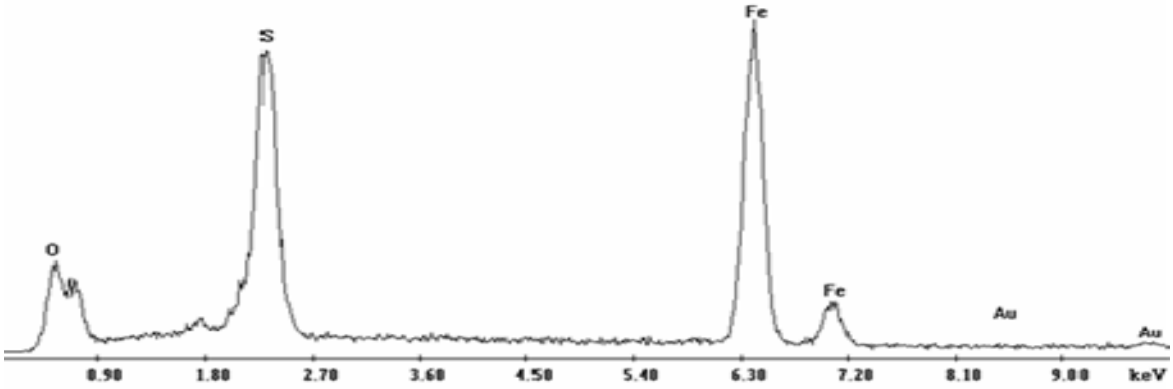

(c) Composition on the coupon surface

Figure 4-100: 2-week test in the enriched Qurrayah water spiked with SRB at 25 ºC (SEM and EDS analysis of coupon surface before acid cleaning; Sample #1)

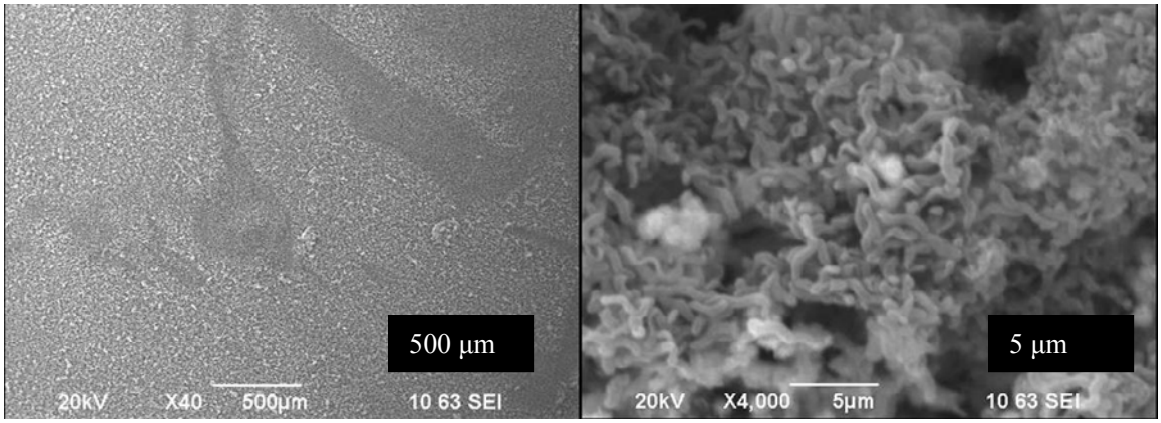

(a) SEM at 40X (b) SEM at 4000X

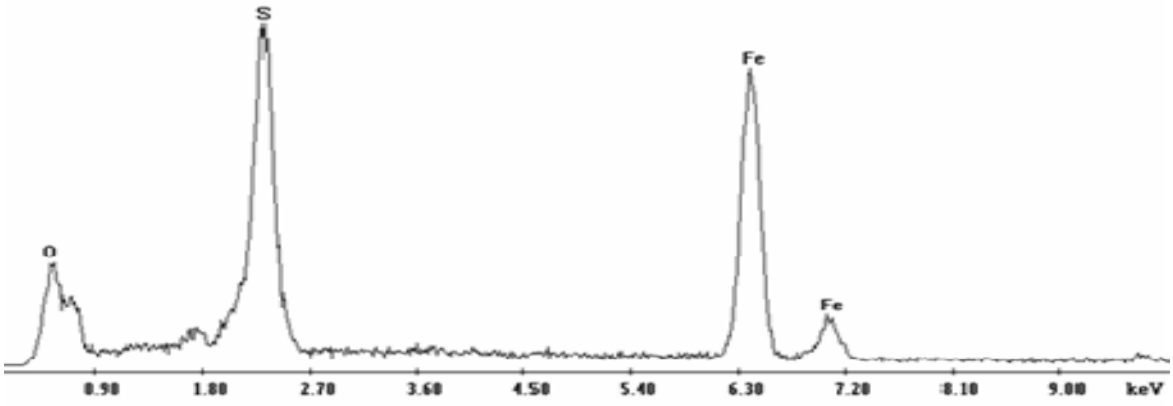

(c) Composition on the coupon surface

Figure 4-101: 2-week test in the enriched Qurrayah water spiked with SRB at 25 ºC (SEM and EDS analysis of coupon surface before acid cleaning; Sample #2 – duplicate sample as Sample #1 in Figure 4-100)

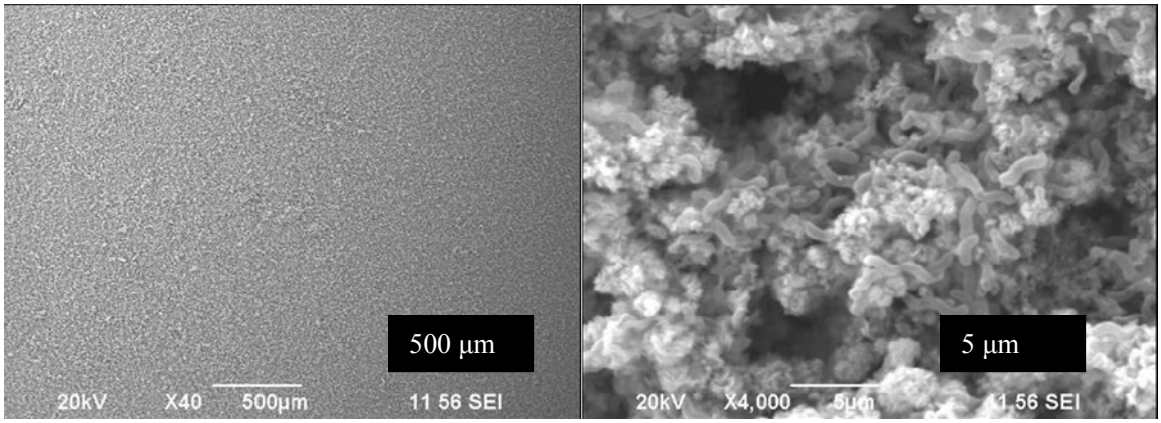

(a) SEM at 40X (b) SEM at 4000X

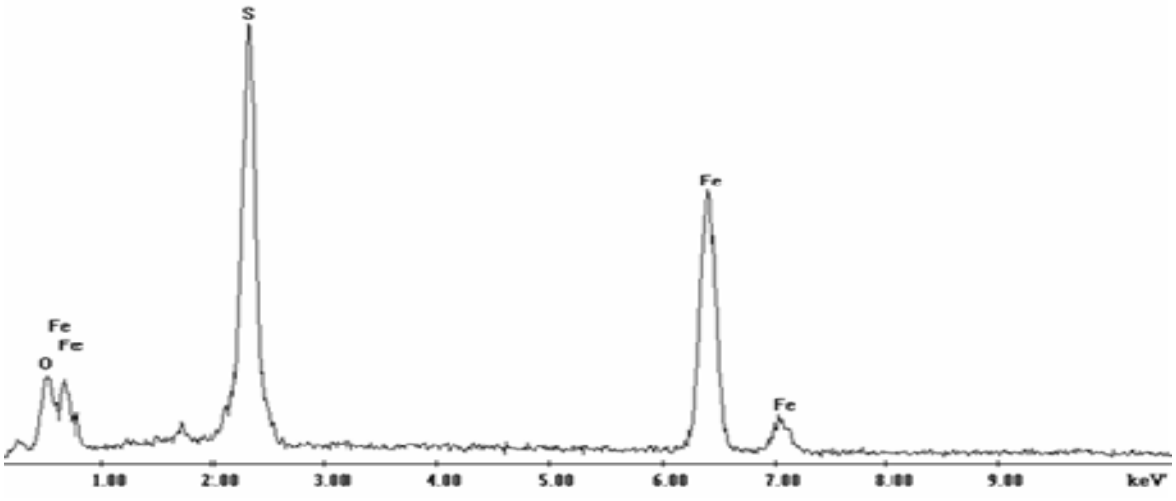

(c) Composition on the coupon surface

Figure 4-102: 2-week test in the enriched Qurrayah water spiked with SRB at 31 ºC (SEM and EDS analysis of coupon surface before acid cleaning; Sample #1)

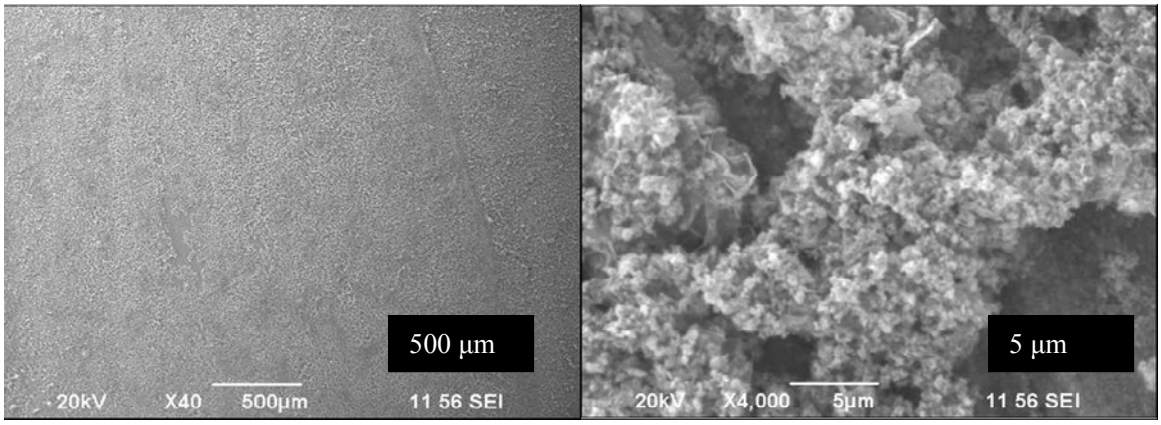

(a) SEM at 40X (b) SEM at 4000X

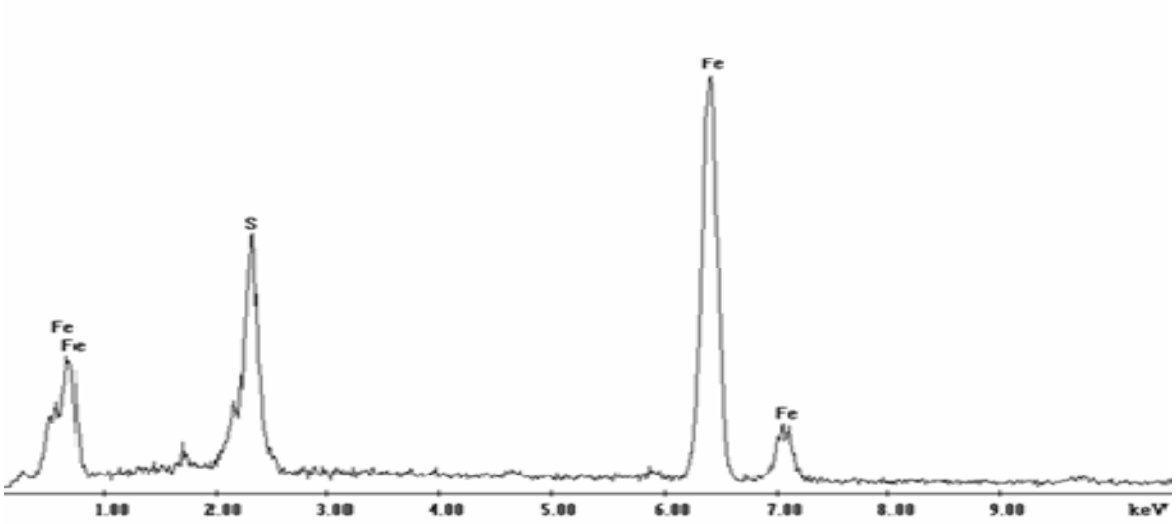

(c) Composition on the coupon surface

Figure 4-103: 2-week test in the enriched Qurrayah water spiked with SRB at 31 ºC (SEM and EDS analysis of coupon surface before acid cleaning; Sample #2– duplicate sample as Sample #1 in Figure 4-102)

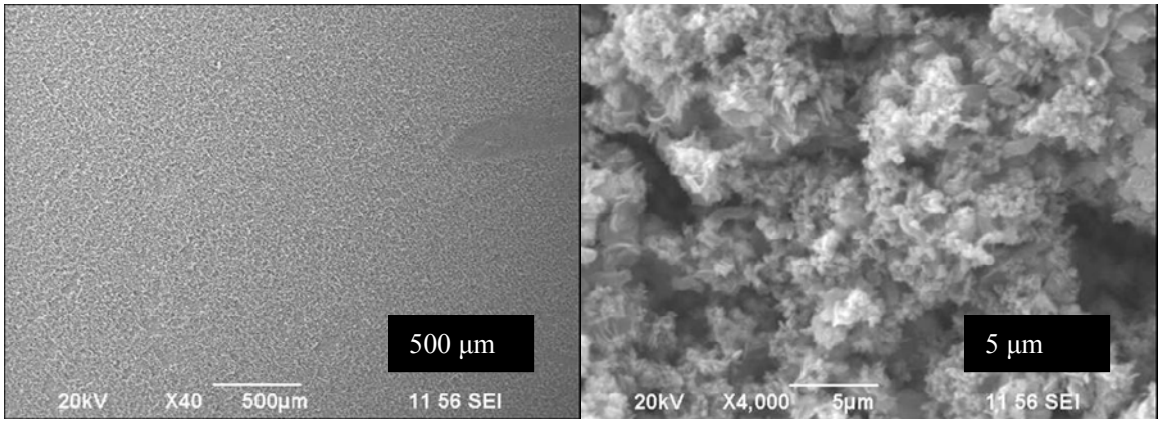

(a) SEM at 40X (b) SEM at 4000X

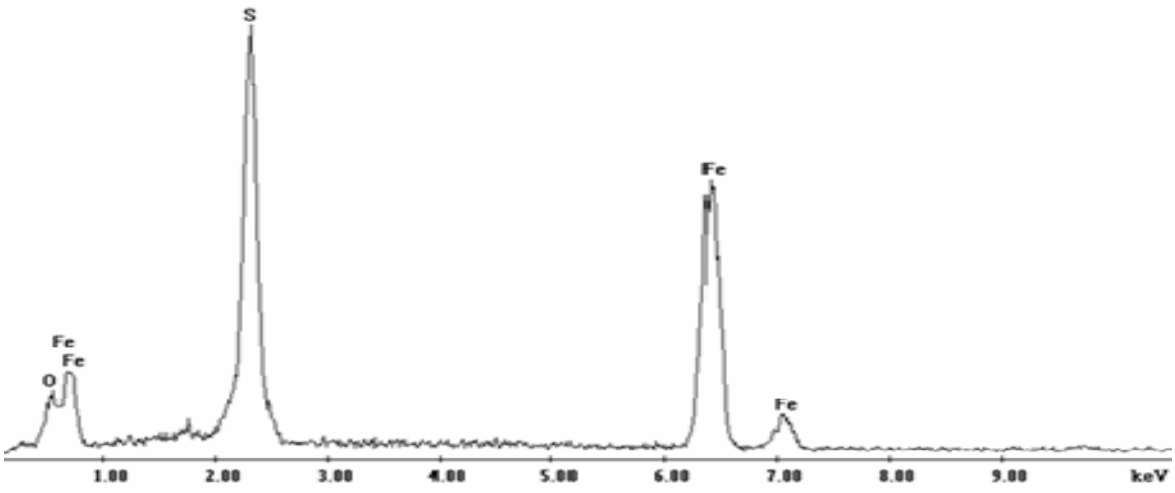

(c) Composition on the coupon surface

Figure 4-104: 2-week test in the enriched Qurrayah water spiked with SRB at 37 ºC (SEM and EDS analysis of coupon surface before acid cleaning; Sample #1)

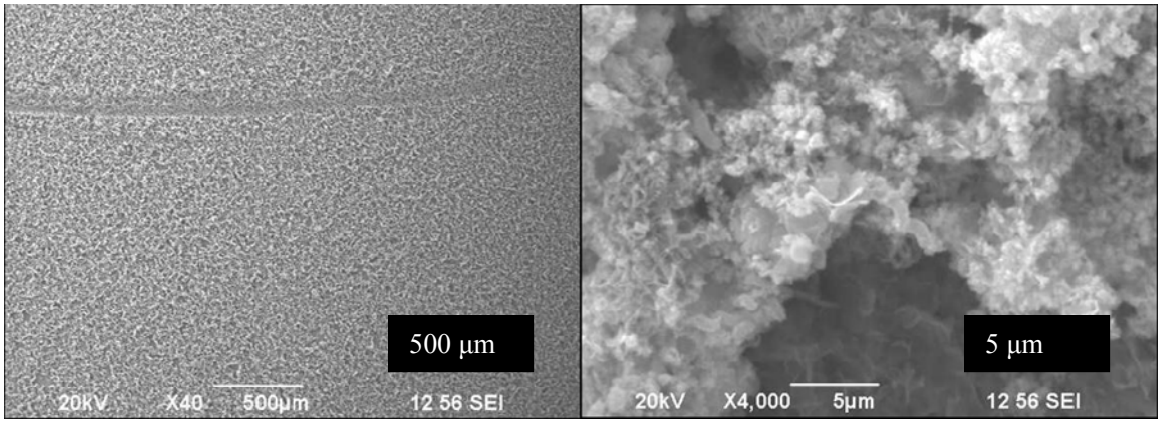

(a) SEM at 40X (b) SEM at 4000X

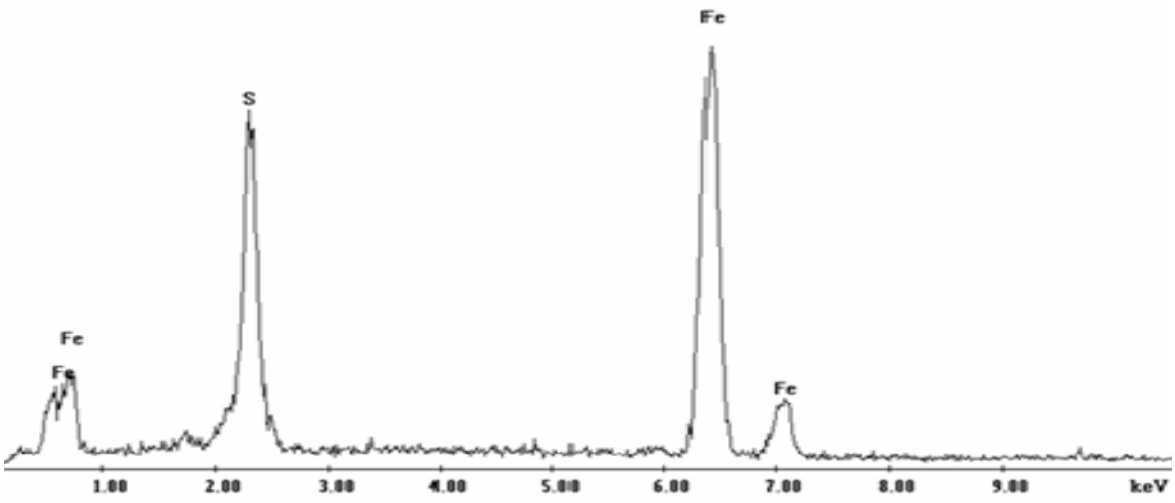

(c) Composition on the coupon surface

Figure 4-105: 2-week test in the enriched Qurrayah water spiked with SRB at 37 ºC (SEM and EDS analysis of coupon surface before acid cleaning; Sample #2– duplicate sample as Sample #1 in Figure 4-104)

Figure 4-106 shows greater weight loss at higher temperatures. Pitting rates were obtained from the samples at 25ºC and 31ºC while corrosion rates were obtained in the samples at 37ºC. In comparing the coupon surfaces after removing the films, it was found that MIC pits appeared at 25ºC (Figure 4-107 and Figure 4-108) or 31ºC (Figure 4-109 and Figure 4-110), but at 37ºC the entire sample surface turned much coarser (Figure 4-111 and Figure 4-112). From this test and the one-week test above, it was found that biofilm and pit formation on the sample surface changed both with time and temperature.

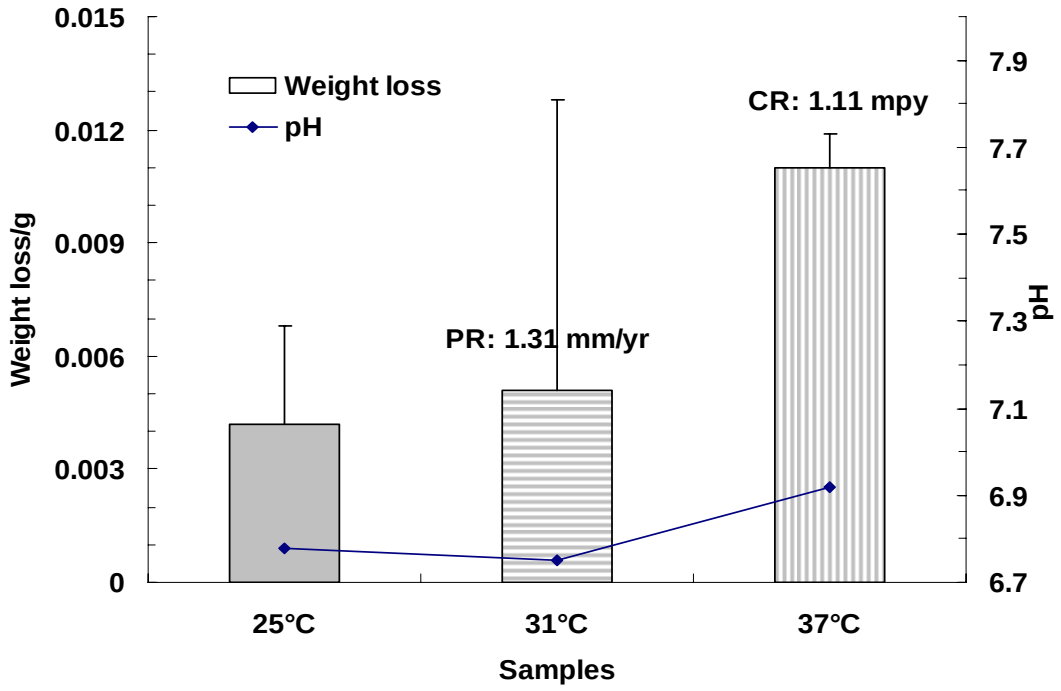

Figure 4-106: X65 coupon weight loss in the enriched Qurrayah water (seawater) spiked with SRB after the 2-week test

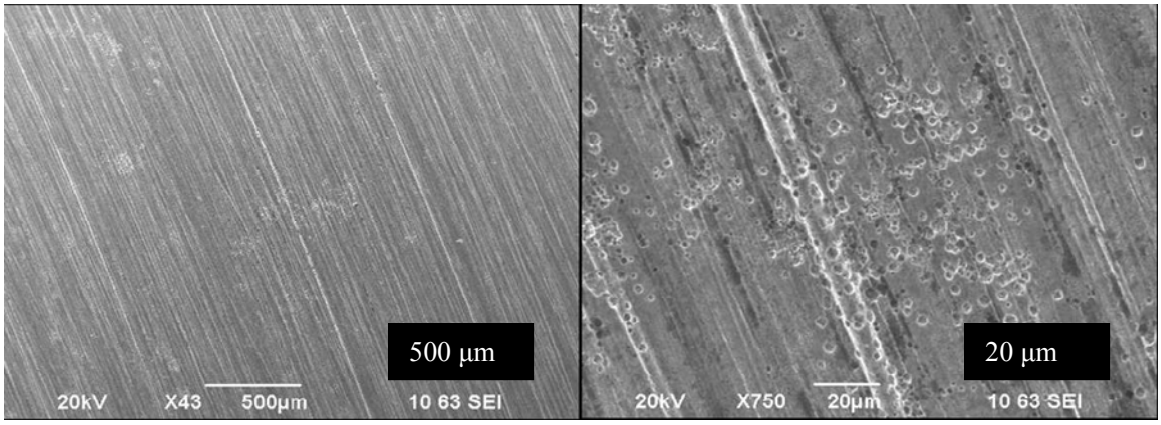

(a) SEM at 43X (b) SEM at 750X

Figure 4-107: 2-week test in the enriched Qurrayah water spiked with SRB at 25 ºC (SEM analysis of coupon surface after acid cleaning; Sample #1)

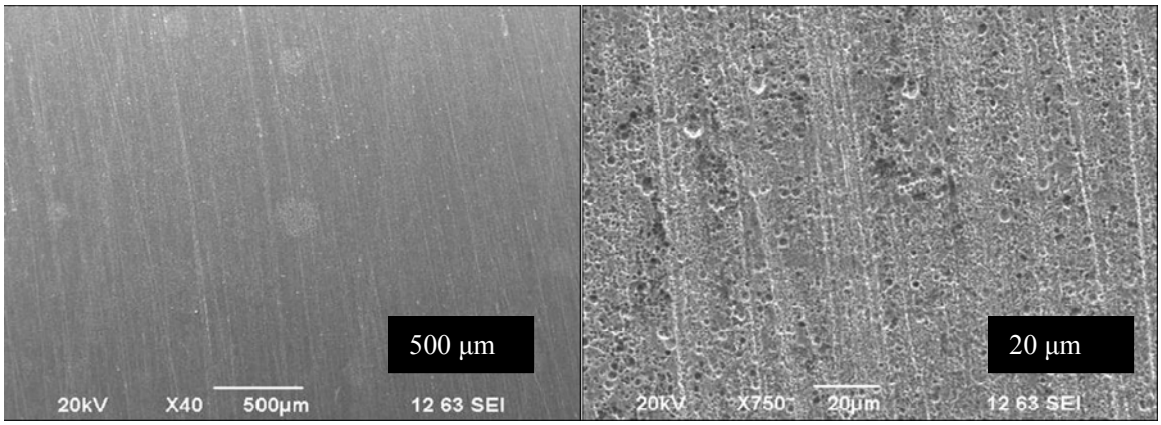

(a) SEM at 40X (b) SEM at 750X

Figure 4-108: 2-week test in the enriched Qurrayah water spiked with SRB at 25 ºC (SEM analysis of coupon surface after acid cleaning; Sample #2– duplicate sample as Sample #1 in Figure 4-107)

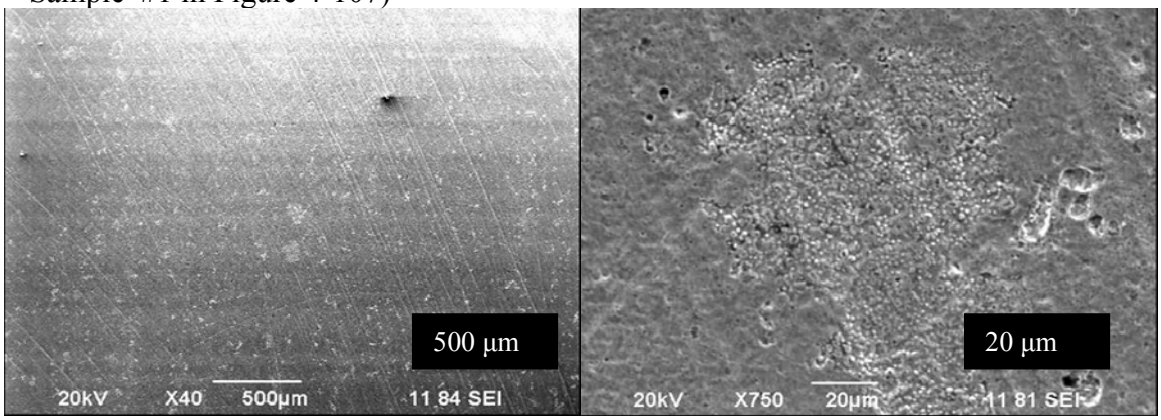

(a) SEM at 40X (b) SEM at 750X

Figure 4-109: 2-week test in the enriched Qurrayah water spiked with SRB at 31 ºC (SEM analysis of coupon surface after acid cleaning; Sample #1)

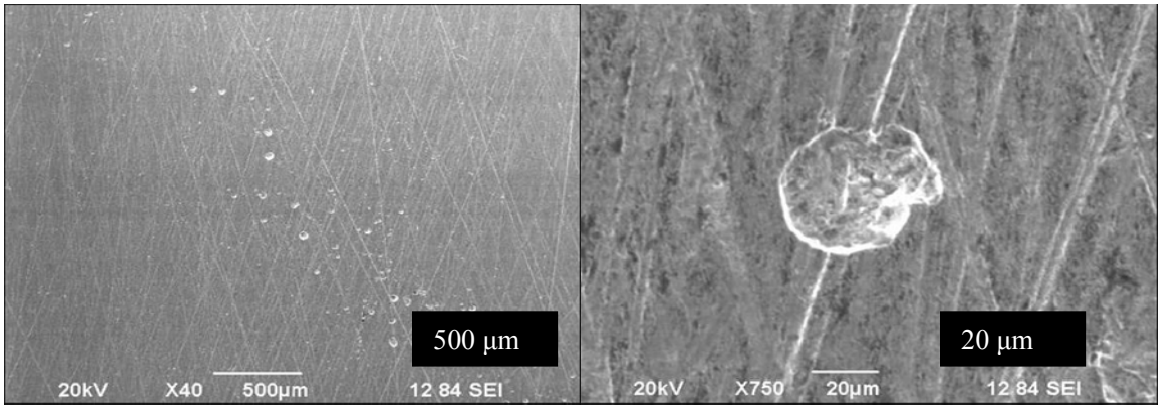

(a) SEM at 40X (b) SEM at 750X

Figure 4-110: 2-week test in the enriched Qurrayah water spiked with SRB at 31 ºC (SEM analysis of coupon surface after acid cleaning; Sample #2– duplicate sample as Sample #1 in Figure 4-109)

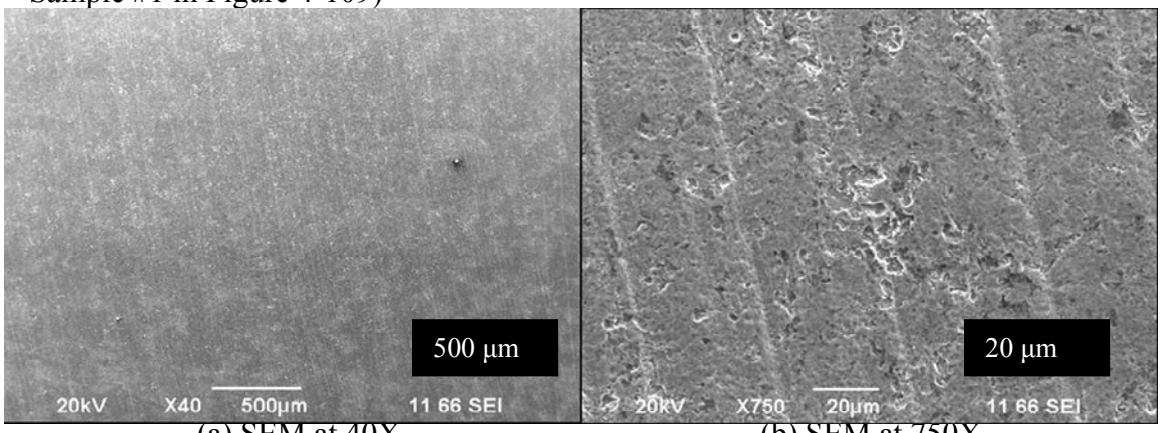

(a) SEM at 40X (b) SEM at 750X

Figure 4-111: 2-week test in the enriched Qurrayah water spiked with SRB at 37 ºC (SEM analysis of coupon surface after acid cleaning; Sample #1)

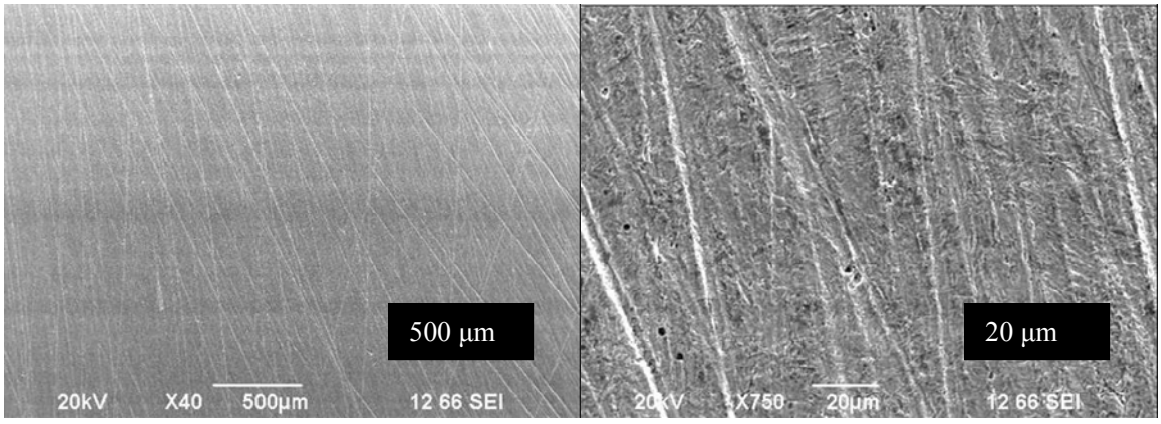

(a) SEM at 40X (b) SEM at 750X

Figure 4-112: 2-week test in the enriched Qurrayah water spiked with SRB at 37 ºC (SEM analysis of coupon surface after acid cleaning; Sample #2– duplicate sample as Sample #1 in Figure 4-111)

As in the two-week test above, in the one-month test, elemental S could be observed on all the sample surfaces at all three test temperatures (Figure 4-113 (c) ~ Figure 4-118 (c)). The presence of biofilm was dependent on the location of the sample surfaces rather than solely on the temperature as in the two-week test. When the upper surface was not covered by FeS film, like the cases in Figure 4-113 ~ Figure 4-115, bacteria could be observed; while at the locations shown in Figure 4-116 and Figure 4-118 where the surface was covered with FeS film, bacteria could not be found. On the coupon surface in Figure 4-117 where there is a film rupture, several solid layers covering the sample surface are clearly evident and show the biofilm layers to be covered by a film resembling FeS film. Unless this surface was broken for a reason, the film prevented the biofilms underneath from being seen, such as in the cases in Figure 4-113 ~ Figure 4-115. Figure 4-119 shows that weight loss increased with the increase of temperature. Pitting rates were obtained from the samples at 25ºC while corrosion rates were obtained from the samples at 31ºC and 37ºC. After the films were removed, the appearances of coupon surfaces looked similar to those in the two-week test. MIC pits were evident at the lower temperature 25ºC (Figure 4-120 and Figure 4-121), but at the higher temperatures of 31ºC and 37ºC, the surfaces became coarser (Figure 4-122 ~ Figure 4-125). It is likely that the smaller pits had coalesced.

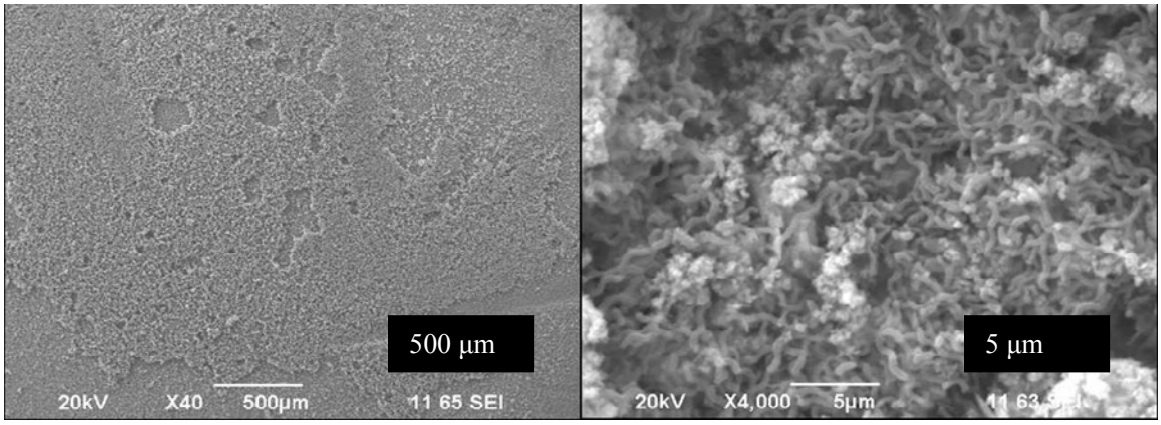

(a) SEM at 40X (b) SEM at 4000X

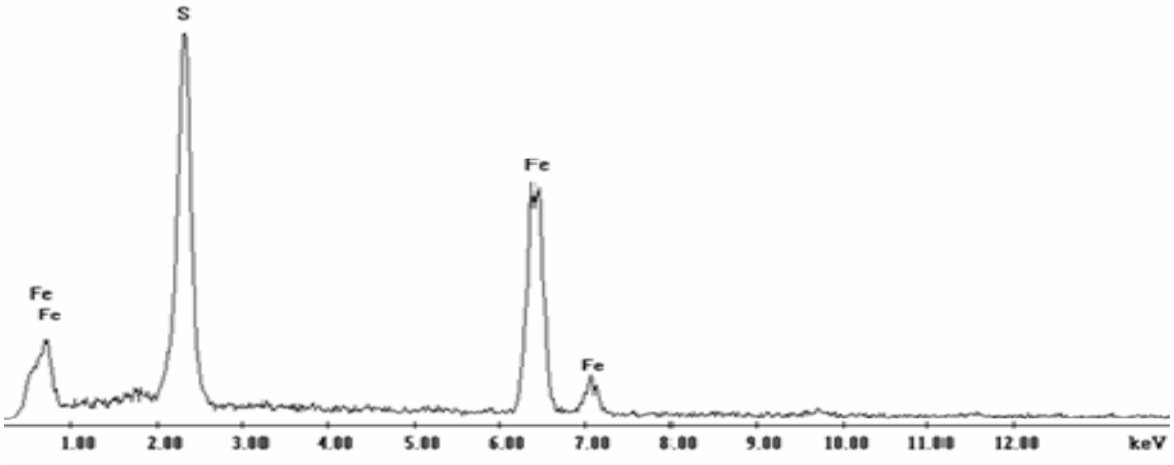

(c) Composition on the coupon surface

Figure 4-113: 1-month test in the enriched Qurrayah water spiked with SRB at 25 ºC (SEM and EDS analysis of coupon surface before acid cleaning; Sample #1)

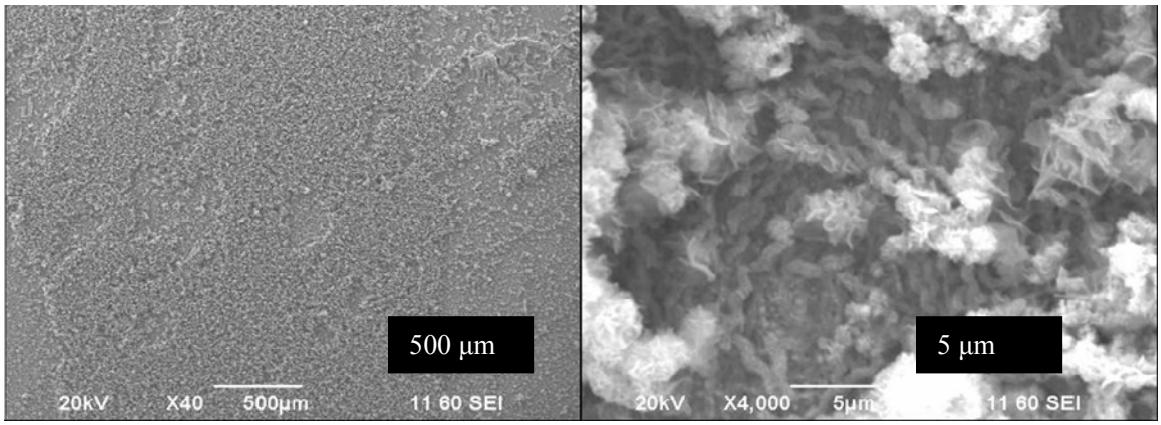

(a) SEM at 40X (b) SEM at 4000X

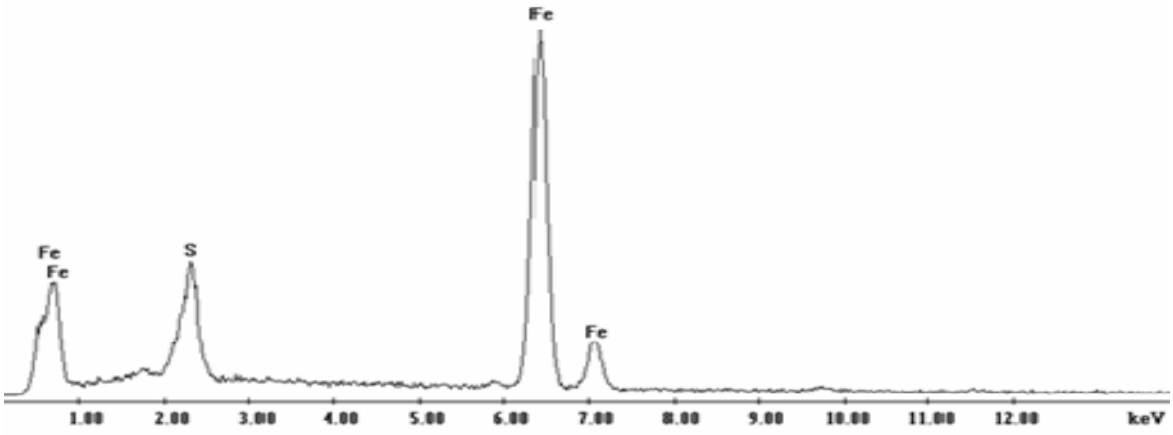

(c) Composition on the coupon surface

Figure 4-114: 1-month test in the enriched Qurrayah water spiked with SRB at 25 ºC (SEM and EDS analysis of coupon surface before acid cleaning; Sample #2– duplicate sample as Sample #1 in Figure 4-113)

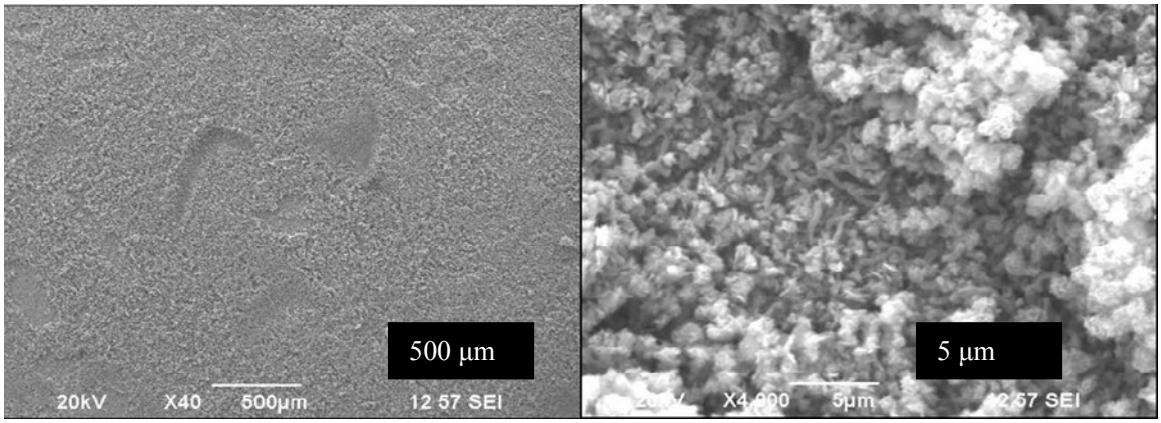

(a) SEM at 40X (b) SEM at 4000X

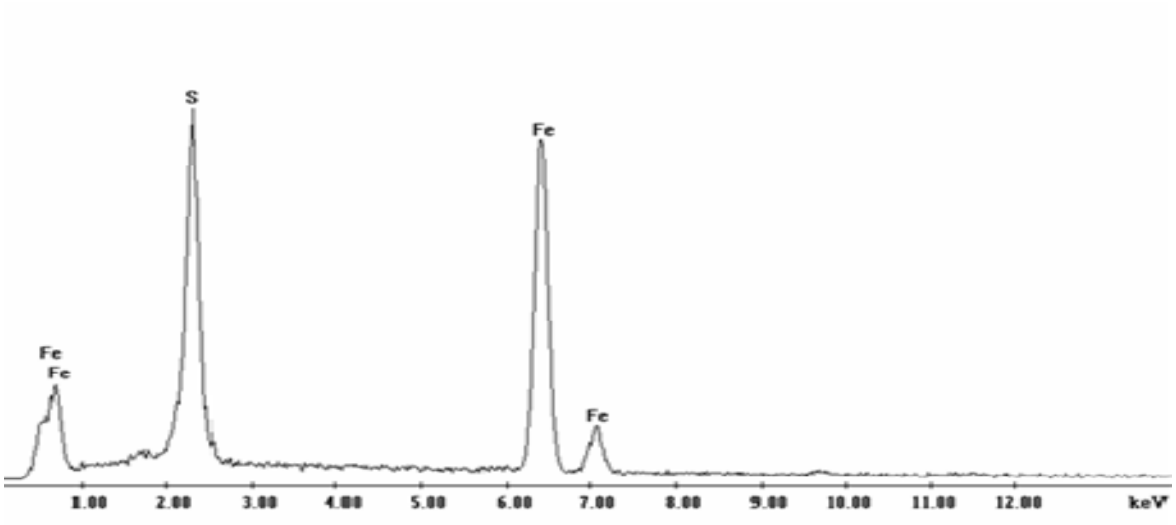

(c) Composition on the coupon surface

Figure 4-115: 1-month test in the enriched Qurrayah water spiked with SRB at 31 ºC (SEM and EDS analysis of coupon surface before acid cleaning; Sample #1)

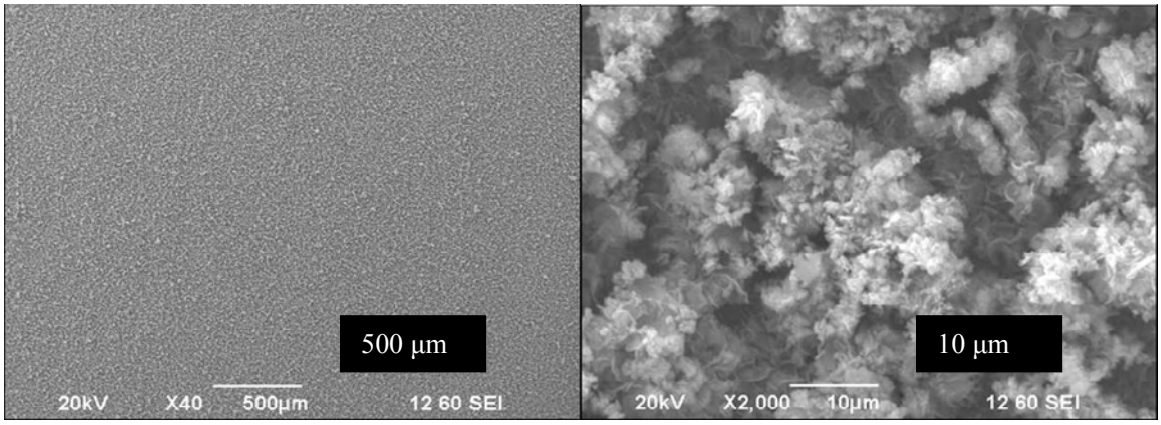

(a) SEM at 40X (b) SEM at 2000X

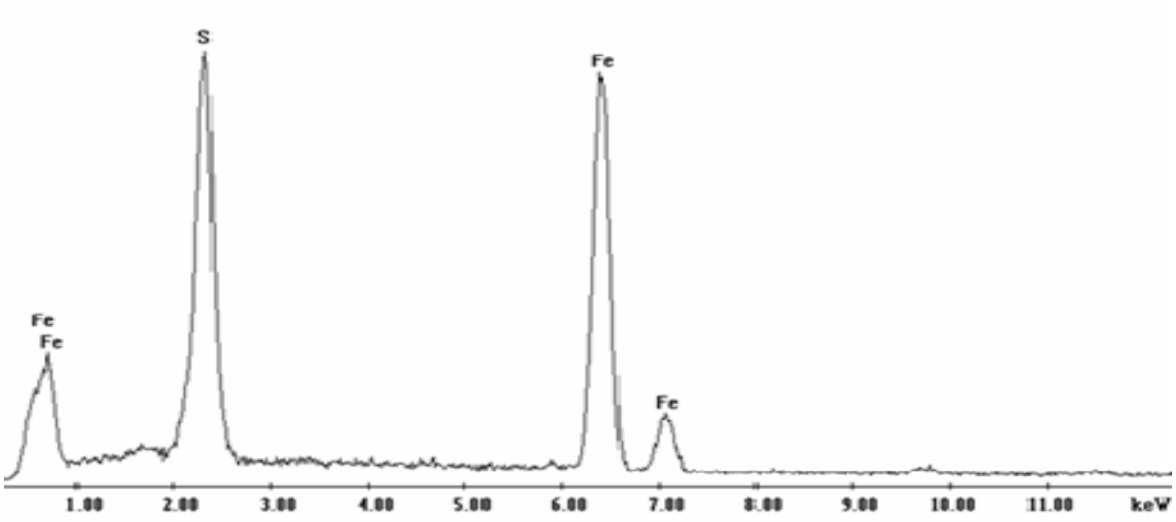

(c) Composition on the coupon surface

Figure 4-116: 1-month test in the enriched Qurrayah water spiked with SRB at 31 ºC (SEM and EDS analysis of coupon surface before acid cleaning; Sample #2– duplicate sample as Sample #1 in Figure 4-115)

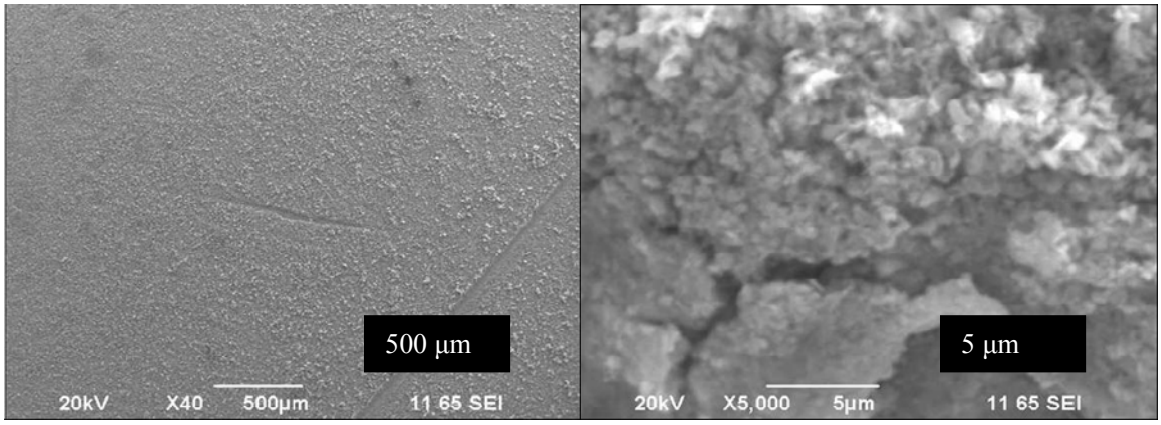

(a) SEM at 40X (b) SEM at 5000X

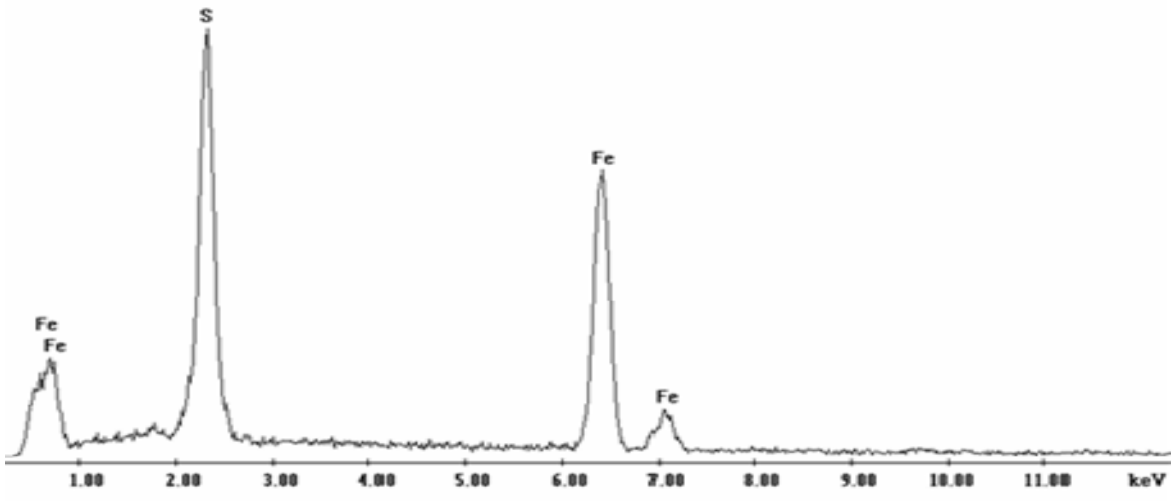

(c) Composition on the coupon surface

Figure 4-117: 1-month test in the enriched Qurrayah water spiked with SRB at 37 ºC (SEM and EDS analysis of coupon surface before acid cleaning; Sample #1)

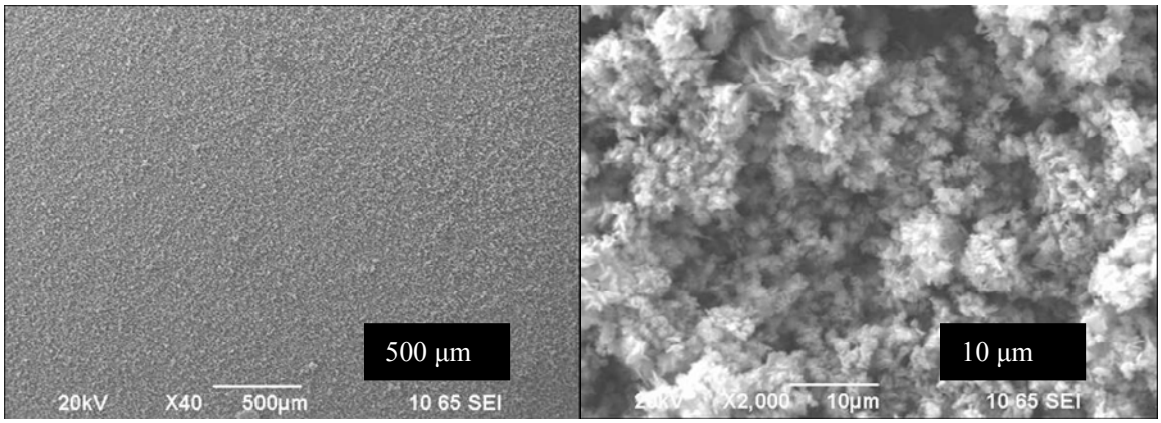

(a) SEM at 40X (b) SEM at 2000X

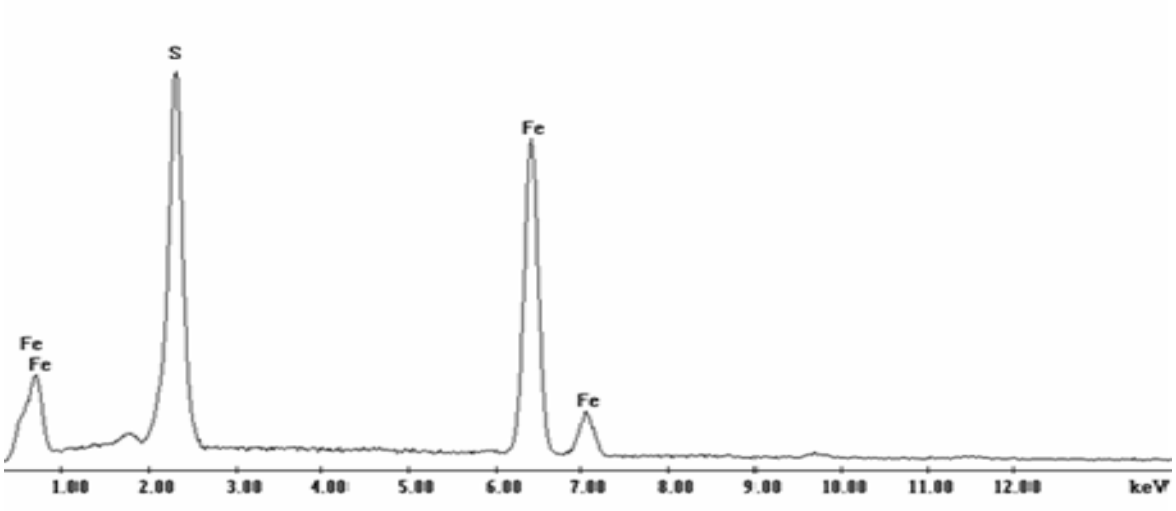

(c) Composition on the coupon surface

Figure 4-118: 1-month test in the enriched Qurrayah water spiked with SRB at 37 ºC (SEM and EDS analysis of coupon surface before acid cleaning; Sample #2– duplicate sample as Sample #1 in Figure 4-117)

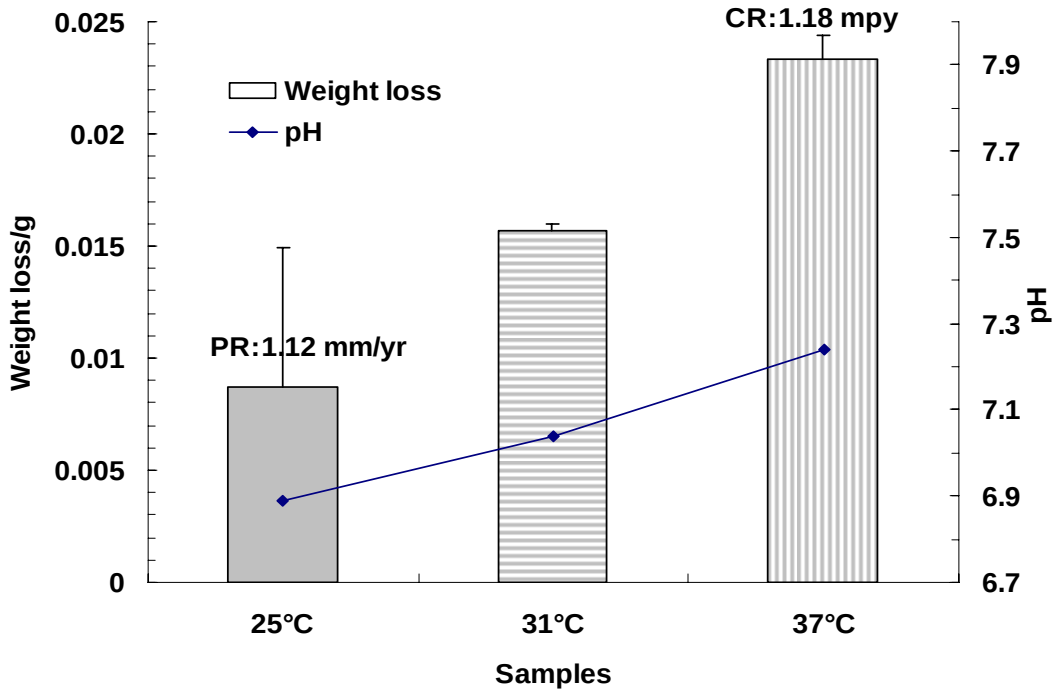

Figure 4-119: X65 coupon weight loss in the enriched Qurrayah water (seawater) spiked with SRB after the 1-month test

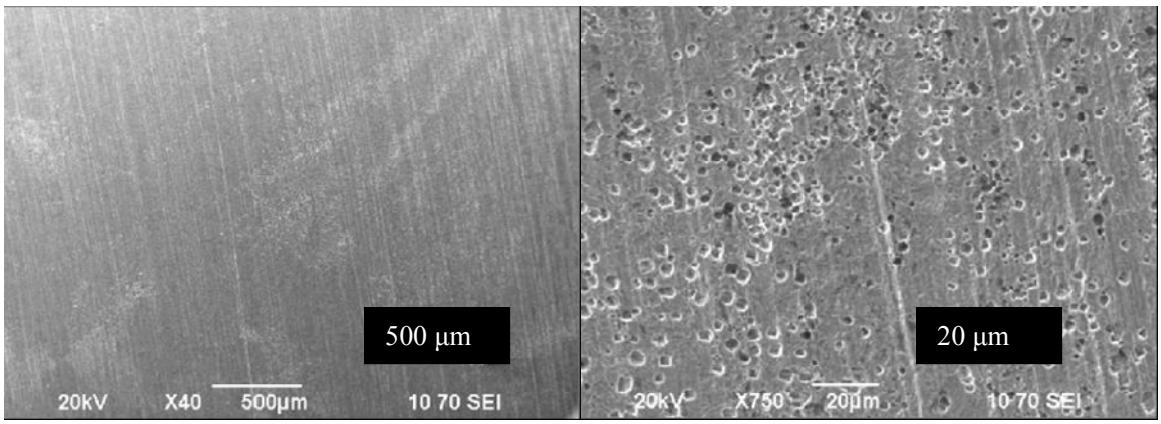

(a) SEM at 40X (b) SEM at 750X

Figure 4-120: 1-month test in the enriched Qurrayah water spiked with SRB at 25 ºC (SEM analysis of coupon surface after acid cleaning; Sample #1)

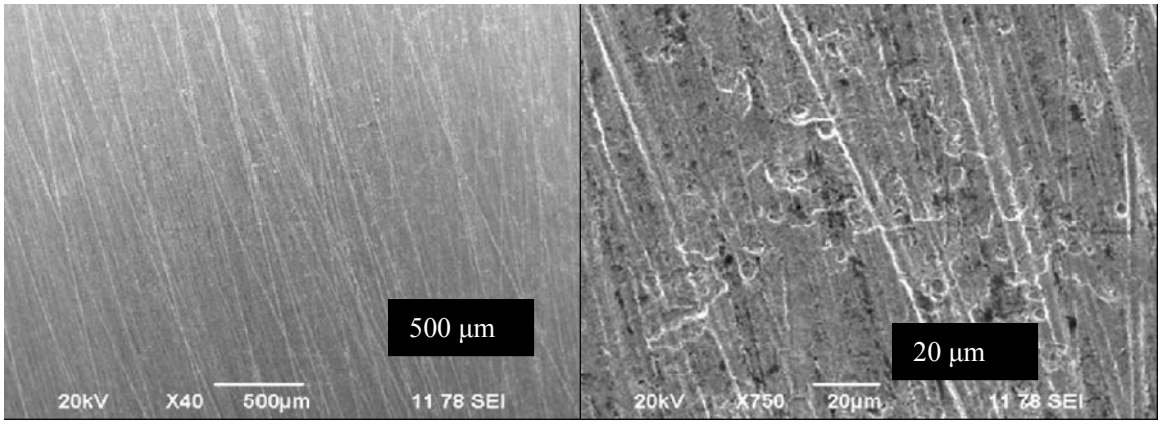

(a) SEM at 40X (b) SEM at 750X

Figure 4-121: 1-month test in the enriched Qurrayah water spiked with SRB at 25 ºC (SEM analysis of coupon surface after acid cleaning; Sample #2– duplicate sample as Sample #1 in Figure 4-120)

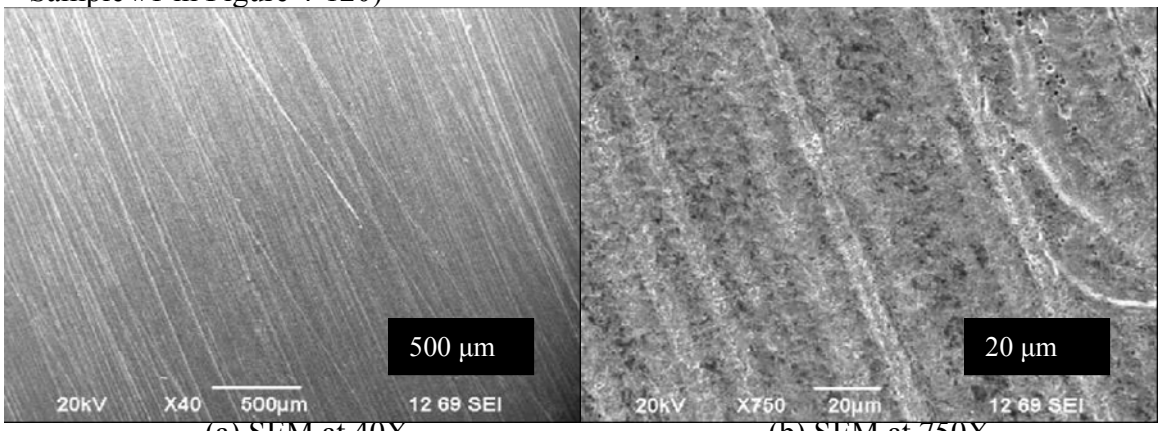

(a) SEM at 40X (b) SEM at 750X

Figure 4-122: 1-month test in the enriched Qurrayah water spiked with SRB at 31 ºC (SEM analysis of coupon surface after acid cleaning; Sample #1)

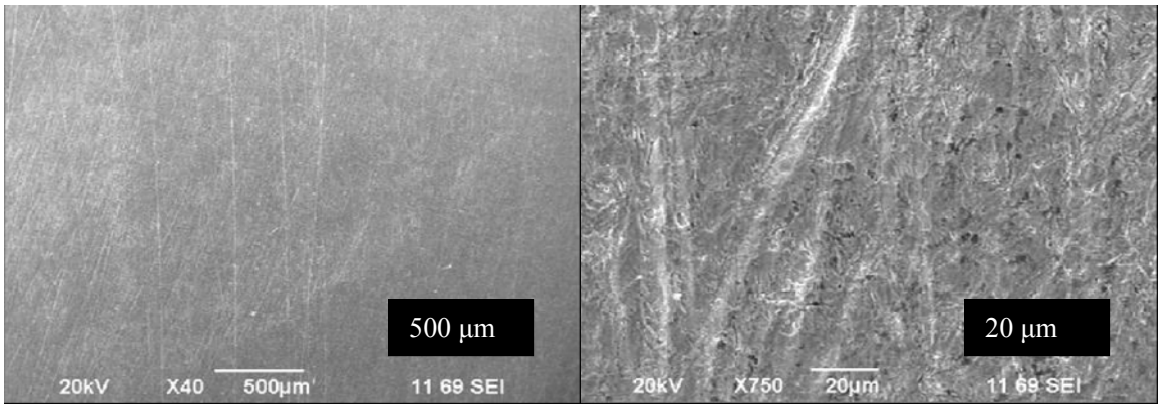

(a) SEM at 40X (b) SEM at 750X

Figure 4-123: 1-month test in the enriched Qurrayah water spiked with SRB at 31 ºC (SEM analysis of coupon surface after acid cleaning; Sample #2– duplicate sample as Sample #1 in Figure 4-122)

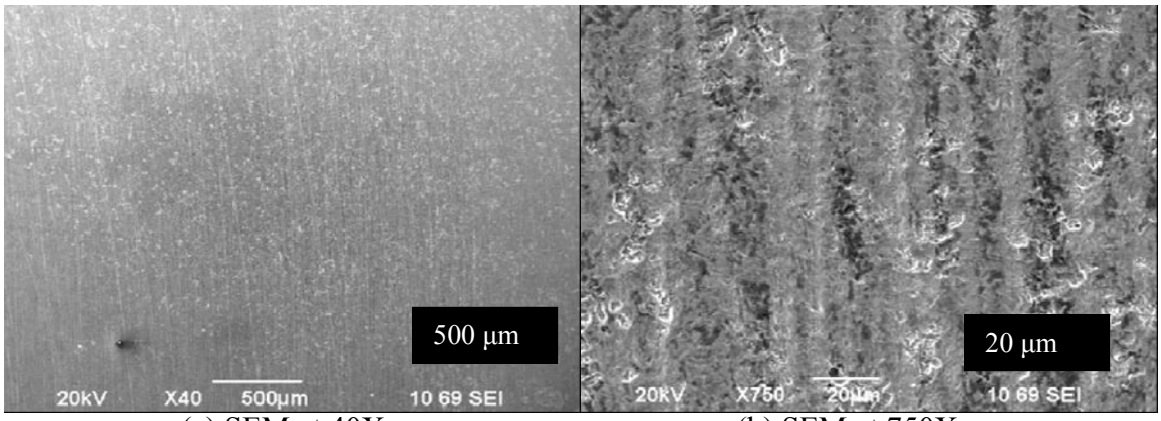

(a) SEM at 40X (b) SEM at 750X

Figure 4-124: 1-month test in the enriched Qurrayah water spiked with SRB at 37 ºC (SEM analysis of coupon surface after acid cleaning; Sample #1)

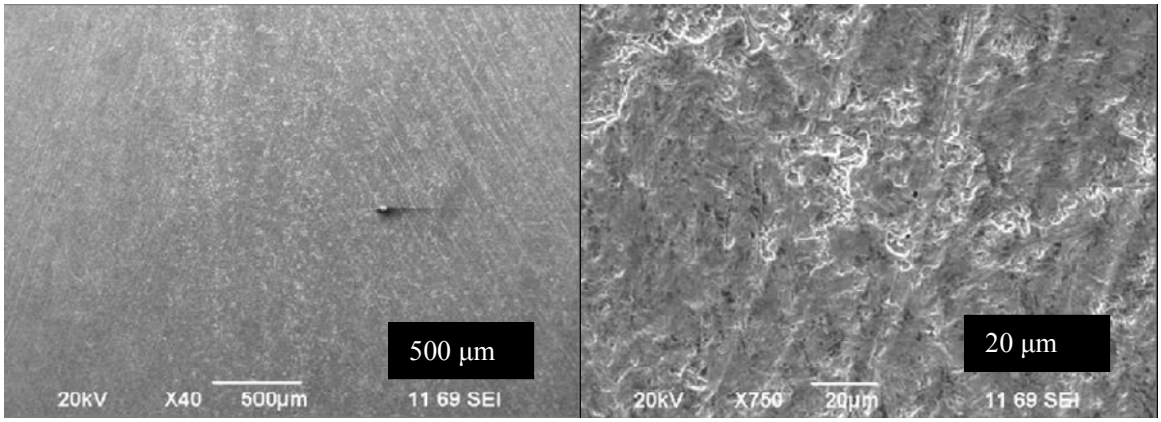

(a) SEM at 40X (b) SEM at 750X

Figure 4-125: 1-month test in the enriched Qurrayah water spiked with SRB at 37 ºC (SEM analysis of coupon surface after acid cleaning; Sample #2– duplicate sample as Sample #1 in Figure 4-124)

In summary, SRB biofilm growth depends on the test environment. A conducive condition like warm temperature can accelerate biofilm formation. In this test, biofilm was first apparent at a higher temperature. FeS film that was found on the top of the biofilms verified the assumption that FeS film is sometimes protective because the film makes supplying the nutrient to bacteria difficult. In field operations, some pipeline

failures were probably due to MIC even when no visible SRB were detected. It was possible that SRB biofilms were hidden under other films deposits.

MIC pits tend to be different from other pitting. Infinite focus microscope (IFM), an excellent tool for analyzing pit morphology, was used to analyze coupon surfaces. The IFM 3D images in Figure 4-126 clearly show the pit configuration after the coupon was cleaned (the coupon from the three-month test in the enriched Wasia water at 25 ºC is the example shown. Refer to Figure 4-55 for the SEM images). The pit depth was obtained by analyzing the IFM images (Figure 4-126). Portion (a) in Figure 4-127 shows there are three pits with different depth, and (b) shows the deepest pit has the depth of 70 μm. Therefore, the pitting rate in this three-month test in the enriched Wasia water at 25 ºC was around 11 mpy (0.28mm/year), which is about 40 times the general corrosion rate (0.27 mpy, Figure 4-54) at the same test condition.

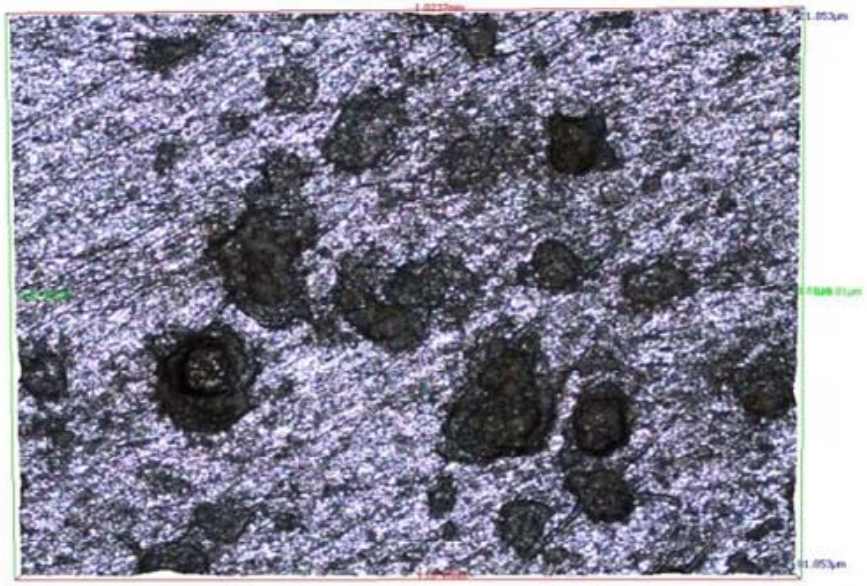

(a)

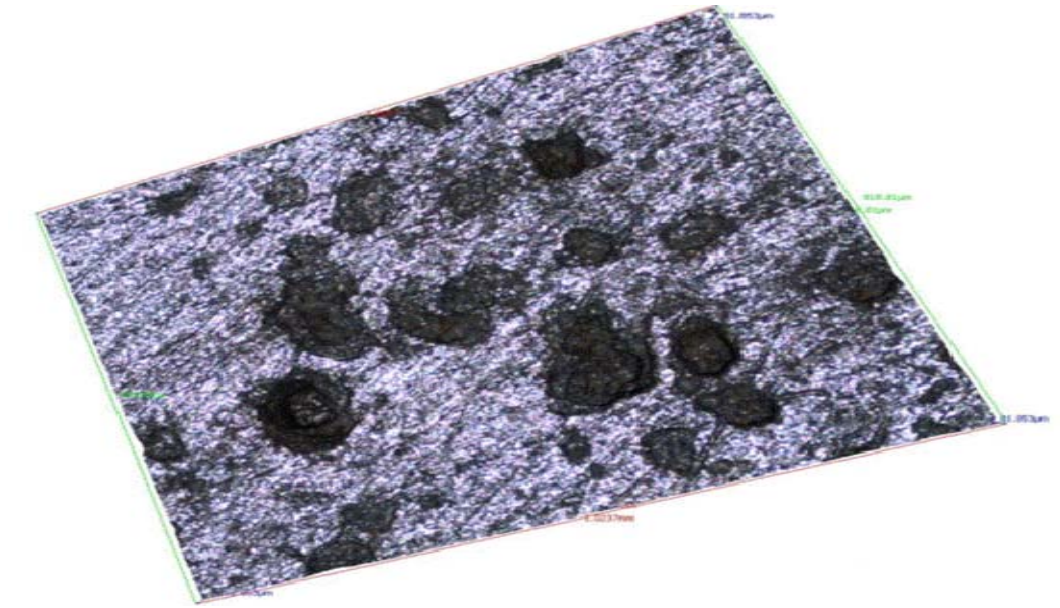

(b)

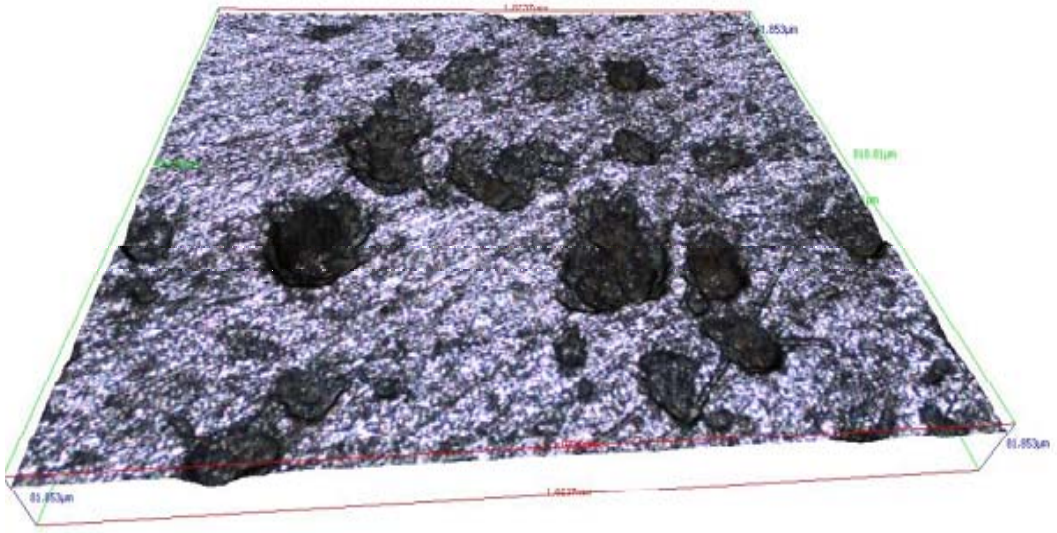

(c)

Figure 4-126: IFM 3D images of X65 coupon surface after acid cleaning (the 3-month test in the enriched Wasia water spiked with SRB at 25 ºC; Refer to Figure 4-55 for the SEM images)

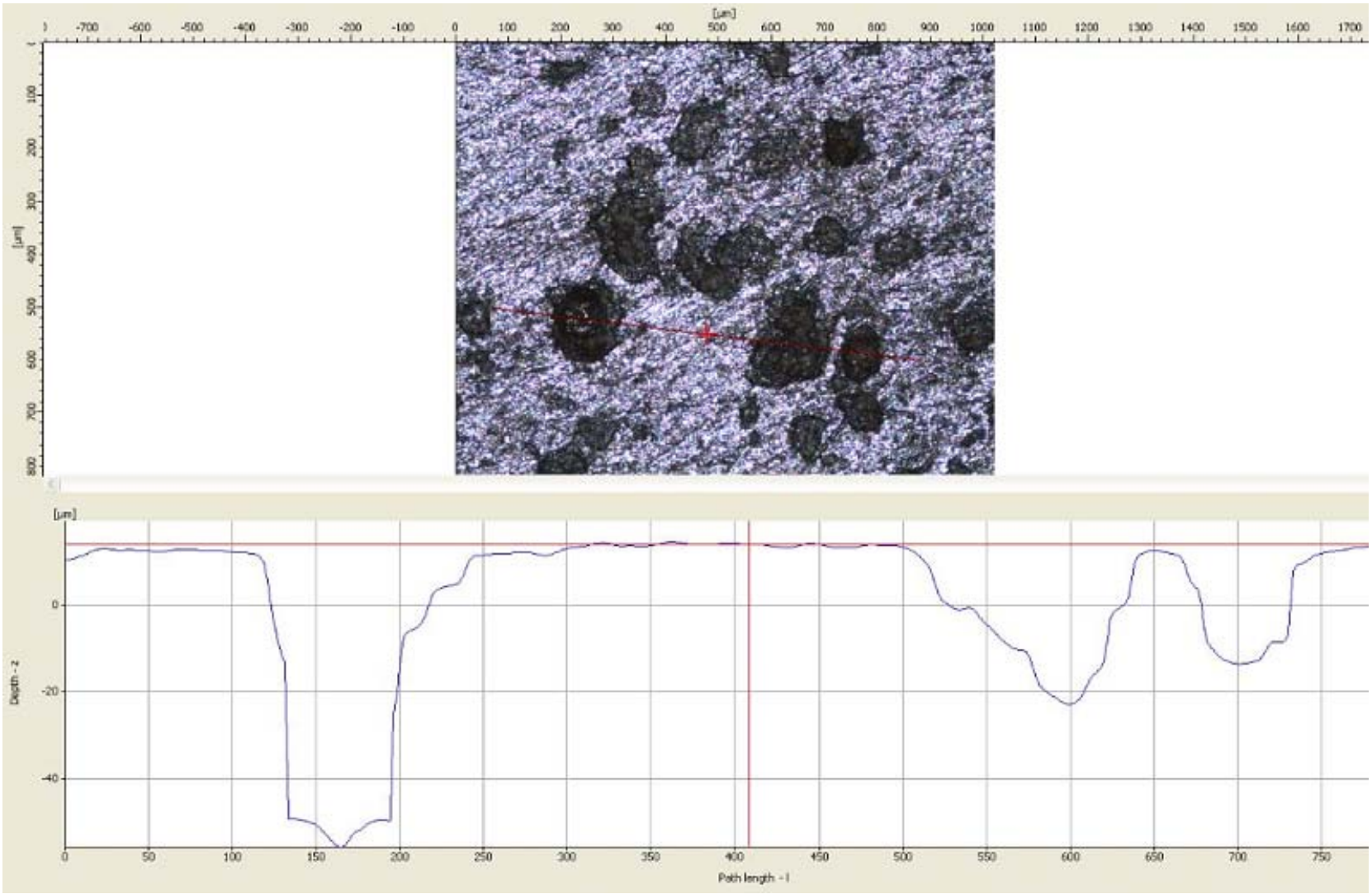
[µm]
-700 -600 -500 -400 -300 -200 -100 0 100 200 300 400 500 600 700 800 900 1000 1100 1200 1300 1400 1500 1600 1700
[µm]
100 200 300 400 500 600 700 800
[µm]
0
-20
-40
Depth - z
0 50 100 150 200 250 300 350 400 450 500 550 600 650 700 750
Path length - l

(a)

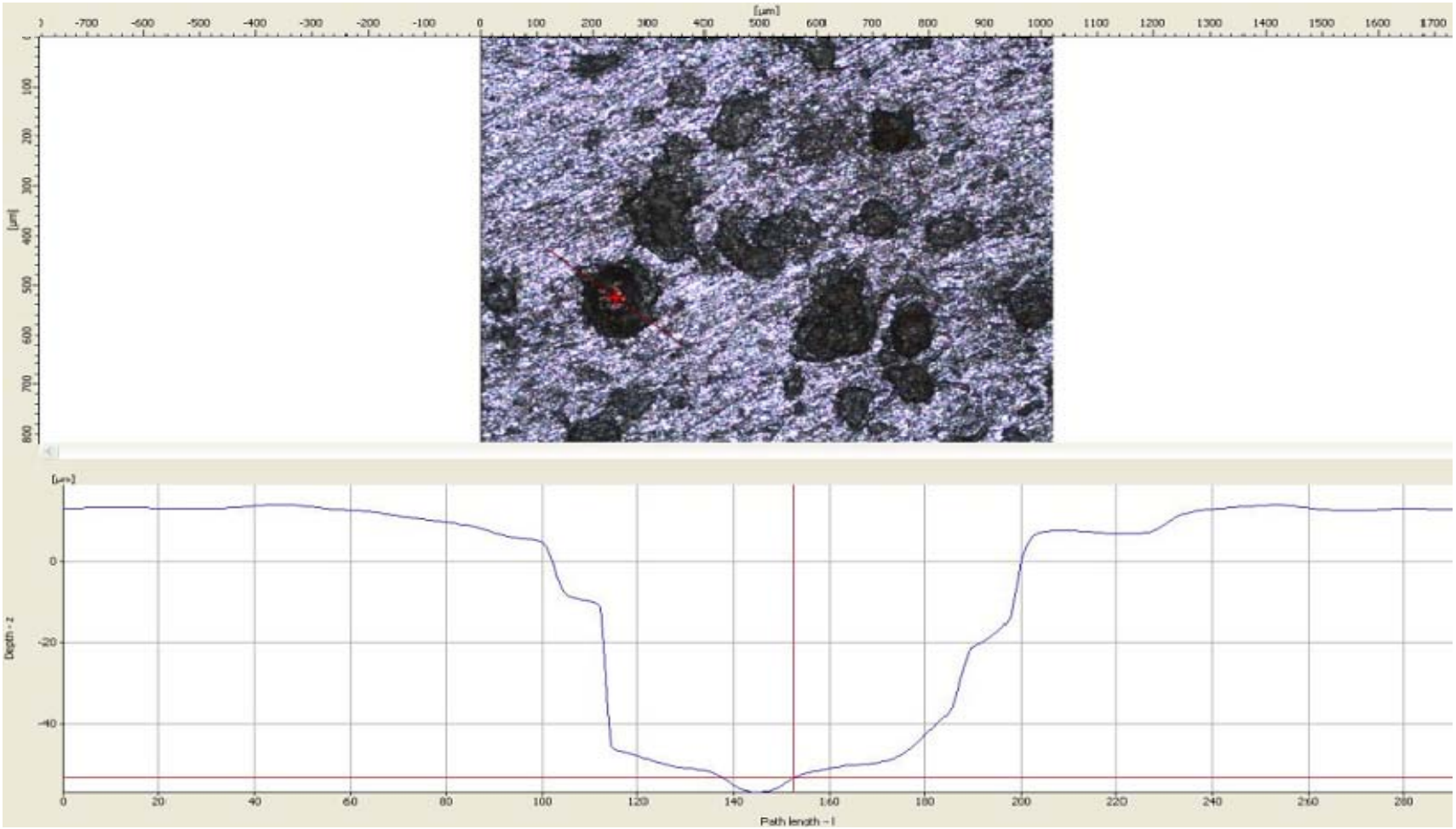

(b)

Figure 4-127: Pit analysis of X65 coupon surface after acid cleaning (the 3-month test in the enriched Wasia water spiked with SRB at 25 ºC; Refer to Figure 4-55 for the SEM images and Figure 4-126 for the IFM 3D images)

4.4.4 "Black powder" study

Black powder which causes damage to end users' gas turbines, line valves and associated instrumentation contamination is a common problem in natural gas pipelines. Black powder has been documented in both "dry" and "wet" lines. Even in parallel lines, there can be a problem in one line and not another (Baldwin, 1998). Black powder may be a wet material like tar or a dry fine powder like soot. The analyses of its chemical composition indicate it may be a mixture, in any form, of iron sulfide or iron oxide or a combination with any number of contaminants such as water, liquid hydrocarbons, salts, chlorides, sand, or dirt. Many corrosion engineers believe black power is a result of poor hydrotesting practices.

Black powder can exhibit as iron sulfide, which can be seen in the test using enriched Qurrayah water. Figure 4-59 clearly shows that a black substance was produced in the test vials in the test environment of enriched Qurrayah water with added SRB. A strong H_2S odor was emitted after the test vials were opened. EDS analysis of the sample surfaces showed elemental S (for example Figure 4-63) indicating the presence of FeS (Baldwin, 1998).

Iron oxides in the black powder could be produced in a test with and without an added O_2 scavenger. The chemical composition of the artificial seawater is similar to that of typical natural seawater (Table 4-3). X65 and C1018 carbon steel were used to test the material effect on black powder occurrence. Figure 4-128 and Figure 4-129 show the images of the vials taken at the beginning and the end of test. There was no black layer in the test when an O_2 scavenger (cysteine) was added (#6 and #8 in Figure 4-129) while a greenish black layer presented on the coupon surfaces when an O_2 scavenger was not

used (#2 and #4 in Figure 4-129,). This suggests that a black powder might be produced by even a very low level of O_2 (less than 10ppb). The collected dried black powder, however, didn't show obvious magnetism when tested using a magnet. According to Genin (2002 and 2004), these greenish black substances attributed to Fe (II-III) hydroxysalts formed by oxidation of $Fe(OH)_2$ and were found as intermediate compounds during the corrosion of iron-based materials and during iron oxide transformations

Left 4
0 ppm O_2 scavenger

Right 4
500 ppm O_2 scavenger

Figure 4-128: Sterilized artificial seawater with and without O_2 scavenger (Images taken at the beginning, initial pH=8.3**)**

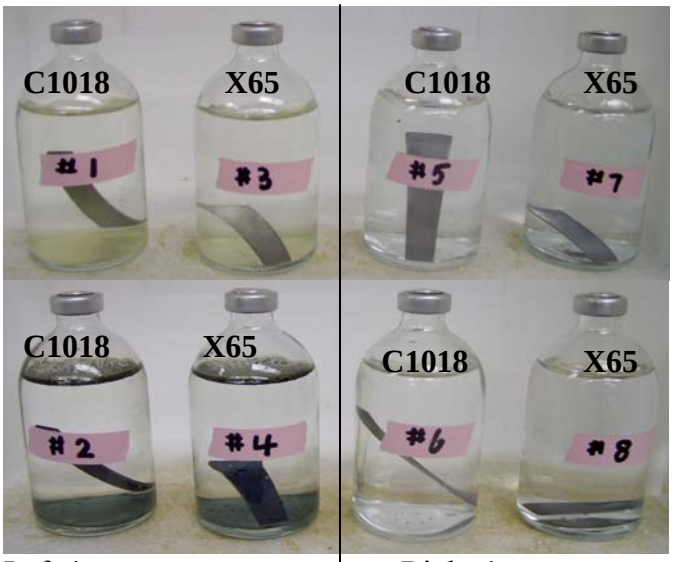

Figure 4-129: Sterilized artificial seawater with and without O_2 scavenger (Images taken after 2 weeks and 2 months)

4.4.5 Polymerase Chain Reaction (PCR) application

Currently, bacteria enumeration is mainly based on such conventional culture methods as the most probable number (MPN) or colony forming-unit (CFU) (Zhu and Kilbane, 2005). These methods, however, generally give biased results because most of the bacterial species do not thrive in an artificial medium and, thus, the concentrations of microbes can be underestimated. To circumvent this problem, the PCR method was developed to detect the bacteria. PCR is used for amplifying DNA in vitro. PCR works by repeated cycles of strand separation, annealing of primers, and extension of the primed strands. It increases DNA numbers exponentially. PCR is capable of amplifying an extremely small amount of DNA for detection. SRB counts in clean natural seawater can

be very low at which MPN is inadequate. PCR is needed because it can detect very low concentration of target bacteria, even at 1 to 2 cells/liter.

Basic ingredients needed in PCR are:

A template - the DNA that contains the target you want to amplify.

Primers - short synthetic oligonucleotide, designed to have a sequence that is the reverse complement of a region of template or target DNA to which the primers anneal.

DNA polymerase - enzyme that assists in DNA replication.

dNTPs - nucleotide precursors

Both DNA polymerase and dNTPs are commercially available from biotechnology supply companies.

Table 4-8 shows the test matrix for the PCR work. It was done in a PCR device (Eppendorf Mastercycler® gradient thermal cycler). The template was the SRB DNA extracted by a FastDNA®SPIN For Soil Kit (www.mpbio.com, Cat #6560-200). The key component primers shown in Table 4-8 having the correct sequence (Wagner et al., 1998) to bind the all known SRB strains' DNA, were chemically synthesized by MWG Biotech, Inc. (www.mwg-biotech.com) and purchased by us. Figure 4-130 shows the PCR operating procedure and parameters. According to the formula in Table 4-8, template (extracted SRB DNA), primers, DNA polymerase, buffer, dNTPs and water were fully mixed, and ran at 94ºC in the PCR device for 5 minutes. The first step aims to separate DNA into two single strands. Then, repeated cycles of strand separation (at 94ºC), annealing of primers (at annealing temperature 55ºC and 65ºC, respectively), and extension of the primed strands (at 72ºC) began, usually for 30 cycles. A final elongation

step of seven minutes at 72ºC after the last cycle was used to ensure that any remaining single-stranded DNA was fully extended. Finally, agarose gel electrophoresis was employed for size separation of the PCR products.

Table 4-8: Test matrix for PCR work

Test conditions	
SRB (*Desulfovibrio desulfuricans*) DNA template (50.84 µg/ml)	1 µl & 2 µl
Primers (100 pmol/µl): sequence from Saudi Aramco 1, 5'-ACG CAC TGG AAG CAC G-3'; 2, 5'-GTG TAG CAG TTA CCG CA-3'	1 µl of each primer
Taq DNA polymerase (5000 units/ml)	1 µl
Buffer (100 mM Tris-HCl, pH 9.0; 500 mM KCl; 0.1% Triton X-100)	5 µl
dNTPs (1.5 µM)	5 µl
Water	37 µl
Annealing temperatures (º C)	55 & 65

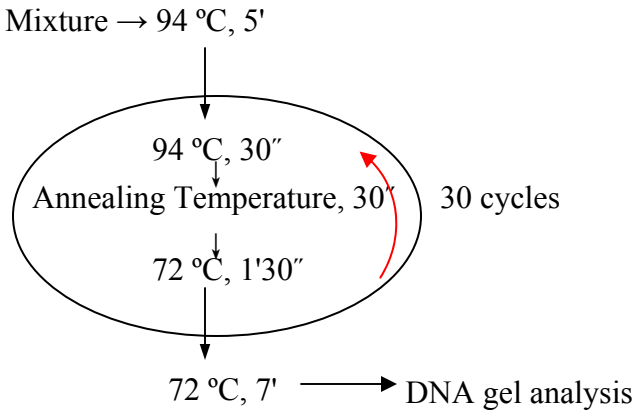

Figure 4-130: PCR operation procedure and parameters

Figure 4-131 shows the results of agarose gel electrophoresis of PCR products. The size of PCR products is determined by comparison with a DNA ladder, which contains DNA fragments of known size, ran on the gel alongside the PCR products (Figure 4-131). At the annealing temperature 55ºC, the gel shows that many bands were observed no matter whether 1µl or 2µl DNA template was used, which indicated the amplified substance was not a single product. At the annealing temperature of 65ºC, fewer bands were found when 2µl DNA template was employed, while when DNA template amount reduced to 1µl, only one band showed up, which indicated that only a single DNA product could be detected at the given test conditions. By comparison with the DNA ladder, the single product size was around 1.9kb, which is the featured SRB DNA fragment. Therefore, the annealing temperature of 65ºC and 1µl DNA template were the optimum conditions to amply the *Desulfovibrio desulfuricans'* DNA sequence. Figure 4-132 shows a standard curve that correlates the known SRB concentration with

the cycle numbers by using quantitative PCR (QPCR), which can tell automatically how many cycles are needed right after the amplified DNA is detected. In the future, after DNA is extracted from an unknown sample and amplified by QPCR, SRB concentration in the sample can be obtained by checking the standard curve. The QPCR method can detect precise and very low bacteria concentrations.

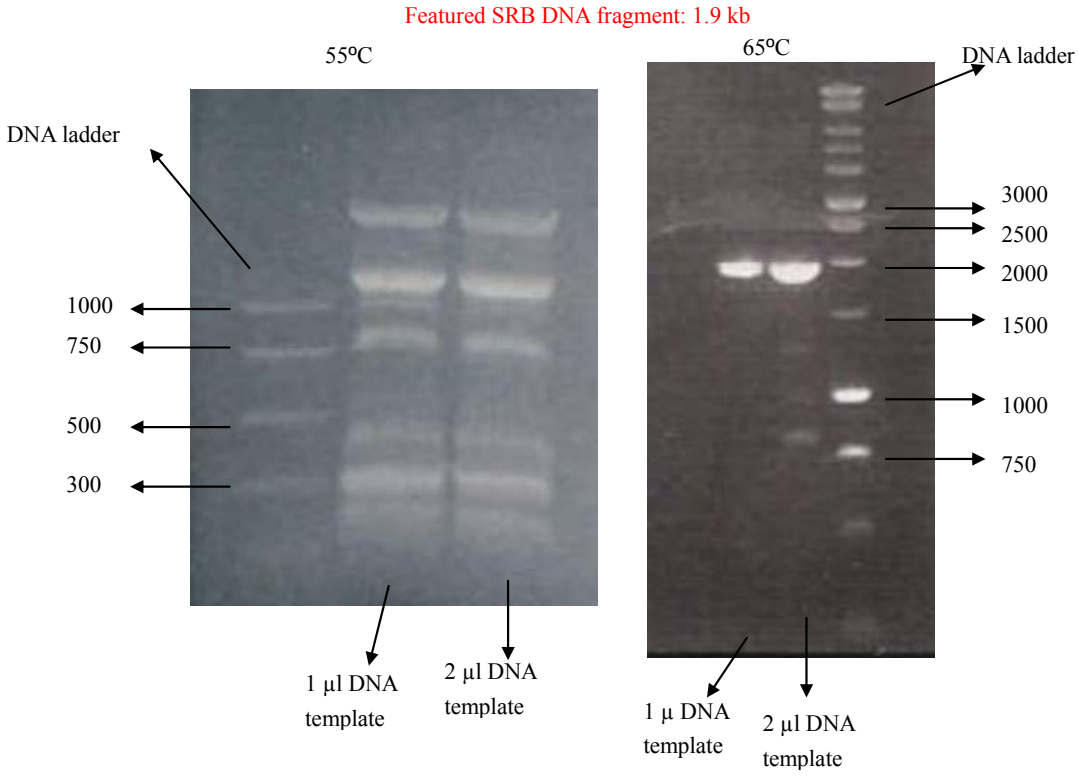

Figure 4-131: Agarose gel electrophoresis analysis of PCR products

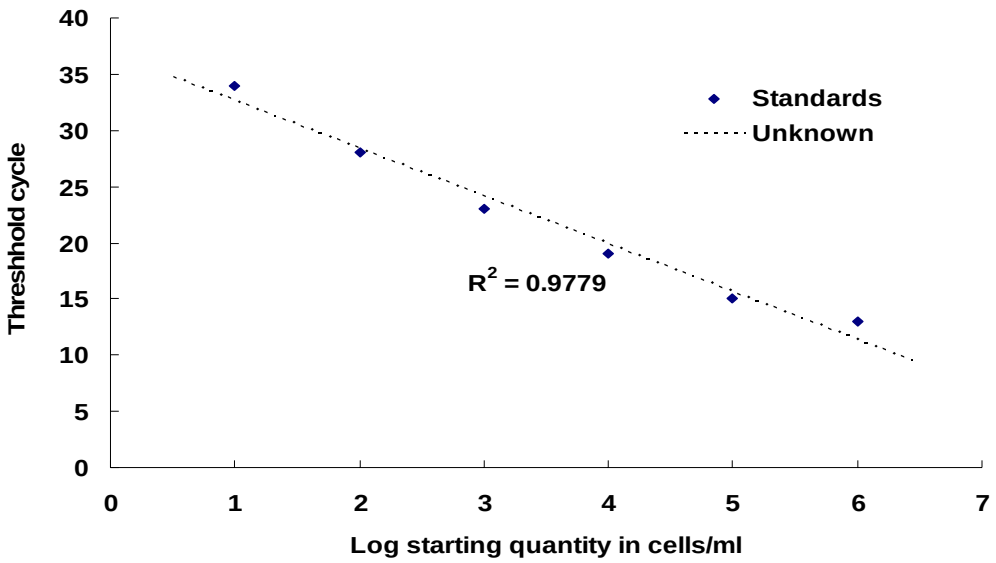

Figure 4-132: Standard curve to calculate SRB concentration

4.5 Conclusions:

- With the supplied untreated SA waters (Wasia water & Qurrayah water), no native biofilm was found in any of the tests up to three-month in duration at temperatures up to 37°C.
- With a possible exception of the three-month test at 37°C, no MIC was observed in any of the tests using untreated SA waters. Corrosion in deoxygenated (DO < 40 ppb) SA waters without MIC was negligible (< 0.4 mpy). Weight loss increased with time and temperature. In the test up to three months or longer, under deposit corrosion may cause non-MIC related pits.

- Corrosion rates in the tests using untreated Wasia water and Qurrayah water were comparable, but with the increase of time and temperature, coupons were more susceptible to pitting attack in the Qurrayah water.
- In enriched artificial seawater tests, it was found that growth of a lab strain SRB at 4^oC was negligible and was quite slow at 10^oC. Much higher growth rates were observed for 25^oC and 37^oC.
- After SA waters were spiked with 10^6 SRB cells/ml, biofilms formed on the coupon surface, and pits characteristic of MIC were observed after biofilm removal. In some cases, pits caused by MIC were significant. S and Fe detected by EDS indicated the presence of FeS. A strong H_2S odor was also noticed when the vials were opened.
- In the tests using enriched SA waters spiked with SRB, biofilm formation and detection were associated with time, temperature and corrosion protective FeS film formation, all of which made pitting prediction difficult. It was found that the corrosion rates in the tests using enriched Qurrayah water spiked with SRB were all higher than those using untreated Qurrayah water, which indicated that the added SRB accelerated the corrosion process. Corrosion rates in the tests using SA water spiked with SRB were all below 2 mpy. One of the tests showed a pitting rate 40 times that of its general corrosion rate.
- The “black powder” shown in the tests without SRB spiking was not FeS. It was likely caused by O_2, even though the dissolved O_2 concentration in the samples

was very low (less than 10ppb). The “black powder” shown in the tests with SRB spiking was found to be FeS.

- Annealing temperature 65^{o}C and 1µl extracted DNA template proved to be optimum conditions for amplifying SRB DNA in the quantitative PCR process.

CHAPTER 5: MITIGATION OF MIC

5.1 Introduction

Material deterioration due to microbial involvement has been recognized as a major problem in gas/oil operations, as well as other such industries as nuclear power generation, water treatment and chemical processing, resulting in enormous economic losses. The microbes commonly implicated in biological corrosion are SRB, acid-producing bacteria (APB), iron/manganese bacteria and slime formers. Currently, the use of biocide is a major measure taken to mitigate MIC. For environmental safety concerns, biocide selection and dosage are restricted, and green biocides are desirable. Given their greater biodegradability, as well as for their efficient control of bacterial growth, and especially SRB, THPS and glutaraldehyde are two popular biocides widely used to prevent MIC.

Glutaraldehyde, structurally, is a five-carbon compound (Figure 5-1). It works by attacking the amine groups (lysine and arginine) in the cell wall, which leads to the inhibition of cellular growth. The metabolic product of glutaraldehyde by microorganism is principally CO_2 under aerobic conditions, while under anaerobic conditions the degradable product is 1, 5-pentanediol which has low toxicity (Union Carbide, 1999, Figure 5-1). Under the requirement of OECD (Organisation for Economic Co-operation and Development) 306 test, Union Carbide (1999) indicated that biodegradation of glutaraldehyde to be 73% in 28 days. The similar characteristic of biocide THPS is discussed in Chapter 6.

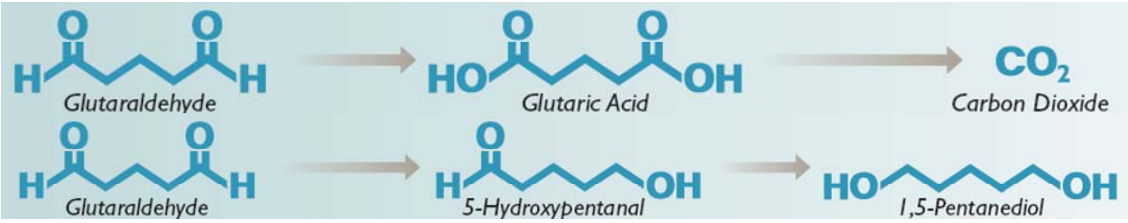

Figure 5-1: Glutaraldehyde structure and its metabolic products (Permission from Union Carbide, 1999)

Biofilms (sessile cells), the main culprits during the MIC process, are the congregation of planktonic cells which adhere to supporter surfaces with the help of extracellular polymer substances (EPS). Although biocide is effective in inhibiting or even killing planktonic cells, it has limited control on biofilms once they are established because biofilm is capable of protecting sessile cells from attacks. The biofilms surrounded by EPS make biocide penetration difficult (Stoodley et al., 1999) and, moreover, according to Fux et al. (2005) the physiology of biofilm may change in order to resist biocide attack. Besides its directly destructive damage to metal, biofilm decreases efficiency of inhibitor application by acting as a barrier to prevent inhibitors from forming a continuous protective film on a metal surface.

Biocides like THPS or glutaraldehyde have effective inhibition on SRB growth. However, being gram-negative bacteria, SRB in nature resist external attack because the outer membranes of gram-negative bacteria have poor permeability for large molecules to pass through and only limited substances can diffuse the lipopolysacharide (LPS) covered surface (Nikaido, 1989). In 1965, Lerve firstly found that EDTA (EthyleneDiamine-TetraAcetic acid) showed the ability to disrupt LPS by chelating and removing cations on

LPS binding sites, which resulted in increased permeability of outer membrane of gram-negative bacteria. EDTA was mostly introduced in medical field to assist macromolecules penetrate target cells. Minocycline combined with EDTA was found not only to synergistically inhibit planktonic *bacilli* and *C. albicans* growth in suspension solution (Wooley et al., 1983), but also Raad et al. (2003) demonstrated that the combined application of both were highly efficacious to minimize harmful microbe colonization embedded in the biofilm on a catheter surface. Because of these outstanding characteristics, EDTA use can be extended to MIC research to enhance the effectiveness of biocides. The practice of using chelators as biocide enhancers was patented by Raad and Sherertz (2001). The MIC group at Ohio University is currently working on this project.

5.2 Objectives

- Compare performance of biocides THPS and glutaraldehyde on SRB growth
- Study the effect of the combination of biocides with EDTA on SRB growth

5.3 Experimental conditions

In this study, *Desulfovibrio desulfuricans* (ATCC strain 7757), a common SRB strain, was used. Laboratory experiments were carried out in 100ml anaerobic vials. The liquid medium used was based on the ATCC 1249 medium (Table 5-1) for the growth of *D. desulfuricans* ATCC strain 7757 (Atlas and Park, 1997).

Table 5-1: Composition of ATCC 1249 medium for SRB (ATCC strain 7757)

Component I		**Component II**		**Component III**		**Component IV**
$MgSO_4$	2.0 g	K_2HPO_4	0.5 g	Sodium Lactate	3.5 g	See below*
Sodium Citrate	5.0 g	Distilled water	200 ml	Yeast Extract	1.0 g	
$CaSO_4$	1.0 g			Distilled water	400 ml	
NH_4Cl	1.0 g					
Distilled water	400 ml					

*Filter-sterilized 5%wt ferrous ammonium sulfate. Add 0.1 ml of this solution to 5.0 ml of medium prior to inoculation.

SRB cell numbers were counted under an optical microscope using a hemacytometer (Neubauer chamber, Hausser Scientific) with serial dilutions (Penn, 1991) if needed. All cell growth experiments were carried out in a 37 ^oC incubator.

5.4 Results and discussion

Table 5-2 and Table 5-3 show the test matrices for experiments in the vials. Coupons were not used.

5.4.1 Effects of biocides on planktonic SRB growth

Figures 5-2 and 5-3 show that glutaraldehyde alone did not inhibit SRB growth when its concentration was 10 ppm and 30 ppm; however, glutaraldehyde became effective when its concentration rose to 50 ppm (Figure 5-4). In contrast, biocide THPS alone could suppress planktonic SRB growth when its concentration was 30 ppm (Figure

5-5), which indicates that THPS is more effective on inhibition of SRB growth than glutaraldehyde.

Table 5-2: Test matrix for glutaraldehyde and EDTA effect on planktonic SRB growth

Test Conditions	
Strain	*Desulfovibrio desulfuricans* (ATCC 7757)
Medium	ATCC 1249 liquid medium
Temperature (ºC)	37
pH	7.0±0.1
Glutaraldehyde concentration (ppm)	0, 10, 30, 50
EDTA concentration (ppm)	0, 50, 100, 200
Experimental setup	100 ml anaerobic vials

Table 5-3: Test matrix for THPS and EDTA effect on planktonic SRB growth

Test Conditions	
Strain, Medium, Temperature, pH and Experimental setup are the same with the above matrix.	
THPS concentration (ppm)	0, 10, 30
EDTA concentration (ppm)	0, 50, 100, 200

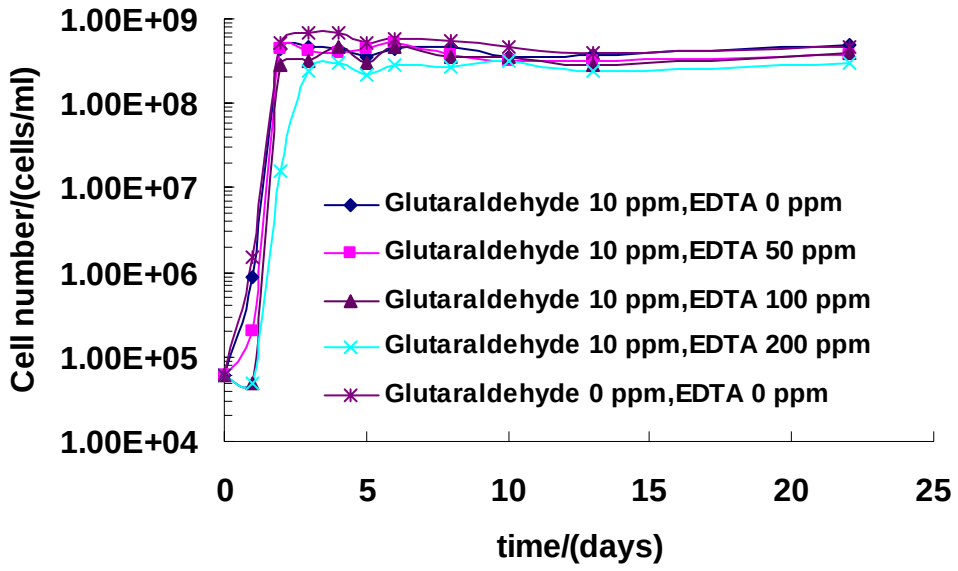

Figure 5-2: The effect of 10 ppm glutaraldehyde with and without EDTA on planktonic SRB growth

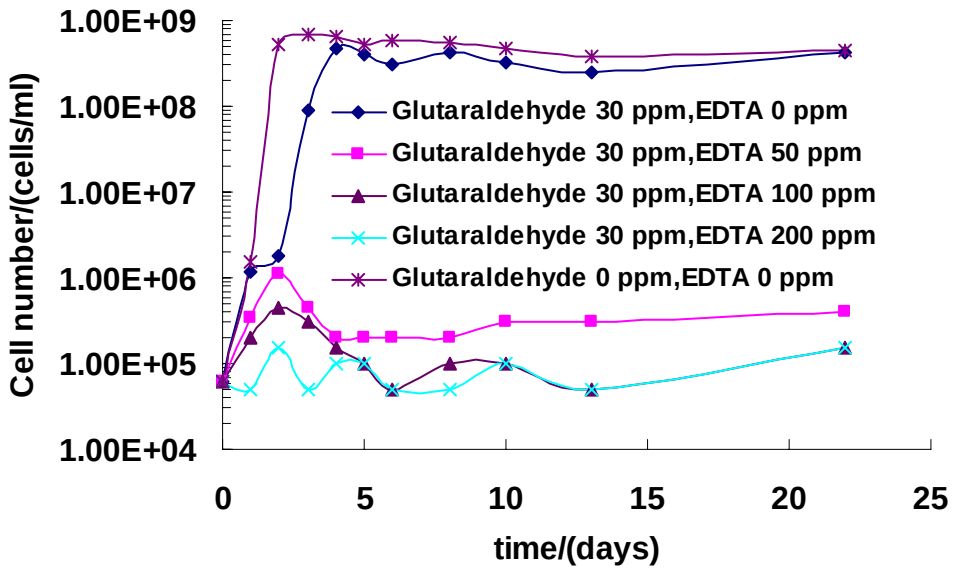

Figure 5-3: The effect of 30 ppm glutaraldehyde with and without EDTA on planktonic SRB growth

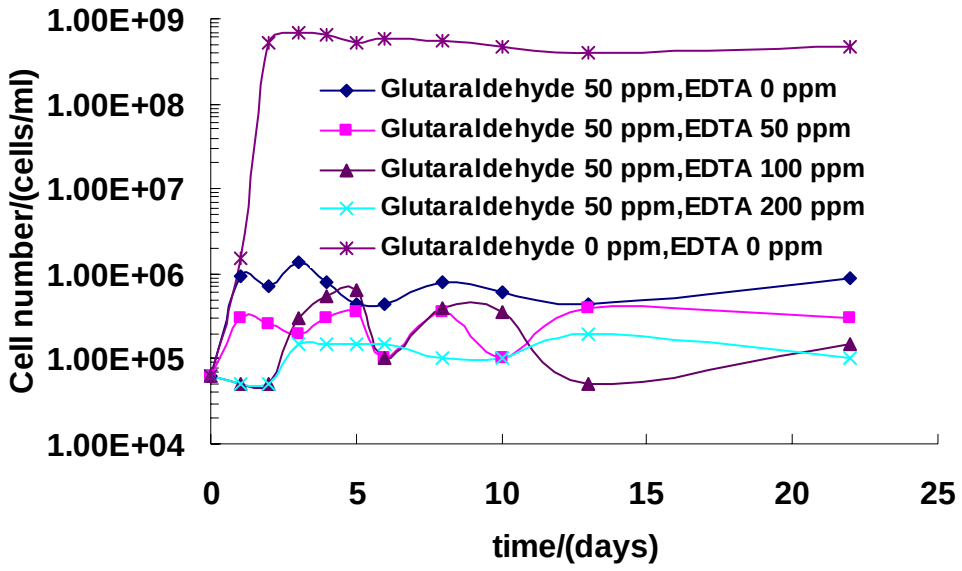

Figure 5-4: The effect of 50 ppm glutaraldehyde with and without EDTA on planktonic SRB growth

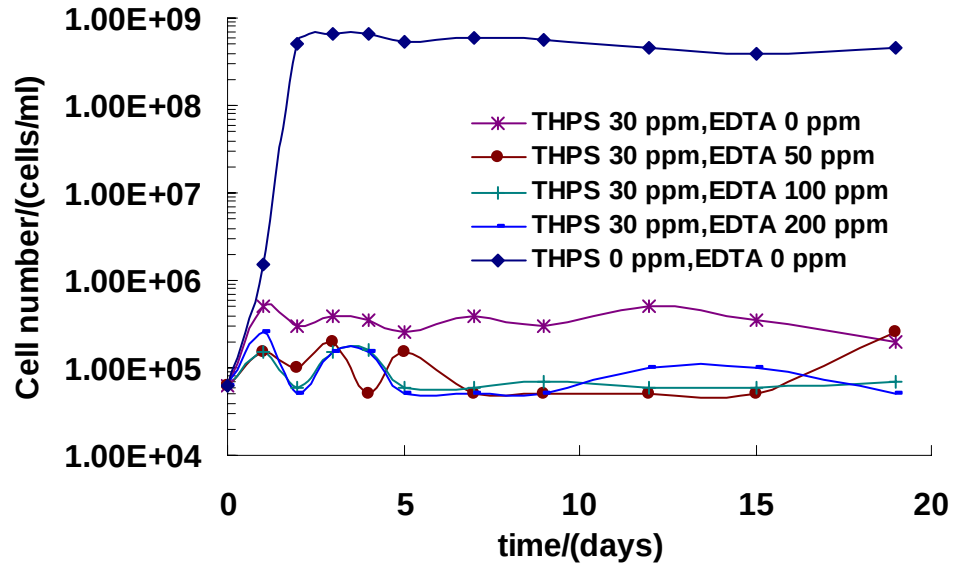

Figure 5-5: The effect of 30 ppm THPS with and without EDTA on planktonic SRB growth

5.4.2 Effects of EDTA on planktonic SRB growth

Figure 5-6 shows that the EDTA did not suppress planktonic SRB growth in the absence of biocides nor in combination with glutaradehyde at a 10 ppm concentration (Figure 5-2). Figure 5-7 shows that EDTA combined with biocide THPS 10 ppm did not significantly suppress SRB growth until the EDTA concentration rose to 200 ppm where it enhanced the THPS suppression of SRB growth at the beginning of the test. When there was exponential SRB growth, it was shown that EDTA can assist THPS inhibition only to a certain extent. EDTA was able to suppress SRB growth until the combined biocide concentration rose above 30 ppm (Figures 5-3 ~5-5). It should be pointed out that Figure 5-3 clearly shows that the combination of EDTA with 30 ppm glutaraldehyde can suppress SRB growth much better than can 30 ppm glutaraldehyde alone.

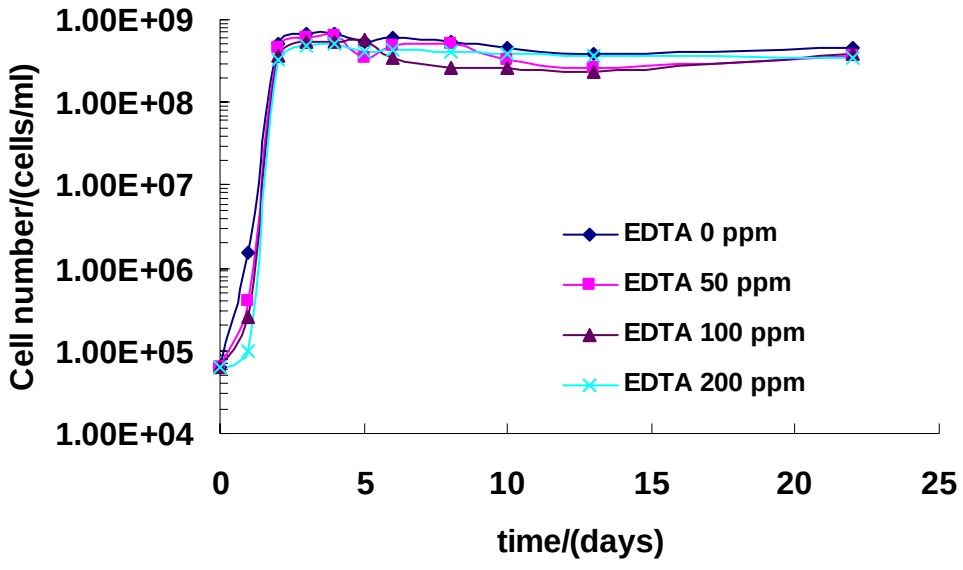

Figure 5-6: The effect of EDTA alone on planktonic SRB growth

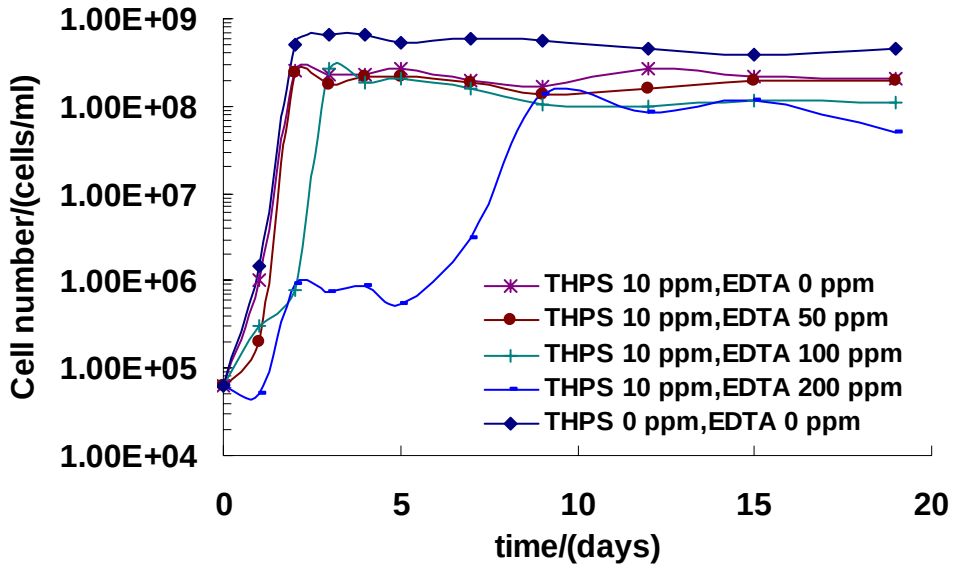

Figure 5-7: The effect of THPS 10 ppm with and without EDTA on planktonic SRB growth

5.5 Conclusions:

- Biocides glutaraldehyde and THPS can both effectively inhibit planktonic SRB growth and THPS is better in that it can work alone at 30 ppm, where glutaraldehyde cannot control SRB growth.
- EDTA alone has no inhibition effect on SRB growth. The use of the EDTA in combination with biocides THPS and glutaraldehyde improved the effectiveness of the biocides on planktonic SRB growth.

CHAPTER 6: MECHANISTIC MODELING OF ANAEROBIC THPS DEGRADATION IN SEAWATER

6.1 Introduction

Microbiologically influenced corrosion (MIC) is becoming an increasingly significant problem in the oil and gas industry due to the increased water-wetting operations. THPS (Tetrakis Hydroxymethyl Phosphonium Sulfate) and glutaraldehyde are the popular choices widely used to mitigate the MIC process because they are environmentally green and non-bioaccumulative, and have the advantage of rapid reaction. THPS is highly effective in controlling SRB because it causes rapid and severe damage to the cell membrane integrity by the way of crosslink with sulfur (Rhodia Water). The key features of THPS include exceptionally rapid action, a favorable environmental profile, and effectiveness over a wide pH range. The most attractive feature is that it is degradable and non-bioaccumulative. THPS vendors recommend acidic pH for THPS use (Rhodia, 2004). However, corrosion engineers are less willing to accept any pH below 7, especially in hydrotesting.

THPS is synthesized in high-yield with a reaction of PH_3, H_2SO_4 and CH_2O. THPS degrades relatively fast under both aerobic and anaerobic conditions. Trihydroxymethyl phosphine oxide (THPO) and bishydroxymethyl phosphonic acid (BMPA) have been identified as two major breakdown products (WHO, 2000). Another breakdown product is possibly a formaldehyde adduct of a trihydroxy compound. Reaction 6-1 below shows the THPS degradation process. (Reaction 6-1 is not

stoichiometrically balanced due to the uncertainty of the third breakdown product.) THPO and BMPA were found to have low toxicities and are not considered hazardous to the environment (Downward et al., 1997). Both of them will further degrade to CO_2 and inorganic matters (ACG, 2003).

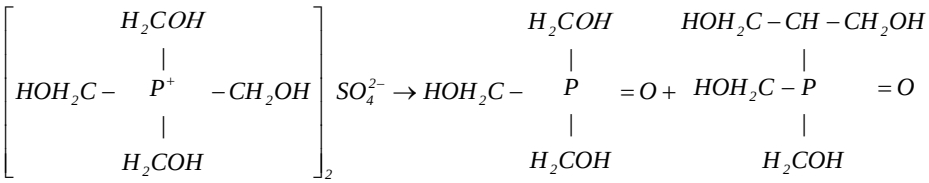

(THPS) (THPO) (BMPA) (6-1)

Apart from THPS degradation itself, in field operations, it is well known that THPS could easily react with oxygen scavengers (Wilfried, 2004). All the factors above can affect the dosing of THPS in the mitigation of MIC. Anecdotes from field operators suggested that the protection against MIC is lost when THPS concentration is below 50 ppm (100 ppm is safer). A much higher biocide concentration is needed once the biofilms are established (Videla, 1996). Thus, it is important to determine residual THPS concentration to make sure that it does not fall below the desired minimum required to prevent biofilm formation. This chapter presents a mechanistic model to predict THPS degradation in seawater from two locations as a function of time, temperature and pH (Zhao et al., 2008). The model was aimed at alkaline pH under which THPS degrades much faster than under acidic pH.

6.2 Objectives

- Investigate light, temperature, pH, mild steel presence and salt effect on THPS degradation
- Establish a THPS degradation prediction model as a function of time, temperature and pH

6.3 Instrumentation and analytical methods

Experiments were carried out in 100 ml anaerobic serum bottles equipped with 20 mm rubber septa and aluminum crimp seals (Figure 3-1). Anaerobic manipulations were performed in a glove box deoxygenated with N_2 gas (Figure 3-2). All liquids in the tests were deoxygenated using N_2 sparging before use and were sterilized to circumvent the involvement of microorganisms. For tests involving coupons to study the presence of mild steel, X65 carbon steel was used with dimensions of 4.76cm×1.09cm×0.16cm (Figure 3-1). The ratio of coupon surface area to liquid volume was set close to that in 0.3m (12″) ID pipes. Prior to use, coupon surfaces were polished successively with 200 and 400 grit SiC abrasive papers, rinsed with propanol, and then sonicated in a beaker with ethanol in an ultrasonic bath. THPS (75% w/w) was provided by Nalco. Artificial seawater made from Instant Ocean® salt mix (see Table 4-3), and two types of natural seawater from the Gulf of Mexico (Table 3-2 in Chapter 3) and the Persian Gulf (Qurrayah, Table 4-1) were used in this test.

Standard iodine titration was applied to test THPS concentration. The assay kit (CODE 8776) from the LaMotte Company (www.lamotte.com) was used. The kit can test

the effective THPS concentration in both fresh water and seawater. A kit from CHEMetrics (www.chemetrics.com, product code: K-7540) was used to test the oxygen concentration in the experimental vials. All pH values were measured at room temperature with a Corning 320 pH meter.

6.4 Results and discussion

A WHO report (2000) suggests that UV could accelerate THPS degradation when its concentration is low. Under exposure to normal fluorescent lighting in the lab, tests lasting five days and using common clear borosilica glass vials that are not UV-transparent failed to show appreciable THPS degradation compared to samples kept in the dark. Therefore, all the test samples for this set of experiments were not kept in the dark. The dissolved oxygen concentration in all the sample fluids was found to be below 40 ppb after the vials were opened at the end of tests.

6.4.1 Effect of temperature

Table 6-1 shows a test matrix to investigate the effect of temperature in six test conditions with fixed pH. The chemical composition of the artificial water is similar to that of typical natural seawater (see Table 4-3).

Table 6-1: Test matrix for THPS degradation investigation

Test conditions	
Test media (all sterilized)	**Stable pH after THPS added with/without X65 coupon**
1. Gulf of Mexico seawater	pH: 7.3; No coupon present
2. Artificial seawater	pH: 8.0; No coupon present
3. Artificial seawater	pH: 7.9; Coupon present
4. Persian Gulf seawater	pH: 7.9; Coupon present
5. pH-adjusted Gulf of Mexico seawater	pH: 8.4, Coupon present
6. pH-adjusted Persian Gulf seawater	pH: 8.4, Coupon present
Initial THPS concentration (ppm)	180 for the #1 medium and 100 for the rest
Test temperature (ºC)	4, 17, 25, 37
Light condition	Normal fluorescent lighting (off in after hours)

Experimental data on THPS degradation in Gulf of Mexico seawater are shown in Figure 6-1. The experimental data shows that THPS degradation follows the first-order kinetics expressed in Equation 6-2 below. Based on Equation 6-3, the values of the specific reaction rate $k_T(T)$ for the four different temperatures were obtained (Figure 6-2). Equation 6-5 was applied to correlate $k_T(T)$ with temperature T (Figure 6-3), and the activation energy E and frequency factor A can be calculated according to the slope and y-axis intercept in Figure 6-3. Equation 6-6 shows a mechanistic mathematic model for

THPS degradation in Gulf of Mexico seawater at different time and temperatures with a fixed pH.

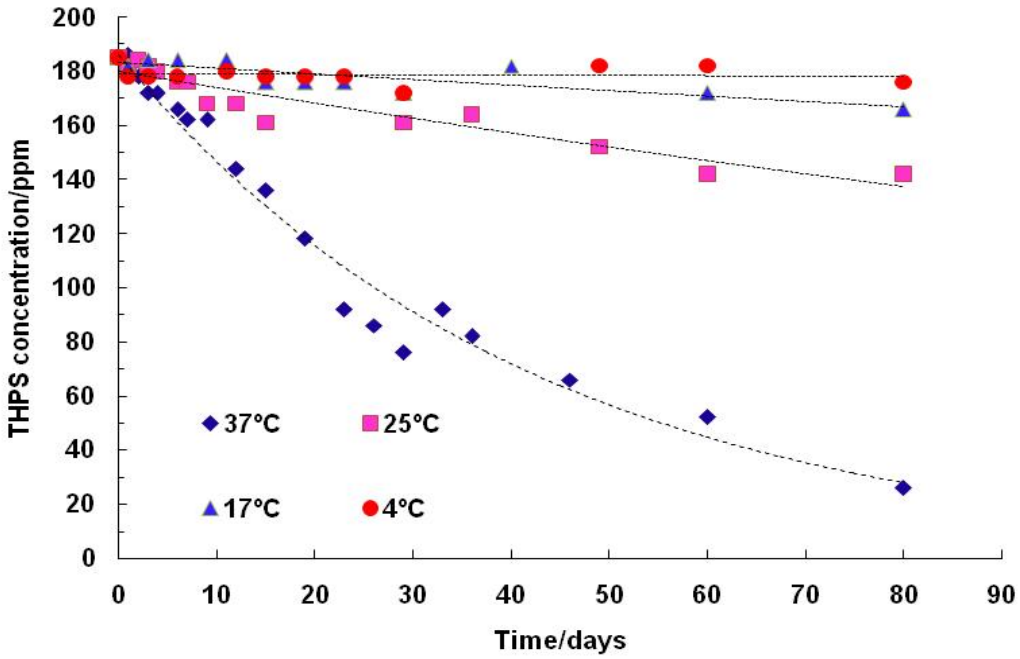

Figure 6-1: THPS degradation in Gulf of Mexico seawater without coupon presence at different temperatures

The following equations that depict the model of THPS degradation with fixed pH are based on first-order kinetics.

$$r = -\frac{dC}{dt} = k_T(T) \bullet C \qquad (6\text{-}2)$$

$$\ln\left(\frac{C}{C_0}\right) = -k_T(T) \bullet t \tag{6-3}$$

$$\text{Arrhenius equation } k_T(T) = A \bullet \exp\left[\frac{-E}{R \bullet (T + 273.15)}\right] \tag{6-4}$$

where A is the frequency factor, E activation energy in J/mol, R gas constant (8.314 J/mol•K), T reaction temperature in ºC and t time in day. Equation 6-4 leads to Equation 6-5.

$$\ln k_T(T) = \ln A - \frac{E}{R \bullet (T + 273.15)} \tag{6-5}$$

Thus,

$$\ln\left(\frac{C}{C_0}\right) = -k_T(T) \bullet t = -A \bullet \exp\left[\frac{-E}{R \bullet (T + 273.15)}\right] \bullet t \tag{6-6}$$

where A and E can be obtained from Figure 6-3 through linear regression.

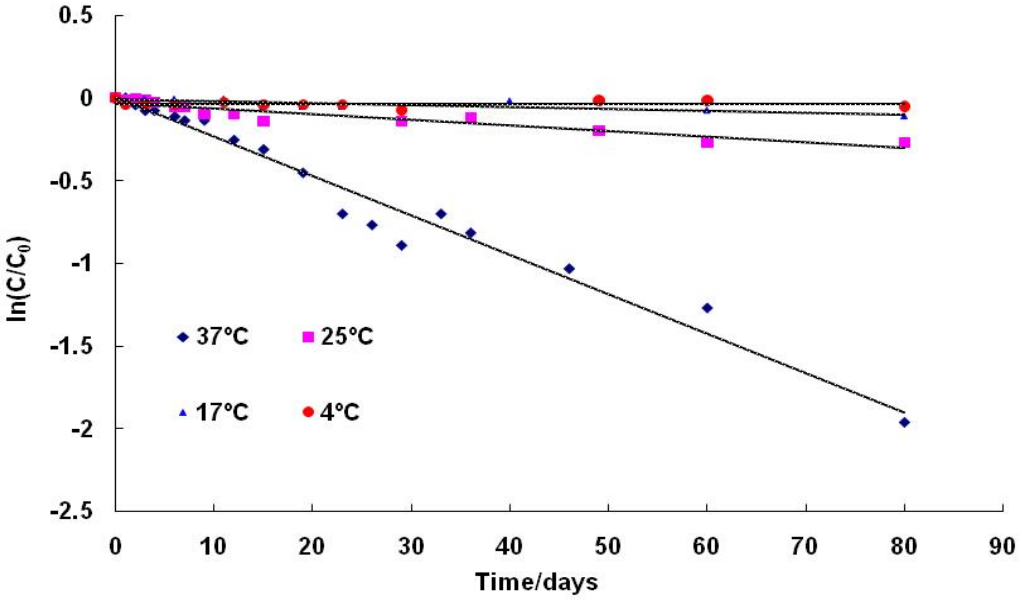

Figure 6-2: The values of specific reaction rate k at different temperatures (Test in Gulf of Mexico seawater without a coupon)

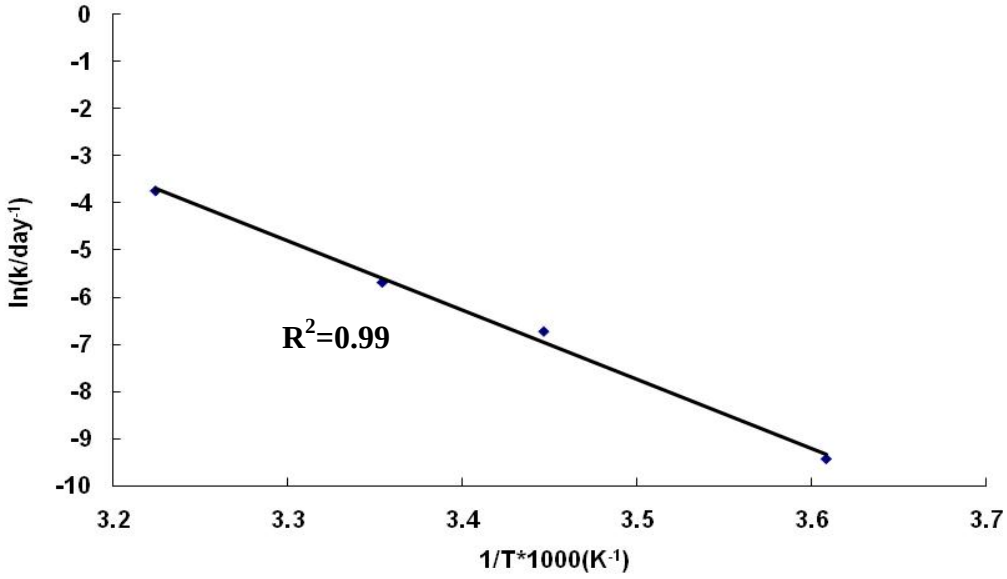

Figure 6-3: The change of specific reaction rate k_T (T) with temperature (Test in Gulf of Mexico seawater without a coupon)

Table 6-2 shows a spreadsheet version of the temperature effect model shown in Equation 6-6 with input parameter time and temperature and initial THPS concentration.

Table 6-2: Preliminary THPS degradation prediction model

Input parameters		
T (^{o}C)	Time (days)	C_o (ppm)
31	10	100
Output		
Residual THPS Concentration (ppm)		
90.83	(In Gulf of Mexico seawater without coupon presence), pH 7.3	
49.3	(In artificial seawater without coupon presence), pH 8	
38.46	(In artificial seawater with coupon presence), pH 7.9	
37.43	(In Persian seawater with coupon presence), pH 7.9	
17.98	(In pH-adjusted Gulf of Mexico seawater with coupon presence), pH 8.4	
15.83	(In pH-adjusted Persian Gulf seawater with coupon presence), pH 8.4	

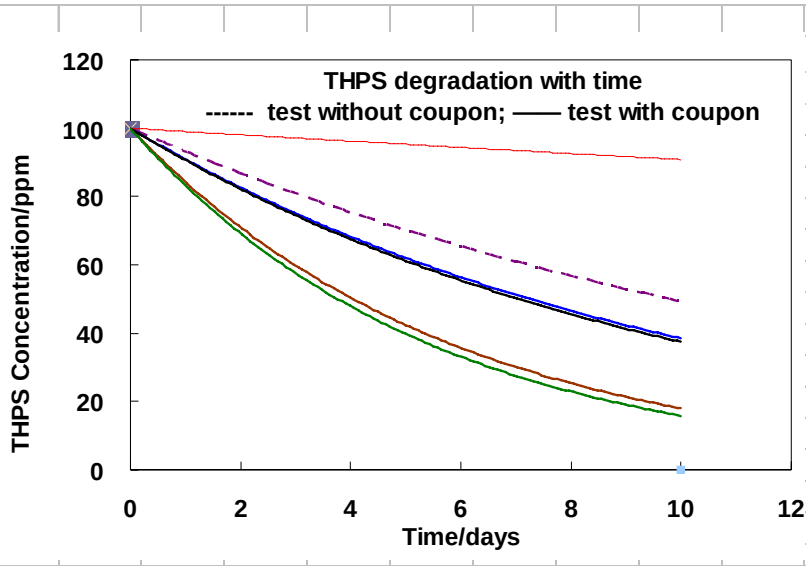

The results showed that THPS degradation rates under six different test conditions increased with increased temperature, and that THPS degrades faster at higher pH. The artificial seawater data in Table 6-2 suggest that the presence of a coupon accelerates THPS degradation. The MSDS sheet from www.accepta.com states that THPS should avoid contact with mild steel (Accepta, 2004). Concentrated THPS has a very low pH that is harmful to mild steel. Even diluted THPS solutions with pH above 7 showed corrosivity in the experimental data (Figures 6-4 ~ Figure 6-6, refer to Figure 3-

30, Figure 3-35, and Figure 3-41, respectively) while samples in sterilized/untreated medium without THPS (Figure 6-7, refer to Figure 3-18; Figure 6-8, refer to Figure 3-15) did not show the particular type of pitting pattern and the associated weight losses. Compared to the five-month image, the eleven-month image showed coalescence of smaller pits. This observation was supported by weight loss data.

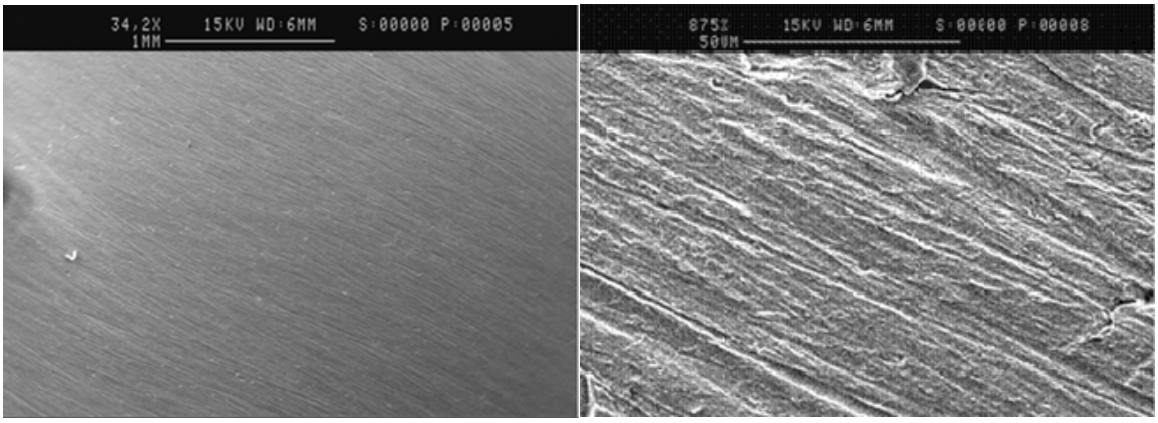

(a) SEM at 34X (b) SEM at 875X

Figure 6-4: 3-month test in Gulf of Mexico seawater with initial THPS 50 ppm at 4 ºC (SEM analysis of coupon surface after acid cleaning; weight loss: 6 mg, initial pH 8.0 and final pH 8.3)

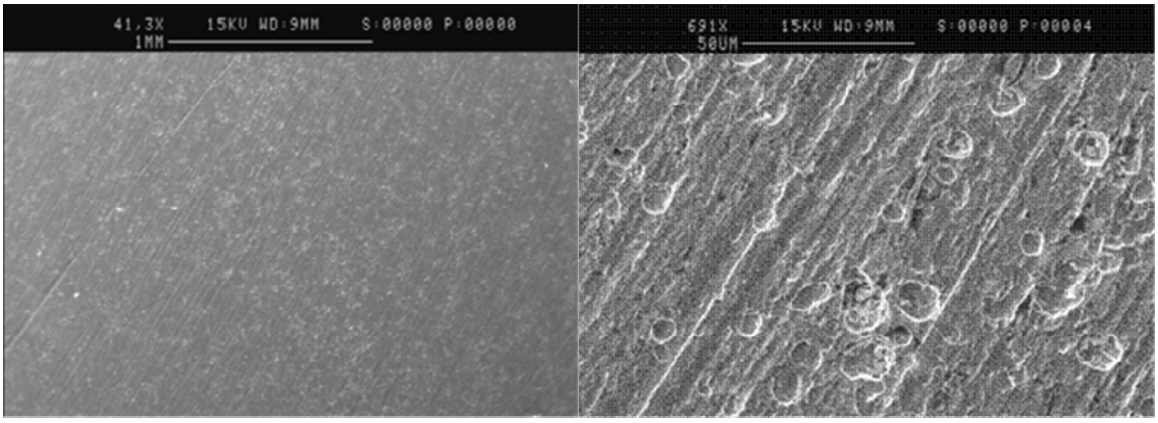

(a) SEM at 41X (b) SEM at 691X

Figure 6-5: 5-month test in Gulf of Mexico seawater with initial THPS 50 ppm at 4 ºC (SEM analysis of coupon surface after acid cleaning; weight loss: 11 mg, initial pH 8.0 and final pH 8.4)

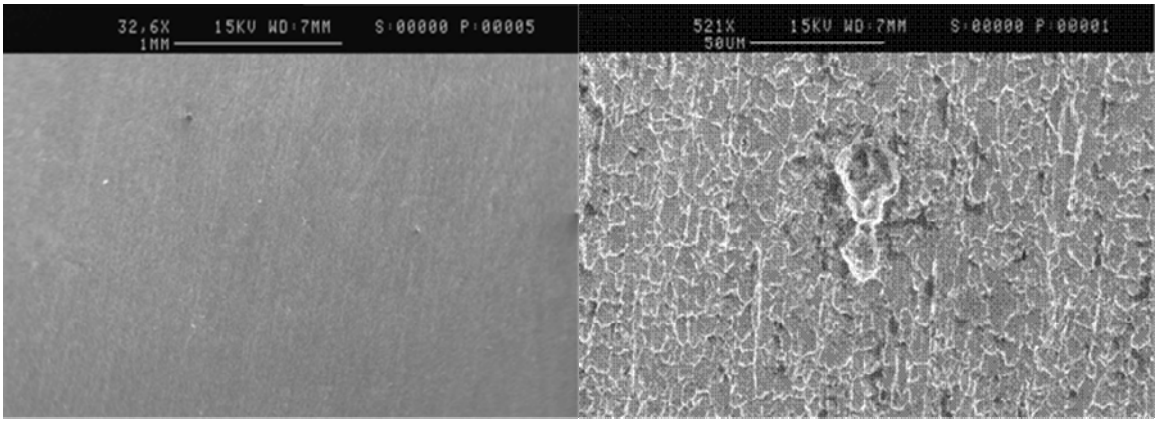

(a) SEM at 33X (b) SEM at 521X

Figure 6-6: 11-month test in Gulf of Mexico seawater with initial THPS 50 ppm at 4 ºC (SEM analysis of coupon surface after acid cleaning; weight loss: 17 mg, initial pH 8.0 and final pH 8.3)

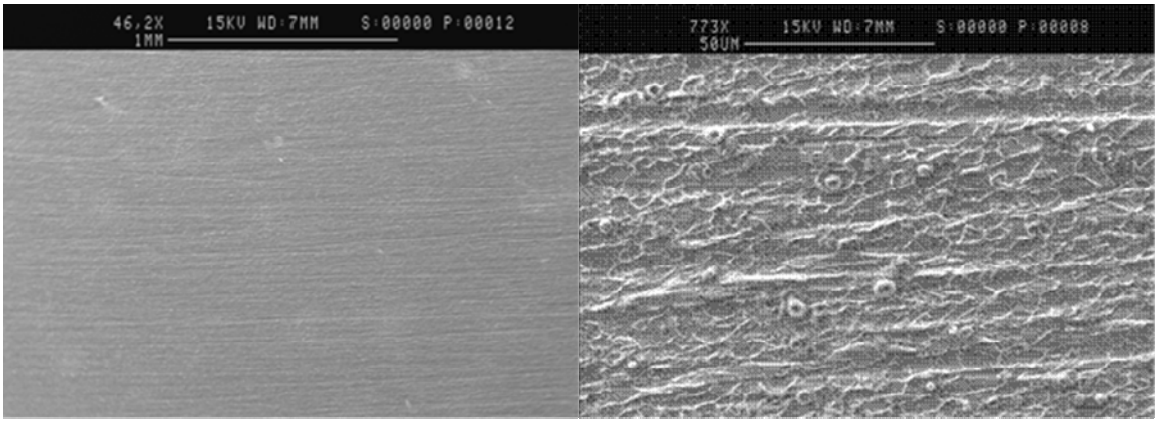

(a) SEM at 46X (b) SEM at 773X

Figure 6-7: 6-month test in the sterilized Gulf of Mexico seawater without THPS at 4ºC (SEM analysis of coupon surface after acid cleaning)

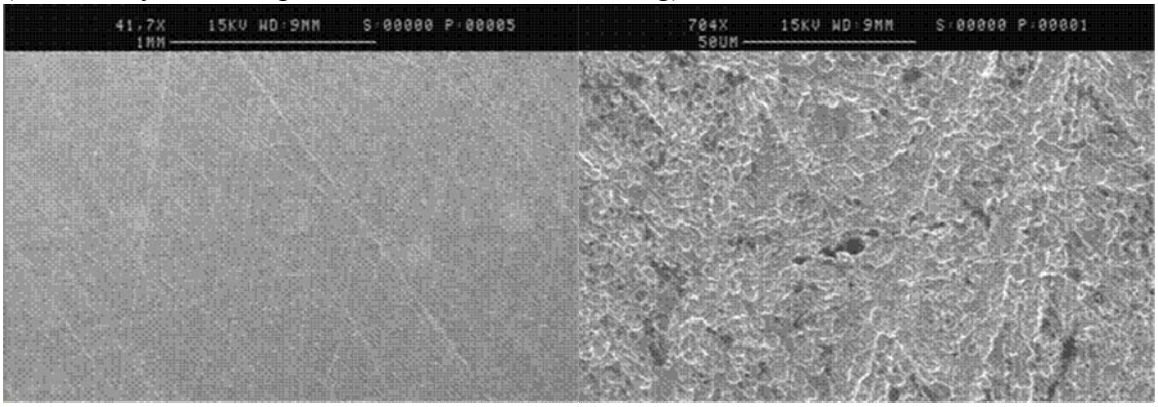

(a) SEM at 42X (b) SEM at 704X

Figure 6-8: 6-month test in the untreated Gulf of Mexico seawater without THPS at 4ºC (SEM analysis of coupon surface after acid cleaning)

6.4.2 Effect of pH

Table 6-3 shows a test matrix used to study the pH effect on THPS degradation in Persian Gulf seawater without coupons. The pH of low and high pH tests was adjusted by using HCl or NaOH after adding THPS. Figure 6-9 shows THPS degrades faster under higher pH conditions.

Table 6-3: Test matrix for pH effect on THPS degradation

Test conditions	
Test media (all sterilized)	**Initial pH after THPS was added without coupon presence**
1. Persian Gulf seawater	8.52
2. pH-adjusted Persian Gulf seawater at low pH	6.76
3. pH-adjusted Persian Gulf seawater at high pH	10.00
Initial THPS concentration (ppm)	55
Test temperature (ºC)	37
Light condition	Normal fluorescent lighting

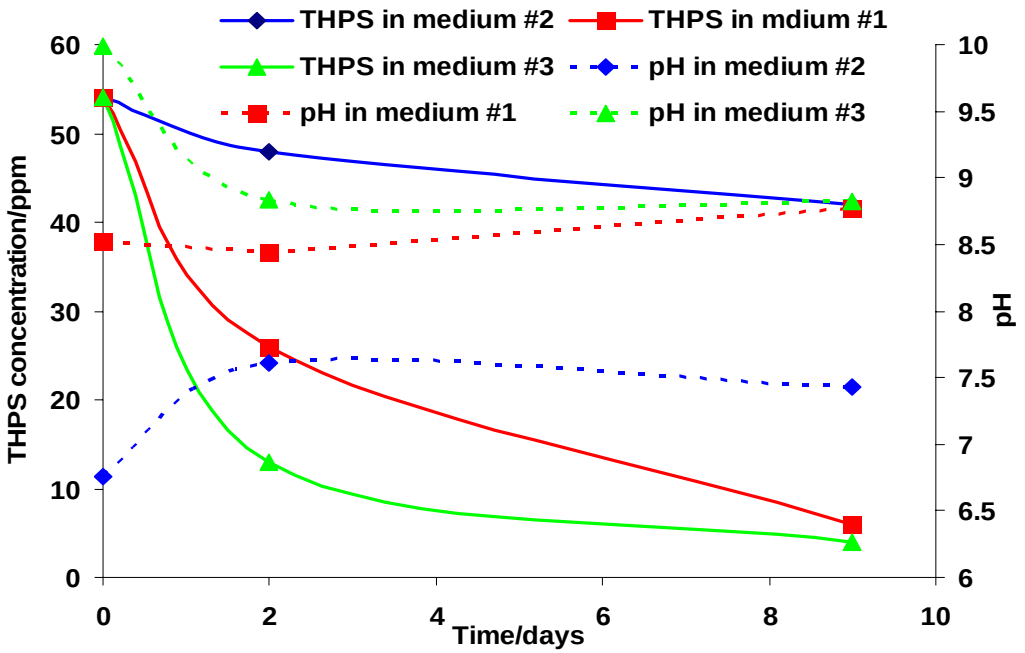

Figure 6-9: pH effect on THPS degradation in Persian Gulf seawater (medium #1: Persian Gulf seawater; medium #2: pH-adjusted Persian Gulf seawater with lower initial pH; medium #3: pH-adjusted Persian Gulf seawater with higher initial pH)

Table 6-4 shows a test matrix using Persian Gulf seawater with different initial pH values at different test temperatures. The effect of pH on THPS degradation initially appeared to be quite complicated. During the first two or three days following the introduction of THPS into seawater, the pH shifted but became quite stable. It was found that THPS reduced the pH immediately after it was added to the seawater. For example, adding THPS to seawater to achieve 160 ppm THPS immediately reduced the initial solution pH from 8.6 to 7.6. It also was found that the first experimental data obtained at two days showed a pH shift from its initial value for all the tests with three different initial pH settings. The solution pH values stabilized after approximately two days. This

could have been due to the slow acting buffering power of the seawater. Therefore, only stabilized pH data were used in modeling. This is permissible since THPS degradation evaluation is typically carried out over an extended period.

Table 6-4: Test matrix for THPS degradation investigation in the presence of mild steel

Test conditions	
Test media (all sterilized)	**Initial pH after THPS was added**
1. Persian Gulf seawater	8.12
2. pH-adjusted Persian Gulf seawater at low pH	6.06
3. pH-adjusted Persian Gulf seawater at high pH	9.33
Initial THPS concentration (ppm)	160
Test temperature (ºC)	4, 23, 31, 37
Light condition	Normal fluorescent lighting

Figure 6-10 shows that when the temperature is fixed, a lower pH slows down THPS degradation and that the degradation still follows the first-order kinetics with respect to THPS concentration. Figure 6-11 shows a surprisingly revealing trend for pH effect on k. All the lines are straight and parallel to each other. This suggests a linear relationship $\ln k \propto pH$ with a slope that is independent of temperature.

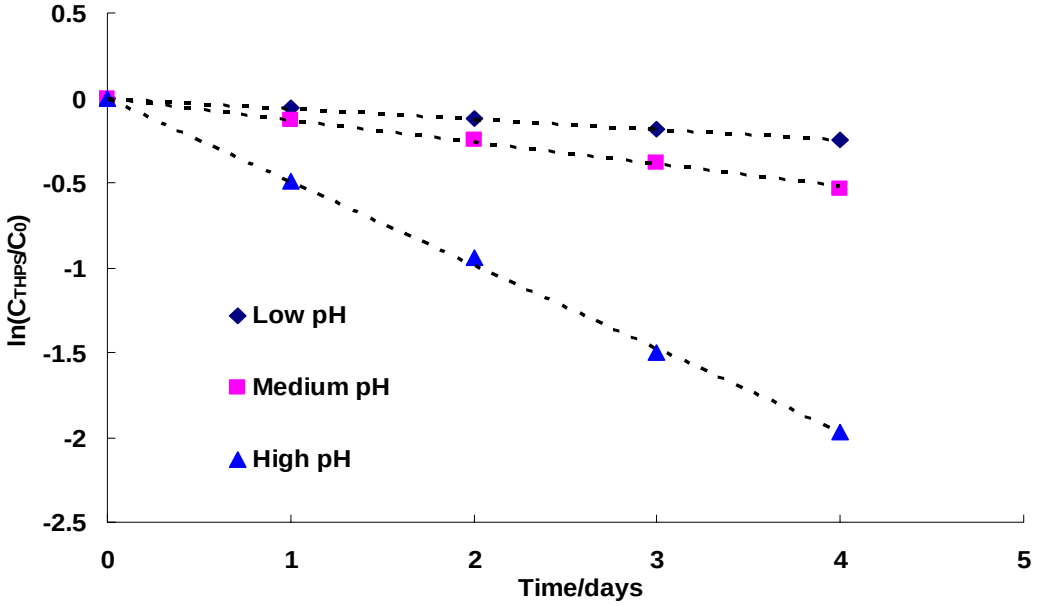

Figure 6-10: The specific reaction k(T, pH) at different pH at temperature 31 ºC (Test in Persian Gulf seawater with coupon)

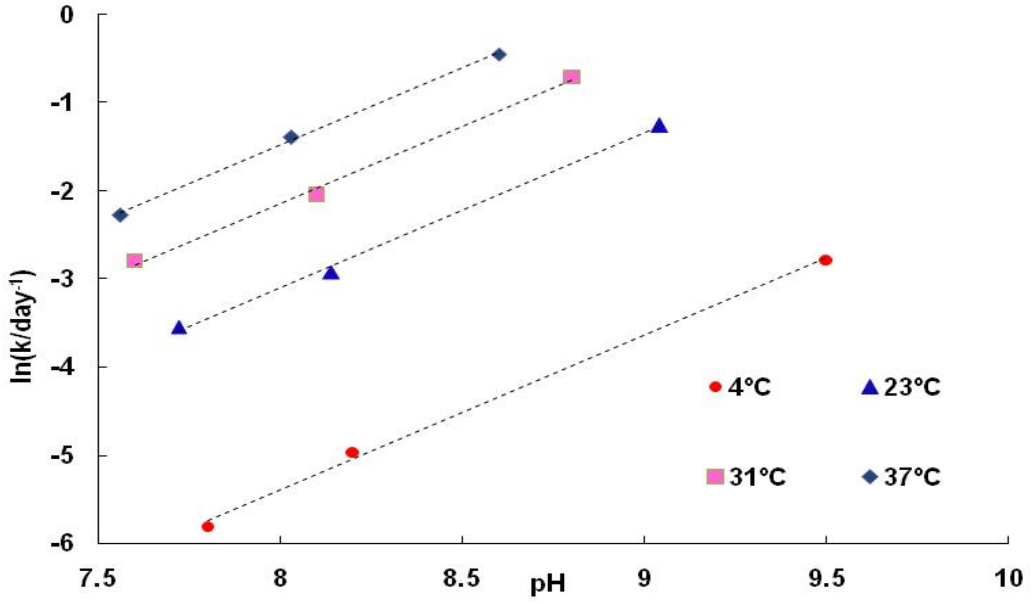

Figure 6-11: The relation of k(T, pH) with pH at four different temperatures (Test in Persian Gulf seawater with coupon)

Based on the definition pH= $-\log_{10}[H^+]$, the lnk vs. pH relationship now translates to a proportional relationship of $k \propto [H^+]^{-n}$, in which the parameter n is positive and independent of temperature. Because n is independent of temperature, we may use $k(T, pH)=k_T(T)\bullet[H^+]^{-n}$ where $k_T(T)$ is the rate constant with a fixed pH. This means that Equation 6-2 can be modified to include $[H^+]$ as shown in equation 6-7.

$$r = -\frac{dC}{dt} = k(T,pH) \bullet C = k_T(T) \bullet [H^+]^{-n} \bullet C \tag{6-7}$$

This suggests that the effect of pH can be viewed as proton inhibiting THPS degradation. In terms of reaction kinetics, $[H^+]$ appears in the rate expression as a negative order (-n) of reaction.

Equation 6-6 can be reformulated to give Equation 6-8 or Equation 6-9.

$$\ln k(T,pH) = \ln\left\{k_T(T) \bullet \left[H^+\right]^n\right\} = \ln\left(k_T(T)\right) - n \bullet \ln\left(\left[H^+\right]\right) = \ln A - \frac{E}{R \bullet (T + 273.15)} + 2.303n \bullet pH$$

(6-8)

Or,

$$\ln k(T,pH) = b + \frac{-E}{R \bullet (T + 273.15)} + 2.303n \bullet pH \tag{6-9}$$

Multi-linear regression of lnk vs. 1/(T+273.15) and pH experimental data would give parameters b, E and n values.

Table 6-5 lists k(T,pH) data obtained from Table 6-4 at different pH values and four different temperatures in Persian Gulf seawater. The pH values in Table 6-5 were stabilized pH values instead of the initial pH values. Multi-linear regression of the data in Table 6-5 using MATLAB (www.mathworks.com) Version 7 quickly yields b=17.25, activation energy $E=8.445\times10^4$ J/mol and a=1.750, i.e. n=0.76. The R^2 of the multi-linear regression is 0.998.

Table 6-5: Data for multi-linear regression

Temperature (°C)	4	4	4	23	23	23	31	31	31	37	37	37
pH	7.8	8.2	9.5	7.72	8.14	9.04	7.6	8.1	8.8	7.56	8.03	8.6
-lnk(T, pH)	5.81	4.96	2.78	3.54	2.92	1.25	2.78	2.04	0.71	2.27	1.39	0.45

Equation 6-9 can now be written as Equation 6-10:

$$k(T,pH)=\exp(17.25)\times\exp\left(\frac{-10161}{T+273.15}\right)\times\exp(1.75\bullet pH) \qquad (6\text{-}10)$$

With the k(T, pH) function known, Equation (6-7) can be solved with the initial THPS condition $C=C_0$ at t=0 to give THPS concentration as a function of temperature (in °C), pH and time (in days) as shown in Equation (6-11).

$$\ln\left(\frac{C}{C_0}\right) = -k(T, pH) \bullet t = -3.1 \times 10^7 \times \exp\left[\frac{-10161}{T + 273.15}\right] \times \exp(1.75 \bullet pH) \times t \qquad (6\text{-}11)$$

where the pH is the stabilized pH of the seawater after THPS introduction.

Table 6-6 compares the experimental data with the model. The dots at 31ºC with pH 7.9 and 8.4 are experimental data from the tests listed in Table 6-1, and the dots at pH 8.1 are the experimental data from the test in Table 6-4. These data in Table 6-1 were not used in the regression to obtain the b, E and n values above. The results show that the model fits the data very well indicating that the mechanism proposed for the pH effect is both reasonable and robust. It is interesting to note that at pH 8.4 and also at 7.9 THPS degradations in two different seawater samples were similar even though the salinity of Persian Gulf seawater is about twice that of Gulf of Mexico seawater and the artificial seawater (see Table 4-1 and Table 3-2). However, further experimental data with a wider range of salt concentrations is needed to determine whether salt content has an intrinsic effect on THPS degradation after pH is fixed.

Table 6-6: Comparison of THPS degradation model predictions with experimental data

Input parameters				
T (^{o}C)	Time (days)	C_o (ppm)	pH	
31	10	100	8.4	(In pH-adjusted Gulf of Mexico seawater with coupon presence)
			8.4	(In pH-adjusted Persian Gulf seawater with coupon presence)
			8.1	(In pH-adjusted Persian Gulf seawater with coupon presence)
			7.9	(In Persian Gulf seawater with coupon presence)
			7.9	(In artificial seawater with coupon presence)

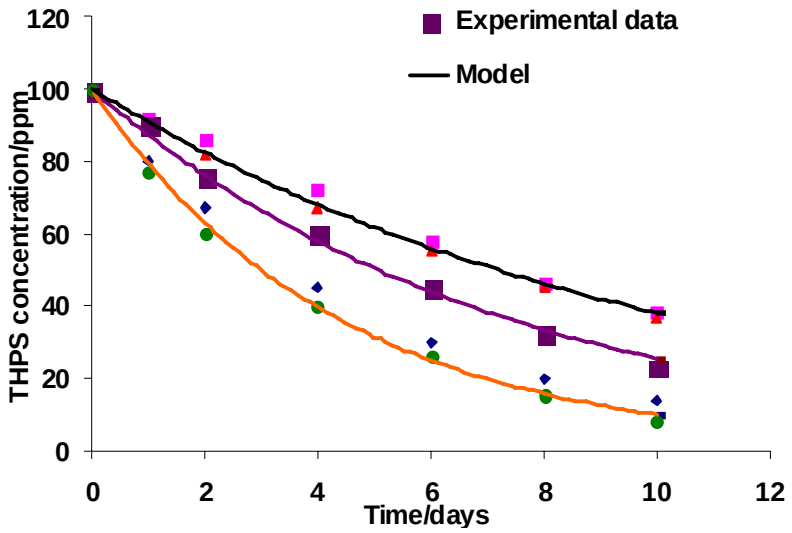

6.4.3 Effect of salts

Table 6-7 shows the test matrix when Persian Gulf seawater and fresh water were used as test media to study the salt effect on THPS degradation at the same fixed pH 6.3. Figure 6-12 shows that THPS degrades faster at higher temperature while the THPS degradation rate remains almost constant in seawater and fresh water at the same test temperature and pH. The results showed that salt has little intrinsic effect on THPS degradation after pH is fixed.

Table 6-7: Test matrix for salt effect on THPS degradation

Test condition	
Test media (all sterilized)	**Stabilized pH after THPS was added without coupon presence**
1. Persian Gulf seawater	6.3
2. Fresh water	6.3
Initial THPS concentration (ppm)	160
Test temperature (ºC)	31, 37
Light condition	Normal fluorescent lighting

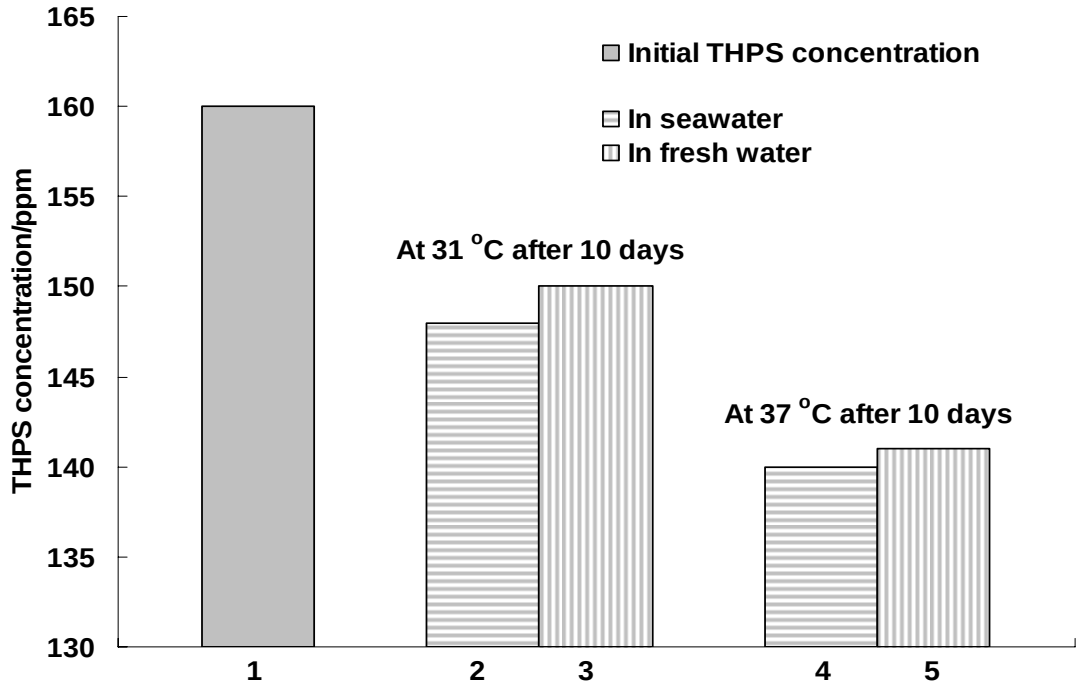

Figure 6-12: Salt effect on THPS degradation at fixed pH 6.3

6.5 Conclusions:

- THPS degradation is a complex process and is affected by many factors. It follows first-order kinetics. Our mechanistic model shows that it is strongly dependent on temperature and pH. THPS degradation increases with the increase of temperature and pH.
- pH effect can be decoupled from temperature. Experimental data indicated that proton acted as an inhibitor of THPS degradation in the form of a negative order reaction.
- The proposed mechanistic model for THPS concentration prediction as a function of time, temperature and pH fits the experimental data very well. The model shows that THPS degradation is highly sensitive to temperature and pH changes while salt has no intrinsic effect on THPS degradation.

CHAPTER 7: A MECHANISTIC MIC MODEL

7.1 Introduction

Current MIC modeling is still immature and existing MIC modeling is confined to probability models based on risk factors. Some drawbacks to these models:

1) The weighing of the risk factors is subjective
2) The interactions of the risk factors are not clear
3) Verifying these models for pipeline systems is difficult

The anaerobic metal corrosion caused by SRB is a growing problem with the aging of reservoirs and pipelines, and increased water-wetting operations. The mechanism of MIC, however, is still controversial. The leading theory is the cathodic depolarization theory (CDT) (von Wolzogen Kuhr and vander Vlugt, 1934; Thierry and Sand, 1995) hinging on SRB hydrogenase to covert the adsorbed hydrogen atoms on the cathode to hydrogen and then to H^+, thus pushing the iron dissolution reaction forward. Costello (1974), however, proposed that hydrogen sulfide H_2S, rather than H^+ could act as cathodic reactant, i.e.

$$2H_2S + 2e^- \Leftrightarrow 2HS^- + H_2 \qquad (7\text{-}1)$$

A number of other studies (Hardy, 1983; Cord-Ruwisch and Widdel, 1986; Rajagopal and LeGall, 1989) also showed that sulfate reduction could occur successively even with the hydrogen formation on the cathodic site. In addition, some corrosive bacteria such as acid producing bacteria (APB) are hydrogenase negative, which means MIC due to APB cannot be explained by the cathodic depolarization theory. The actual reaction steps of

MIC mechanism are complicated; however, there is no doubt about the iron oxidation and sulfate reduction

$$Fe \rightarrow Fe^{2+} + 2e^{-} \quad (7\text{-}2)$$

$$SO_4^{2-} + 9H^{+} + 8e^{-} \rightarrow HS^{-} + 4H_2O \quad (7\text{-}3)$$

$$2HS^{-} + 2H^{+} \rightarrow 2H_2S \quad (7\text{-}4)$$

A simplified approach to microbial corrosion involving SRB is to view the sulfate reduction as a single process that removes electron from the metal because iron does not corrode in neutral water without the presence of oxygen and SRB, so the process of proton reduction is neglected. The hydrogenase system in the SRB cells at the interface of biofilm and metal surface is treated as a bio-electrocatalyst for sulfate reduction. Based on Reactions 7-2 and 7-3, this study presents a mechanistic model based on a biocatalytic cathodic sulfate reduction (BCSR) theory for MIC due to SRB. The BCSR theory assumes that MIC occurs because the electrons released by iron dissolution at the anode are utilized in the sulfate reduction at the cathode with the help of biocatalyst, and anodic and cathodic sites are both on the interface of biofilm and the metal.

7.2 Modeling development

7.2.1 Assumptions

Compared to a conventional electrochemical study, the MIC process is far more complex due to the uncertainty of biological behavior. For this study, the following assumptions were made:

1. Only one single strain of SRB species was investigated.
2. The test was conducted in a well turbulent condition.
3. No nutrients were involved except for the key substrate sulfate.

Sulfate reduction also happens if lactate is used as the carbon source in the medium even without iron. In the following reaction, lactate acts as the electron donor for sulfate reduction.

$$SO_4^{2-} + 2CH_3CHOCOO^- \rightarrow 2CH_3COO^- + 2CO_2 + HS^- + OH^- \quad (7\text{-}5)$$

The assumption was made to reduce the uncertainty of sulfate reduction, indicating that iron acts as the only electron donor in the sulfate reduction process (see Reaction 7-3).

4. It was assumed that there were no iron sulfides present in the system.

If there is a production of iron sulfides, galvanic corrosion may be involved, but it has not been proven yet. Some experments need to be done to verify the hypothesis; otherwise the presence of iron sulfides adds an extra diffusion layer like biofilms. The effect of iron sulfides will be incoporated into the MIC model in the future.

5. This MIC model focused on the single effect of biofilm on iron corrosion, and assumed that there were no planktonic SRB cells in the medium.

This assumption is practical because in a real operation, concentrations of planktonic cells are low whereas biofilm colony is in a high concentration of cells.

6. In the simulated MIC process, test conditions at temperature=37^oC and pH=7 in anaerobic environment (deoxidization with N_2) with ambient (atmosphere) pressure are applied.

7.2.2 Electrochemical process

The electrochemical method in MIC research was proven to be practical and feasible as early as 1997 by Rainha and Fonseca (1997). They used a three-electrode glass cell similar to the one shown in Figure 7-1 used at Ohio University to investigate anodic and catholic behavior by applying a polarization potential approach.

In electrochemistry, the Butler-Volmer equation (7-6) is a fundamental tool used to describe electrical current relationship to the electrode. Both anodic and cathodic electrical current on the same electrode can be expressed by the following equation:

$$I = A \cdot i_0 \cdot \left\{ exp\left[\frac{(1-\alpha) \cdot n \cdot F}{R \cdot T} \cdot \left(E - E_{eq}\right) \right] - exp\left[-\frac{\alpha \cdot n \cdot F}{R \cdot T} \cdot \left(E - E_{eq}\right) \right] \right\} \quad (7\text{-}6)$$

I: electrode current, A

A: electrode active surface area, m^2

i_o: exchange current density, A/m^2

E: electrode potential, V

E_{eq}: equilibrium potential, V

T: absolute temperature, K

n: number of electrons involved in the electrode reaction

F: Faraday constant

R: universal gas constant

α: symmetry factor, dimensionless

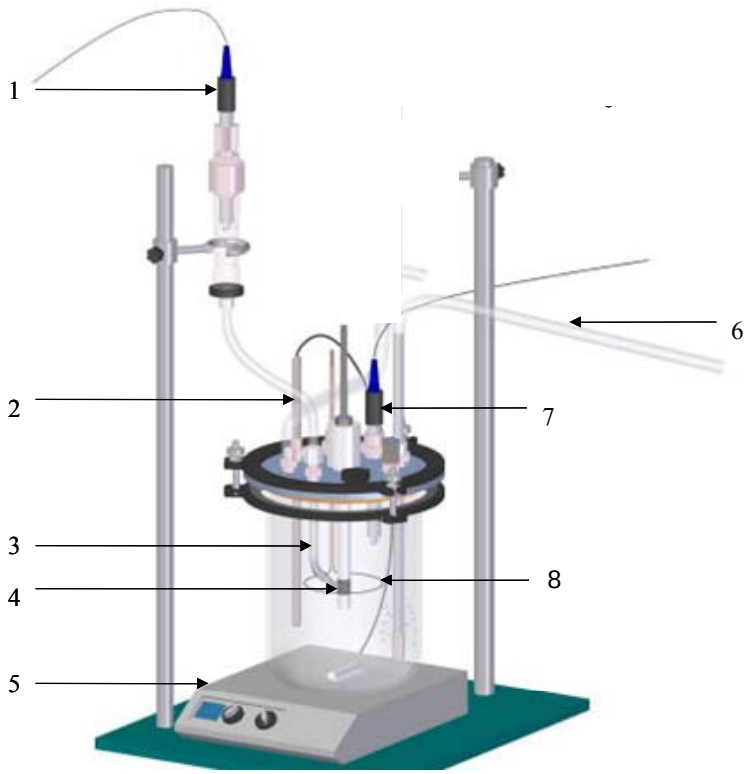

Figure 7-1: Schematic of an electrochemical glass cell: 1. Reference electrode; 2. Temperature probe; 3. Luggin capillary; 4. Working electrode; 5. Hot plate; 6. Bubbler for gas; 7. pH electrode; 8. Counter electrode (Picture drawn by Mosser Danniel, 2004)

At the high overpotential region, the Butler-Volmer equation can be approximated by the Tafel equation.

$$i = i_0 \cdot 10^{\frac{E-E_{eq}}{\beta}} \tag{7-7}$$

The Butler Volmer equation simplifies to Equation (7-8) when symmetry factor α=0.5 is used, i.e.

$$i = i_0\left[e^{\frac{nF(E-E_{eq})}{2RT}} - e^{-\frac{nF(E-E_{eq})}{2RT}}\right] = 2i_0\, sinh\left[\frac{nF(E-E_{eq})}{2RT}\right] \quad (7\text{-}8)$$

For anodic dissolution of metal iron and cathodic reduction of sulfate, Equation (7-8) can give

$$i_{a(Fe)} = 2i_{0(Fe)}\, sinh\left[\frac{nF(E-E_{eq_{(Fe)}})}{2RT}\right] \quad \text{for anodic iron oxidation} \quad (7\text{-}9)$$

$i_{0(Fe)}$: exchange current density for Fe, A/m^2

$E_{eq(Fe)}$: equilibrium potential for Fe, V

$$i_{ct(SO_4^{2-})} = 2i_{0(SO_4^{2-})}\, sinh\left[-\frac{nF(E-E_{eq_{(SO_4^{2-})}})}{2RT}\right] \quad \text{for cathodic reaction} \quad (7\text{-}10)$$

$i_{0(SO_4^{2-})}$: exchange current density, A/m^2

$E_{eq(SO_4^{2-})}$: equilibrium potential, V

Equations (7-9) and (7-10) are the electrical currents expressed in the condition of charge transfer control. In general, for each species of cathodic reactions, cathodic current i_c is expressed as:

$$\frac{1}{i_c} = \frac{1}{i_{ct}} + \frac{1}{i_{lim}} \quad (7\text{-}11)$$

i_{ct}: cathodic charge transfer controlled current, A/m^2

i_{lim}: limiting current, A/m^2

i.e.

$$\frac{1}{i_{c(SO_4^{2-})}} = \frac{1}{i_{ct(SO_4^{2-})}} + \frac{1}{i_{lim(SO_4^{2-})}} \qquad \text{for cathodic } SO_4^{2-} \text{ reduction} \qquad (7\text{-}12)$$

$i_{ct(SO_4^{2-})}$: cathodic charge transfer controlled current for SO_4^{2-}, A/m^2

$i_{lim(SO_4^{2-})}$: limiting current for SO_4^{2-}, A/m^2

where $$i_{ct(SO_4^{2-})} = 2i_{0(SO_4^{2-})} \sinh\left[-\frac{nF(E - E_{eq(SO_4^{2-})})}{2RT}\right] \qquad (7\text{-}13)$$

$i_{0(SO_4^{2-})}$: exchange current density for for SO_4^{2-}, A/m^2

$E_{eq(SO_4^{2-})}$: equilibrium potential for SO_4^{2-}, V

$i_{0(Fe)}$ and $E_{eq(Fe)}$ in anodic iron dissolution reaction (7-2) are available in the literature or can easily be obtained from experiment, while $i_{0(SO_4^{2-})}$ in cathodic SO_4^{2-} reduction (7-3) by SRB have not been found in the literature and must be obtained through experimental method. The exchange current density for the cathodic sulfate reduction is a key parameter in this mechanistic MIC model. Without the biocatalysis from biofilm on the cathode, the sulfate reduction reaction on the cathode is negligible due to an extremely small $i_{0(SO_4^{2-})}$. $i_{0(SO_4^{2-})}$ is a direct measurement of how "aggressive" a particular SRB species is meaning how capable their enzymeatic ability is for the catalysis of sulfate reduction. We define its value on the $\log_{10}$ scale as bioaggressiveness. Typical range is expected to be around -10 to 2. The unknown potential E (known as corrosion potential) in the above equations can be determined by a charge balance

equation (7-14) which states that the sum of anodic currents (7-9) is equal to the sum of cathodic currents (7-10) at the metal interface (Lee, 2004).

$$\sum i_a = \sum i_c \qquad \text{i.e.} \qquad i_{a(Fe)} = i_{c(SO_4^{2-})} \tag{7-14}$$

7.2.3 Transport process

As shown in Figure 7-2, under stagnant conditions, each species migrating towards or away from a metal surface must pass through both liquid diffusion and biofilm layers, resulting in concentration gradients that influence the electrochemical reactions on the metal surface. Therefore, the electrochemical processes in Section 7.2.2 need to be coupled with a transport process to study the microbially caused corrosion. Sulfate consumption by bulk sessile SRB cells for maintenance and growth in pits is ignored here.

According to Grady (1983), mass transfer resistance in the liquid layer under turbulent condition was found to be minimal, and moreover, Bailey and Ollis (1986) calculated the Biot number ($Bi = \frac{hL_C}{k_b}$) for a biofilm system and found it to be larger than 200. Therefore, the external mass transfer resistance in the development of the model can be ignored, which indicates that C_1 is equal to C_0, i.e. C_1=C_b= bulk concentration.

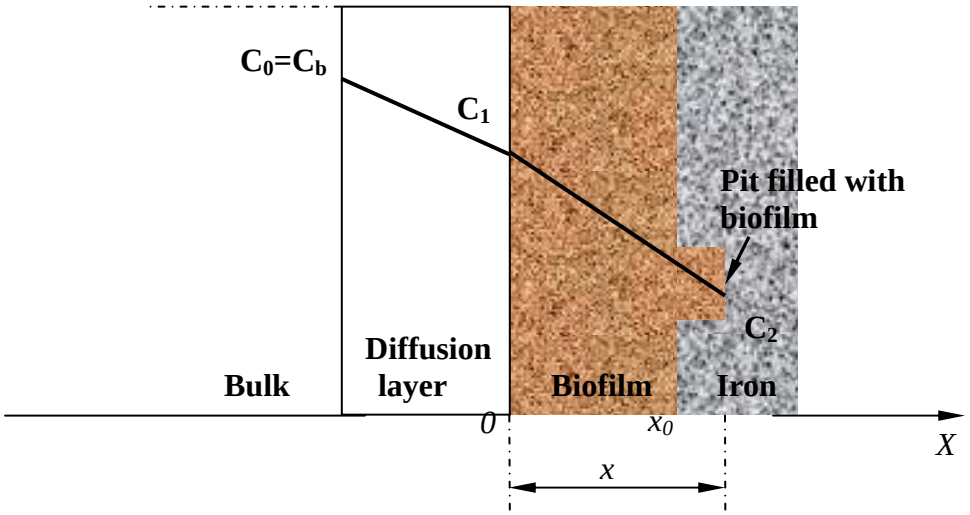

Figure 7-2: Schematic of a domain from metal to bulk solution

In the case of SO_4^{2-} reduction, SO_4^{2-} limiting current $i_{lim(SO_4^{2-})}$ in the absence of charge transfer resistance and negligible diffusion resistance in the liquid diffusion layer (i.e., $C_1=C_b$) can be expressed as:

$$i_{lim(SO_4^{2-})} = \left(\frac{D_{(SO_4^{2-})} nF}{x}\right) C_{b(SO_4^{2-})} \qquad (7\text{-}15)$$

$D_{(SO_4^{2-})}$: SO_4^{2-} diffusion coefficient

n: the number of electrons consumed by the reduction rate

F: Faraday's constant

x: the thickness of the diffusion layer

$[SO_4^{2-}]_b$: bulk concentration of SO_4^{2-} ion

The diffusion coefficients of each species within biofilm can be determined by the following Equation (7-16) (Fan et al., 1990), which shows that diffusivity in the biofilm is related to the biofilm density. Aqueous diffusivity D_w of each species is available in the literature.

$$\frac{D_{eff}}{D_w} = 1 - \left[\frac{0.43X^{0.92}}{\left(11.19 + 0.27X^{0.99}\right)} \right] \tag{7-16}$$

D_{eff}: effective diffusivity in the biofilm, m^2/s

D_w: aqueous diffusivity, m^2/s

X: biofilm dry density, mg/cm^3

This research focused on 1-D study of biofilm development, i.e. biofilm growth along z axis instead of spreading along x and y axis.

In this simplified system, there are five soluble species, Fe^{2+}, SO_4^{2-}, H^+, S^{2-}, and OH^-. Irrespective of whether or not the species are involved in the electrochemical reactions, each of the species *j* has its own spatial distribution of concentration, which is governed by the mass balance as demonstrated in (7-17).

$$\frac{\partial C_j}{\partial t} = \frac{\partial}{\partial x}\left(D_{eff} \frac{\partial C_j}{\partial x} \right) + R_j \qquad \text{j=1, 2…} \quad \text{(species)} \tag{7-17}$$

C_j: concentration of species *j*, mol/m^3

t: time, s

x: spatial coordinate, m

R_j: the source or sink of species *j* due to chemical reactions, mol/ (m^3 ·s)

To simplify the system, this study only considers sulfate mass transfer and ignores the sulfate consumption by SRB, i.e., R=0. For a mature biofilm, the sulfate consumption in the bulk biofilm ($R_{SO_4^{2-}}$ <0) is used either for cell growth to fill pits, and to compensate for cell death or provide maintenance energy. To solve the diffusion equation above, a pseudo-steady state is assumed. In a small time frame (say 1 hour or day), the sulfate concentration can be considered time independent across the biofilm. The iron dissolution (corrosion) rate CR is then determined by the following expression: $CR = \frac{M_{Fe}}{2F\rho_{Fe}} i_{a(Fe)} = 1.155 i_{a(Fe)}$, after $i_{a(Fe)}$ is calculated from the charge balance Equation (7-14). It is noted that the iron dissolution (corrosion) rate here is the pitting rate in mm/y.

7.2.4 Numerical method

To solve the model, a time loop is used to calculate CR from t= 0 to t=365 days (or longer as needed). Since the time step is sufficiently small (say 1 hour or day), CR rate can be considered constant because the biofilm thickness increase during that time frame due to pitting is negligible.

In the numerical solution, the current SRB biofilm thickness will be the thickness carried over from the previous one plus CR multiplied by the time step size. This assumes that the biofilm will fill in the pit void, thus increasing the biofilm thickness. The biofilm surface exposed to the bulk liquid is assumed not moving for a mature biofilm. It may be

explained by that the bulk fluid flow in a pipe restricts the biofilm from expanding toward the pipe center due to shear. The resistance ratio, $\left(\frac{1}{i_{lim(SO_4^{2-})}}\right) \Big/ \left(\frac{1}{i_{ct(SO_4^{2-})}}\right)$, can be used to characterize the relative importance of mass transfer resistance over charge transfer resistance.

7.2.5 Results and discussion

MATLAB was used to solve the model, and the parameters used in the model are listed in Table 7-1. Some of them are available from the literature, and the others have to be obtained from experiments and were assumed in the model using reasonable values. The first generation of the mechanistic MIC model is named BCSR model. Figure 7-3 shows the interface for BCSR V1.0 with input parameters: bioaggressiveness and time in days. The final pit depth and several simulated figures (Figure 7-4 ~ Figure 7-6, and Figure 7-8 ~ Figure 7-9) will pop up when pushing the button simulation.

Figure 7-4 shows that the resistence ratio is 0.40 at time zero and it becomes 4.6×10^5 at day 365, indicating that mass transfer resistence becomes increasingly important over time. This fact is manifested in Figure 7-5, which shows that the initially increasing biofilm thickness causes the corrosion rate to decrease quickly. It means that mass transfer control quickly takes over the corrosion process after the charge transfer control takes effect at the very beginning. Figure 7-5 also shows the pit depth increases over time. The pitting rate is large initially when mass transfer resistance is less important. As pit grows, the overall thickness of the SRB biofilm (between the pit bottom and the

top biofilm surface) increases and mass transfer starts to control the corrosion process. For a deep pit, this is a major mass transfer barrier hampering the sulfate migration from the bulk fluid to the pit bottom. Eventually, the growth of all deep pits will be severely limited by this.

Figure 7-6 shows that the corrosion potential decreases over time corresponding to a decreasing corrosion rate. As expected, the corrosion potential values are between the anodic equilibrium potential (-0.458) and cathodic equilibrium potential (-0.226) (based on the values from Barton and Hamilton, 2007 with temperature adjustment). Sulfate concentration is important in this model. Increased sulfate concentration in the bulk-fluid phase will make more sulfate available for cathodic reduction on the iron and biofilm interface leading to more corrosion as shown in Figure 7-7. This is only true in the mass transfer control region (often meaning deep pit growth region).

Figures 7-8 and Figure 7-9 show the simulated potentiodynamic sweep profiles. The intersection of the anodic and cathodic curves yields the corrosion potential and corrosion current density. Figure 7-9 shows that the intersection point is clearly in the almost vertical cathodic curve region on the right. This is known as concentration polarization or mass transfer control region in the electrochemical reaction theory.

Figure 7-10 shows the calibrated model prediction using calibrated bioaggressiveness (-8.5). The pit depth data at one-week (see Section 4.4.3, Part II: (ii)) and 2-week (see Section 4.4.3, Part II: (i)), were obtained from the previous tests at 37^{o}C in the enriched Qurrayah water spiked with SRB.

To better simulate the real situation, the bulk sulfate concentration in the calibrated model was adjusted to 44 mole/m^3 (mM) because the sulfate concentration in Qurrayah water (Arabian seawater) is higher than in typical seawater (28 mole/m^3). Figure 7-10 shows that the calibrated model matches the 2-week experimental data very well. The MIC model calibrated using one-week pit depth data is under the control of charge transfer during which pit grows linearly with time. This is demonstrated in Figure 7-11 that pit depth increases little with the increase of sulfate concentration.

Table 7-1: Model parameters at 37°C

Parameters	Symbol	Value	Units	Source
SO_4^{2-} concentration in bulk solution	$C^0_{SO_4^{2-}}$	28	mol/m^3	Assumed
Initial biofilm thickness	x_0	100	μm	Assumed
Biofilm dry density	X	60	mg/cm^3	Assumed
Equilibrium potential for iron	$E_{eq(Fe)}$	-0.458	V,SHE	Calibrated from Barton and Hamilton, 2007 (-0.44V @25°C)
Equilibrium potential for sulfate	$E_{eq(SO4^{2-})}$	-0.226	V, SHE	Calibrated from Barton and Hamilton, 2007 (-0.217V @25°C)
Exchange current density for iron dissolution	$i_{0(Fe)}$	0.018	Am^{-2}	Calculated from Eq. (7-19) at $i^{ref}_{0(Fe)} = 0.01$ @ 25°C
Exchange current density for SO_4^{2-} reduction	$i_{0(SO_4^{2-})}$	0.1	V, SHE	Assumed
Diffusion coefficient of SO_4^{2-} in water	$D_{SO4^{2-}}$	1.41×10^{-9}	$m^2 s^{-1}$	Calculated from Newman, 1991 (1.10×10^{-9} m^2s^{-1} @25°C)

The exchange current density of iron is temperature dependent:

$$i_{0(Fe)} = i^{ref}_{0(Fe)} e^{\frac{-\Delta H_{Fe}}{R}\left(\frac{1}{T_c+273.15}-\frac{1}{T_{c,ref}+273.15}\right)} \qquad \Delta H_{Fe}=37.5 \text{ KJ/mol} \qquad (7\text{-}18)$$

And diffusion coefficient of species in water is related to temperature and viscosity:

$$D = D_{ref}\left(\frac{T_c+273.15}{T_{c,ref}+273.15}\right)\left(\frac{\mu_{H_2O,ref}}{\mu_{H_2O}}\right) \qquad (7\text{-}19)$$

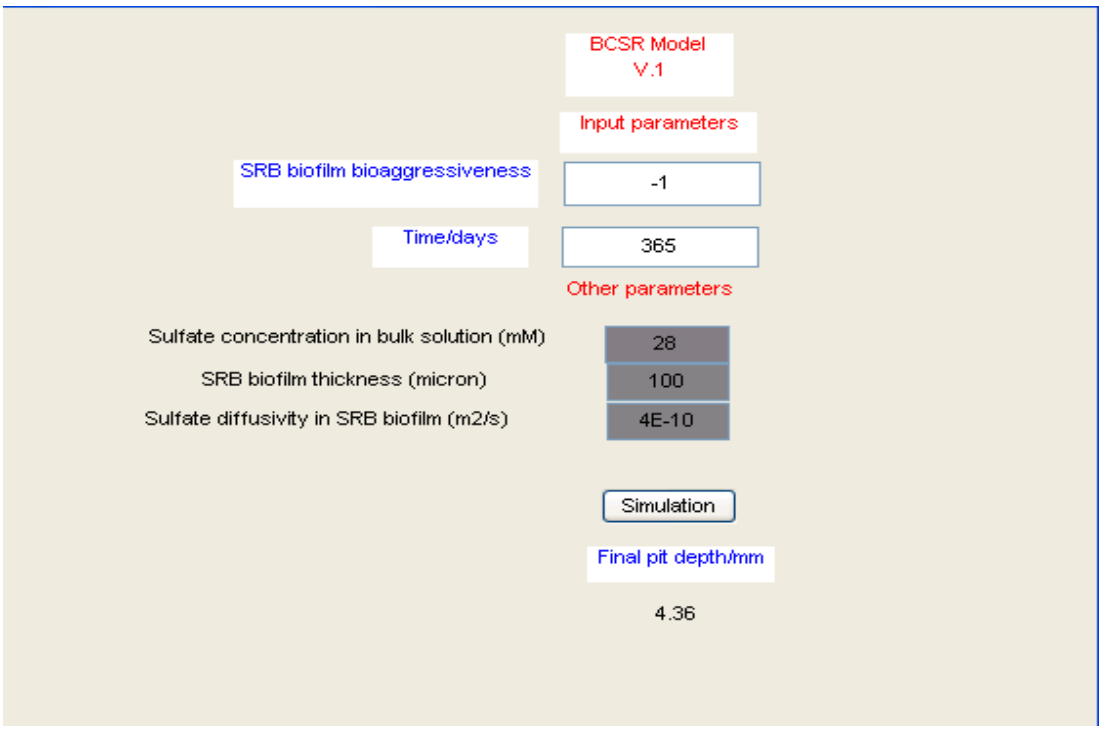

Figure 7-3: Interface for BCSR Version 1

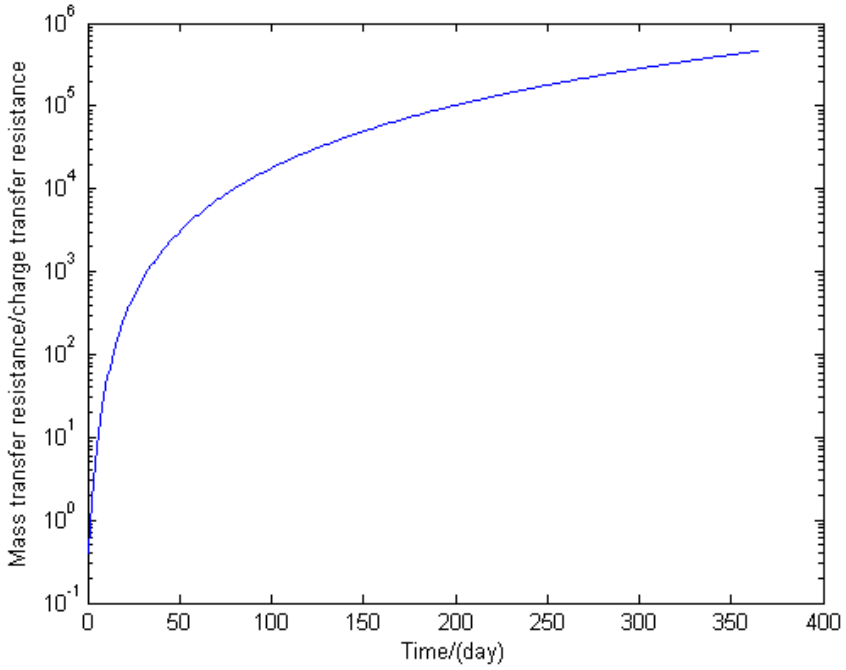

Figure 7-4: Simulated corrosion resistence ration using parameters in Table 7-1

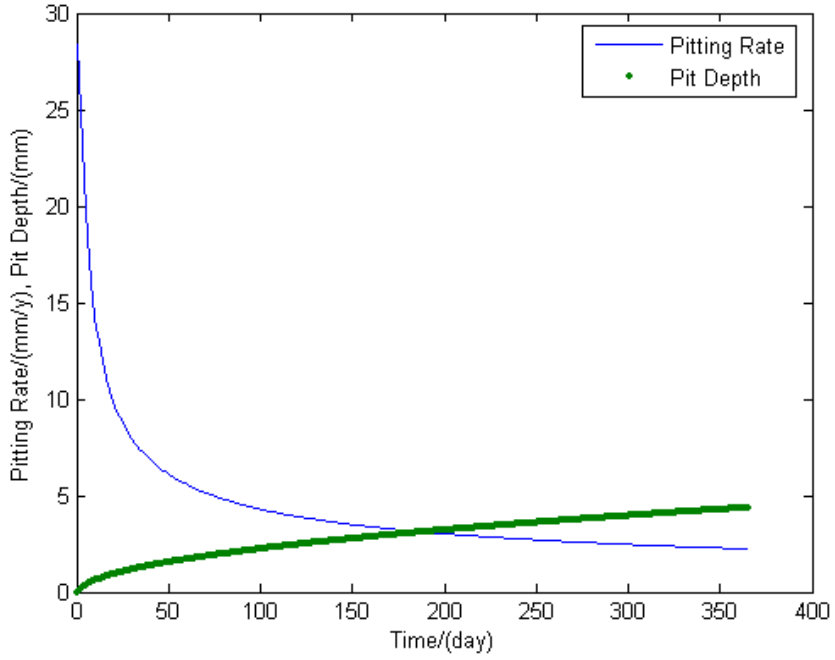

Figure 7-5: Simulated corrosion rate and pit depth using parameters in Table 7-1

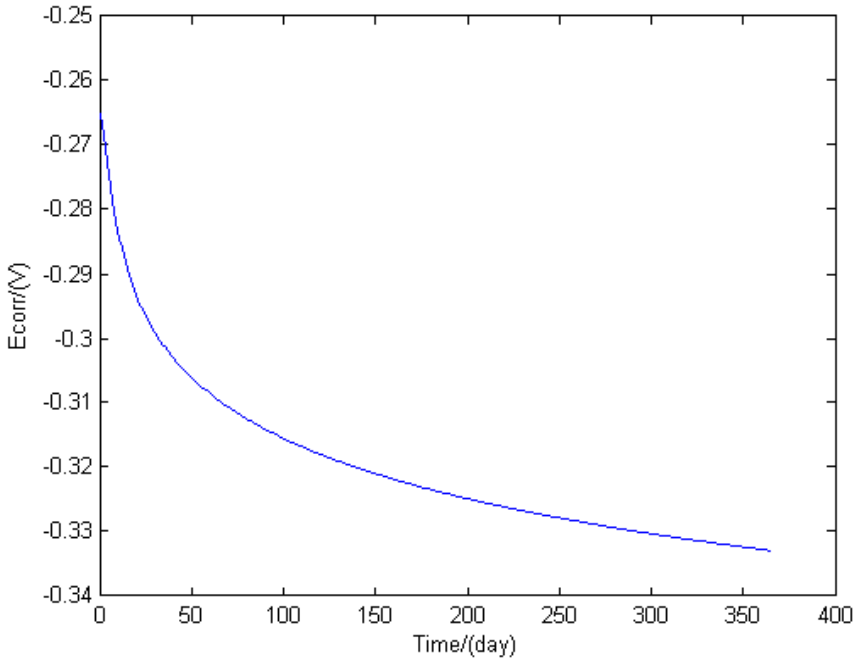

Figure 7-6: Simulated corrosion potential using parameters in Table 7-1

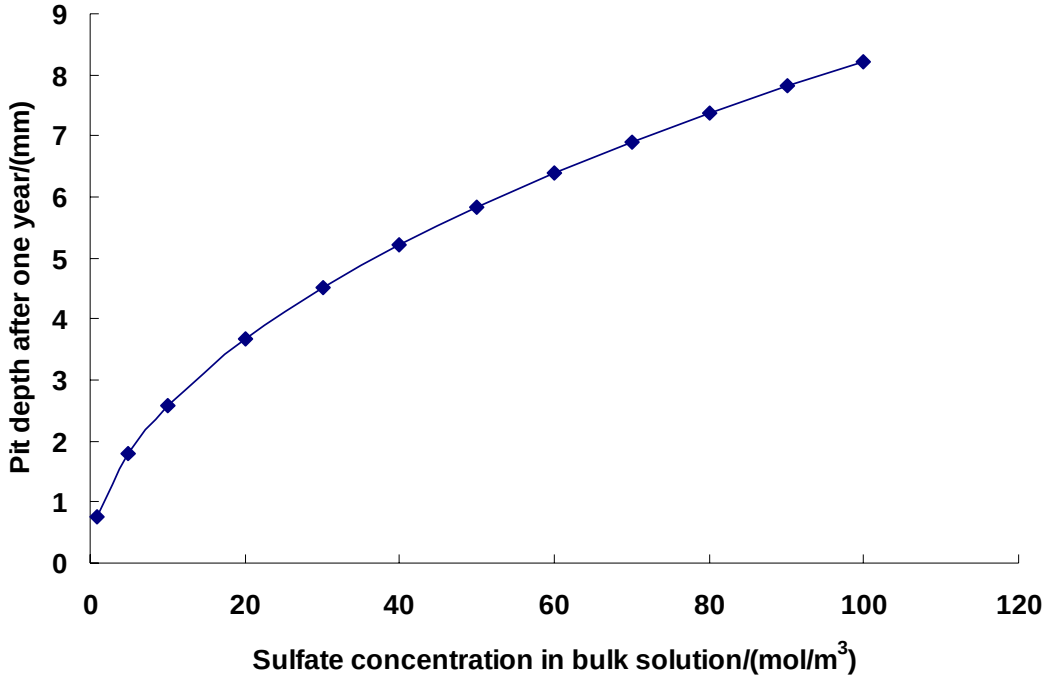

Figure 7-7: Simulated effect of sulfate concentration on pit depth using parameters in Table 7-1 after one year

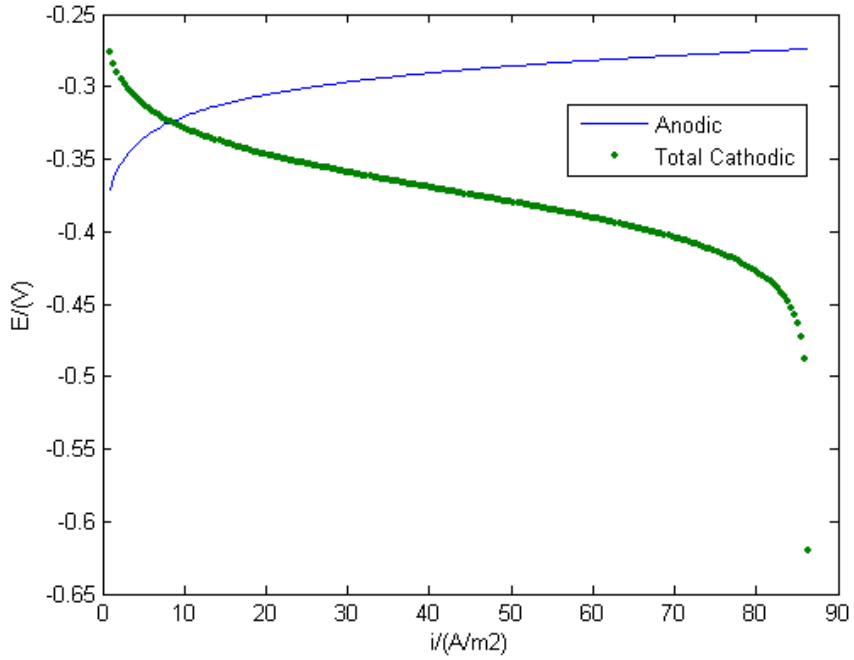

Figure 7-8: Simulated potentialdynamic sweeps at time=0 using parameters in Table 7-1

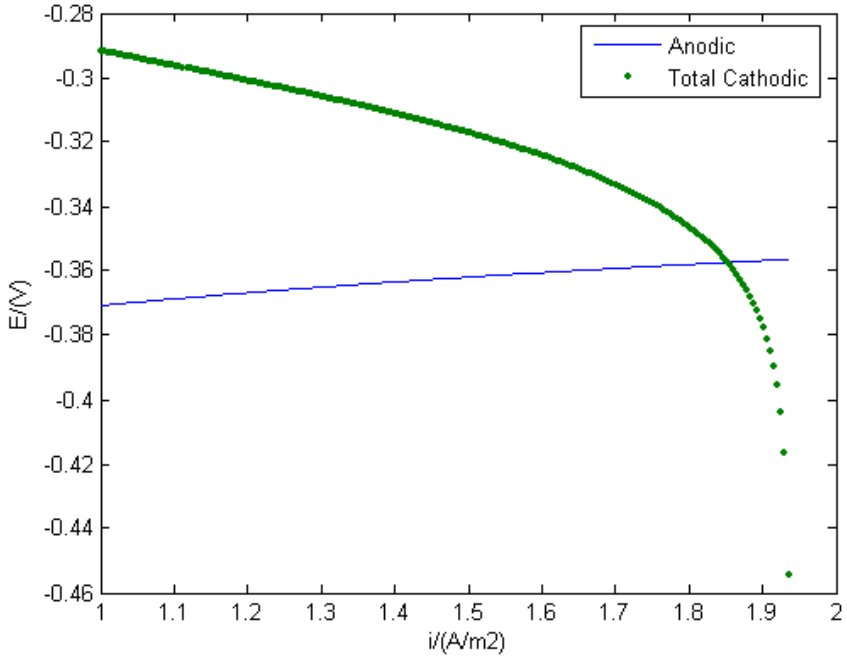

Figure 7-9: Simulated potentialdynamic sweeps at day 365 using parameters in Table 7-1

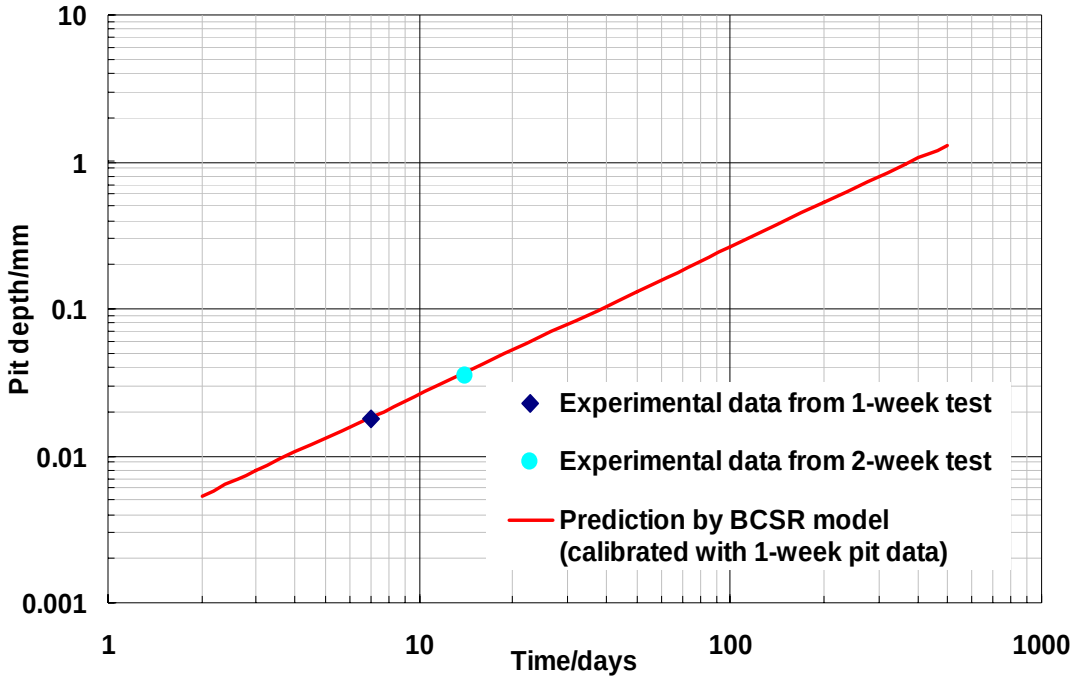

Figure 7-10: Calibrated MIC model prediction using the bioaggressiveness (-8.5) calibrated from the 1-week pit depth data point (18μm) (The slow pitting corrosion is likely due to the lack of organic carbon in the seawater.)

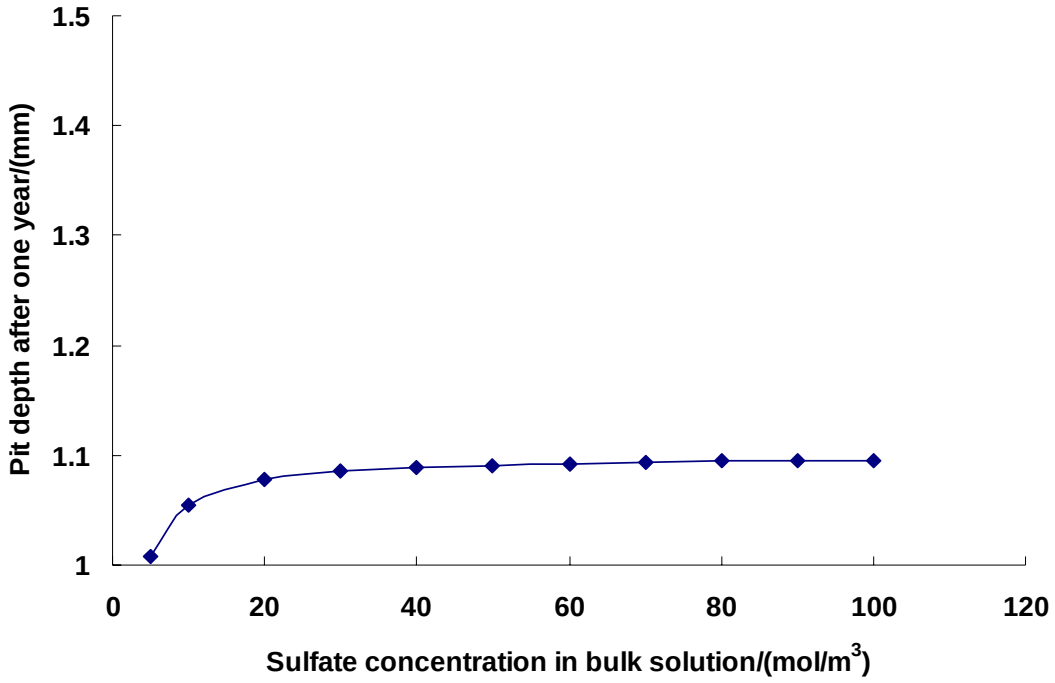

Figure 7-11: Simulated effect of sulfate concentration on pit depth using calibrated bioaggressiveness (-8.5) after one year

MIC pitting attacks do not occur without the presence of a biofilm. The mechanistic MIC model above was developed based on the corrosion process underneath a biofilm. Therefore, to apply the MIC model to predict localized corrosion rates caused by biofilms, a good method for detecting biofilm locations is needed. The following Section (7.3) proposed a new biomarker for locating biofilms.

7.3 Biomarker for biofilm monitoring

7.3.1 Introduction

The current NACE biofilm assay standards all require actual biofilm samples (NACE Standard TM0194, 2004). Existing DNA and enzyme assays cannot distinguish between planktonic cells and the elusive sessile (biofilm) cells. Further, these assays are not sensitive enough for extremely dilute systems. A new class of biomarkers is needed for more reliable and quantitative prediction of MIC. It is desirable to investigate biomarkers released by sessile cells in relatively large quantities, and when biomarkers are released into the bulk fluid they could be easily sampled. For a flow system, it is foreseeable that a self-propelled capsule with multiple chambers could be deployed. The chambers could be opened at pre-programmed times, taking in the bulk fluid at different locations. In analyzing the biomarker concentration profiles, biofilm locations could be indentified.

One such biomarker, extracellular polymeric substances (EPS) was explored in this work. EPS, secreted by cells, glue themselves and adhere a biofilm to solid surfaces. EPS account for 50% to 90% of the organic matter in a biofilm (Wingender et al., 1999). Some EPS molecules are released into the bulk-fluid due to cell metabolism and natural death. This allows for the detection of biofilms at their source as well as downstream when sampling the bulk fluid.

EPS means extracellular polysaccharides, exopolysaccharides or exopolymers. To be inclusive, EPS now often stands for extracellular polymeric substances. Bacterial EPS consist mostly of polysaccharides, proteins, nucleic acids, phospholipids and humic

substances (Jahn and Nielsen, 1998). The two most abundant components are polysaccharides and proteins. The protein content varies from a few percentages to up to 50%.

EPS exist in several forms: capsules (firmly attached to the cell surface), sheaths, slimes (loosely attached to the cell surface), and a soluble form found in suspensions according to Nielsen and Jahn (1999). Usually, EPS in the biofilm matrix and EPS released by the matrix are called biofilm EPS while planktonic EPS are those that are attached to the planktonic cells or released by the planktonic cells. Because of their low solubility, some undissolved biofilm and planktonic EPS will be suspended in the liquid medium.

Currently, EPS studies focus on the analysis of its two main components, polysaccharides and proteins. Some studies have demonstrated that composition differences among EPS from different sources are apparent. For example, it has been documented that in some bacterial strains uronic acids (polysaccharide subunits) and protein contents and structures are different for EPS in capsule and in free forms (Beech et al., 1999). Experimental work has already confirmed that cellular compositions between planktonic and sessile cells are different (Trémoulet et al., 2002). Since EPS from sessile and planktonic cells serve different biological functions, this inevitably leads to the differences in EPS molecular compositions. A recent paper by Kives et al. (2006) showed that the EPS harvested from the biofilm of *Pseudomonas fluorescens* strain B52 (associated with the food industry) differed in the relative amounts of polysaccharide subunits and proteins. It contained roughly 1:1.4:2 weight ratios for neutral and amino

sugars vs. proteins vs. uronic acids for EPS associated with biofilm growth on a stainless steel surface, while the ratio for EPS associated with planktonic cells became 1:11.2:54. For this microorganism, biofilm EPS detection can obviously overcome the interference from other EPS because biofilm EPS contains much more neutral and amino sugars, and much less protein.

Although EPS polysaccharides contain many different polysaccharide subunits (monosaccharides), only a few are dominant. Beech et al. (1991) identified glucose, mannose and galactose as dominant sugar subunits in the biofilms of *Pseudomonas fluorescens* and *D. desulfuricans* grown on mild steel coupons. Rhamnose was a dominant polysaccharide subunit in *Desulfovibrio desulfuricans,* but was not detected in *P. fluorescens* or *Desulfovibrio esulfuricans*. Staats et al. (1999) found that glucose, galactose, mannose, rhamnose and xylose were dominant in the EPS both in the biofilms and in the medium for *Cylindrotheca closterium* and *Navicula salinarum.* Leriche et al. (2000) found that EPS in the biofilms of coryneform bacteria contained large amounts of glucose and mannose residue. Wozniak et al. (2003) studied EPS in the biofilms of four strains of *Pseudomonas aeruginosa* and found that rhamnose, mannose and glucose and, to a lesser extent, xylose were dominant polysaccharide subunits. The same was true for biofilms of *Desulfobacterium autotrophicum*, *Desulfovibrio sp.* (stain H0401_12.1Lac and LM1, respectively) (Braissant et al., 2007). Hu et al. (2003) found that glucose, galactose, mannose, rhamnose and xylose were also dominant in the biofilms of four filamentous cyanobacteria *Microcoleus vaginatus, Scytonema javanicum, Phormidium tenue* and *Nostoc sp.* Some researchers have also targeted monomeric uronic acids in

addition to monosaccharides in EPS analysis and glucuronic acid was often found to be relatively abundant (Hu et al., 2003; Singh et al., 2006; de Brouwer et al., 2006).

Almost all the existing literature focuses on assaying EPS attached to biofilms, and to a much less extent, planktonic cells with the exception of two papers. Beech et al. (1991) found that there were other significantly more neutral sugars in the culture media for *D. desulfuricans* cultures when steel or stainless steel coupons were present. They also indicated that glucose, mannose and galactose were the dominant polysaccharide subunits in the EPS found in the culture media of *P. fluorescens* and *D. desulfuricans* after biofilms had been removed. Staats et al. (1999) found that polysaccharides (from EPS) suspended in the culture media for *C. closterium* and *N. salinarum,* concentrations were in the range of several grams per liter. This means EPS are rather abundant compared to other biomolecules.

As likely dominant polysaccharide subunits, five hexoses and one uronic acid, namely glucose, galactose, mannose, rhamnose, xylose and glucuronic acid can be used to distinguish biofilm EPS from planktonic EPS. EPS proteins can also be analyzed as an auxiliary tool. In EPS studies, accurate control is necessary because EPS production and composition can be influenced by various factors. Carbon, nitrogen and phosphate were found to influence the yields of bacteria *Vibrio* sp. EPS (Majumdar et al., 1999), and growth conditions, species and even presence of metal could lead to a difference of EPS chemical composition (Sutherland, 1985; Zinkevich et al., 1996; Sponza, 2003). However, certain similarities are expected in biofilm EPS and the variations may not prevent interference by planktonic EPS during the detection of biofilm EPS. In some field

situations, planktonic EPS in the bulk media are expected to be completely negligible compared to biofilm EPS because microbes in synergistic consortia flourish only in local environments. The presence of planktonic cells can be detected using MPN or 16S rRNA fingerprinting (Zhu et al., 2005).

Advances in immunoassay techniques have made it possible to detect EPS components at extremely low levels, making their detections even more sensitive than PCR-based DNA/RNA fingerprinting. Thus, using EPS as a new biomarker for biofilm detection is a practical proposition. Although EPS as a biomarker may not indicate specific microbes, once the biofilm is located, more concentrated samples can be taken at the location for 16S rRNA fingerprinting to determine whether or not the biofilm contains corrosive microbes. Furthermore, because biofilm EPS are involved in cell adhesion to a metal surface, it is possible that as MIC pitting progresses, certain types of EPS polysaccharides or proteins may be released from the metal surface to the bulk fluid. Thus, it may be possible to use EPS as a new biomarker for MIC detection as well. To date, the MIC research community has not paid enough attention to the importance of EPS.

7.3.2 Sample preparation and analysis

7.3.2.1 Sample preparation for EPS assays

The bulk culture medium containing planktonic cells can be decanted from a biofilm culture to separate it from the biofilm and the biofilm can be removed from the

solid surface by using a scraper or sonication. The medium and biofilm need to be processed separately.

(a) EPS in the biofilm-free bulk medium can be isolated by microfiltration. EPS in the filtrate can be precipitated using ethanol (Braissant et al., 2007) and lyophilization can be used to remove ethanol and to concentrate EPS.

(b) EPS from the biofilm cells can be separated using centrifugation (Beech et al., 1991; Staats et al., 1999). EPS in the supernatant stage can be precipitated using ethanol and lyophilized as indicated in Part (a).

(c) The lyophilized EPS sample can be purified by using diafiltration (Beech et al., 1999).

7.3.2.2 Assays for polysaccharides

There are several popular methods for assaying polysaccharide. They are GC (Beech et al., 1991; Staats et al., 1999), lectin binding (Neu et al., 2001), XPS (Chan et al., 2002), LC (Kives et al., 2006), ^{1}H-NMR (Singh et al., 2006), and FTIR (Chan et al., 2002; Singh et al., 2006). Lectin binding can be used to directly analyze EPS in biofilms (Strathmann et al., 2002) using a confocal laser scanning microscope, as well as hydrolyzed EPS. EPS samples for ^{1}H-NMR, FTIR, and XPS are easy to prepare and do not require hydrolysis, but their peak information must be corroborated using GC or LC. Before GC or LC is used, polysaccharides must be hydrolyzed to become monosaccharides. To use GC, monosaccharides must be converted to volatile methyl-glycosides. Anion exchange LC can be used instead of GC without methylation (Kives et

al., 2006). However, GC usually provides much better resolutions and is cheaper to operate than LC for a large number of samples. The procedure for using GC is described below.

(a) Firstly, EPS need to be hydrolyzed to generate monosaccharides and monomeric uronic acids by using trifluoroacetic acid (TFA) (Stroop et al., 2002; Talaga et al., 2002; Asker et al., 2007) or H_2SO_4 hydrolysis (Singh et al., 2006). If necessary, a subsequent ultrafiltration can be used to remove large undigested molecules such as proteins.

(b) The monosaccharides and glucuronic acid need to be methylated with acidified methanol. The resulting methylglycosides need to be converted to their trimethylsilyl derivatives and separated in a gas chromatograph equipped with a flame ionization detector. Pure glucose, galactose, mannose, rhamnose, xylose and glucuronic acid can be used as GC standards after they are converted to volatile trimethylsilyl derivatives. If an unknown sugar component appears to be a major species, GC-MS can be applied to identify it (Zinkevich et al., 1996).

7.3.2.3 Protein Assays

Protein contents can be obtained by applying the Bradford method (Bradford, 1976) using protein standards such as bovine serum albumin. A proteomic analysis of planktonic EPS and biofilm EPS can be carried out by SDS-PAGE, 2-D gel electrophoresis, matrix-assisted laser desorption ionization-time of flight mass

spectrometry (MALDI-TOF-MS) and database searching (Trémoulet et al., 2002). If needed, purified proteins can be sequenced after 2-D gel electrophoresis.

7.3.2.4 Ultra-sensitive assays for EPS polysaccharides and proteins

The analytical procedures above, however, may not be sensitive enough for bulk-liquid samples from the field in which EPS released by biofilms in unknown locations are greatly diluted by the bulk solution, ultra-sensitive assays would be preferable.

Immunoassays such as quantitative ELISA (Enzyme-Linked ImmunoSorbent Assay) assays are used in many fields to detect trace amounts of chemicals or pathogens. ELISA is widely used in molecular biology and medical diagnostics. It relies on extremely strong antibody and antigen binding for separation and tagging. Antibodies have been widely used to detect both specific protein molecules and other molecules (Madoff et al., 1991; Goueli et al., 1998; Huang, 2001). Tens of thousands of antibodies are commercially available. They can also be custom-made by a commercial antibody supplier for any given molecules (antigens).

Figure 7-6 illustrates how ELISA works. Two antibodies with different binding specificities are needed. The capture antibody is immobilized on a plate well's surface (this helps separate the target molecule; an example would be a protein from a liquid sample). The target molecule (antigen) in a sample solution will bind with the capture antibody and impurities will be washed off. A detection antibody will then be used to bind with the antigen. The enzyme (E) conjugated to the detection antibody will digest added substrate molecules to produce a color change that can be detected using a plate

reader. For the reason of convenience, in a typical sandwich ELISA, a secondary antibody will be added first to bind the antigen and, then, detection antibody is added. Newer ELISA assays use fluorogenic substrates instead of chromogenic substrates to provide a much higher sensitivity. A 96-well microtiter plate is a popular choice allowing for simultaneous assaying of up to 96 samples.

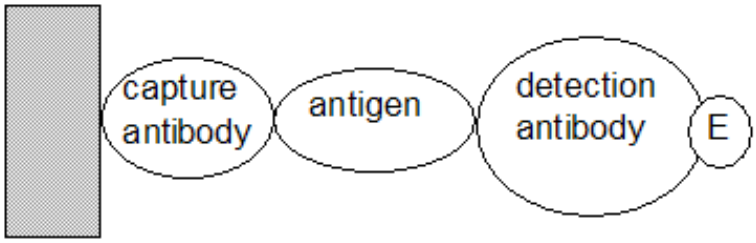

Figure 7-12: Illustration for ELISA assay

The assay in Figure 7-6 can be used directly for EPS protein detections. Because some of the EPS proteins are common proteins, there may already be commercially available ELISA assays. There are also commercial companies that will custom develop ELISA assays.

Lectin is a class of naturally occurring proteins or glycoproteins in plants that bind carbohydrates noncovalently. They are highly specific for their sugar moieties and have been employed as an enzyme-linked lectinsorbent assay to study biofilm development. Similar to what happens in ELISA, different lectins can bind with different carbohydrate molecules. Lectins with different sugar specificities are used to detect

different polysaccharide subunits (Michael and Smith, 1995; Neu and Lawrence, 1997; Johnsen et al., 2000; Neu et al., 2001). Table 7-2 shows an example taken from Johnsen et al. (2000). Commercially available lectins (Sigma Chemical) can be used to form lectin-sugar conjugates that replace the capture antibody in Figure 7-6. A detection antibody for the lectin-sugar conjugate instead of the sugar is illustrated in Figure 7-7, because the sugar, being a subunit for a polysaccharide, may be too small.

Table 7-2: Lectin specificities (Johnsen et al., 2000)

Lectin	Fluorescent label	Specificity of sugar
UEA1	TRITC	α-L-Fucose
Pha-E	TRITC	Galactose
ConA	TRITC Cy5	Terminal α-D-mananose Terminal α-D-glucose
PNA	TRITC	β-Galactose (1→3) N-acetylgalactosamine
WCA	Texas red	N-Acetyl- β-D-glucosamine, N- acetylneuraminic acid N- acetylmuraminic acid

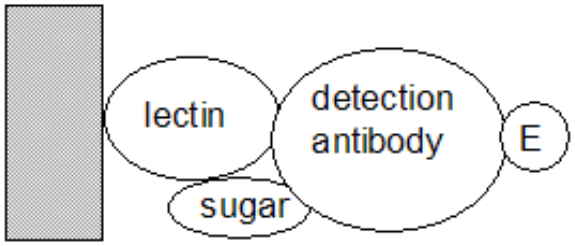

Figure 7-13: ELISA assay of a polysaccharide subunit using lectin binding

Signal-amplification in ELISA relies on the fact that one enzyme molecule can catalyze the digestion of many substrate molecules. This amplification mechanism can be replaced with a more powerful technique such as PCR. The so-called immuno-PCR technique is a modification of the above ELISA immunoassay. Instead of the enzyme molecule attaching to the detection antibody, a small DNA molecule attaches as a label. PCR is used to exponentially amplify the amount of the DNA after binding. A one-million fold increase in the DNA amount is readily achieved with 25 PCR cycles, making the immuno-PCR assay typically $10^4 - 10^5$ times more sensitive than ELISA. Immuno-PCR can detect as few as 580 antigen molecules (9.6×10^{-22} moles or 6.6×10^{-17} g for BSA) according to Sano et al. (1992) and Kricka (1996). Because there are far more polysaccharide subunit molecules and protein molecules from EPS than DNA molecules released by a biofilm, using immuno-PCR will make EPS far more detectable. This means EPS as a biomarker will allow for far more extensive dilutions in the bulk fluid than DNA before the detection limit is reached. ELISA schemes in Figures 7-6 and Figure 7-7 can be modified by replacing the enzyme molecule with a DNA label so that it

can then be used to assay EPS polysaccharide subunits and EPS proteins at extremely low concentrations quantitatively.

To prepare immuno-PCR test tubes, capture antibodies and lectins will be purchased from commercial vendors. A capture antibody or lectin for a particular polysaccharide subunit or protein from EPS will be immobilized on the wall of a test tube using a commercially available ELISA development kit. A sample solution can be added to a tube coated with capture antibodies or lectins. After incubation and washing, a detection antibody-DNA conjugate solution is added to the tube. The solution is removed after incubation and a test tube is inserted into the sample block of a PCR machine for DNA amplification.

It should be noted that rapid advances in proteomics have pushed forward the development of antibody microarrays (biochips) that are designed to detect thousands of proteins on a single chip (http://en.wikipedia.org/wiki/Protein_microarray; Mitchell, 2002). Signal amplification technologies other than enzymatic reaction and PCR are emerging. One example is the Tyramide Signal Amplification (TSA) technology (http://las.perkinelmer.com/applicationssummary/applications/TSA+-+Main.htm) that has been used in antibody microarrays. It is foreseeable that a dedicated field instrument may be developed in the future to process antibody microarrays for on-site analysis of biofilm EPS components.

7.4 Conclusions:

- The mechanistic MIC model shows that pitting rate decreases with time due to increased mass transfer resistance over time, charge transfer resistance is important initially when pit depth is small.
- Mass transfer becomes increasingly important when the pit grows deeper, and for deep pits, mass transfer resistance is always a controlling factor.
- The proposed new biomarker EPS for locating biofilm is theoretically proven practical and can be a potential replacement of exsiting biofilm probes.

CHAPTER 8: SUMMARY

The existing MIC research during and after hydrotesting has been confined to field practice after facility failure. The well designed experiments in a laboratory setting in this work have proven to be efficient and convenient, and have contributed to the establishment of guidelines for real operations.

MIC during hydrotesting is dependent on the composition of water sources, containing bacterial concentration and species as well as varying test temperatures and length of time. In the untreated water sources with low concentrations of nutrients and native organisms, it was found that test carbon steels in the laboratory were subject to pitting attacks in seawater, but not in the Wasia well water. This phenomenon, which agrees with current understanding of the effects of seawater on carbon steel, may be attributed to the high concentration of chloride. Other than the corrosion caused by the seawater, the experimental results on the test carbon steels did not demonstrate severe corrosion. However, in the experiments in which a marine strain of sulfate-reducing bacteria (SRB) and necessary nutrients were added, there were biofilms and typical MIC pits, and greater corrosion rates, proving that MIC can result in serious consequences both during and after hydrotesting.

The so called “black powder” problem during hydrotesting was found to most likely originate from oxygen contamination if no SRB were present; otherwise, iron sulfide (FeS), as one of the components, was apparent. This provided a key for a better understanding of the phenomenon.

The use of biocides THPS and glutaraldehyde proved effective in the control of planktonic SRB growth, and the application in combination with EDTA improved the bactericidal effect, which might be a novel and promising complement for treating water sources used in hydrotesting.

A technique for polymerase chain reaction (PCR) was used to detect very low levels of SRB in water samples. In the case of biofilm monitoring, the newly proposed biomarker EPS can be used to locate biofilm distribution and might be a preferable replacement for prevailing biofilm probes.

A mechanistic THPS degradation model as a function of time, temperature and pH was developed. It follows first-order kinetics and fits the experimental data very well. The model shows that THPS degradation is highly sensitive to temperature and pH changes while salt has no intrinsic effect on THPS degradation. Experimental results indicate that pH effect can be decoupled with temperature, and protons can act as an inhibitor of THPS degradation in the form of a negative order reaction. This model can provide an accurate guideline for THPS dosage strategy to minimize MIC in field hydrotesting practice.

Based on the mechanism of biocatalytic cathodic sulfate reduction, a simplified mechanistic MIC model was developed to predict MIC pitting rate under a certain condition; thus providing a basis for a more comprehensive mechanistic MIC modeling.

CHAPTER 9: RECOMMENDATIONS AND FUTURE WORK

Further investigations are recommended for a better understanding of MIC during hydrotesting. Below is a list of future work.

1. To collect a mixture of microbial culture from the field for use in testing. In a real world situation, SRB often grow in a synergistic microbial community. Even in natural seawater with a low level of organic carbon content, some microbes continue to thrive and their metabolites enrich the local organic carbon content. SRB can benefit from this.
2. To perfect the quantitative PCR technique for the detection of very low concentrations of microbes which might otherwise go undetected using microbiological tests.
3. To apply the combination of biocides and biocide enhancers (EDTA, EDDS, or other green metal chelants) to treat the water sources for hydrotesting.
4. To upgrade the existing THPS degradation model by incorporating more parameters, such as microbes, surfactant, O_2 scavenger, corrosion inhibitor, scale inhibitor and mild steel reactivity, given that in field applications, THPS is often blended with other chemicals. Because glutaraldehyde is a widely used green biocide, mechanistic modeling for its degradation will continue to prove valuable to the oil and gas industry.
5. The mechanistic MIC model will not predict MIC pitting for reasons other than biocatalytic cathodic sulfate reduction. This may include galvanic effects and H_2S attack. More work need to done to incorporate these factors.

REFERENCES

1. "ACG Phase I - supplementary lenders information package, executive summary." http://www.bp.com/liveassets/bp_internet/bp_caspian/bp_caspian_en/STAGING/local_assets/downloads_pdfs/t/ACG_English_SLIP_Content_ACG_Phase_1_SLIP.pdf, April 2003.
2. "Glutaraldehyde: the right biocide for many environments," Union Carbide Corporation, published by Union Carbide, Danbury CT, 1999.
3. "Performance biocides in industry applications"-brochure, Rhodia Water, Phosphorus and Performance Derivatives, http://www.rhodia-ppd.com/index.asp.
4. "Phosphonium Sulfate (THPS): a new industry biocide with low environmental toxicity," Paper No.401, NACE International, Houston, TX; 1997.
5. "Standard test method: field monitoring of bacterial growth in oil and gas systems," NACE Standard TM0194, NACE International, 2004.
6. Accepta, MSDS sheet for Accepta 2102 (a THPS formulation). Uhttp://www.accepta.com/prod_docs/2102.pdf, 2004.
7. Andrade C. de A., da Silva E.D., Licina G.J., "Real time monitoring of biofilms in seawater injection environments," Paper No.06660, NACE International, Houston, TX, 2006.

8. Asker M.S., Manal, Mahmoud G., Ghada Ibrahim S., "Structural characterization and biological activity of acidic polysaccharide fractions isolated from *Bacillus polymyxa* NRC-A," *Journal of Applied Sciences Research*, 3, 10, 1170-1177, 2007.
9. Atlas R.M., Park L.C., *Handbook of Microbiological Media*, 2nd ed., CRC Press, Boca Raton, 1997.
10. Badziong W., Ditter B., Thauer R.K., "Acetate and carbon dioxide assimilation by *Desulfovibrio vulgaris* (Marburg), growing on hydrogen and sulfate as sole energy source," *Archives of Microbiology.*, 123, 301-305, 1979.
11. Bahr M., Crump B.C., Ceraj V.K., Teske A., Sogln M.L., Hobble J.E., "Molecular characterization of sulfate-reducing bacteria in a new England salt marsh," *Environmental Microbiology*, 7 (8), 1175-1185, 2005.
12. Bailey J.E., Ollis D.F., "Biochemical Engineering Fundamentals," 2nd ed., McGraw-Hill, New York, 373-453, 1986.
13. Baldwin R. M., "Black powder in the gas industry – sources, characteristics and treatment," Mechanical and Fluids Engineering Division, Southwest Research Institute, May 1998.
14. Barton L.L., Hamilton W.A., *Sulfate-Reducing Bacteria: Environmental and Engineered Systems*, Cambridge University Press, 2007.
15. Beech I.B., Cheung C.W.S., Johnson D.B., Smith J.R., "Comparative studies of bacterial biofilms on steel surfaces using atomic force microscopy and environmental scanning electron microscopy," *Biofouling*, 10, 65-77, 1996.

16. Beech I.B., Gaylarde C.C., "Microbial polysaccharides and corrosion," *International Biodeterioration*, 27 (2), 95-107, 1991.
17. Beech I.B., Gaylarde C.C., "Recent advances in the study of biocorrosion-an overview," *Revista de Microbiologia*, 30, 177-190, 1999.
18. Beech I.B., Gaylarde C.C., Smith J.J., Geesey G.G., "Extracellular polysaccharides from *Desulfovibrio desulfuricans* and *Pseudomonas fluorescens* in the presence of mild and stainless steel," *Applied Microbiology Biotechnology*, 35, 65-71, 1991.
19. Beech I.B., Sunner J., "Biocorrosion: towards understanding interactions between biofilms and metals," *Current Opinion in Biotechnology*, 15, 181-186, 2004.
20. Berges, J.A., Franklin, D.J., "Evolution of an artificial seawater medium: improvements in enriched seawater, artificial water over the last two decades," *Journal of Phycology*, 37, 1138-1145, 2001.
21. Bibb M., "Bacterial corrosion in the South African power industry," *Biologically Induced Corrosion*, NACE International, Houston, TX, 96-101, 1986.
22. Borenstein W.S., Lindsay P.B., "MIC failure of 304L stainless steel piping left stagnant after hydrotesting," *Materials Performance*, 41 (6), 70-73, 2002.
23. Bradford, M.M., "A rapid and sensitive method for the quantitation of microgram quantities of protein utilizing the principle of protein-dye binding," *Analytical Biochemistry*, 72, 248-254, 1976.

24. Braissant O., Decho A.W., Dupraz C., Glunk C., Przekop K.M., Visscher P.T., "Exopolymeric substances of sulfate-reducing bacteria: interaction with calcium at alkaline pH and implication for formation of carbonate minerals," *Geobiology*, 5, 401-411, 2007.

25. Brennenstuhl A.M., Doherty P.E., "The economic impact of microbiologically influence corrosion at Ontario Hydro's nuclear plants," *Microbiologically Influenced Corrosion and Biodeterioration*, University of Tennessee, Knoxville, TN, 5-10, 1990.

26. Bryant R.D., Jansen W., Bovin J., Laishley E.J., Costerton J.W., "Effect of hydrogenase and mixed sulfate reducing bacterial populations on the corrosion of steel," *Applied and Environmental Microbiology*, 57, 2804-2809, 1991.

27. Caldwell D.E., Korber D.R., Lawrence J.R., "Confocal laser microscopy in digital images analysis in microbial ecology," *Advances in Microbial Ecology*, 12, 1-67, 1992.

28. Castro H.F., Williams N.H., Ogram A., "Phylogeny of sulfate-reducing bacteria," *FEMS Microbiology Ecology*, 31, 1-9, 2000.

29. Chan K.Y., Xu L.C., Fang H.H.P., "Anaerobic electrochemical corrosion of mild steel in the presence of extracellular polymeric substances produced by a culture enriched in sulfate-reducing bacteria," *Environmental Science & Technology*, 36, 1720-1717, 2002.

30. Chexal V.K., et al, Proceedings International Corrosion Conference, paper IWC-97-84, Eng. Soc. W. PA, Pittsburgh, PA, 1997.

31. Cord-Ruwisch R., Widdel F., "Corroding iron as a hydrogen source for sulphate reduction in growing cultures of sulphate-reducing bacteria," *Applied Microbiology Biotechnology*, 25, 169-174, 1986.
32. CSLC-MFD, "California State Lands Commission, a procedure for the hydrostatic pressure testing of marine facility piping," http://www.slc.ca.gov/Division_Pages/MFD/SLPT/Revised_SLPT_Guidelines_12-03-03.pdf
33. Davis, J.R., *Corrosion: understanding the basics*, ASM International, Materials Park, Ohio, 2000.
34. de Brouwer J.F.C., Neu T.R., Stal L.J., "On the function of secretion of extracellular polymeric substances by benthic diatoms and their role in intertidal mudflats: A review of recent insights and views," in Functioning of Microphytobenthos in Estuaries, 45-61, edited by Kromkamp J.C., de Brouwer J.F.C., Blanchard G.F., Forster R.M., Créach V., Royal Netherlands Academy of Arts and Sciences, Amsterdam, 2006.
35. Donlan R.M., "Biofilm: microbial life on surfaces," *Emerging Infectious Diseases*, 8 (9), 881-890, 2002.
36. Duan J.Z., Hou B.R., Yu Z.G., "Characteristics of sulfide corrosion products on 316L stainless steel surfaces in the presence of sulfate-reducing bacteria," *Materials Science and Engineering,* 26, 624-629, 2006.

37. Dzierzewicz Z., Szczerba J., Weglarz L., Swiatkowska L., Jasinska D. Wilczok, T., "Intraspecies variability of *Desulfovibrio desulfuricans* strains determined by genetic profiles," *FEMS Microbiology Letter*, 219, 69-74, 2003.

38. Eckford R.E, Fedorak P.M., "Chemical and microbiological changes in laboratory incubations of nitrate amendment "sour" produced waters from three western Canadian oil fields," *Journal of Industrial Microbiology & Biotechnology*, 29, 243–254, 2002a.

39. Eckford R.E., Fedorak P.M., "Planktonic nitrate-reducing bacteria and sulfate-reducing bacteria in some western Canadian oil field water," *Journal of Industrial Microbiology & Biotechnology*, 29, 83-92, 2002b.

40. Edyvean R.G.J., Benson J., Thomas C.J., Beech I.B., Videla H., "Biological influences on hydrogen effects in steel in seawater," *Materials Performance*, 37, 40-44, 1998.

41. Efird K.D., "Galvanic corrosion in oil and gas production," Galvanic Corrosion, *ASTM STP 978*, Hack, H.P., Ed., American Society for Testing and Materials, 260-282, Philadelphia, 1988.

42. Electric Power Research Institute, "Microbiologically Influenced Corrosion", TM1001, EPRI Palo Alto, CA, 1994.

43. Escher A., Characklis, W.G., "Modeling the initial events in biofilm accumulation," *In Biofilms*. Edited by Characklis W.G., and Marshall K.C., Wiley, New York, 445-86, 1990.

44. Evans P., Dunsmore B., "Reservoir simulation of sulfate-reducing bacteria activity in the deep sub-surface," Paper No.06664, NACE International, Houston, TX, 2006.

45. Fan L.S., Leyva-Ramos R., Wisecarver K.D., Zehner B.J., "Diffusion of phenol through a biofilm grown on activated carbon particles in a draft-tube three-phase fluidized-bed bioreactor," *Biotechnology and Bioengineering*, 35, 279-286, 1990.

46. Flemming H–C., "Biofouling and microbiologically influenced corrosion (MIC) – an economical and technical overview," *Microbial Deterioration of Materials*, Springer, Heidelberg, 5-14, 1996.

47. Flemming H-C., Geesey, G. G., "Biofouling and biocorrosion in industrial water systems," Springer, Berlin, Heidelberg, 162, 1991.

48. Fonseca I.T.E., Feio M.J., Lino A.R., Reis M.A., Rainha V.L., "The influence of the media on the corrosion of mild steel by *Desulfovibrio desulfuricans* bacteria: an electrochemical study," *Eletrochemica Acta*, 43, 213, 1998.

49. Ford T.E., Maki J.S., Mitchell R., "Metal binding bacterial exopolymers and corrosion process," Paper No.380, NACE International, Houston, TX, 1987.

50. Fukui M., Takii S., "Survival of sulfate-reducing bacteria in oxic surface sediment of a seawater lake," *FEMS Microbiology Ecology*, 73, 317-322, 1990.

51. Fux C.A., Costerton J.W., Stewart P.S., Stoodley P., "Survival strategies of infectious biofilms," *Trends in Microbiology*, 13 (1), 34-40, 2005.

52. Genin, J.M. R., Refait, P., Abdelmoula M., "Green rusts and their relationship to iron corrosion; a key role in microbially influenced corrosion," *Hyperfine Interactions*, 139/140, 119-131, 2002.

53. Genin, J.M.R., "Fe (II-III) hydroxysalt green rusts; from corrosion to mineralogy and abiotic to biotic reactions by Mossbauer spectroscopy," *Hyperfine Interactions*, 156/157, 471-485, 2004.

54. Gorman M., "Anaerobic aquatic metabolism of $_{14}$C-tetrakishhydroxylmethyl phosphonium sulfate (THPS): Final report," 1997.

55. Goueli S.A., O'Brien M., Hsiao K., "Anti-ACTIVE™ antibody for specific detection of phosphorylated CaM KII protein kinase," *Promega Notes*, 67, 9-12, 1998.

56. Grady C.P.L., "Modeling of biological fixed films - a state of the art review," In: Fixed Film Biological Process for Wastewater Treatment, Wu Y.C., Smith E.D. (Eds), Noyes Data Corporation, New Jersey, 75-134, 1983.

57. Gu T., "From probability models to quantitative mechanistic models for MIC prediction," Calgary MIC Workshop, October, 2007.

58. Hardy J.A., "Utilisation of cathodic hydrogen by sulphate-reducing bacteria," *British Corrosion Journal*, 18, 190-193, 1983.

59. Hardy J.A., Hamilton W.A., "The oxygen tolerance of sulfate-reducing bacteria isolated from North Sea waters," *Current Microbiology*, 6, 259-262, 1981.

60. Hardy, J.A., "The enumeration, isolation and characterization of sulfate-reducing bacteria from North Sea waters," *Journal of Applied Bacteriology*, 51, 505-516, 1981.

61. Hu A., "Investigation of sulfate-reducing bacteria growth behavior for the mitigation of microbiologically influenced corrosion (MIC)," Master thesis, Ohio University, Athens, OH, 2004.

62. Hu C., Liu Y., Paulsen B.S, Petersenc D., Dag Klavenessd D., "Extracellular carbohydrate polymers from five desert soil algae with different cohesion in the stabilization of fine sand grain," *Carbohydrate Polymers*, 54, 33–42, 2003.

63. Huang R.P., "Detection of multiple proteins in an antibody-based protein microarray system," *Journal of Immunological Methods*, 255, 1-13, 2001.

64. Huber C., Nemati M., Jenneman G.E., Voordouw G., "Containment of biogenic sulfide production in continuous up-flow packed-bed bioreactors with nitrate or nitrite," *Biotechnology Progress,* 19, 338-345, 2003.

65. Jacobson G.A., "Corrosion at Prudhoe Bay-A lesson on the line," *Materials Performance*, 26-34, 2007.

66. Jahn A., Nielsen P.H., "Cell biomass and exopolymer composition in sewer biofilms," *Water Science and Technology*, 37, 17-24, 1998.

67. Javaherdashi R., "A review of some characteristic of MIC caused by sulfate-reducing bacteria: past, present and future," *Anti-Corrosion Methods and Materials*, 46, 173-180, 1999.

68. Javaherdashi R., "Enhancing the effects of hydrotesting on microbiologically influenced corrosion," *Materials Performance*, 40-43, 2003.

69. Johnsen A.R., Hausner M., Schnell A., Wuertz S., "Evaluation of fluorescently labeled lectins for noninvasive localization of extracellular polymeric substances in *Sphingomonas* biofilms," *Applied and Environmental Microbiology*, 66, 3487-3491, 2000.

70. Jones, D.A., *"Principles and Prevention of Corrosion,"* 2nd eds., Prentice Hall, 1996.

71. Kives J., Orgaz B., SanJose C., "Polysaccharide differences between planktonic and biofilm-associated EPS from *Pseudomonas fluorescens* B52," *Colloids and Surfaces B: Biointerfaces,* 52, 123–127, 2006.

72. Koch G.H., Brongers M.P.H., Thompson N.G., Virmani Y.P., Payer J.H., "Corrosion costs and preservative strategies in the United States FHWA-RD-01-156," Federal Highway Administration, Washington, D.C., 2001.

73. Kricka L.J., "Strategies for immunoassay," *Pure & Applied Chemistry*, 68, 1825-1830, 1996.

74. Kuang F., Wang J., Yan L., Zhang D., "Effects of sulfate-reducing bacteria on the corrosion behavior of carbon steel," *Electrochimica Acta*, 52, 6084-6088, 2007.

75. Larsen J., Skovhus T.L., Thomas T.R., "Bacterial diversity study applying novel molecular methods on Halfdan produced waters," Paper No. 06668, NACE International, Houston, TX, 2006.

76. Lee, J. K-L., "A mechanistic modeling of CO_2 corrosion of mild steel in the presence of H_2S," PhD dissertation, Ohio University, Athens, OH, 2004.

77. Lee, J. S., Ray, R. I., "Comparison of Key West and Persian Gulf seawaters," Paper No. 518, NACE International, Houston, TX, 2007.

78. Leive L., "Release of lipopolysaccharide by EDTA treatment of *E.coli.*," *Biochemical Biophysical Research Communications*, 21, 290-296, 1965.

79. Leriche V., Sibilie P., Carpentier B., "Use of enzyme-linked lectinsorbent assay to monitor the shift in polysaccharide composition in bacterial biofilms," *Applied and Environmental Microbiology*, 1851-1856, 2000.

80. Lewandowski, Z., Cloete T.E., Dexter S.C., et al., "MIC issues: commentary from the corrosion 2002 MIC panel discussion," Paper No. 03560, NACE International, Houston, TX, 2003.

81. Li J., Bishop P.L., "Time course observations of nitrifying biofilm development using microelectrodes," *Journal of Environmental Engineering and Science*, 3 (6), 523-528, 2004.

82. Li J., Xu Z.Y., Zhang W.Y., Du Y.L., Xie S.Y., "Impact of sulfate reducing bacteria biofilm on the corrosion of copper-nickel alloy of condense in power plant," *Proceedings of the Chinese Society of Electrical Engineering*, 25 (25), 305-308, 2005.

83. Lloyd G. R., "UV degradation of THPS," Oldbury, United Kingdom, Albright & Wilson UK Ltd, Specialties Technical Laboratory, 1994.

84. Lovley D.R., Philips E.J.P., "Novel processes for anaerobic sulfate production from elemental sulfur by sulfate-reducing bacteria," *Applied Environmental Microbiology*, 60, 2394-2399, 1994.

85. Lutey, R. W. Stein, A., Proceedings 14th International Corrosion Conf., paper 5.6-263, Sept. 27, Cape Town, SA, 1999.

86. Madoff L.C., Michel J.L., Kasper D.L., "A monoclonal antibody identifies a protective C-protein Alpha-Antigen epitope in group B *Streptococci,*" *Infection and Immunity*, 204-210, 1991.

87. Majumdar I., D´souza F., Bhosle N., "Microbial exopolysaccharides: effect on corrosion and partial chemical characterization," *Journal of Indian Institute of Science,* 79, 539-550, 1999.

88. Marschall C., Frenzel P., Cypionka H., "Influence of oxygen on sulfate reduction and growth of sulfate-reducing bacteria," *Archives of Microbiology*, 159, 168-173, 1993.

89. Mattila K., Carpen L., Hakkarainen T., Salkinoja-Salonen M.S., "Biofilm development during ennoblement of stainless steel in Baltic Sea water: a microscopic study," *International Biodeterioration & Biodegradation*, 40 (1), 1-10, 1997.

90. Maxwell S., Campbell S., "Monitoring the mitigation of MIC risk in pipelines," Paper No.06662, NACE International, Houston, TX, 2006.

91. McWilliam P., "Tolcide PS355A: Biodegradability in seawater-closed bottle test," 1994.

92. Michael T., Smith C.M., "Lectins probe molecular films in biofouling: characterization of early films on non-living and living surfaces," *Marine Ecology Progress Series*, 119, 229-236, 1995.

93. Mitman R., "Getting serious about slime," *Materials Performance*, 46, April, 2006.

94. Mohanty S.S., Das T., Mishra S.P. Chaudhury G.R., "Kinetics of SO_4^{2-} - reduction under different growth media by sulfate reducing bacteria," *BioMetals*, 73-76, 2000.

95. Mudryk Z.Y., Podgórska B., Bolalek J., "The occurrence and activity of sulphate-reducing bacteria in the bottom sediments of the Gulf of Gdańsk," *Oceanologia*, 42 (1), 105-117, 2000.

96. Neu T.R., Lawrence J.R., "Development and structure of microbial biofilms in river water studied by confocal laser scanning microscopy," *FEMS Microbiology Ecology*, 24, 11-25, 1997.

97. Neu T.R., Swerhone G.D.W., Lawrence J.R., "Assessment of lectin-binding analysis for in situ detection of glycoconjugates in biofilm systems," *Microbiology*, 147, 299-313, 2001.

98. Newman J.S., "Electrochemical systems," 2nd eds., Prentice Hall, 1991.

99. Nikaido H., "Outer membrane barrier as a mechanism of antimicrobial resistance," *Antimicrobial Agents and Chemotherapy*, 33, 1831-1836, 1989.

100. O'Connor J., "THPS: Determination of hydrolysis as a function of pH," *Eye*, United Kingdom, Life Science Research Limited, 1992.

101. Odom J.M., "Industrial and environmental activities of sulfate-reducing bacteria," in the *Sulfate-reducing bacteria: contemporary perspective*, Springer-Verlag, NY, 1993.

102. Parra A., Capio J.J., Martinez I., "Microbial corrosion of metals exposed to air in tropical marine environment," *Materials Performance*, 35 (10), 1996.

103. Penn C.W., *Handling Laboratory Microorganism*s, Bristol. PA, USA, 1991..

104. Picioreanu C., van Loosdrecht M.C.M., "A mathematical model for initiation of microbiologically influenced corrosion by differential aeration," *Journal of The Electrochemical Society*, 149 (6), 211-223, 2002,

105. Postgate J.R., *The sulfate-reducing bacteria* (2nd eds.,), Cambridge University Press, Cambridge, 1984.

106. Pots B.F.M., John R.C., Rippon I.J., et al., "Improvements on DeWaard-Milliams corrosion prediction and applications to corrosion management," Paper No.02235, NACE International, Houston, TX, 2002.

107. Prasad R., "Chemical treatment for hydrostatic test," US Patent No.6815208 B2, 2004.

108. Raad I., Chatzinikolaou I., Chaiban G., Hanna H., Hachem R., Dvorak T., Cook G., Costerton W., "In vitro and ex vivo activities of minocycline and EDTA against microorganisms embedded in biofilm on catheter surfaces," *Antimicrobial Agents and Chemotherapy*, 47 (11), 3580-3585, 2003.

109. Radd, I., Sherertz, R., US Patent 6267979−Chelators in combination with biocides: treatment of microbially induced biofilm and corrosion, 2001.

110. Rainha V.L., Fonseca I.T.E., "Kinetic studies on the SRB influenced corrosion of steel: a first approach," *Corrosion Science*, 39 (4), 807-813, 1997.

111. Rajagopal B.S., LeGall J., "Utilization of cathodic hydrogen by hydrogen-oxidizing bacteria," *Applied Microbiology and Biotechnology*, 31, 406-412, 1989.

112. Rhodia, Product Technical Data on TOLCIDE®PS75, Issue No. 6, October, 2004.

113. Rossmoore H.W., Handbook of biocide and preservation use, Blackie Academic & Professional, Chapman & Hall, UK, 1995.

114. Sanders P.F., "Overview of souring, corrosion and plugging due to reservoir organisms," *UK Corrosion 98*, Paper 15, Sheffield, UK, Oct. 20-21, 1998.

115. Sano T., Smith C.L., Cantor C.R., "Immuno-PCR: very sensitive antigen detection by means of specific antibody–DNA conjugates." *Science*, 258, 120–122, 1992.

116. Schultz G.L., Hampton B.E., Proceedings EPRI SWSRI, EPRI NDE Center, Charlotte, NC, June 22-27, 1997.

117. Shams El Din, A.M., Saber T.M.H., Hammoud A.A., "Biofilm formation on stainless steels in Arabian Gulf water," *Desalination*, 107, 251-264, 1996.

118. Sharpley J. M., "Microbiological corrosion in waterflood," *Corrosion*, 17, 386, 1961.

119. Singh V.B., Kumar A., Kirubakaran S.I., Ayyadurai N., Sunish Kumar R., Sakthivel N., "Comparison of Exopolysaccharides Produced by *Xanthomonas*

oryzae pv. *oryzae* Strains, BXO1 and BXO8 that Show Varying Degrees of Virulence in Rice (*Oryza sativa* L.)," *Journal of Phytopathology* 154, 410-413, 2006.

120. Sooknah R., Papavinasam S., Revie R.W., Romero M.D., "Modeling the occurrence of microbiologically influenced corrosion," Paper No. 07515, NACE International, Houston, TX, 2007.
121. Sponza D.T., "Investigation of extracellular polymer substances (EPS) and physicochemical properties of different activated sludge flocs under steady-state conditions," *Enzyme and Microbial Technology*, 32, 375-385, 2003.
122. Staats N., Winder B. D., Stal L. J., Mur. L. R., "Isolation and characterization of extracellular polysaccharides from the epipelic diatoms *Cylindrotheca closterium* and *Navicula salinarum*," *European Journal of Phycology*, 34, 161-169, 1999.
123. Stoodley P., Dodds I., Boyle J.D., Lappin-Scott H.M., "Influence of hydrodynamics and nutrients on biofilm structure," *Journal of Applied Microbiology Symposium Supplement*, 85, 19-28, 1999.
124. Strathmann M., Wingender J., Flemming H. -C., "Application of fluorescently labelled lectins for the visualization and biochemical characterization of polysaccharides in biofilms of *Pseudomonas aeruginosa*," *Journal of Microbiological Methods*, 50, 237-248, 2002.
125. Stroop C.J.M., Bush A., Marple R.L., LaCourse W.R., "Carbohydrate analysis of bacterial polysaccharides by high-pH anion-exchange chromatography and

online polarimetric determination of absolute configuration," *Analytical Biochemistry*, 303, 176-185, 2002.

126. Sutherland I.W., "Biosynthesis and composition of gram-negative bacterial extracellular and cell wall polysaccharides," *Annual Review of Microbiology*, 39, 243-262, 1985.
127. Talaga P., Vialle S., Moreau M., "Development of a high-performance anion-exchange chromatography with pulsed-amperometric detection based quantification assay for pneumococcal polysaccharides and conjugates," *Vaccine*, 20, 2474-2484, 2002.
128. Tatnall R.E., "Introduction" in *Practical Manual on Microbiologically-Influenced Corrosion*, NACE International, Houston, TX, 1995.
129. Thierry D., Sand W., "Microbially influenced corrosion," In: *Corrosion Mechanisms in Theory and Practice*, Marcus, P., Oudar, J. (eds.), 457-499, Marcel Dekker, New York, 1995.
130. Trémoulet F., Duché O., Namane A., Martinie B., Labadie J. -C., "A proteomic study of *Escherichia coli* O157:H7 NCTC 12900 cultivated in biofilm or in planktonic growth mode," *FEMS Microbiology Letters*, 215, 7-14, 2002.
131. Vester F., Ingvorsen K., "Improved most-probable-number method to detect sulfate-reducing bacteria with natural media and a radiotracer," *Applied and environmental microbiology*, 1700-1707, 1998.
132. Videla H. A., *Manual of Biocorrosion*, Lewis Publishers, Boca Raton, Florida, 1996.

133. Videla H.A., Herrera L.K., "Microbiologically influenced corrosion: looking to the future," *International Microbiology*, 8, 169-180, 2005.

134. Viera M.R., Guiamet P.S., de Mele M.F.L., Videla H.A., "Use of dissolved ozone for controlling planktonic and sessile bacteria in industrial cooling systems," *International Biodeterioration & Biodegradation*, 44, 201-207, 1999.

135. von Wolzogen Kuhr C.A.H., van der Vlugt I.S., "Graphication of cast iron as an electrochemical process in anaerobic soils," *Water*, 18, 147-165, 1934.

136. Wagner M., Roger A.J., Flax J.L., Brusseau G.A., Stahl D.A., "Phylogeny of dissimilatory sulfite supports an early origin of sulfate respiration," J*ournal of Bacteriology*, 2975-2982, 1998.

137. Walker J.T., Hanson K., Cadwell D., Keevil C.W., "Scanning confocal laser microscopy study of biofilm induced corrosion on copper plumbing tubes," *Biofouling*, 12, 333-444, 1998.

138. Weinbauer M.G., Wenderoth D.F., "Microbial Diversity and Ecosystem Functions – the Unmined Riches," *Electronic Journal of Biotechnology*, April 15, 2002.

139. White D.C., Nivens P.D., Nichols A.T., Kergrer B. D., Henson J.M., Geesey G.G., Clarke C.K., "Corrosion of steel induced by aerobic bacteria and their extracellular polymers," In proceedings of International Workshop on Biodeterioration held at the University of La Plata, Argentina, 73-86, 1985.

140. WHO, "Flame Retardants: Tris(2-Butoxyethyl) Phosphate, Tris(2-Ethylhexyl) Phosphate And Tetrakis(Hydroxymethyl) Phosphonium Salts,"

http://www.inchem.org/documents/ehc/ehc/ehc218.htm, Environmental Health Criteria 218, World Health Organization, Geneva, 2000.

141. Wilfried P., *Directory of microbicides for the protection of materials, a handbook,* Kluwer Academic Publishers, 2004.
142. Wingender J., Neu T.R., Flemming H.-C., "What are bacterial extracellular polymeric substances?" in Microbial Extracellular Polymeric Substances: characterization, structure and function, 1-19, edited by Wingender J., Neu T.R., Flemming H.-C., Springer, Berlin-New York, 1999.
143. Wooley R.E., Jones M., Gilbert J.P., Shotts E.B., "In vitro action of combination of antimicrobial agents and EDTA-tromethamine on *Pseudomonas aeruginosa*," *American Journal of Veterinary Research*, 44, 1521-1524, 1983.
144. Wozniak D.J., Wyckoff T.J.O., Starkey M., Keyer R., Azadi P., O´Toole G.A., Parsek M.R., "Alginate is not a significant component of the extracellular polysaccharide matrix of PA14 and PA01 *Pseudomonas aeruginosa* biofilms," *Proceedings of the National Academy of Sciences*, 100, 7907-7912, 2003.
145. Xu C.M., Zhang Y.H., Cheng G.X., Zhu W.S., "Localized corrosion behavior of 316L stainless steel in the presence of sulfate-reducing and iron-oxidizing bacteria," *Materials Science and Engineering,* 443, 235-241, 2007.
146. Xu L.C., Chan K.Y., Fang H.H.P., "Application of atomic force microscopy in the study of microbiologically influenced corrosion," *Materials Characterization*, 48, 195-203, 2002.

147. Zhao K.L., Wen J., Gu T., Kopliku A., Cruz I., "Mechanistic modeling of anaerobic THPS degradation in seawater under various conditions," Paper No. 08512, NACE International, Houston, TX, 2008.

148. Zhao K.L., Wen J., Gu T., Nesic S., "Effects of biocides and a biocide enhancer on SRB growth," AIChE Annual Meeting, Conference Proceedings, Cincinnati, OH, United States, 2005.

149. Zhao X.D., Duan J.Z., Hou B.R., Wu S.R., "Effect of sulfate-reducing bacteria on corrosion behavior of mild steel in sea mud," *Journal of Material Science and Technology*, 23 (3), 323-328, 2007.

150. Zhu X., Kilbane J. II, Ayala A., Modi H., "Application of quantitative, real-time PCR in monitoring microbiologically influenced corrosion (MIC) in gas pipelines," Paper No.493, NACE International, Houston, TX, 2005.

151. Zinkevich V., Bogdarina I., Kang H., et al., "Characterisation of exopolymers produced by different isolates of marine sulphate-reducing bacteria," International Biodeterioration & Biodegradation, 163-172, 1996.